

Mud volcanoes from the Alboran Sea: materials and vulcano-sedimentary and diagenetic processes involved.

*Los volcanes de lodo del mar de Alborán: materiales y procesos
vulcano-sedimentarios y diagenéticos involucrados.*

Editor: Universidad de Granada. Tesis Doctorales
Autora: Carmen Fátima López Rodríguez
ISBN: 978-84-9125-421-8
URI: <http://hdl.handle.net/10481/41550>



Instituto Andaluz de Ciencias de la Tierra
Consejo Superior de Investigaciones Científicas-
Universidad de Granada (CSIC - UGR)



Tesis Doctoral

Mud volcanoes from the Alboran Basin: materials and volcano - sedimentary and diagenetic processes involved

Los volcanes de lodo del Mar de Alborán: materiales y procesos vulcano - sedimentarios y diagenéticos involucrados

Programa de doctorado Ciencias de la Tierra (UGR)
2015

Carmen Fátima López Rodríguez

Granada, Noviembre 2015

La Doctoranda

Carmen Fátima López Rodríguez

Vº Bº de las directoras

Francisca Martínez Ruiz

Menchu Comas Minondo

Para el desarrollo de esta Tesis Doctoral se ha contado con una beca-contrato (2+2) del Programa JAE-Predoc del Consejo Superior de Investigaciones Científicas (CSIC) y cuatro ayudas complementarias para la realización de Estancias Breves en el Extranjero tres de ellas concedidas por el Programa JAE-Predoc (Consejo Superior de Investigaciones Científicas -CSIC) y una de ellas por el Programa de Movilidad Internacional de Posgrado Universidad de Granada y CEI BioTic. El trabajo de investigación se ha desarrollado mayormente en el Instituto Andaluz de Ciencias de la Tierra (IACT) del Consejo de Investigaciones Científicas (CSIC). Parte del trabajo también fue realizado durante las estancias en el extranjero en “Departament of Marine Geosciences” (Octubre-Diciembre 2009; Universidad de Aveiro, Portugal); “Marine Biochemie-Marine Geosysteme” (Septiembre-Noviembre 2010; IFM-GEOMAR, Kiel, Alemania); “Department of Marine Organic Biogeochemistry, NIOZ, Holanda” (Febrero-Agosto 2011) y en “Department of Earth Sciences – Department of Earth Sciences and Geochemistry, Universidad de Utrecht, Holanda) (Enero-Abril y Agosto-Noviembre 2013). Este trabajo ha sido financiado dentro de los proyectos del Plan Nacional CGL2008-03474-E/BTE, CTM2009-07715 y CGL2011-14141-E financiados por el Ministerio de Ciencia e Innovación (MICINN) del Gobierno de España. También se agradece la financiación de los Fondos Europeos de Desarrollo Regional (FEDER) de la Comunidad Económica Europea, a la acción especial CGL2011-14141-E financiada por el Ministerio de Ciencia e Innovación (MICINN) del Gobierno de España, los proyectos RNM-3713 y Grupo de Investigación RNM215 de la Junta de Andalucía y a los programas Topomed CGL2008-03474 y Consolider Ingenio 2010- CSD2006-00041 del Ministerio de Ciencia e Innovación del Gobierno de España. Igualmente es de agradecer la colaboración del Training Through Research Program UNESCO-IOC/MSU así como a los jefes científicos de la campaña Ristretto & Lungo M83/3 G.J. De Lange y A. Stadnitskaia por la obtención de los testigos de sedimento marino y materiales volcánicos estudiados en esta Tesis Doctoral. Al Departamento de Mineralogía y Petrología de la Universidad de Granada (UGR) donde se ha realizado parte del trabajo de laboratorio así como al Centro de Instrumentación Científica (CIC) de Granada.

“El científico no estudia la naturaleza por la utilidad que le pueda reportar, la estudia por el gozo que le proporciona, y este gozo se debe a la belleza que hay en ella. La belleza intelectual se basta en sí misma, y es por ella más quizá que por el bien futuro de la humanidad, por lo que el científico consagra su vida a un trabajo largo y difícil”

Henri Poincaré . Filósofo y matemático francés

“Iré a cualquier parte, siempre que sea hacia adelante”

David Livingstone. Médico y misionero británico

A Juan y Carmen, mis padres

A todos los que valoran y reconocen el esfuerzo

Table of contents

Abstract	5
Resumen	9
Chapter 1. Introduction and background	13
1.1. Mud volcanoes: an overview	15
1.2. Diagenetic processes associated with mud volcanism	18
1.3. Environmental hazards and socio-economic importance of mud volcanism	20
1.4. Regional setting	22
1.5. Motivation	24
1.6. Objectives	25
1.7. Thesis outline	25
Chapter 2. Data and Methodology	27
2.1. Geophysical survey and data	29
2.1.1. Oceanographic cruises and core locations	29
2.1.2. Seismic images	29
2.1.3. Morphology of the seafloor	31
2.2. Sedimentological and mineralogical analyses	34
2.3. Geochemical analyses	36
2.3.1. X-ray fluorescence (XRF)	36
2.3.2. Inductively coupled plasma mass spectrometry (ICP-MS)	38
2.3.3. Total Organic Carbon (TOC), Total Inorganic Carbon (TIC) and Total Nitrogen (TN)	38
2.3.4. Inductively coupled plasma atomic emission spectrometry (ICP-AES)	38
2.3.5. Gas Chromatography (GC), gas chromatography mass spectrometry (GC-MS) and high performance liquid chromatography mass spectrometry (HPLC-MS)	38
2.3.6. Stable carbon ($\delta^{13}\text{C}$), oxygen ($\delta^{18}\text{O}$) and hydrogen (δD) isotopes of pore waters	38
2.3.7. Stable carbon ($\delta^{13}\text{C}$) and hydrogen (δD) isotopes of methane	39
2.4. Radiocarbon dating	39
Chapter 3. Sedimentology and mineral composition of mud volcano products and related sediments	41
Abstract	43
3.1. Introduction	44
3.2. Regional Setting	45
3.3. Sediment Recovery and Sampling	46
3.3.1. Sediment Recovery	46
3.3.2. Sampling	47

Hand-sized pieces	47
Hemipelagic sediments and mud breccia matrices	47
Methane derived authigenic (MDAC) concretion & chimney	47
3.4. Methods	47
3.5. Results	52
3.5.1. Hemipelagic sediments and mud breccias	52
3.5.2. Core lithologies	53
Kalinin MV	53
Perejil MV	53
Granada MV	53
Marrakech MV	53
Dhaka MV	53
Carmen MV	53
Mulhacen MV	54
Maya MV	54
3.5.3. Mineral composition	54
Hemipelagic drapes	54
Mud breccia	54
MDAC concretion & chimney	59
3.5.4. Dating	60
3.6. Discussion	60
3.6.1. On the activity of mud volcano from core recovering	60
3.6.2. On the nature and source of mud breccias	63
3.6.3. Role of clay dehydration on fluid flow	68
3.7. Conclusions	70
 Chapter 4. Major and trace elements in mud-volcano solid phases and involved sediments from the West Alboran Basin	 71
Abstract	73
4.1. Introduction	74
4.2. Geological background	74
4.3. Core sediment and sampling	75
4.4. Methods	76
4.5. Elemental ratios	77
4.6. Results	78
4.6.1. Geochemical composition	78
Hemipelagic drapes	78
Mud breccia	78
Methane derived authigenic carbonates (MDAC).	85
4.7. Discussion	85
4.7.1. Control of fluid venting in hemipelagic drapes	85
4.7.2. Geochemical constrains on the nature of mud breccias from the Alboran mud volcanoes	 86

4.7.3. Influence of fluid venting on sediment geochemistry	87
Paleo-tracer of SMZT and AOM occurrence	87
Current discharge and sources of MDAC related fluids	89
4.8. Conclusions	90
Chapter 5. Fluid venting and methane seep in active mud volcanoes from the Alboran Sea	93
Abstract	95
5.1. Introduction	96
5.2. Geological background and site description	96
5.2.1. Mud volcanism in the West Alboran Basin	97
Carmen mud volcano	98
5.3. Sampling and analytical procedures	99
5.3.1. Sediment sampling and core lithology	99
5.3.2. Pore waters and hydrocarbon gases	101
Gas extraction and analysis	101
Pore water extraction	101
Pore water analyses	102
Geo-thermometer calculations	103
5.4. Results	103
5.4.1. Fluid composition	103
Dissolved major and trace elements	103
Stable and radiogenic isotopes ($\delta^{13}\text{C}$, δD , $\delta^{18}\text{O}$ and $^{87}\text{Sr}/^{86}\text{Sr}$)	103
5.4.2. Methane isotopic composition	104
5.5. Discussion	105
5.5.1. Geochemical evidences of seawater intrusion	105
5.5.2. Relative rates of fluid venting activity	107
5.5.3. Potential associated processes	109
5.5.4. Deep-source signature for deep sediments	110
5.6. Conclusions	111
Chapter 6. Origin of lipid biomarkers in mud volcanoes from the Alboran Sea, western Mediterranean	113
Abstract	115
6.1. Introduction	116
6.2. Geological background	117
6.3. Materials and methods	118
6.3.1. Samples	118
6.3.2. Extraction and separation	118
6.3.3. Analysis and identification of lipid biomarkers	119
6.3.4. Methane and sulfate analyses	120
6.4. Results	121
6.4.1. Core lithologies	121

Perejil MV	121
Kalinin and Schneider's Heart MVs	121
6.4.2. Lipid biomarker distributions	121
6.4.3. Methane and sulphate	128
6.5. Discussion	128
6.5.1. Source of organic matter in mud breccia and hemipelagic sediments	128
6.5.2. Maturity of the organic matter	130
6.5.3. Probable source strata	130
6.5.4. Recent microbial activity	132
6.5.5. MV dynamics	132
6.6. Conclusions	135
 Chapter 7. Conclusions/Conclusiones	 137
 References	 143
 Appendix	 165
 Acknowledgments/Agradecimientos	 191
 <i>Curriculum Vitae</i>	 201

Abstract

In the westernmost Mediterranean, a broad field of mud volcanoes (MVs) and pockmarks occurs in the West Alboran Basin (WAB). These typical sea-floor structures can be found in the inner part of the Gibraltar Arc and occur above a major sedimentary depocenter encompassing early Miocene to Holocene sedimentary sequences, up to 7 km thick. In this region the development of mud volcanism is related to the presence of a large shale-diapiric province in the WAB. The shale-diapiric province underlying the MV fields is derived from deep overpressured units (undercompacted Miocene shales and olistostromes), which in turn overlie a metamorphic basement. MV occurrences are related to tectonic features (faults): they rise under Holocene tectonics, and grow atop diverse diapiric structures. Various studies have focused on the tectonic context and morphology of these mud volcanic edifices. Still, however, little is known about the nature and components of the extruded materials (solid and fluids phases).

This PhD thesis involves mineralogical, geochemical and biogeochemical investigations of mud-volcanic products and related sediments from some MVs and pockmarks of the Alboran Sea, named Perejil, Kalinin, Schneider's Heart, Carmen, Maya Dhaka, Marrakesh, Granada and Mulhacen, and also Crow's foot pockmark. The research is performed on gravity cores that comprised extruded materials' from the MVs (mud breccias) and associated hemipelagic sediment samples. A entailed multi-proxy approach including organic (lipid biomarkers) and inorganic (mineralogy, sedimentology and pore water geochemistry) determinations have been performed both on fluids and solid phases. This study provides important insights about the composition and provenance of the volcanic extruded material (mud breccia) and hemipelagic sediments involved also including biogeochemical results closely related with the discharge of hydrocarbon-rich fluids to the seafloor through MVs. It also pursues a better understanding of the origin of the extruded muds as well as of the mud volcanism in the WAB.

Hemipelagic facies draping mud volcanic structures exemplify mud volcanic activity. The existence of several interbedded intervals of hemipelagic sediments between mud breccias indicates the recurrence of volcanic pulses (episodes of mud extrusions), which result in discrete and successive emission of volcanic fluxes in the form of mud breccia intervals. Presence or absence of hemipelagic facies drapping mud edifices inform about the age of the mud volcanic events. Active edifices present a lack of hemipelagic drapes covering the last (uppermost) mud breccia interval. Only craters of Carmen and Perejil MVs lack hemipelagic drapes which indicate current or very recent mud flow and fluid eruptions as well as their current activity. This is supported by further evidence of most recent activity at these two MVs, such as gas bubbling or living chemosynthetic fauna. Thus, the occurrence of hemipelagic intervals intercalated with mud breccias points to successive episodes of volcanic activity resulting in mud flows that were draped by normal marine sediments.

Inactive MVs present well developed hemipelagic drapes that lay covering the MV deposits. The absence of detectable methane discharge and nonexistence of living chemosynthetic fauna at these MVs support their inactivity. These features are found at Kalinin, Maya, Dhaka, Marrakech, Granada and Mulhacen which are considered inactive.

The relative homogeneity in mineralogy and geochemistry of these sediment drapes, covering or interbedded with mud breccia intervals, indicates that they are generally not affected by the seepage venting. Radiocarbon dating of *Globigerina Bulloides* in hemipelagic intervals reveals the age of the older eruption occurred 10.8 Ka BP at Carmen whereas the most recent eruption happened 0.7 ka BP at Marrakech.

All extruded materials (mud breccia) from all studied MVs have similar bulk/clay mineral and geochemical composition (major and detrital element content; Al, Si, Mg, Rb, Th and REE ratios, $Al_2O_3+TiO_2 - SiO_2 - Fe_2O_3$, $MgO+CaO - SiO_2 - Al_2O_3+Fe_2O_3$ and PAAS-normalized REE patterns). These similarities indicate that mud breccia preserves the composition of the parental beds despite the eruptive processes during their ascent. Such widespread similarities, even among MVs located at distant sites along the WAB, reveal a common source-rock for the extruded mud breccias.

Materials expelled by MVs are rich in clay minerals, particularly in smectite and illite. The existence of illite-smectite-mixed layers (IS) extremely rich in illite (up to 95%) at all MVs shows that dehydration of clay minerals plays an essential role in the release of water, and confirms smectite to illite transformation at depth. The isotopic $\delta^{18}O$ and δD compositions of some pore waters likewise confirm that smectite dehydration is a fluid source mechanism that contributes to mud volcanic water freshening at the Alboran MVs. Water formation temperatures calculated through the application of empirical geo-thermometers (K-Na, K-Mg and K-Ca) reveal that fluids generate at temperatures up to 200 °C. This temperature is reached at 8 km depth, where the volcanic source is located (Unit VI and Unit Va), that form shale diapirs overlain MVs and endorses that these strata are within the oil window (i.e. under favorable diagenetic conditions for transformation of smectite to illite as well as hydrocarbon generation).

Pore waters signatures indicate that mud-volcanic waters derive from a deep source, and radiogenic isotopic ratio values ($^{87}Sr/^{86}Sr$) suggest the influence of cortical crust and sediments. This assumption is further supported by the n-alkane distribution and n-alkane-derived indices (CPI and ACL), in combination with the epimerization degree of hopanes [$22S/(22S+22R)$] found in several mud breccias. Particularly, the seawater-like composition of the pore fluids in the upper part of some mud breccia, together with the constant stable carbon isotopes of methane throughout this interval, would suggest that certain zones of the MVs may undergo downward advection of seawater after each episode of gas expulsion.

Most of the organic matter indicates it is mostly thermally immature and has an admixture of petroleum-derived compounds. Pore water composition of Carmen MV confirms a distinct $SO_4^{2-}-CH_4$ transition zone (SMT) coinciding with enhancement of HS^- concentrations, which suggests the methane oxidation is mediated under anaerobic conditions, with sulfate as the electron acceptor. Active anaerobic oxidation of methane (AOM) also occurs at Perejil MV, as supported by the presence of specific lipid biomarkers related to anaerobic methanotrophic (ANME) archaeas (irregular isoprenoids and DGDs), the low amounts of GDGTs, and the depleted carbon isotopic composition ($\delta^{13}C$) of crocetane/phytane. In this particular case, the presence of these lipid biomarkers specific for ANME- archaea furthermore reveals the dominance of anaerobic methanotrophs of the ANME-2 group over ANME-1.

Evidences of fossil AOM is corroborated at Crow's foot pockmark by the stable carbon isotopic composition of the methane-derived authigenic carbonate (MDAC) chimney and concretion encountered at this site. The enhancements of redox sensitive elements (Mo, S) as well as disseminated MDAC-enriched fronts (Sr/Ca, Mn/Ca) within mud breccias at dormant MVs also demonstrate that ancient pulses of methane occurred at these edifices, and served to constrain the mud volcanic activity in past times. Regarding the origin of the mud volcanic material expelled by the Alboran MVs, data conclude that the source-rocks feeding these structures is thought to be overpressured shales and megabreccias (rich in fluid) that constitute the lowermost and the second deepest units of the WAB infill (Unit VI and Unit Va; Early to Middle Miocene in age) which at same time generate de shale diapirism within the Mud Dipir Province (MDP) in the Alboran Sea.

Resumen

En el Mar de Alboran (Mediterráneo Occidental) existe un amplio campo de volcanes de lodo y pockmarks. Estas estructuras de escape de fluidos profundos al fondo marino se localizan en la Cuenca Oeste de Alboran (COA) que corresponde al mayor depocentro existente en la Cuenca del Mar de Alboran. En la COA la cobertera sedimentaria, alcanza potencias de hasta 7 km de espesor y contiene depósitos con edades comprendidas entre el Mioceno inferior y el Holoceno. La ubicación y el desarrollo del vulcanismo de lodo y pockmarks en la COA está relacionado con la presencia en profundidad de una extensa Provincia Diapirica de Lodo bajo el campo de volcanes, y con la actividad tectónica reciente o actual en la cuenca. Datos geofísicos y geológicos previos indican que los diapiros comportan facies sobrepresurizadas (arcillas verdes y olistostromas o megabrechas) pertenecientes a las unidades sísmo-estratigráficas Va y VI, de edad Mioceno inferior y medio, y que la posición de los volcanes de lodo está condicionada por estructuras tectónicas recientes.

Esta Tesis Doctoral aborda el estudio mineralógico, geoquímico y biogeoquímico de los productos volcánicos, y sedimentos relacionados con diversos volcanes de lodo existentes en el Mar de Alboran llamados Perejil, Kalinin, Schneider's Heart, Carmen, Maya, Dhaka, Marrakech, Granada y Mulhacen, y además del Crow's foot pockmark. Las investigaciones se han realizado en testigos de gravedad de esas estructuras volcánicas que recuperaron materiales extruidos por los volcanes (brechas de lodo) y sedimentos hemipelágicos asociados. Se han determinado e integrado diversos indicadores orgánicos (biomarcadores) e inorgánicos (mineralogía, sedimentología y geoquímica) en las fases sólidas extruidas (brechas de lodo), y la composición de sus fluidos intersticiales; asimismo, se han analizado (mineralogía, geoquímica y dataciones) los sedimentos pelágicos involucrados en los edificios volcánicos. Este trabajo aporta resultados importantes sobre la naturaleza del material extruido (brechas y fluidos) por los volcanes, incluyendo resultados biogeoquímicos estrechamente relacionados con la descarga volcánica al fondo marino de fluidos ricos en hidrocarburos. Además, se precisan el origen del material volcánico y los procesos determinables en los flujos extruidos, y se contribuye a conocer mejor la dinámica del vulcanismo de lodo en la COA.

Las facies pelágicas en los edificios volcánicos ilustran sobre la actividad volcánica. La existencia de varios intervalos de sedimentos hemipelágicos intercalados entre los de brechas de lodo indica que los eventos de actividad volcánica en la COA son múltiples, resultando en discretas y sucesivas efusiones de flujos volcánicos expresadas por los intervalos de brecha. La presencia o ausencia de facies hemipelágicas cubriendo las estructuras volcánicas determina la antigüedad de los episodios de extrusión del volcán. Los volcanes actualmente activos carecen de cobertera hemipelágica y las brechas volcánicas se exponen al fondo marino en sus cráteres. Únicamente los cráteres de los volcanes Carmen y Perejil carecen de cobertera hemipelágica, indicando así que estos dos volcanes son activos hoy día. Evidencias, tales como la presencia de fauna quimiosintética viva y el burbujeo de gases visible encontrados en los cráteres de esos dos volcanes corroboran su actividad volcánica actual. Los volcanes inactivos presentan sedimentos hemipelágicos bien desarrollados cubriendo los cráteres y diversas intercalaciones de sedimentos pelágicos entre intervalos de brecha. La ausencia de descargas de metano visible o de fauna quimiosintética viva confirma que esos volcanes son inactivos. Estas características las

presentan los volcanes Kalinin, Maya, Dhaka, Marrakesh, Granada y Mulhacen por lo que se consideran actualmente inactivos.

La relativa homogeneidad mineralógica y geoquímica que presentan las facies hemipelágicas, tanto si aparecen tapizando o intercaladas entre intervalos de brechas de lodo, indica que estos sedimentos se han visto poco afectados por la descarga de fluidos. Las dataciones de radiocarbono sobre foraminíferos planktónicos *Globigerina Bulloides* de los intervalos hemipelágicos han permitido saber que la erupción más antigua determinada en los testigos de gravedad estudiados tuvo lugar hace aproximadamente 10.8 Ka BP en el volcán Carmen y que la más reciente ocurrió hace unos 0.7 ka BP en el volcán Marrakech.

Los materiales extruidos (brechas de lodo) por todos los volcanes estudiados tienen composición mineralógica total, similar asociación de los minerales de las arcillas, y similar composición geoquímica (elementos mayores y detríticos; relaciones Al, Si, Mg, Rb, Th y REE, $Al_2O_3+TiO_2 - SiO_2 - Fe_2O_3$, $MgO+CaO - SiO_2 - Al_2O_3+Fe_2O_3$ y patrones de REE normalizados al PAAS). Estas similitudes sugieren, que en las brechas se preserva la composición de los materiales fuente del volcanismo de lodo, a pesar de los diferentes procesos que los flujos volcánicos pudieron sufrir en su ascenso. La similitud del material extruido por los distintos volcanes estudiados indica que los flujos extruidos tienen el mismo origen, a pesar de la lejanía entre los edificios volcánicos.

Los materiales que expulsaron los volcanes contienen una alta proporción de minerales arcillosos, particularmente esmectitas e illitas. Interestratificados de smectita/illita (IS), extremadamente ricos en capas de illita (hasta un 95%), se han identificado en todos los volcanes, revelando que la deshidratación de los minerales de la arcilla juega un papel fundamental en los procesos de generación de fluidos, a la vez que confirman las transformaciones esmectita-illita en profundidad. La composición isotópica $\delta^{18}O$ y δD de ciertos fluidos intersticiales indica que la deshidratación de las esmectitas afecta a la signatura geoquímica de los fluidos intersticiales de las brechas. La aplicación de geo-termómetros empíricos (K-Na, K-Mg y K-Ca) permite calcular las temperaturas de formación de esos fluidos e indica que se generaron en un rango de temperaturas que llega a los 200 °C. En la COA, esta temperatura se puede alcanzar a unos 8 km de profundidad. A esta profundidad se localizan los diapiros de lodo de la COA que consecuentemente se consideran la principal fuente del material volcánico estudiado. Este dato geotérmico sugiere que las Unidades sismo-estratigráficas VI y Va que conforman los diapiros de lodo infrayacentes a los volcanes se encuentran sometidos a procesos diagenéticos que favorecen tanto la transformación de esmectitas en illitas, como la generación de hidrocarburos.

La signatura geoquímica de los fluidos intersticiales en brechas también indica que los flujos volcánicos derivan de una fuente profunda, y los valores de isótopos radiogénicos ($^{87}Sr/^{86}Sr$) sugieren la influencia de una corteza continental subyacente. Esta hipótesis se confirma por la existencia de biomarcadores tales como los n-alkanos y los índices relacionados con n-alkanos (CPI y ACL), junto con los grados de epidermización de los hopanos [$22S/(22S+22R)$] en ciertos intervalos de brechas. Los fluidos intersticiales a techo de los intervalos de brecha tienen una signatura geoquímica parecida a la del agua marina, con valores constantes de isótopos estables de carbono, lo que indica que el agua marina percoló en los materiales extruidos tras cada episodio de actividad volcánica.

Resultados del estudio de biomarcadores indican que la materia orgánica presente en las brechas de lodo tiene unas características fundamentalmente inmaduras, y que presenta mezcla con compuestos derivados del petróleo. Los fluidos intersticiales del volcán Carmen determinan una zona de transición $\text{SO}_4^{2-}\text{-CH}_4$ que coincide con un incremento en la concentración de HS^- , lo que sugiere que la oxidación del metano ocurrió en condiciones anaeróbicas, con el sulfato como aceptor de electrones. El volcán Perejil presenta oxidación anaeróbica del metano (OAM), determinada por la presencia de ciertos biomarcadores lipídicos relacionados con arqueas anaeróbicas metanotróficas (ANME) (isoprenoides irregulares y DGDs, baja cantidad de GDGTs, e isótopos estables de carbono empobrecidos ($\delta^{13}\text{C}$) del compuesto crocetano/phytano). Además, la presencia de estos biomarcadores relacionados con arqueas-ANME revela que predominan los metanótrofos anaeróbicos del grupo ANME-2 sobre los del grupo ANME-1.

Evidencias de una OAM fósil se encuentran en el Crow's foot pockmark, y quedan reflejadas por la composición isotópica $\delta^{13}\text{C}$ de los carbonatos autigénicos derivados del metano (MDAC) analizados. En las brechas de los volcanes inactivos, el incremento de elementos sensibles a procesos de oxidación-reducción (Mo, S) así como la presencia de frentes ligeramente enriquecidos en MDAC (Sr/Ca, Ma/Ca) demuestra que en esos volcanes inactivos ocurrieron pulsos de metano en el pasado. Las concentraciones en metano y sulfato de los fluidos intersticiales en las brechas de los volcanes activos constatan que actualmente se están produciendo descargas de metano en el Mar de Alboran.

Respecto al origen del material volcánico extruido, se concluye que la fuente que nutre los volcanes de lodo de la COA corresponde a las arcillas y megabrechas sobrepresurizadas (subcompactadas) que forman las unidades basales del relleno sedimentario de la cuenca (Unidad VI y Unidad Va; de edad Mioceno inferior y medio), que a su vez generan el diapirismo de lodo de la Provincia Diapirica de Lodo del Mar de Alboran.

1

Introduction
& background

Chapter 1

Introduction and Background

1.1 Mud volcanoes: an overview

Mud volcanoes (MVs) constitute geological features through which overpressured clayed material and fluids are transported from deep sedimentary strata and expelled to the Earth's surface (Milkov, 2000; Dimitrov, 2002; Kopf, 2002a).

Their occurrence is known to be linked to hydrocarbon-rich fluids and seepage fields (Whelan et al., 2005; Mazzini et al., 2009a; Martinelli et al., 2012; Oppo et al., 2014, among others), and they located on land, where more than 900 terrestrial MVs are supposed to exist, or offshore, where the amount of mud edifices may significantly exceed the quantified number of these structures on land (Fig.1.1) (Milkov, 2000; Dimitrov, 2002; Mazurenko and Soloviev, 2003; Tinivella and Giustiniani, 2013).

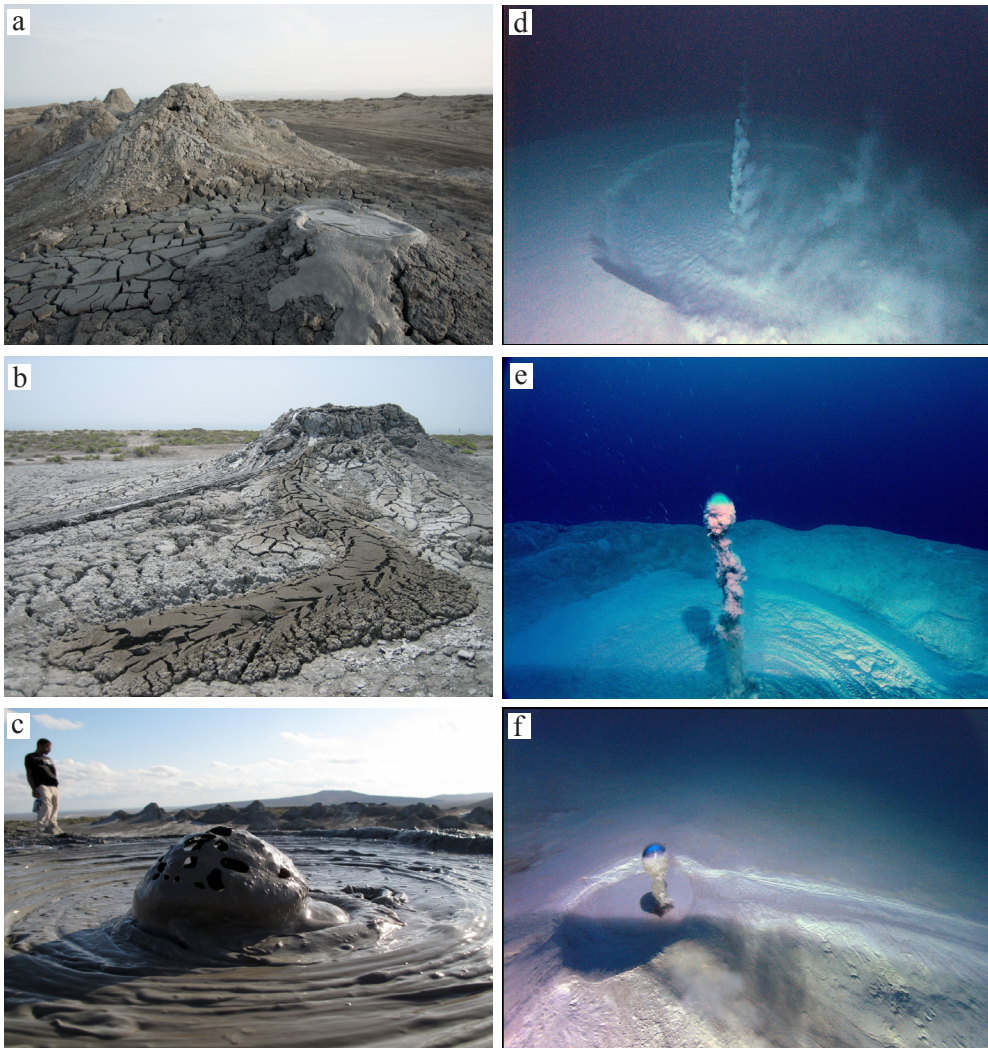


Figure 1.1. Examples of the main seeping features of MVs on land and off shore: a) MV field showing different mud-cones, b) mud-flows with desiccation cracks, c) active vent vigorously erupting water and gas-rich mud, d-f) submarine seepages showing the typical cone-shape and crater of a MV. Active venting is evidenced by gas bubbling to the water column. Source GFDL via Wikimedia Commons

In marine realms, MVs occur at different depths, from shallow to deep waters (from 500 to 5000 m deep). Exceptional examples have been described in areas such as the Black Sea, the Mediterranean Ridge, the Nankai Trough or the Barbados (Dimitrov, 2002). Since the 1970's, a large number of MVs has been discovered at seafloor due to the exploration of active fluid venting regions, supported by the rapid development in recent decades of underwater research technologies. Still, the total number of MVs remains uncertain and future research will no doubt engross the number of known MVs (Mazurenko and Soloviev, 2003; Martinelli and Panahi, 2005).

MVs are geological structures that expel large volumes of detrital material (rock and clast fragments), together with hydrocarbon-rich fluids (e.g. methane), subsequently representing "natural windows to the deep geosphere" (Fig. 1.1). This eruptive behavior provides key geological and geochemical information on the nature of deep sources feeding the MVs, and offers insights into the diagenetic processes operating at depth, such as the formation/dissociation of gas hydrates, mineral transformations, the degradation of organic matter and high pressure/temperature-reactions (Martin et al., 1996; Hensen et al., 2007; Liu et al., 2009; Li et al., 2014). In certain cases this information would be economically and technically more difficult to obtain by means of standard drilling operations.

The expelled materials are typically known as "mud breccia" (Cita et al., 1981). The solid phase of mud breccia is composed of a sedimentary mixture or *mélange* mainly deriving from the over-pressurized source strata, with a secondary incorporation of clastic material through the triggering of the overlying stratigraphic units as a consequence of the upward migration of mud-rich fluids (Akhmanov, 1996; Akhmanov and Woodside, 1998).

The existence of source strata having low density and pore-fluid overpressure favors mud fluid

ascension, piercing the sediments and giving rise to MV edifices at surface (Milkov, 2000; Dimitrov, 2002). The occurrence of MVs moreover depends on the regional setting.

To this regard, the mechanisms that may promote high pore-fluid overpressure are 1) recent tectonic activity, in particular compressional activity; 2) high sedimentation rates; 3) intense development of salt/shale diapirism; 4) the occurrence of diagenetic reactions such as clay mineral dehydration or destabilization of gas hydrates; 5) post-depositional transformation of organic matter leading to hydrocarbon generation; and 6) hydrothermal pressuring (Milkov, 2000; Brown et al., 2001; Dimitrov, 2002; Kopf, 2002a; Planke et al., 2003).

According to Milkov (2000), MVs most likely develop on top of seafloor-piercing shale diapirs (Fig. 1.2a), although in some cases diapirs are completely unrelated to MV generation (Fig. 1.2b). At times the diapir does not completely pierce the sediment cover and rises only to a level beneath the surface (Fig. 1.2b and c). Yet during diapir emplacement the fluidized mud can migrate further upward and reach the surface. Thus, the ascent of the semi-liquid and plastic material along faults and fractures is described as the most common mechanism for MV formation (Fig. 1.2d and e) and the expulsion of mud breccia with high fluid contents. The expelled material can be extremely rich in fluids (brine, gas, water), which may be the main phase of mud breccia or even the only material that migrates. In such situations, pockmarks and seepage related-structures are formed on the seafloor instead of mud volcanic edifices (Fig. 1.2f). MVs can be also connected to petroleum reservoirs where fluids are discharged to the seafloor through underwater cold-venting (Fig. 1.3). The worldwide distribution of hydrocarbon fluid venting, both on active and passive continental margins, is generally associated to gas hydrate accumulations (Fig. 1.4) (Milkov, 2000).

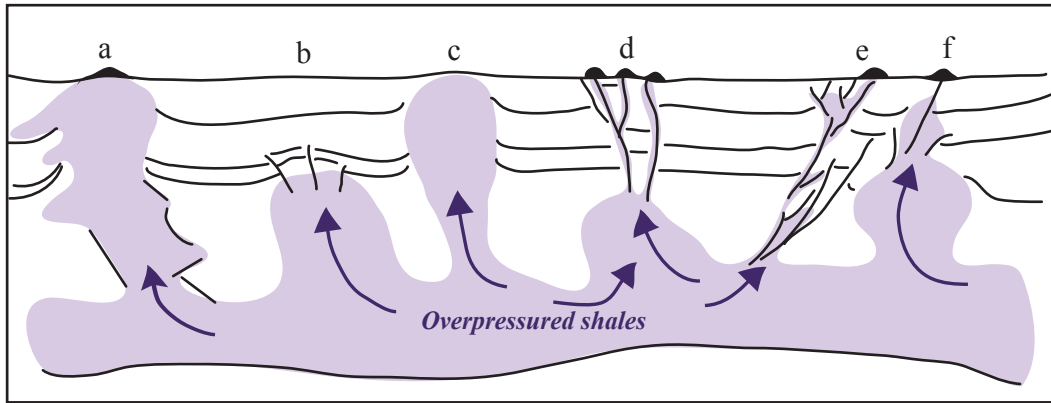


Figure 1.2. Scheme showing submarine MVs formed by a) MV formed on top of a sea-floor-piercing shale diapir; b) buried mud diapir; c) sea-floor-piercing shale diapir without MV; d-e) MVs formed by the rising of fluidized sediments along faults; f) sea-floor seepage. Arrows show the migration paths of fluids. Modified after Milkov, 2000

In light of the tectonic context, MVs can be linked to convergent plate settings and accretionary complexes, e.g. Barbados (Olu et al., 1997; Deville et al., 2006), the Nankai Trough (Kuramoto et al., 2001), Makran accretionary prism (von Rad et al., 2000), Eastern Mediterranean (Cita et al., 1994; Ivanov et al., 1996; Lykousis et al., 2004), the Gulf of Cadiz (Kenyon et al., 2000; Mascle et al., 2014) the Alboran Sea (Talukder et al., 2003;

Comas et al., 2010; Somoza et al., 2012); or passive continental margins, e.g. Niger Delta (Graue, 2000), the Black Sea (Ivanov et al., 1998; Mazzini, 2009b), the Caspian Sea (Ginsburg and Soloviev, 1994), the Barent Sea (Pape et al., 2011), the Nile deep-sea fan (Mascle et al., 2001), the Norwegian Sea (Vogt et al., 1999; Perez-Garcia et al., 2009) and the Gulf of Mexico (Sager et al., 2003).

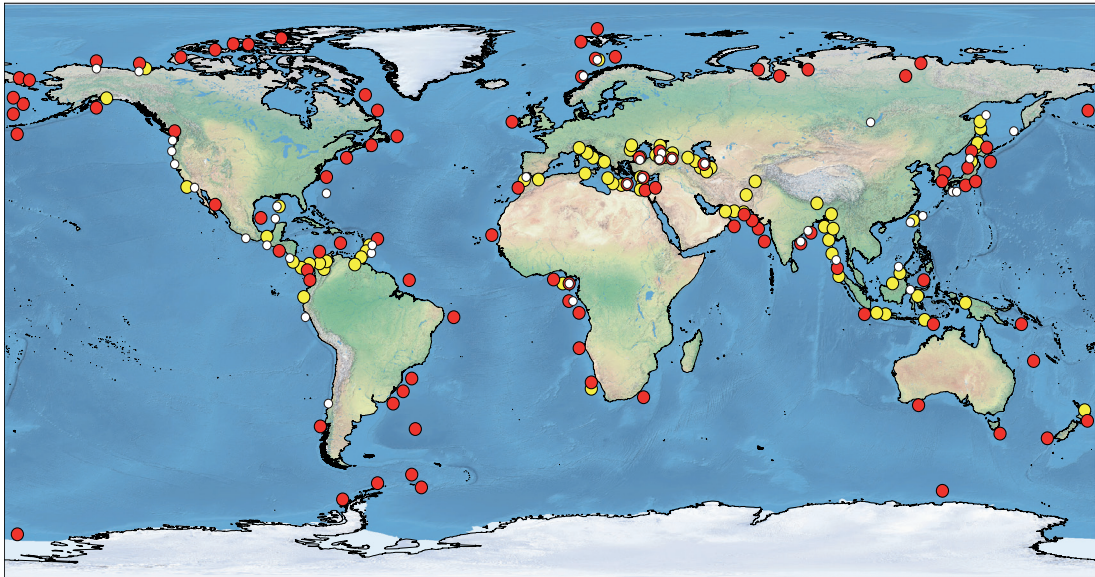


Figure 1.3. Topographic and bathymetric map showing the worldwide occurrence of MVs and natural gas hydrate deposits deduced from recovered gas hydrate samples and inferred gas hydrate occurrences, based on seismic evidence (bottom simulating reflector; BSR) and well logs. Yellow dots correspond with MVs, red dots mark places where the presence of gas hydrates is inferred from seismic or well logs, and white dots indicate recovered gas hydrate samples. Modified after Kholodov, 2002, Kopf, 2002 and Judd and Hovland, 2007.

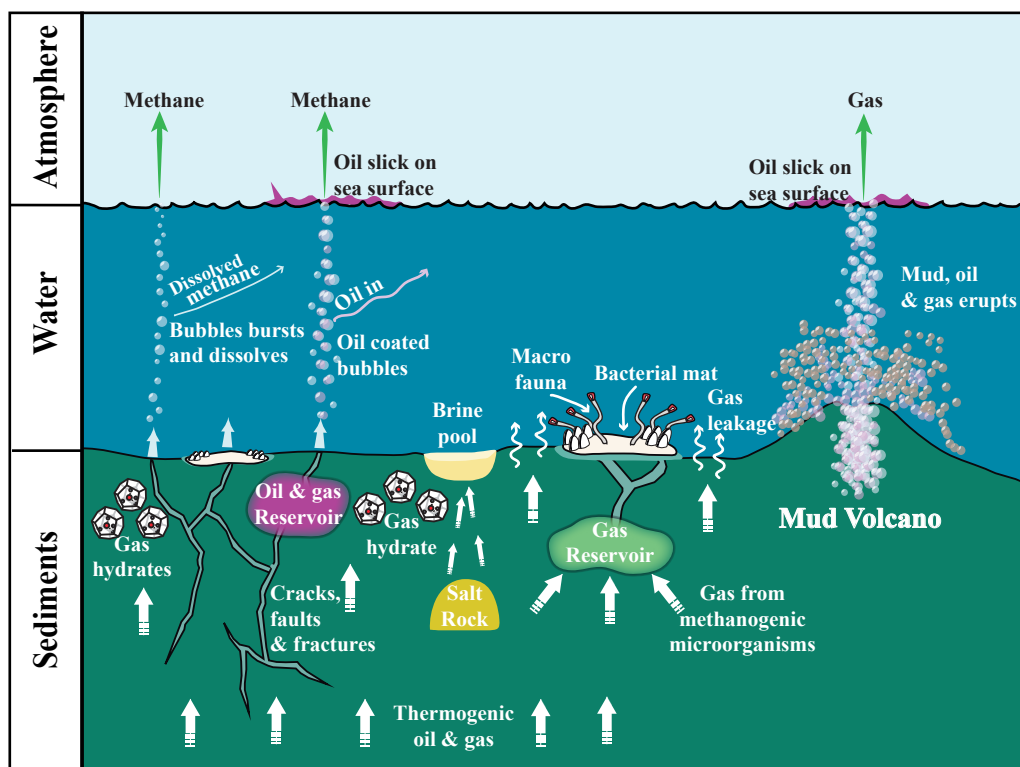
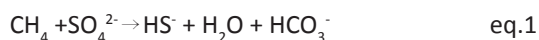


Figure 1.4. Scheme summarizing all processes related with gas seepage at marine seafloor. They include the generation of thermogenic oil and gas, and biogenic methane. Either source of gas can migrate upward rapidly through faults and fractures, or more slowly by diffusion within sediments to overlying oil and gas reservoirs. In either case, most of the gas transfer from the reservoir and migrates upward reaching the sediment-water interface where hydrocarbons can be deposited or vented to the water column. If methane concentration does not reach the saturation level, the gas is dissolved and largely biodegraded in the water column. In marine sediments where sufficient methane concentration is present, gas bubbles may form; if the methane flux is vigorous enough, they can reach the atmosphere. The bubbles are sometimes coated with oil. Chemosynthetic macro and micro-communities tend to develop on the surface of gas hydrates and within bacterial mats as they are fueled by these gas seeps. Modified after Whelan et al., 2005

1.2 Diagenetic processes associated with mud volcanism.

In marine sediments, methane decomposition is mediated by the biological process of anaerobic oxidation of methane (AOM) and is considered an important sink of methane in the Earth (Knittel and Boetius, 2009; Holler et al., 2011; Milucka et al., 2012; and references therein). AOM mainly takes place in oxygen-free sediments, within the topmost layers affected by sulfate penetration (Knittel et al., 2005; Knittel and Boetius, 2009; Reeburgh, 2007), and is regulated by a consortium of anaerobic methane oxidizer archaeas (ANMEs) together with sulfate-reducing bacteria (SRB)

(Boetius et al., 2000; Orphan et al., 2001a; Knittel et al., 2005; Niemann et al., 2006b; Lösekann et al., 2007; Pernthaler et al., 2008; Knittel and Boetius, 2009; Boetius and Wenzhöfer, 2013). During AOM (eq.1) more than 90% of methane is anaerobically consumed by microbes in the presence of sulfate (SO_4^{2-}) as the electron acceptor (Martens and Berner, 1974; Reeburgh, 1976; Barnes and Goldberg, 1976; Treude et al., 2003; Cui et al., 2015).



In marine sediments, the interval where AOM takes place is known as the sulfate-methane transition zone (SMTZ), where sulfate is nearly deple-

ted and methane concentration starts to dramatically increase. Hence, a distinctive concave-up shape of the methane concentration distribution and a reverse profile of sulfate concentration in depth are recognized, giving a typical intersection indicative of AOM occurrence (Fig. 1.5) (e.g., Reeburgh 1976, 1980; Boetius et al., 2000; Knittel and Boetius, 2009; Milucka et al., 2012). Such zones have a variable thickness, from a few centimeters to a few meters below the seafloor. Moreover, during active cold seeps the thickness of this zone can vary significantly. In some cases it extremely thin and pulled up to the seafloor or even appears very close to it.

Likewise, during AOM processes the consumption of dissolved sulfate in the pore waters affects the carbonate system (Fig 1.5; eq.1) and methane reactions produce bicarbonate (HCO_3^-), which can further react with dissolved calcium ions

(Ca^{2+}), and generate calcium carbonate (CaCO_3) precipitates. At the same time hydrogen sulphide (H_2S) is produced, serving as a source of energy for chemosynthetic communities, including symbiotic clams and tubeworms (Fig. 1.5).

In this sense, hydrocarbon seep venting also supports specific methane-dependent microbial communities. AOM is mediated by a putative consortium of methanotrophic archaea with sulfate reducing bacteria (SRB). This leads to an accumulation of biomass in methane seeps (Niemann, 2005; Elvert et al., 2000; Michaelis et al., 2002) while controlling, to some extent, the modern network of methane flux emissions to the atmosphere (Hinrichs and Boetius, 2002; Reeburgh, 2007; Cui et al., 2015).

The current classification of both methanotrophic archaea and sulfate-reducing bacteria involved in AOM processes was established through the

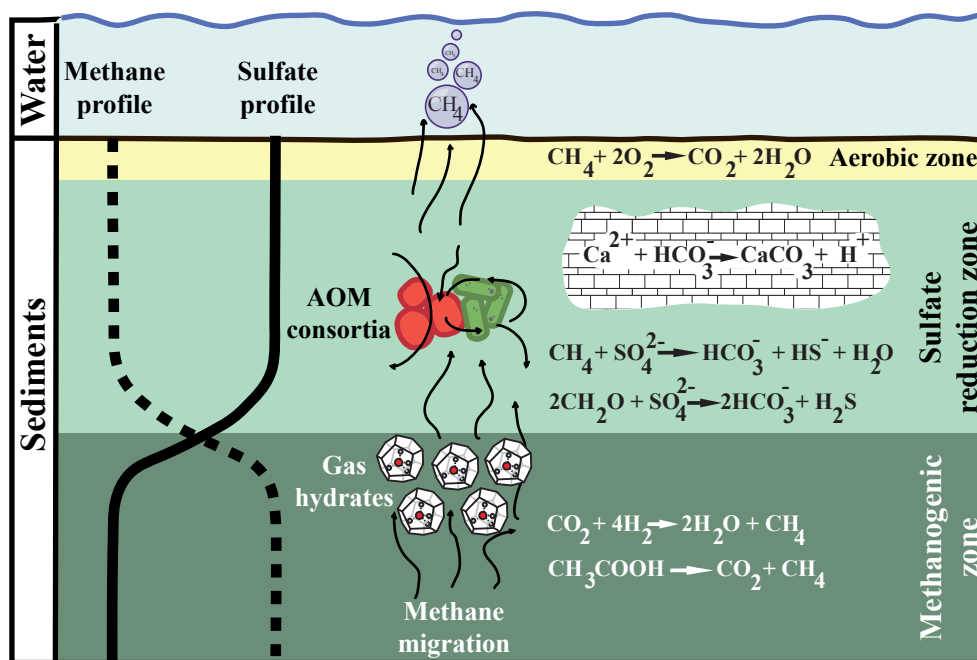


Figure 1.5. Scheme of the marine methane cycle showing depth distribution profiles of methane and sulfate concentrations in interstitial waters. The sulphate-methane transition zone (SMTZ) corresponds with the break of methane and sulfate profiles and represents the zone of maximum anaerobic oxidation of methane. Red and green balls signal methanotrophic archaeas and sulfate-reducing bacteria, respectively. Gridded zone denotes precipitation of methane-derived authigenic carbonates. Modified after Stadnitskaia, 2007a

phylogenetic analysis of 16S rDNA gene sequences (Hinrichs et al., 1999; Boetius et al., 2000; Orphan et al., 2001a, 2001b; Cui et al., 2015, and references therein). They revealed three distinct clusters of Euryarchaeota capable of mediating AOM, and namely Anaerobic MEthanotrophs (ANME-1, -2 and -3).

Whereas members of ANME-2 and ANME-3 archaeal clusters are respectively related to the cultured members of the methanogenic *Methanosarcinales* (Orphan et al., 2002b; Knittel et al., 2005; Niemann et al., 2006; Lösekann et al., 2007; Lazar et al., 2011) and to the cultivated genera *Methanococoides* spp., members of the ANME-1 cluster do not contain any culture relatives (Michaelis et al., 2002; Orphan et al., 2001a; Knittel et al., 2005). Specific lipid biomarkers and their stable carbon isotope signatures are widely used for the identification of ANME populations, as they serve as fingerprints and relative indicators of ANME biomasses (Schouten et al., 2012 and references therein) and consequently as reliable proxies for past-or-recent MV activity reconstructions.

MVs are also tied to particular marine ecosystems as a consequence of the upward migration of hydrocarbon rich-fluids (mainly methane). Once these fluids reach the seafloor, they induce the development of specific biological activity or chemosynthetic fauna (Sibuet and Olu, 1998; Boetius et al., 2000; Orphan et al., 2001a, 2001b; Vanreusel et al., 2009; Fischer et al., 2012), being rich in inorganic and organic compounds, hence sources of carbon, energy and nutrients for the methane-dependent macro-organisms. The production of benthic organisms such as mollusks, siboglinid tubeworms, microbial mats or even microbial chemosynthetic communities (i.e. archaeas and bacteria, as addressed above) would constitute direct bio-indicators of a recent release of methane-rich fluids to the subsurface, as well as the activity of MVs.

1.3 Environmental hazards and socio-economic importance of mud volcanism

Research into MVs holds great geological interest because these particular structures facilitate the outcropping of materials placed several kilometers in depth. Mud volcanism is also of relevance for economic issues and geo-hazard assessments, owing to their associations with hydrocarbon-oil, gas, and gas-hydrate fields (i.e. Azerbaijan, Gulf of Mexico, deep water Nigeria). Not to be underestimated are the effects that mud eruptions (i.e. submarine landscapes) may entail for human risk and environmental safeguarding.

In MVs, the upward migration of hydrocarbon-rich fluids can be linked to destabilization of gas hydrates. These are ice-like crystalline forms composed of water and low molecular weight gas (e.g. methane), trapped and hosted inside the “iced cage” (Ginsburg and Soloviev, 1997; Ivanov et al., 1998). They are stable under very specific ranges of pressure and temperature (Liu et al., 2013, and references therein), and any alteration of these conditions may lead to the destabilization of the methane hydrates. Thus, massive and episodic eruptions of MVs may contribute to a gas hydrate dissociation and discharge of mud fluids which, ultimately, might destabilize the seafloor. Gas hosted inside gas hydrates escapes within sediments, and volumes occupied by gas hydrates are replaced by water and sediment particles, which can generate an excess of pore pressure.

Mud volcanism may therefore play a noteworthy role in the degassing and dewatering processes of buried sediments (Dimitrov, 2002; Kopf et al., 2002a). The discharge of hydrocarbon-rich fluids during mud volcanic eruptions changes the landscape of the MV, as a consequence of the rapid expansion of trapped gasses followed by their gradual release, leading to significant disturbances of seafloor morphology (Feseker et al., 2014). This would also favor the generation of giant landslides and instabilities on the sediment

surface near the mud edifices. Accordingly, the hazardous implications of MVs are not limited to seafloor operations and infrastructures, as they represent a possible risk for humans and the environment.

Because MVs are particularly sensitive to external perturbations, they constitute ideal natural laboratories to test the effects of dynamic stress generated by remote seismic events. Systems of MVs are most often directly associated with active tectonic settings and aligned trending bands (i.e., Thyrrenian Sea; South Caspian Sea; the Gulf of Cadiz, among others) (Dimitrov, 2002; Huseynov and Guliyev, 2004; Manga and Brodsky, 2006; Gutscher et al., 2012; Lupi et al., 2014; Oppo et al., 2014; Rovere et al., 2014). Under instable conditions, a sudden tremor may provoke irregular and unexpected events of mud eruptions, reactivating dormant MVs. This could entail the shake-up of sediments, inducing instabilities of the ground floor or even the generation of landslides and faulting, which could affect the composition of deep fluids promoting a significant increase in gas release and gas hydrate dissociation. The catastrophic release of methane into the Earth's atmosphere may have noteworthy implications for global warming and climatic change. Methane is a significant greenhouse gas (Etiope and Klusman, 2002; Etiope, 2012) due to its availability to absorb and emit infrared radiation; its global warming potential is 20 times greater than that of carbon dioxide over a 100-year period. This signals MVs as natural sources of hydrocarbons, with a key role in the geochemical carbon cycle (Kopf and Deyhle, 2002) and, in turn, in the world greenhouse gas budget and its impact on the present and past global climate (Dickens et al., 1995; Dimitrov, 2002).

Such is the case of the Paleocene-Eocene Thermal Maximum (PETM; Dickens, 2001; Thomas et al., 2002; Zachos et al., 2008; McInerney and Wing, 2011, among others): an abrupt global warming along with oceanographic changes triggered by

a massive release of carbon altered the carbon cycle, climate, ocean chemistry, and marine and continental ecosystems. The resulting emission of free methane by gas hydrate destabilization to the oceans and atmosphere is considered as a potential source of carbon, and may contribute to global warming (McInerney and Wing, 2011).

Methane does not only occur in the form of gas hydrate, but also as free gas trapped in the deep-frozen permafrost. Methane deposits in permafrost and hydrates are particularly sensitive in expansive shallow-shelf regions, because under relatively low pressures a release of large amounts of methane is more likely to be promoted by minor temperature changes (Collett et al., 2011, and references therein).

In these regions the occurrence of MVs and other cold-seep venting features constitute direct indicators of the hydrocarbon content of the deeper sediments, hence of the petroleum potential of the area (e.g. Guliev and Feizullayev, 1996; Ivanov, et al., 1998; Kholodov, 2002; Stadnitskaia et al., 2008). This fact has generated extraordinary interest in the study of MVs, especially to understand their connection with petroliferous accumulations. The existence of hydrocarbon reservoirs beneath MVs— containing methane as well as other more complex organic compounds (e.g. wet gas, petroleum)— is primarily traced to their eruptive behavior and the discharge of hydrocarbon-rich mud flows and sediments to the surface. Still, the importance of the understanding of hydrocarbon gases (either thermogenic or of a microbial/biogenic nature) is primarily tied to their economic implications. There is a need for more accurate estimations of petroliferous potential in areas where cold seep and fluid venting discharge occurs. MVs understood as “natural free holes to the deep geosphere” heighten the interest of the scientific research community and of oil companies looking for reliable petroliferous insights to identify new natural reservoirs of hydrocarbons.

1.4 Regional Setting

The Alboran Sea is a marginal basin located in the westernmost Mediterranean Sea. Differences in structural architecture, sedimentary infill and seafloor morphology allow for discerning the western, eastern and southern Alboran Basins. The Alboran Sea Basin is a remnant of the Miocene back-arc basin from the Gibraltar Arc System (Fig. 1.6). This System comprises the Betics (Spain) and Rif (Morocco) orogenic arc, the Alboran and Algerian back-arc basins, and the forearc accretionary prism on the Atlantic side. Within the Gibraltar Arc System, the Alboran Basin evolved since the Late Oligocene in a geodynamic setting characterized by a pervasive north-south convergence between the Eurasian and African plates (Dewey et al., 1989).

Geological and geophysical data demonstrate that the Alboran Sea originated in the Early Miocene, and evolved first through extensional tectonics (from Middle to Upper Miocene), later undergoing significant contractive tectonics (from Late Miocene onwards). Post-Miocene contractive tectonics caused a major reorganization of the

basin, which resulted in prominent north-south shortening of the marine realm and uplifting and emersions of the surrounding Betics and Rif chains. The recent and actual active tectonics conditioned the present coastline as well as the current seafloor morphology (Comas et al., 1999, and references therein).

Basement and sedimentary cover beneath the Alboran Sea are known from commercial wells and ODP Leg 161 drilling. The thicker sedimentary depocenter is located in the West Alboran Basin, where more than 7 km of sediments lie atop the metamorphic basement (Fig. 1.7) (Jurado and Comas, 1992; Comas et al., 1996; Soto, et al., 1996).

The West Alboran Basin is characterized by the presence of extensive shale diapirism and shale tectonics determined by the existence of overpressured units at depth (Comas et al., 1999, 2012; Soto et al., 2010). The overpressure is limited to the basal units of the West Alboran Basin (Unit VI and Unit Va; Jurado and Comas, 1992; Fig. 1.7), as reported by logging data (sonic velocity, density and resistivity) from Andalucía-G1 and

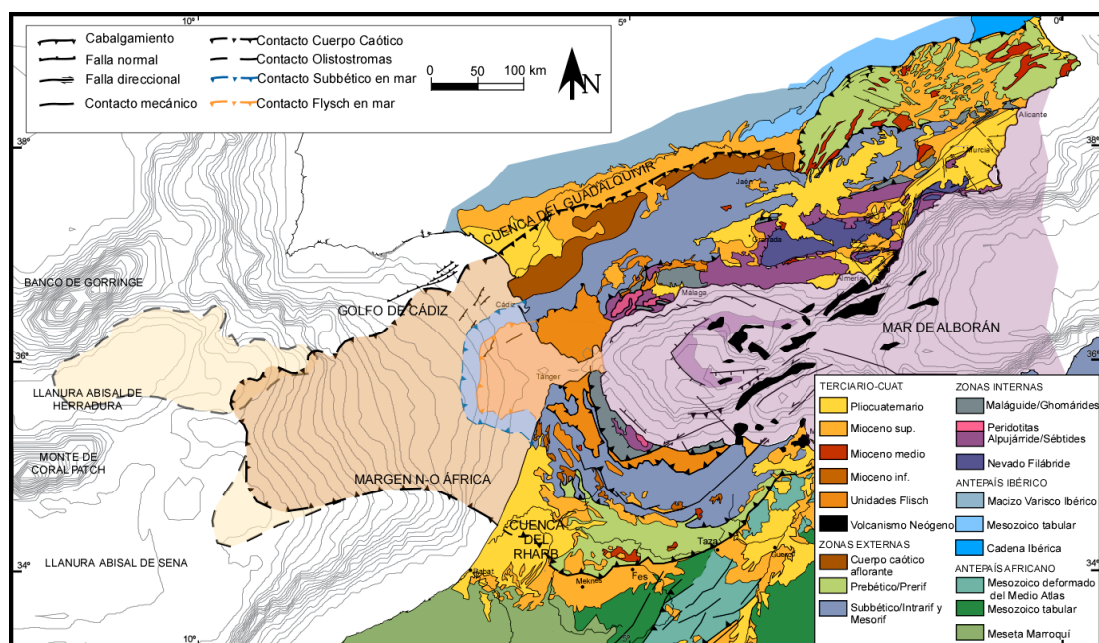


Figure 1.6. The Gibraltar Arc System (GAS). From Iribarren et al., 2009

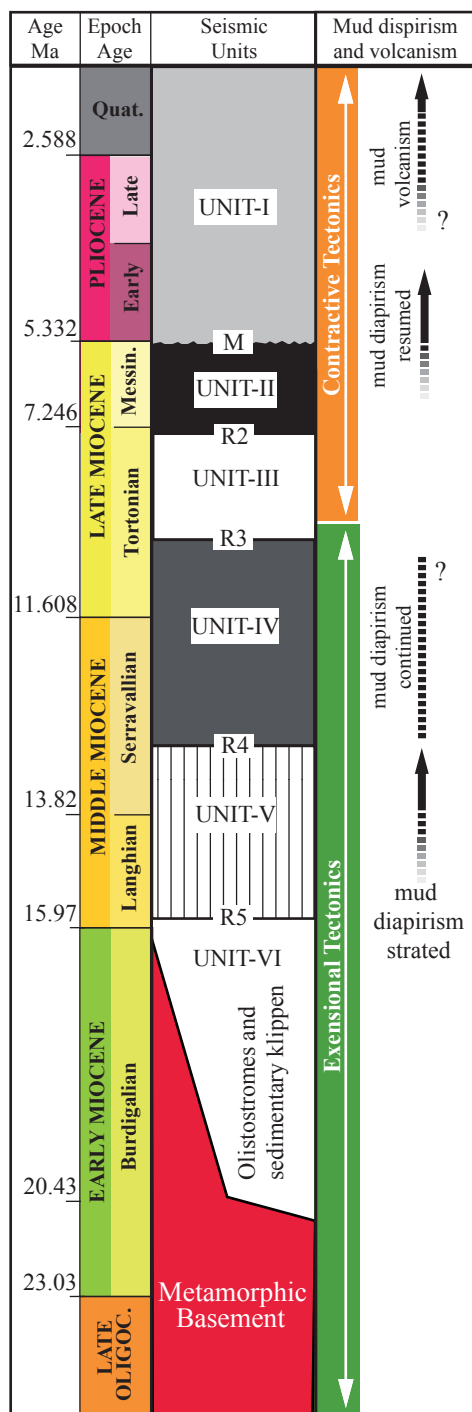


Figure 1.7. Tectonic evolution and main processes in the Alboran Sea basin related to seismo-stratigraphy infill ages. Note the position of Unit VI –comprising overpressured clay and olistostromes— and pulses and ages of mud diapirism in the framework of tectonic evolution. Modified from Comas et al., 1999

Alboran-A1 boreholes drilled in the West Alboran basin. Furthermore, borehole sampling indicates that Unit VI (Burdigalian in age) is made up of under-compacted (pressurized) olistostromic or brecciated materials containing heterogeneous rock fragments (blocks, boulders and clasts) of different ages embedded in a shale matrix intercalated with clay, marly and sandy intervals, while Unit Va (Langhian in age) also contains under-compacted green clays (Jurado and Comas, 1992; Díaz-Merino et al., 2003) (Fig. 1.7).

Mud volcanism and pockmarks occurring in the West Alboran Basin overlie the huge Mud Diapir Province that extends from the Iberian to the Moroccan margins (Fig. 1.8). As evidenced by previous work, the mud volcanism is linked to recent stages of shale diapirism taking place during compressive tectonics (Plio-Quaternary, from 4-5 Ma onwards), which conditioned pierced diapirs and led subsequently to mud volcanism at the seafloor (Comas et al., 2010, Soto et al., 2012 and references therein). Seismic profiles show that volcano-feeding channels are con-

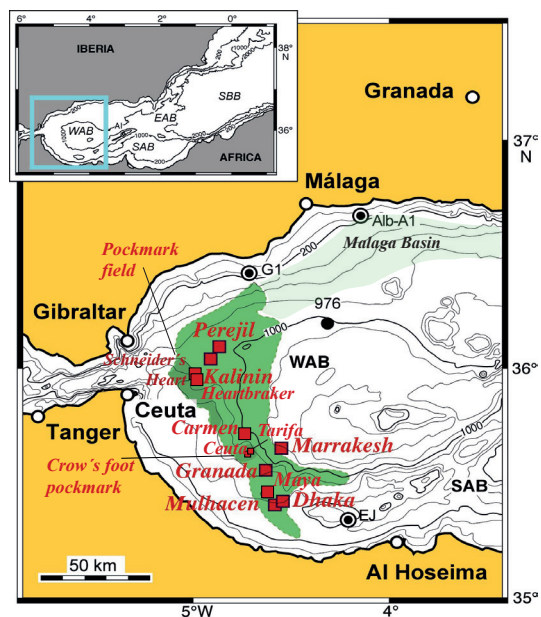


Figure 1.8. The Mud Diapir Province of the Alboran Sea showing position of the recorded MVs. WAB: West Alboran Basin; SAB. South Alboran Basin. Dark green: Mud Diapiric Province. Light green: Area occupied by Unit VI in the Malaga Basin

nected to deeper shale-diapir structures, evidencing that volcanic processes bring up to the seafloor overpressured shales and olistostromes from Unit VI (Fig. 1.7) lying at a depth of over 6 km (Talukder et al., 2003; Comas et al., 2012).

The extruded mud breccias contain exotic rocks from different sedimentary units embedded in minor-sized mud breccias (matrices) (Fig.1.9). Micropaleontological data from core sampling indicates that MVs can bring up to the seafloor sedimentary rocks ranging from the Late Cretaceous to the Late Miocene (Sautkin et al., 2003; Gennari et al., 2013). A deep thermogenic source of fluids expelled by the Alboran MVs has been suggested on the basis of $\delta^{13}\text{C}$ isotope determinations in authigenic carbonates, pore-water analyses, gas composition and lipid biomarkers (Blinova et al., 2011; López-Rodríguez et al., 2014). The abundance of chemosynthetic habitats (bivalves, tube worms) above some MVs indicates current methane/hydrocarbon seeping (Hilário et al., 2011). However, most of the Alboran MVs appear to be inactive, or dormant (Comas et al., 2010).



Figure 1.9. Fragments of exotic rocks and clasts from megabreccias from Units VI.

1.5 Motivation

Biogeochemical processes related to methane production are subjected to intensive research, since methane is an important greenhouse gas that plays a major role in the global carbon cycle. Hence, investigations of microbiological and

diagenetic processes in marine sediments involving methane production and emissions are crucial for our understanding of the carbon cycle. At the present time, innovative technologies for data acquisition as well as heightened scientific interest in this topic have led to a vast literature on methane emission into the atmosphere from marine sediments and on gas hydrates as a potential source of atmospheric methane. Special attention has been paid to estimations of the rates of microbial processes (sulfate reduction, methanogenesis, and methane oxidation) as well as the fluxes of biogenic methane from marine sediments to the water column and to the atmosphere. Seepage areas and MVs in particular are held to be hot spots for biogeochemical processes related to methane cycling. MVs also hold great interest because they represent unique geological structures. The widespread interest in MV investigation is further justified in that they are key settings for the study of Geosphere-Biosphere coupling processes and an exceptional natural laboratory to explore the interplay between tectonics, detrital sediments, authigenic mineral precipitation, deep fluids and the deep biosphere. Increasing site surveying and coring in seepage areas provides for a global picture of MV distribution, though the total number of submarine MVs is still uncertain and further investigations are clearly required.

The recent discovery, in the late nineties, of an MV province in the Western Alboran has added a new hotspot to the picture, with numerous MVs, pockmarks, authigenic carbonates and chemosynthetic fauna reportedly linked to fluids expelled from a overpressurized shale deep source. Although seepage and MV activity have been well documented in the nearby regions of Gulf of Cadiz and the Eastern Mediterranean, much less is known about MV dynamics in the Alboran sea basin. The UNESCO/IOC Training Through Research Program (e.g., Comas et al., 1999; Kenyon et al., 2000; Kenyon et al., 2006; Ivanov et

al., 2010) has significantly contributed to MV exploration in this region. Distribution of MVs, source rocks and tectonic processes have been previously addressed, whereas the nature of MV derived materials and processes related to deep fluid circulation are poorly understood (e.g., Comas et al., 1999; Talukder, 2003; Somoza et al., 2012).

Within this context, the present Thesis is intended to provide new insights into the reconstruction of MV dynamics (source and provenance of extruded mud breccia) and fluid venting in this tectonically active region by using a multiproxy approach that embraces two types of investigation of the fluid and solid phases: organic (lipid biomarkers) and inorganic (mineralogy, sediment and pore water geochemistry). All investigations were performed on finer part of mud breccias (matrix).

This will contribute substantial information to the body of knowledge surrounding biogeochemical processes related to hydrocarbon-rich fluid venting in this basin. It will likewise shed light on the significance of the West Alboran MV province in the context of the West Mediterranean Sea.

1.6 Objectives

The general aim of this Thesis is to improve the scientific understanding of mud volcanism occurring in the Alboran Sea basin. To achieve this, a general overview of the Alboran MVs is presented, based on the study of their expelled products (mud breccia and fluids) and hemipelagic marine sediments, leading to a characterization of the MV-related materials. This helps to elucidate the MV dynamics as well as to identify the diagenetic processes operating at these edifices. Within this context, the specific objectives of the Thesis are:

- To characterize and compare the volcano related materials of the Alboran MVs.
- To describe the nature of the expelled materials

(mud breccia matrices and fluids) as well as their origin and source. This entails evaluation of the organic matter of mud breccias and hemipelagic marine sediments.

- To understand the role of sediment-fluid interactions during diagenetic processes, and their association with hydrocarbon generation (i.e. methane, gas hydrates), clay mineral transformations (smectite-to-illite) or authigenic mineral precipitation (methane-derived authigenic carbonates; MDACs).
- To determine the current activity of the Alboran MVs, in order to distinguish the most active structures as well as the dormant ones, and document the occurrence of mud volcanic eruptions in past times.

1.7 Thesis Outline

Chapter 1 offers a general overview about mud volcanoes and their relationship with cold seepages and active methane seep venting worldwide. It presents an introduction as to the nature and scope of this research, describing the scientific problem and main objectives of the Thesis.

Chapter 2 provides a detailed data set and a specific description of the methodology used during the development of this research.

Chapter 3 relays a study of sedimentology and mineralogical composition, involving both the bulk and clay mineral assemblages of mud breccia matrices and hemipelagic sediments from the Alboran mud volcanoes. Mud volcanism timing is based on radiocarbon dating on the sedimentary covers overlying inactive volcanoes. A characterization of the solid materials and explanation about the source of the expelled mud breccias are provided, along with discussion of certain mineral transformations as the source of fluids.

Chapter 4 presents inorganic geochemical results of mud breccia matrices and hemipelagic sediments. The data reveal complementary information about the source of extruded materials. This

chapter provides new insights into diagenetic processes operating at the studied volcanoes, and into authigenic mineral formation; it also addresses the occurrence of anaerobic oxidation processes at present and in the past.

Chapter 5 focuses on the geochemical composition of the expelled fluids from Alboran mud volcanoes. In view of methane-related processes (e.g. anaerobic oxidation of methane) and volcano dynamics, the nature and origin of the expelled fluids are discussed, and the occurrence of secondary processes possibly affecting the geochemical signature of fluids is debated.

Chapter 6 describes the study of lipid biomarkers performed on mud breccia matrices and hemipelagic sediments upholstering the mud volcanoes. In addition to new insights about source strata feeding the Alboran MVs, the nature of the organic matter and the hydrocarbon contents, this Chapter offers tentative interpretations about the ANME communities operating in these MVs.

Chapter 7 gives summarized conclusions regarding the dynamics of Alboran mud volcanism, expounding the nature and provenance of the expelled mud breccias as well as the occurrence of biogeochemical and diagenetic processes closely related to hydrocarbon discharge to the Alboran seafloor.



2



Data
& Methodology

Chapter 2

Data and Methodology

2.1 Geophysical survey and data

2.1.1 Oceanographic cruises and core locations

The data and materials used for this study were collected during several oceanographic cruises (Fig. 2.1):

- UNESCO/IOC Training Through Research (TTR) cruises, on board RV Professor Logachev (St. Petersburg, Russia): TTR-9 BASACALB Cruise in 1999 (Kenyon et al., 2000), TTR-12 Leg 3, MARSIBAL-1 Cruise in 2002 (Kenyon et al., 2003) and TTR-17 Leg 1 cruise SAGAS-08 in 2008 (Ivanov et al., 2010).
- Ristretto & Lungo M83-3 cruise on board RV Meteor (Hamburg, Germany) in 2010/2011.
- GASALB-Pelagia cruise on board RV Pelagia (NIOZ, Texel, The Netherlands) in 2011.

Geophysical data considered in this work come from the UNESCO/IOC Training Through Research (TTR) program cruises, in particular from TTR-12 (MARSIBAL-1 Cruise 2002; Kenyon et al., 2003) and TTR-17 (SAGAS-08 Cruise 2008; Ivanov et al., 2010). Additionally, geophysical data were acquired from the GASALB-Pelagia cruise (2011).

During the TTR-Cruises the positioning was acquired by the combination of GPS and GLO-NASS satellite configurations, achieving up to 60% greater satellite availability. Positioning had an accuracy of +/- 35 cm (75 cm at 95% confidence limits), whereas realistic positioning accuracy under normal satellite configuration for European waters is assumed as ca. 5 m. Precise back navigation was ensured by the location of the GPS+GLONASS receiver on the central part of the vessel, with accurate leveling of sampling and equipment deployment positions. The combination of the two systems permitted us to acquire the desirable precision in position determination, as well as the necessary yaw corrections to

be used by the multibeam systems and sampling operations (Kenyon et al., 2003).

During the GASALB cruise positioning was determined by a differential GPS system, and the data from the GPS receiver and gyro compass were recorded by an underway data logging system. An additional Sea path dual antenna GPS receiver determined the direction. The speed above ground and course over ground were determined from the GPS positions for successive one minute periods. After removal of occasional spikes, the data were smoothed with a 5 min running mean and sub-samples every 5 minutes.

The selected core materials analyzed came from twenty-one different sites, at nine mud volcanoes (Perejil, Kalinin, Schneider's Heart, Carmen, Granada, Marrakech, Maya, Dhaka, Mulhacen) and the "Crow's foot" pockmark (Fig. 2.2). Among them, fifteen are gravity cores, three are piston cores and three are box-cores (Fig. 2.3; Table 2.1). Sediment cores were retrieved at the top or flank of the MV edifices. More cores were taken from the most active structures; from dormant or inactive edifices only one single core was selected. Moreover, one core was recovered from the mud volcanic province as a reference site. This provided a continuous sedimentary archive to compare MV materials and distinguish "normal" pelagic sediments within the basin.

2.1.2 Seismic images

High-resolution seismic profiles, acoustic profiles and side scan sonar images used in this study encompass the purpose of illustrating the location where the studied sediment and fluids were recovered.

The acquisition system for the high-resolution seismic profiles consisted of a long streamer with one single air-gun of 3 l as the energy source at a pressure of 12 MPa. The air-guns were towed at a depth of 2-2.5 m and fired every 10 seconds. The streamer consisted of one active section 30 m

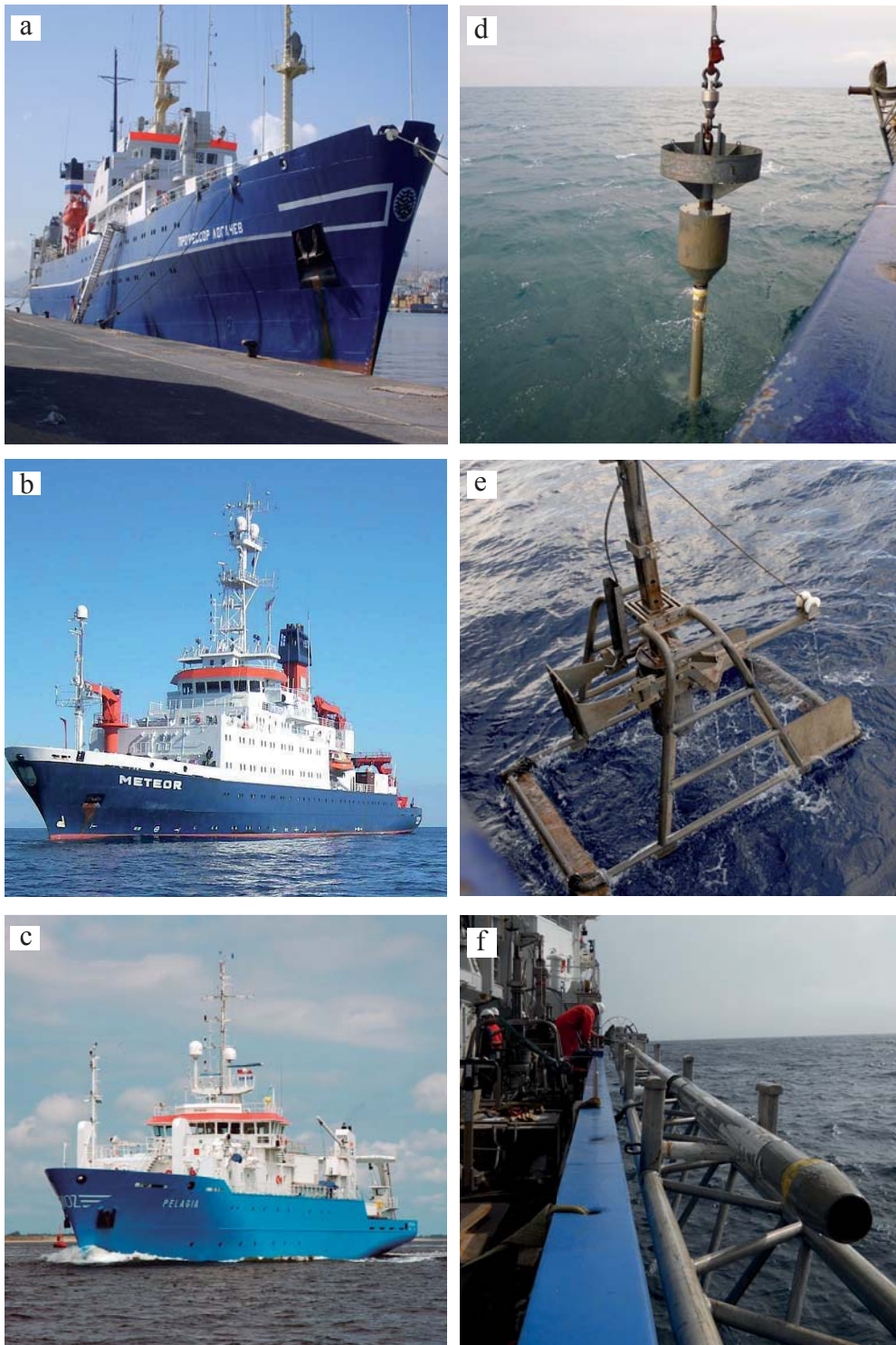


Figure 2.1. Oceanographic cruise research vessels: a) RV Professor Logachev (St. Petersburg, Russia), b) RV Meteor (Hamburg, Germany), c) RV Pelagia (NIOZ, Texel, The Netherlands); and bottom sampling techniques: d) gravity corer, e) box-corer, f) piston corer

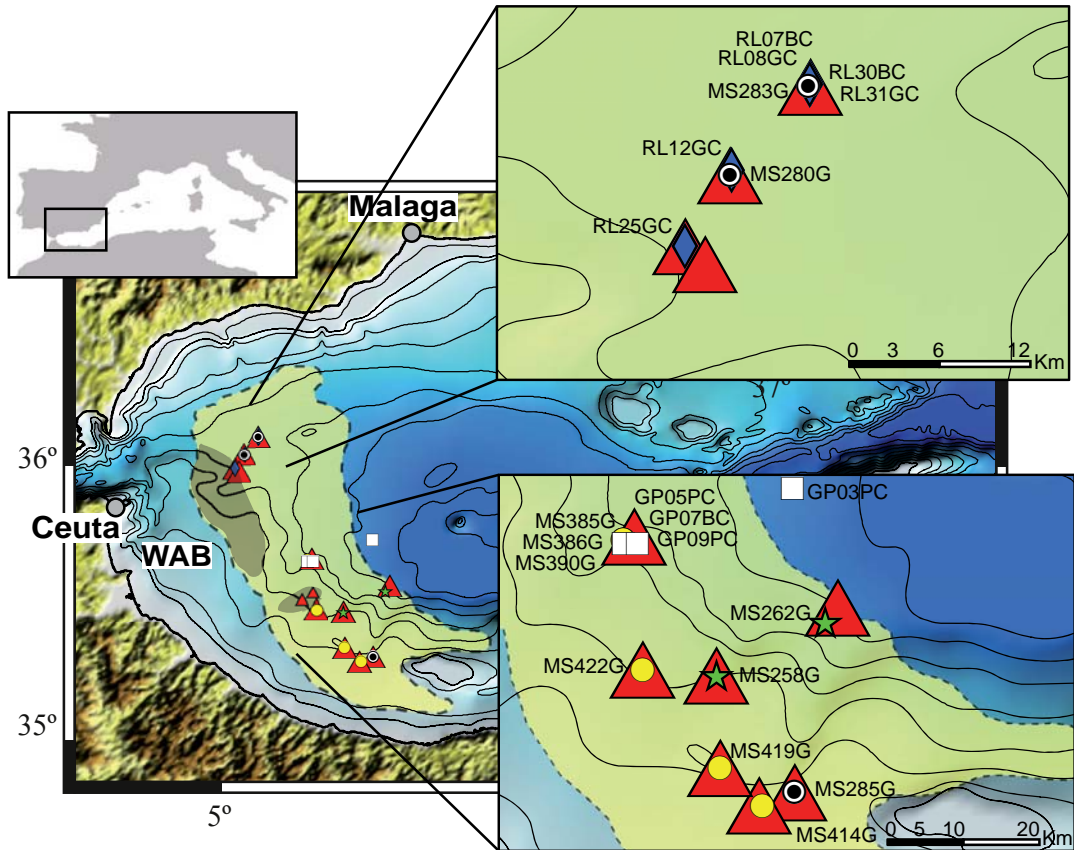


Figure 2.2. Location of the Alboran Sea showing the position of MVs and pockmark fields. Bathymetry contours are in meters, contour interval is 200 m. Red triangles represent mud edifices (mud volcano or pockmark). Green stars correspond to TTR-9 cruise cores, white-black filled dots to TTR-12 cruise cores, yellow dots to TTR-17 cruise cores, blue diamonds to Ristreto & Lungo cruise cores, and white squares to GASALB-Pelagia cruise cores

long, with 50 hydrophones, towed at a depth of approximately 2.5-3 m. The offset between the seismic source and the center of the live hydrophone array was 135 m. High resolution seismic data were preliminary processed with RadExPro software, then filtered analogically to 250 Hz.

High-resolution side scan sonar images of MVs were acquired using the MAK-1 deep-towed hydroacoustic system (30-100 kHz); concurring acoustic profiles were also recorded by a sub-bottom penetrating echosounder (5 kHz) and reported variable resolution of approximately 7 to 1 (Fig. 2.4). Swath bathymetry images were acquired from multibeam SIMRAD systems.

2.1.3. Morphology of the seafloor

Along the West Alboran Basin several structures associated with mud fluid discharge have been documented in a wide area known as the Mud Volcanic Province (Kenyon et al., 2000, 2003; Comas et al., 2010; Ivanov et al., 2010). MVs occur at relatively shallow depths, between 350 and 1100 m water depth (Table 2.1). Variable shapes have been recognized, mainly being circular (e.g. Carmen) or elliptical (e.g. Marrakech) (Fig. 2.5). They also build up as dome-like edifices or even as collapsed structures (e.g. Perejil and Kalinin; Fig. 2.6). MVs usually appear as isolated mounds (e.g. Carmen) or grouped in small clusters (e.g. Mulhacen). They range between 120 and 1630 m in diameter and reach heights

Table 2.1. Site identification, location, water depth, recovery and section lengths of the core used for this study

Core Code	Cruise	Structure	Latitude	Longitude	Sampling Site	Water Depth (m)	Core Recovery (cm)	Section Length (cm)
MS258G	TTR-9	Granada MV	35° 33.719' N	04° 37.398' W	Crater	583.0	144.0	60
MS262G	TTR-9	Marrakech MV	35° 37.509' N	04° 29.663' W	Crater	1086.0	210.0	60
MS280G	TTR-12	Kalinin MV	36° 02.828' N	04° 55.973' W	Crater	908.0	334.0	60
MS283G	TTR-12	Perejil MV	36° 06.018' N	04° 53.158' W	Crater	841.0	233.0	60
MS285G	TTR-12	Dhaka MV	35° 25.398' N	04° 31.853' W	Crater	360.0	244.0	60
MS385G	TTR-17	Carmen MV	35° 43.306' N	04° 44.060' W	Flank	806.0	258.0	60
MS386G	TTR-17	Carmen MV	35° 43.309' N	04° 44.008' W	Crater	809.0	259.0	60
MS390G	TTR-17	Carmen MV	35° 43.306' N	04° 44.017' W	Crater	806.0	480.0	60
MS414G	TTR-17	Mulhacen MV	35° 24.426' N	04° 34.126' W	Crater	365.0	96.0	60
MS419G	TTR-17	Maya MV	35° 27.114' N	04° 37.138' W	Flank	410.0	167.0	60
MS422G	TTR-17	Crow's foot pockmark	35° 34.120' N	04° 42.667' W	Flank	572.0	60.0	60
RL07BC	R & L	Perejil MV	36° 6.110' N	04° 53.080' W	Flank	818.9	40.0	40
RL08GC	R & L	Perejil MV	36° 6.110' N	04° 53.080' W	Flank	822.4	262.5	30
RL30BC	R & L	Perejil MV	36° 6.070' N	04° 53.110' W	Crater	807.8	30.0	40
RL31GC	R & L	Perejil MV	36° 6.070' N	04° 53.110' W	Crater	807.8	270.5	30
RL12GC	R & L	Kalinin MV	36° 3.000' N	04° 55.900' W	Flank	872.6	280.0	30
RL25GC	R & L	Schneider's Heart MV	36° 0.280' N	04° 57.570' W	Flank	924.0	310.0	30
GP03PC	G.P.	Reference Site	35° 47.261' N	04° 32.089' W	Hemipelagic	1306.0	950.0	50
GP05PC	G.P.	Carmen MV	35° 43.333' N	04° 44.046' W	Crater	795.0	820.0	30
GP07BC	G.P.	Carmen MV	35° 43.319' N	04° 44.050' W	Crater	795.0	35.0	40
GP09PC	G.P.	Carmen MV	35° 43.332' N	04° 43.975' W	Crater	795.0	260.0	30

of 35 to 185 m (Table 2.2). Flanks can vary from steep (~ 12°, e.g. Mulhacen) to smooth slopes (~ 2°, e.g. base of Perejil). MV cones appear bounded by concentric echelons that look like narrow rings or moats and reach depths of 15 m (e.g. Mulhacen). Elongated mud flows have also been documented flanking the mud volcanoes, most often covered by hemipelagic sediments. Their longitude is variable and they occasionally

extend up to 2000 m length.

Within the MV province, some semi-circular depressions or pockmarks were observed. They appeared either as individual features or clustered in systems of pockmarks, e.g. the Crow's foot pockmark field (Blinova et al., 2011; Ivanov et al., 2010).

Another interesting feature of the seafloor that appears closely related to MVs is the occurrence

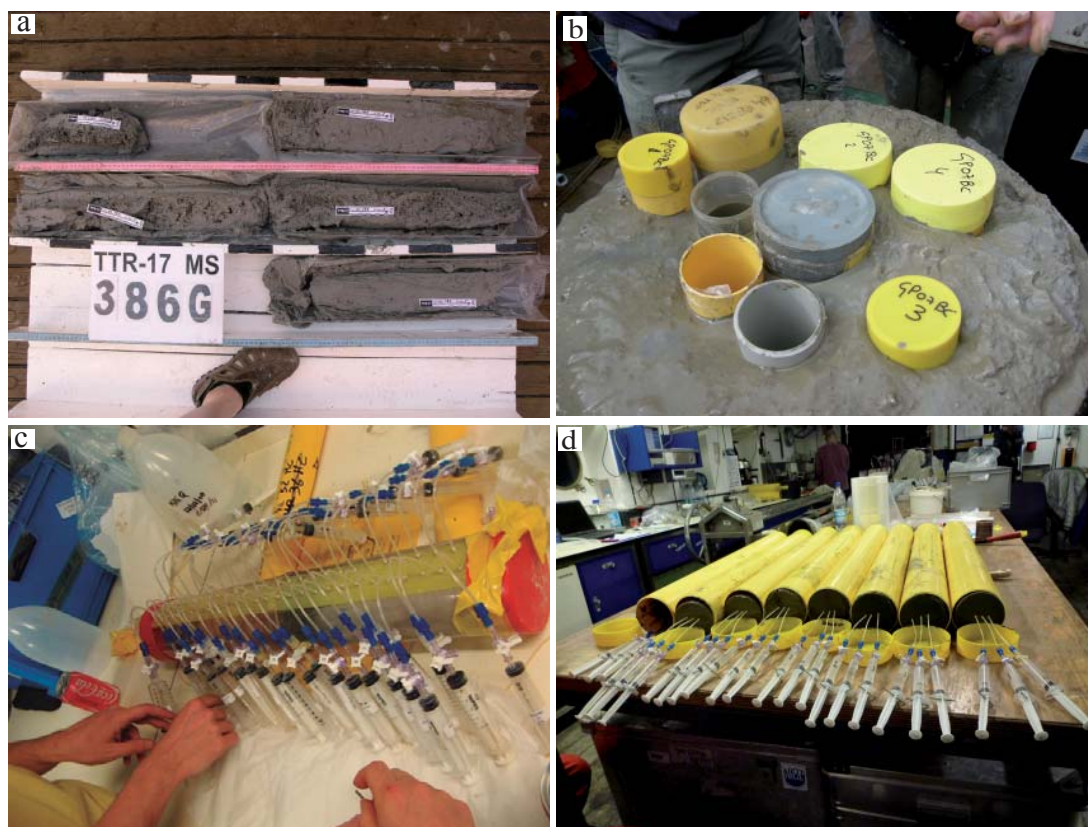


Figure 2.3. a) Half-split sections showing sediments recovered by gravity and piston corers, b) liner tubes inserted on sediments recovered by box-corer, c) box-core drilled liner for high-resolution pore-water extractions with rhizons, and d) tops of gravity core sections showing pore water extraction with rhizons

of cold water corals (CWC). They grow in the topmost part of MVs, leading to the development of a CWC fragment-rich unit underneath a hemipelagic sediment cover, as is the case of Dhaka and Maya MVs (Margreth et al., 2011).

Sediments and materials cored at the Alboran MVs belonged to two main lithofacies: hemipelagic marine sediments and mud breccias (Fig. 2.7). Differences in sediment texture (mostly in mud breccias) were recorded between sites.

The gravity cores were cut into 30 or 60 cm sections, whereas the piston cores were cut into 30 or 50 cm sections before opening (Table 2.1). All of them were split longitudinally into two halves, one used as the working half and one for the archive. The working halves were described with particular detail to changes in lithology, color and

sedimentary structures. Part of the core sections were packed and stored at 2-4°C in the cold camera at the Andalusian Earth Sciences Institute (CSIC-University of Granada, Spain). In the case of materials used for organic determinations, the core sections were sub-sampled on board in a +4°C container as soon as possible after recovery. Afterwards, these cores and samples were stored and transported at -20°C to the Royal Netherlands Institute for Sea Research (NIOZ, The Netherlands).

Once on land, the working halves were carefully cleaned and photographed. The strategy of sub-sampling was determined ad hoc, in view of the type of analysis involved. The sampling interval was established depending on the type of sediment (hemipelagic marls or mud breccia) and

Table 2.2. Morphological parameters and shapes of the studied MVs

Mud Volcano	Shape	Base Diameter (m)	Maximum Elevation (m)	Slopes (°)
Granada	circular dome	1630	185	10
Marrakech	elongated dome	650x470	40	7-9
Kalinin	circular collapse	820	36	4-25
Perejil	circular dome	1200	82	2-7
Dhaka	asymmetrical dome	700	63	7-8
Carmen	circular dome	1130	70	7-12
Mulhacen	asymmetrical dome	700x500	50	8-12
Maya	elongate dome	120x70	-	-
Schneider's Heart	asymmetrical collapse	-	-	-

the analysis to be carried out. High-resolution sampling was done every 2 cm from hemipelagic layers and from their limits with breccias (above and below the sedimentary boundary). Mud breccias were sampled every 2, 5, or 10 cm, according to the textural features.

Box-cores were sub-sampled using pvc tubes c.a. 50 cm long, pushed vertically into the sediment. The sampling tubes were split lengthwise and lithologically described as well as sampled every 2 and 5 cm, taking into consideration lithological variations.

Pore water extraction was performed directly after core recovery, at $\pm 14^{\circ}\text{C}$, using either cut-off syringes with subsequent centrifugation and/or Rhizons (for details see *Chapter 5*).

2.2 Sedimentological and mineralogical analyses

A total of 35 hand-sized pieces of mud breccia matrices were air-dried over a flat surface. The pieces were then carefully polished in a Struers Planopol to obtain a shiny side. To obtain a visual estimation of mud breccia matrices and clasts,

eight thin sections were prepared from these air-dried pieces, performing standard petrographic description and photography.

Mineral composition was determined in 135 samples of hemipelagic sediments and 361 samples of mud breccias. Bulk and clay mineral content were obtained by X-ray diffraction (XRD). This semi-quantitative analysis aims to show changes or gradients in mineral abundances rather than absolute values. For bulk mineralogy, samples were air-dried and ground in a mechanical mortar. Separation of the clay fraction and preparation of the samples for XRD were performed following the international recommendations compiled by Kirsch (1991). X-ray diffractograms were obtained using a Panalytical diffractometer with $\text{Cu-K}\alpha$ radiation and an automatic slit. Scans were run from $4-70^{\circ} 2\theta$ for bulk-sample diffractograms and untreated clay preparations, and from $3-30^{\circ} 2\theta$ for glycolated clay-fraction samples. Resulting diffractograms were interpreted using X Powder 12 software (Martin, 2004 .www.xpowder.com). Peak areas were measured in order to estimate semi-quantitative mineral content. The clay mineral

proportions were estimated from the glycolated diffractograms (estimated semi-quantitative analysis error of 5% for bulk mineral content and 5-10% for clay minerals). Morphological data on two hemipelagic sediment samples and 27 mud breccia matrix samples were obtained by Field Emission Scanning Electron Microscopy (SEM) analyses conducted with a LEO (Carl Zeiss) GEMINI-1530 at the Analytical Facilities of the University of Granada (CIC, *Centro de Instrumentacion Cientifica*, Universidad de Granada). An Energy Dis-

persive X-Ray microanalysis system (EDAX) was used to check the mineralogical composition of selected mineral grains (e.g. clays, pyrite and barite). Determinations of the structural formula of smectites on 23 samples of mud breccia were obtained by Transmission and Analytical Electron Microscopy (TEM-AEM). TEM-AEM analyses were performed on diverse samples deposited on a Cu grid. Individual mineral particles were chemically analyzed in situ by means of Energy Dispersive X-ray fluorescence (EDX).

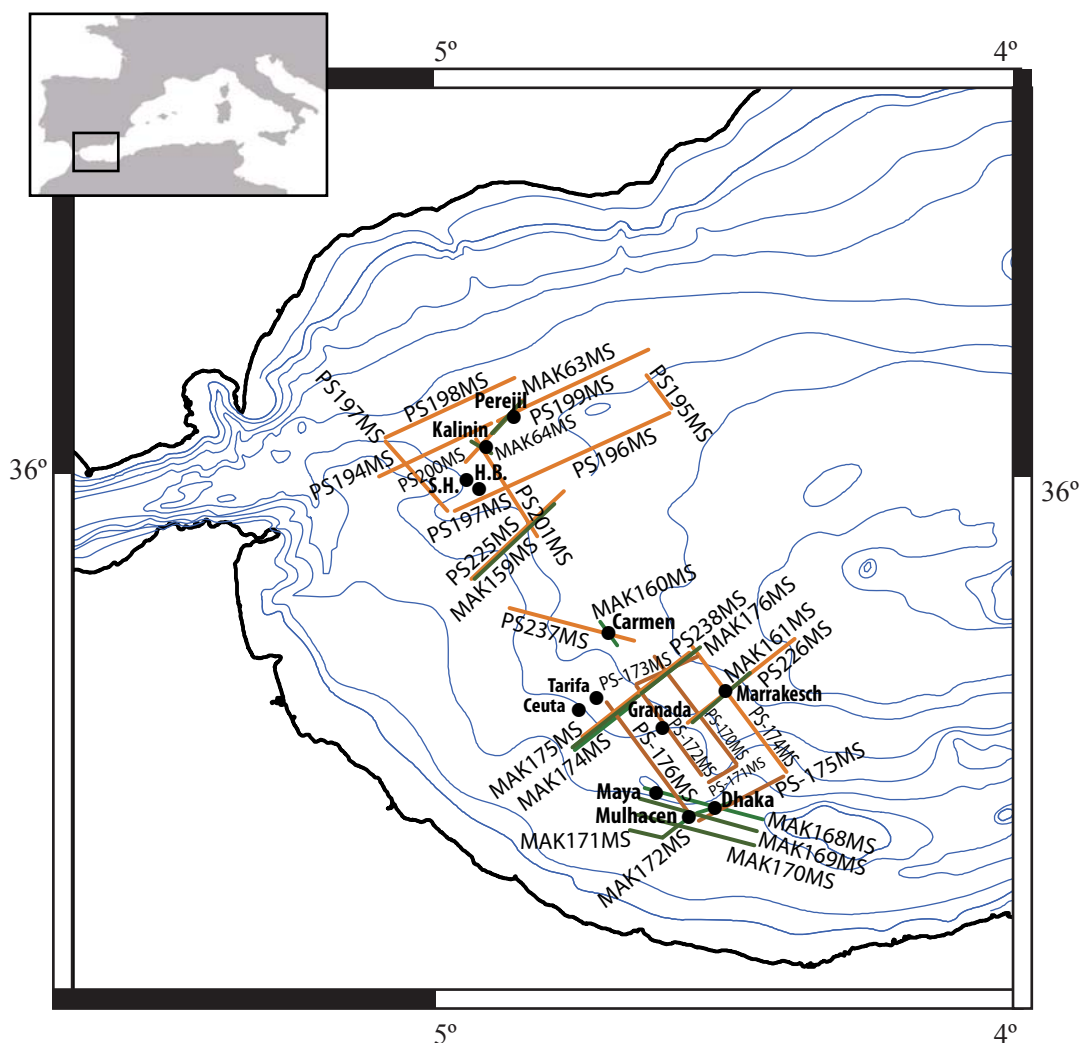


Figure 2.4. Location of high-resolution seismic profiles (orange lines) and side scan sonar profiles (green lines) acquired by MAK-1 from the BASACALB, MARSIBAL-1 and SAGAS-08 cruises. Bathymetry contours are in meters, contour interval 200 m. Black dots represent mud volcanoes

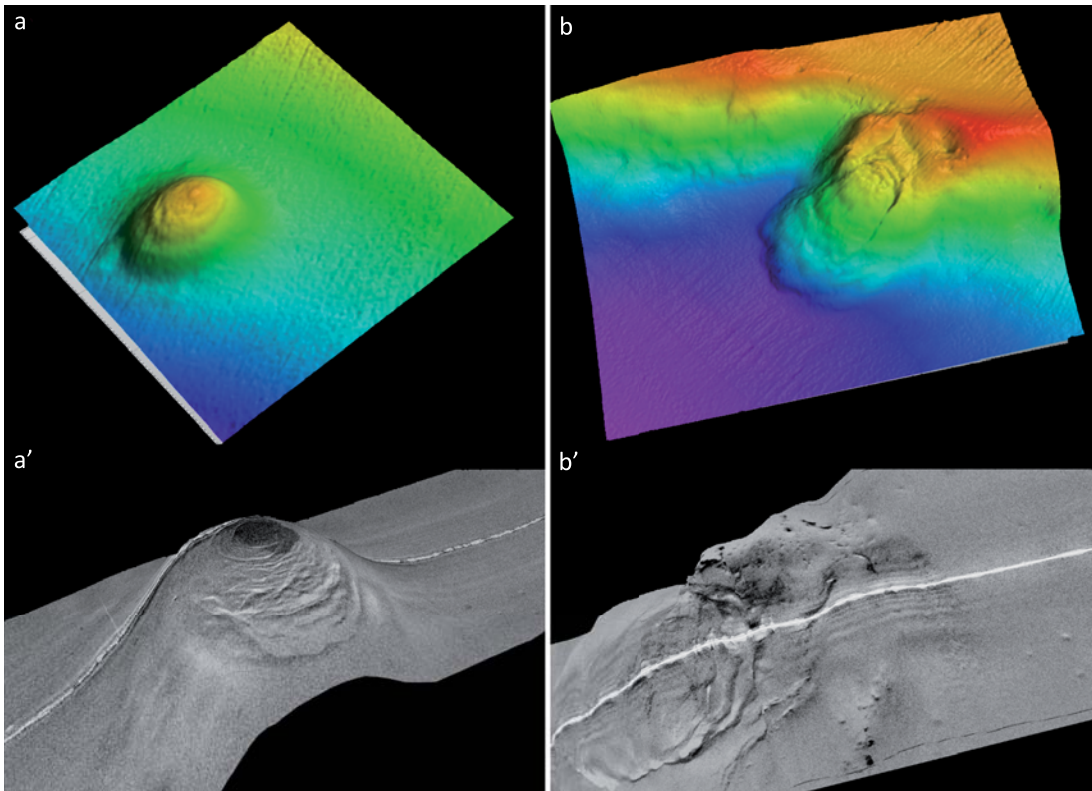


Figure 2.5. a) Carmen MV (1) Swath bathymetry and (2) MAK160MS line and Marrakech MV (1) swath bathymetry and (2) MAK161MS showing typical edifice shapes these MVs. Line position are shown in Fig.2.4

2.3 Geochemical analyses

2.3.1 X-ray fluorescence (XRF)

X-ray fluorescence (XRF) was performed, respectively, on 135 and 361 discrete samples of hemipelagic sediments and mud breccias so as to determine their major elements. Samples were prepared as pressed pellets using 5 g of ground bulk sediment, pretreated and homogenized, then pressed. A commercial wavelength dispersive X-Ray fluorescence device (Bruker AXS S4 Pioneer) with an error of 2% and equipped with an Rh anode X-ray tube (60 Kv and 150 mA) was used for analysis.

2.3.2. Inductively coupled plasma-mass spectrometry (ICP-MS)

Inductively Coupled Plasma-Mass Spectrometry (ICP-MS) was performed on the same number of

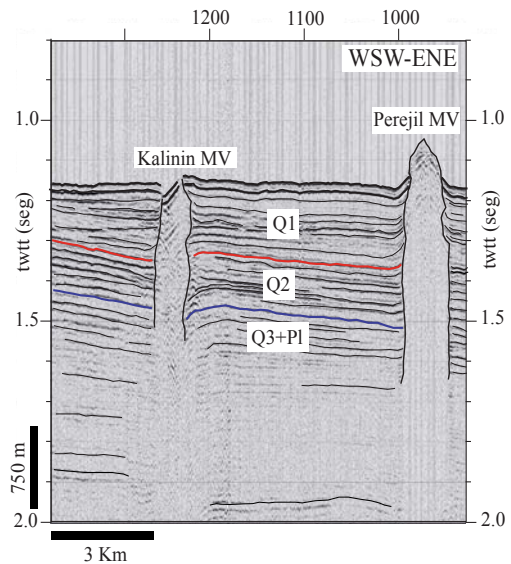


Figure 2.6. Seismic profile line PS200MS across the Kalinin and Perejil MVs showing dome-like and collapsed structures. Line position are expressed in Fig.2.4

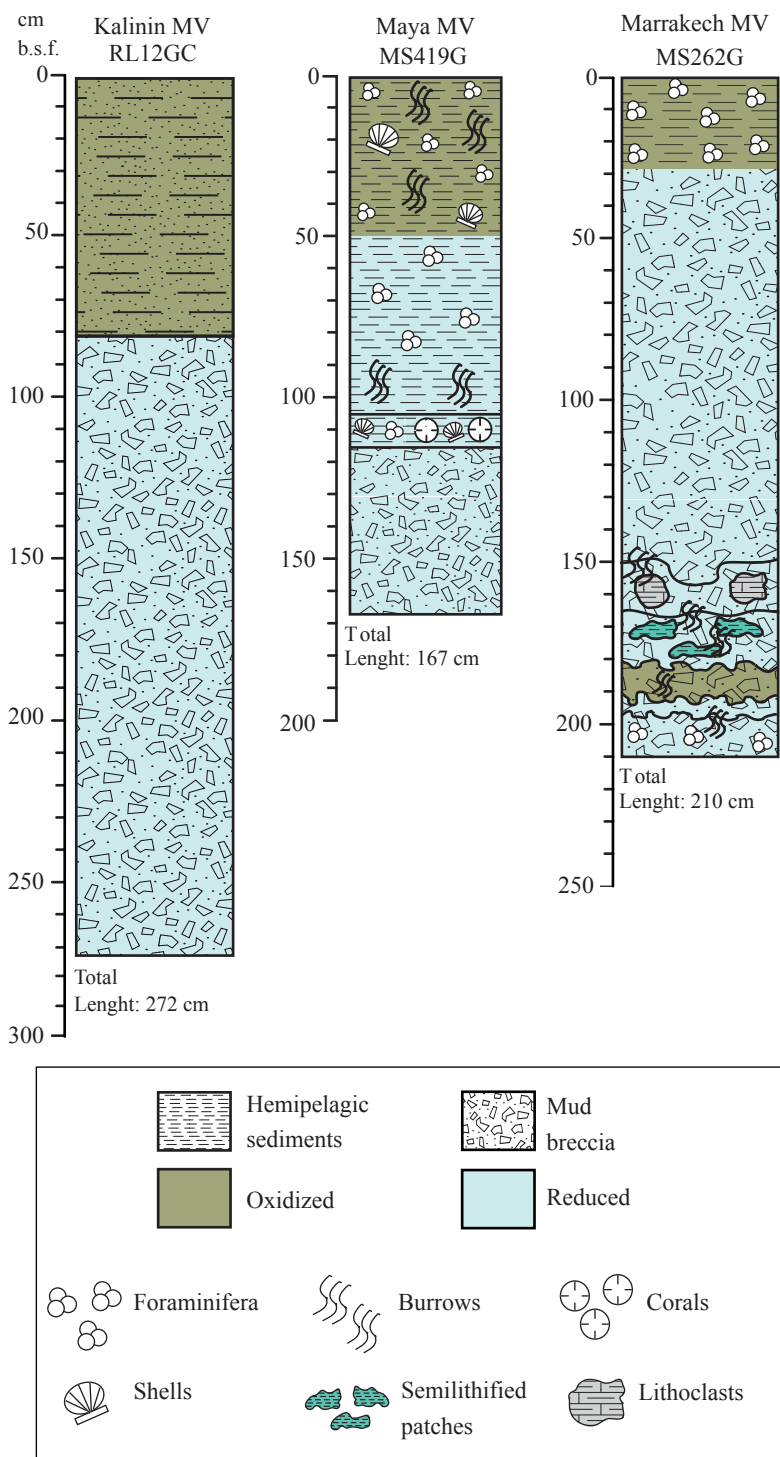


Figure 2.7. Core logs from Kalinin, Maya and Marrakech MVs showing the main lithofacies found at the studied cores.

samples as XRF for trace element and rare earth element (REE) determinations. Measurements were done by spectrometry via a Perkin Elmer Scienx-Elan 5000 spectrometer at the University of Granada (CIC, *Centro de Instrumentacion Cientifica*, Universidad de Granada). The instrumental error was $\pm 2\%$ for elemental concentrations of 50 ppm and $\pm 5\%$ for concentrations of 5 ppm (Bea, 1996).

2.3.3. Total Organic Carbon (TOC), Total Inorganic Carbon (TIC) and Total Nitrogen (TN)

A total of 36 samples of hemipelagic sediments, 113 mud breccia matrices and 25 clasts were analyzed for Total Organic Carbon (TOC), Total Inorganic Carbon (TIC) and Total Nitrogen (TN). TOC, TIC and TN were measured in the CHN elemental analyzer using a LECO CNS-TruSpec and a CM5240 UIC inorganic carbon analyzer in the laboratories of the Andalusian Center for Environmental Research (CEAMA, University of Granada).

2.3.4. Inductively coupled plasma atomic emission spectrometry (ICP-AES)

Dissolved anion and cation concentrations in the pore water of 79 samples were measured using an inductively coupled plasma atomic emission spectrometer (ICP-AES, Perkin Elmer Optima 3000) at the shore-based laboratory of the Department of Earth Sciences (Utrecht University, The Netherlands). Replicate analyses indicated that the relative error for the pore water analyses was $< 5\%$.

2.3.5. Gas Chromatography (GC), gas chromatography-mass spectrometry (GC-MS) and high performance liquid chromatography-mass spectrometry (HPLC-MS)

A total of 13 and 36 aliquot samples of hemipelagic sediments and mud breccias were analyzed by Gas Chromatography (GC), performed using a Thermo Finnigan TRACE instrument equipped with a fused silica capillary column (CP Sil-5, 25m

x 0.32 mm, $df = 0.12 \mu\text{m}$), having a flame ionization detector and helium as a carrier gas.

All fractions were further analyzed by gas chromatography-mass spectrometry (GC-MS) for compound identification. The GC-MS was coupled to a Thermo Finnigan TRACE DSQ quadrupole mass spectrometer with an ionization energy of 70 eV, and a mass range of m/z 50-800. GC conditions of GC-MS were the same as those described for GC.

A total of 48 aliquot samples from sediments and mud volcanic materials were measured by means of high performance liquid chromatography-mass spectrometry (HPLC-MS) (Hopmans et al., 2000) using an Agilent 1100 series/1100 MSD series instrument, with an auto-injection system and HP Chemstation software. MS analysis and quantification of both isoprenoidal and branched GDGTs followed methods reported by Weijers et al. (2006).

2.3.6. Stable carbon ($\delta^{13}\text{C}$), oxygen ($\delta^{18}\text{O}$) and hydrogen (δD) isotopes of pore waters

The stable carbon ($\delta^{13}\text{C}$ -DIC) isotope from four pore water samples was obtained by elemental analyzer-continuous flow isotope ratio-mass spectrometry using a Fisons 1500 NCS elemental analyzer coupled to a Finnigan Mat Delta Plus mass spectrometer. The accuracy of the internal standards was $\pm 0.06\text{‰}$. The $\delta^{13}\text{C}$ was reported in standard delta notation (‰) relative to the VPDB standard. Average analytical precision based on routine analysis of internal laboratory reference material demonstrated a standard deviation of 0.15 ‰.

Stable hydrogen (δD) isotopes from 16 pore water samples and stable oxygen ($\delta^{18}\text{O}$) isotopes from 13 pore water samples were measured in triplicate and determined by the $\text{H}_2\text{O}-\text{CO}_2$ equilibration method using a continuous flow technology with helium carrier gas performed in a GasBench II interfaced with a Finnigan Mat-253 and a Kiel-device mass spectrometer. The accuracy of the internal standards was $\pm 0.1\text{‰}$ for $\delta^{18}\text{O}$

and $\pm 1\text{‰}$ for δD . The $\delta^{18}\text{O}$ and δD of pore water were reported in light of the standard delta notation (‰) relative to the SMOW standard. Average analytical precision based on routine analysis of internal laboratory reference material demonstrated respective standard deviations of 1.2 and 3‰ (Nelson, 2000).

2.3.7. Stable carbon ($\delta^{13}\text{C}$) isotopes of methane

Only five samples for isotopic signatures of methane were measured with continuous flow isotope ratio mass spectrometry systems at the Royal Holloway University of London (RHUL) for $\delta^{13}\text{C}$.

Subsamples were extracted from the headspace present in the sealed flasks and injected to the sample loop of each system to be mixed with a carrier gas (Helium). High precision measurements of $\delta^{13}\text{C}$ were obtained by sample pre-concentration and subsequent pyrolysis to H_2 or combustion to CO_2 for measurement of either stable isotope, before entering the mass spectrometers a Trace Gas and Isoprime mass spectrometer (Isoprime Ltd) for $\delta^{13}\text{C}$. Isotope data are given in δ -notation relative to the Vienna Pee Dee Belemnite (VPDB) for carbon isotopic signatures (Sapart et al., 2011).

2.4 Radiocarbon dating

Absolute age determinations were performed on nine samples of hemipelagic sediments overlying the mud volcanic deposits, using Accelerator Mass Spectrometry (AMS). All samples were sieved and oven dried at c.a. 40°C. Although all samples contained multi-species, AMS radiocarbon focused on just specimens of planktonic foraminifera. Consequently, 10-15 mg of clean and well preserved *Globigerina Bulloides* were hand-picked from the size $> 125\ \mu\text{m}$. The samples were treated and measured at the "Poznan Radiocarbon Laboratory" in Poznan, Poland.

All ages were calibrated and converted to calen-

dar years (calyr BP, the present being AD 1950) using CALIB 7.1 software and the Marine09 calibration curve (Stuiver and Reimer, 1993), with a correction of 400 yr for ocean surface reservoir effects (Reimer et al., 2009).

3

CRUISE 1482/3
SCORE OF SEC
TOP

Sedimentology
and mineral composition of
mud volcano products and
related sediments

Chapter 3

Sedimentology and mineral composition of mud volcano products and related sediments

Abstract

Undercompacted shales and olithostromes proceeding from the deepest sedimentary units feed diapir structures and mud volcanoes in the West Alboran Basin. They are also associated with the generation and upward migration of hydrocarbon-rich fluids. Material ascending through layers of diverse ages assimilates further material from the feeder channels, and this complex mixture is transported to the seafloor. These mud breccia deposits usually feature a clay or silty-clay matrix with diverse rock clasts of heterogeneous composition, shape and size. The mineral makeup this complex mixture of clasts, mud and fluids provided relevant information regarding the nature of source rocks and diagenetic processes associated with fluid flow at depth. Sedimentological and mineralogical analyses were performed on core sediment material from diverse mud volcanoes, including mud breccia, drapes and intercalated pelagic sediments, and on authigenic carbonates from chimneys related to hydrocarbon-rich fluid seepage. Although fluid discharge did not significantly affect the mineral composition of pelagic sediments, intense mixing is recognized between mud breccia and pelagic material at the transition intervals. Similar bulk and clay mineral compositions of the mud breccias from different mud volcanoes further support a common source for the extruded muds. Predominant clay minerals in the mud breccias are smectite and illite, while mixed-layers of illite/smectite are also observed. They span an ample range of ordering, from 10% up to 95% of illite layers. This finding is particularly relevant for constraining diagenetic conditions, since clay dehydration constitutes an essential mechanism that generates fluids and causes subsequent overpressure at depth. Hence, smectite dehydration may have been an important contribution to deep fluid generation within this basin, and would support the thermal maturity of certain MV-derived materials. At the surface, fluid discharge led to the precipitation of authigenic carbonates forming crusts and chimneys, whose predominant aragonite contents also evidence hydrocarbon-rich fluid venting.

3.1 Introduction

Mud volcanoes (MV) are the surface expression of deeply rooted structures that extrude slurries of gas, liquids and poorly sorted solids that migrate upwards from zones of overpressure (Kopf, 2002, 2015). Yet the mud and the embedded clasts may derive from different sources than the fluids (Kopf, 2002; Dupré et al., 2014). Hence, the composition of the diverse phases sheds light onto the source materials and the ample range of processes involved in MV origin. Given the significance of seepage activity and methane emissions, as well as the contribution of MV to fluid reflux from the geosphere to the hydrosphere, the fluid phase has been a major research focus in this field (i.e. Dählmann and de Lange, 2003; Niemann et al., 2006a; Hensen et al., 2007; Mastalerz et al., 2007; Scholz et al., 2010; Magalhães et al., 2012; Pierre et al., 2014a; Hensen et al., 2015; Lash, 2015, among others). Notwithstanding, the solid phase also contributes key information on MV processes. The extruded materials serve as a tectonic window of deeper units, while both clasts and matrix provide provenance information regarding the composition of source rocks (e.g., Robertson and Kopf, 1998; Ovsyanikov, 2003; Pinheiro et al., 2003; Giresse et al., 2010). Furthermore, because authigenic solid phases are closely related to fluid generation and fluid flow, their composition may provide insights into the origin of deep fluids (i.e. clay dehydration at depth) and products of fluid flow activity and discharge (i.e. authigenic carbonates).

Overpressured sediments are usually involved in volcanic processes (Dimitrov, 2002; Kopf, 2002, 2003; Planke et al., 2003; Deville et al., 2003). Among the numerous causes for sediment overpressure, mineral dehydration reactions at depth can be of major significance and responsible for deep fluid generation. In general, smectites are abundant clays in MV settings (e.g., Jurado-Rodriguez and Martínez-Ruiz, 1998; Robertson and Kopf, 1998; Martín-Puertas et al., 2007), and

they are transformed into illite at burial when temperatures increase over ≈ 80 °C in a sequence from randomly interstratified (R0) illite-smectite (I-S) to more ordered I-S (R1-R3). The nature of these clays may therefore constitute a reliable indication of thermal maturity. An increase in illite layers may be linked to greater water release contributing to the deep fluid flow. The nature of clays is also essential in these settings owing to the swelling capacity of smectites and their interaction with methane hydrate complexes. It has been demonstrated that clays can incorporate significant amounts of methane that may be adsorbed on clay surfaces or stored in pores of clay-rich rocks (e.g., Martos-Villa et al., 2014 and references therein). Indeed, the methane adsorbed on clay surfaces can be a major component of shale gas (e.g., Ross and Marc Bustin, 2009; Heller and Zoback, 2014).

Fluid migration and methane cycling may also cause the precipitation of authigenic minerals that subsequently serve as proxies for seepage activity. In fact, authigenic carbonates have been the focus of intensive research because they result from the anaerobic oxidation of methane in seeping fluid areas and thus play an important role in the global carbon cycle (e.g., Milkov, 2003; Judd and Hovland, 2007; Reeburgh, 2007; Knittel and Boetius, 2009; Boetius and Wenzhöfer, 2013).

The Gulf of Cadiz has been extensively studied in recent decades, and numerous MVs and gas-related fluid escape structures have been described there (Kenyon et al., 2000, 2003; Pinheiro et al., 2003). Previous work has helped constrain the mineralogical characteristic of these structures as well as the diagenetic processes resulting in clay dehydration and authigenic mineral precipitation linked to the anaerobic oxidation of methane (AOM) (e.g., Martín-Puertas et al., 2007; González et al., 2009; Magalhães et al., 2012; Martos-Villa et al., 2014). MV sediments from the Gulf of Cadiz show a smectite content similar to that of

the underlying clay-rich unit, and they present a weak thermal maturity suggesting a depth source of just a few km. The abundance of smectite, clast lithologies and micropaleontological data come to support a substantial contribution from Miocene formations to the mud breccia in this region (e.g., Ovsyannikov, 2003; Pinheiro et al., 2003, Martín-Puertas et al., 2007). In the eastern Mediterranean, abundant smectite in the breccia matrix of the Napoli and Milano MVs and its composition —typical detrital beidellite— support Messinian formations as a major sediment source feeding these MVs (Jurado-Rodriguez and Martínez-Ruiz, 1998). The systematic increase of smectite that formed in soils under temperate and sub-arid climate conditions is a representative characteristic of Mediterranean Messinian sediments (Chamley et al., 1980).

In the Gulf of Cadiz, meanwhile, authigenic minerals resulting from the AOM in discharge areas have been extensively described. Methane-derived authigenic carbonates are indicative of active fluid seepage in this area, and they often reach exceptional length and thickness, allowing them to be geophysically mapped (e.g., León et al., 2006; Magalhães et al., 2012 and references therein).

Within the MVs of the West Alboran Basin, an active MV (Carmen) and several pockmarks have also shown evidence of significant seepage activity, and authigenic carbonate crusts and chimneys associated with living chemosynthetic fauna have been described; they moreover present a light carbon isotope signature evidencing their methane-derived origin (Blinova et al., 2011). However, a comparative mineralogical analysis of MV sediments at different locations in the Alboran Sea has not yet been performed, nor have the clasts and matrix from mud breccia been thoroughly investigated. The present work addresses bulk mineral composition and clay mineral assemblages from MV breccia, along with the associated hemipelagic and sedimentological characteristics

of several MVs, the aim being to provide new insights into the origin of mud breccia, the nature of the parent units, and the potential diagenetic processes leading to clay dehydration and the generation of fluids. New data are provided from authigenic carbonates to further evidence seepage activity and AOM-related processes within this basin.

3.2 Regional Setting

The Alboran Sea is a marginal basin located in the westernmost Mediterranean Sea. On the basis on its intricate seafloor morphology, with differences in the structural architecture and sedimentary infill, it can be divided into the Western, Southern and Eastern Alboran Basin (Fig. 1.8).

Geological and geophysical data have suggested that the Alboran Sea evolved first through extensional tectonics (from Middle to Late Miocene) and then under significant contractive tectonics (from Late Miocene onwards) (Fig. 1.7). Post-Miocene contractive tectonics caused a major reorganization, which resulted in prominent north-south shortening and subsidence of the marine realm and uplifting and emersions of the surrounding Betics and Rif chains. Such active neo-tectonics conditioned the actual coastline as well as the seafloor morphology (Comas et al., 1999 and references therein).

The lithology and ages of the basement and sedimentary drape beneath the Alboran Sea are known from commercial wells and ODP Leg 161 drilling (Fig.1.7). The thicker sedimentary depocenter is located in the West Alboran Basin (Fig. 1.6), where more than 7-8 km of sediments accumulated from the Early Miocene to Present on top of the metamorphic basement (Fig. 1.8; Jurado and Comas, 1992; Comas et al., 1996; Soto et al., 1996)

The West Alboran Basin is characterized by the presence of extensive shale (mud rock) diapirism and the existence of overpressured units at dep-

th (Comas et al., 1999, Soto et al., 2010, 2012). Overpressure is conditioned by significant gas and fluid contents in the basal units of the West Alboran Basin (Unit VI and Unit V from Jurado and Comas, 1992; Fig. 1.8), as has been reported by logging data (sonic velocity, density and resistivity) from Andalucía-G1 and Alboran-A1 boreholes drilled in the West Alboran Basin (Comas et al., 1996).

Furthermore, borehole sampling indicates that Unit VI (Burdigalian in age) is formed of under-compacted (overpressured) olistostromic or brecciated materials made of heterogeneous rock fragments (blocks, boulders and clasts) of different ages embedded in a shale matrix intercalated with clayey, marly and sandy intervals; and that Unit Va (Langhian in age) also contains under-compacted green clays (Jurado and Comas, 1992; Díaz-Merino et al., 2003) (Fig. 1.7).

Mud volcanism and pockmarks occurring in the West Alboran Basin lie on top of the huge Mud Diapir Province (MDP) that extends from the Iberian to the Moroccan margins (Fig. 1.6). As evidenced by previous works, the mud volcanism is linked to recent stages of shale diapirism during compressive tectonics (Plio-Quaternary, from 4-5Ma onwards), which gave rise to pierced diapirs and subsequently to mud volcanism at the seafloor (Comas et al., 2010; Somoza et al., 2012; and references therein). Reactivations of the mud volcanism have been explained by the triggering due to erosional episodes related to major sea-level falls, affecting the neutral buoyancy conditions of the overburden above the shale units and causing mud extrusion (Somoza et al., 2012). Seismic profiles show that volcano feeder-channels connect to deeper shale-diapir structures, thus proving that volcanic processes bring up to the seafloor over-pressured shales and olistostromes from Unit VI, over 5 km deep (Talukder et al., 2003; Comas et al., 2012).

The extruded mud breccias contain exotic rocks from Cretaceous to Miocene sedimentary units.

Micropaleontological data from core sampling indicate that the sedimentary rocks brought up to the seafloor by MVs range from Late Cretaceous to Late Miocene in age (Sautkin et al., 2003; Genari et al., 2013). A deep thermogenic source of fluids expelled by the Alboran MVs has been suggested on the basis of $\delta^{13}\text{C}$ isotope determinations in authigenic carbonates, pore-water analyses and gas composition (Blinova et al., 2011; López-Rodríguez et al., 2014). The abundance of chemosynthetic fauna (bivalves, tube worms) atop some MVs, together with direct indicators of activity such as gas bubbling, would suggest current hydrocarbon seeping (most likely methane) (Hilário et al., 2011; Ivanov et al., 2010). Most of the Alboran MVs appear, however, be inactive or dormant (Comas et al., 2010; Ivanov et al., 2010).

3.3 Sediment Recovery and Sampling

3.3.1. Sediment Recovery

The sediment cores selected for sedimentological and mineral determinations were obtained during four oceanographic cruises. The first three expeditions were performed throughout the framework of the UNESCO/IOC Training Through Research Programme (TTR), during the TTR-9 BASALB Cruise (Cruise Report Kenyon et al., 2000), TTR-12 Leg 3, MARSIBAL-1 Cruise (Cruise Report Kenyon et al., 2003) and TTR-17 Leg 1 cruise SAGAS-08 (Cruise Report in Ivanov et al., 2010) in 1999, 2002, and 2008, respectively, aboard the RV Professor Logachev. The fourth oceanographic survey, the GASALB-Pelagia cruise, was accomplished on board RV Pelagia in 2011 (Fig. 2.1). In order to obtain a wide net of sedimentary record for sediment and mineral characterization, a total of ten cores were selected from seven MVs (Pe-rejil, Kalinin, Marrakech, Granada, Maya, Dhaka, and Mulhacen MVs; Table 2.1; Fig. 3.1). One gravity core was investigated at each volcano except at Carmen MV, where four gravity cores were selected because of its current activity. Additiona-

lly, one gravity core from the “Crow’s foot” pothole field was studied, and within this core a piece of a chimney and a concretion of methane-derived authigenic carbonate (MDAC) (Table 2.1; Fig. 3.1).

During the TTR-cruises, coring operations were performed following the standard TTR-procedures (Ivanov et al., 1992 a, b; Kenyon et al., 2002) using a 6 m long gravity corer (ca. 1500 kg) with an internal diameter of 14.7 cm. After recovery of the plastic inserts, the cores were cut into 60 cm sections, split open lengthwise, and described lithologically onboard. During the GASALB cruise, coring operations were performed using a 24 m long piston corer (ca. 1200 kg) with an internal diameter of 11 cm. The recovered piston core was cut into 30 cm sections, split open lengthwise and lithologically described.

During the TTR-17 cruise, a TV-assisted grab was used for underwater observations and collection of large samples. The TV grab consisted of a 1500 kg system able to sample dense clayey and sandy sediments as well as deep water crusts and boulders at water depths up to 6000 m. Sediment and boulder collection (Fig. 1.9) was performed using a system that closed by the difference in hydrostatic pressure. The triggering mechanism was set off once the seabed was touched.

Sediment cores were immediately packed and stored at +4 °C for subsequent laboratory sampling.

3.3.2. Sampling

The two main lithologies generally present at the investigated MVs were hemipelagic drapes and mud breccia intervals (Fig. 3.1). Sampling procedures and resolution were determined according to lithological variations.

Hand-sized pieces

The lowermost part of mud breccia intervals was sampled at 3-5 cm intervals, depending on the availability of material, for hand-sized pieces (Fig.

3.1 and Fig. 3.2). These pieces were air-dried over a flat surface in order to avoid textural alteration; once dried and consolidated, the obtained pieces were polished for further textural characterization and hand-sized photography. Thin sections from the consolidated mud breccias were also obtained for petrographic description (Fig. 3.3).

Hemipelagic sediments and mud breccia matrices

The hemipelagic sedimentary drapes and the first centimeters of the mud breccia intervals were sampled to obtain discrete samples, at a continuous interval every 2 cm. The rest of the mud breccia matrices were sampled every 5 cm or 10 cm at 2 cm thick intervals avoiding rock fragments. Samples were dried in an oven at 40 °C, then ground and homogenized in an agate mortar. They were subsequently processed for mineralogical analyses.

Methane derived authigenic (MDAC) concretion & chimney

A concretion and a chimney formed by methane-derived authigenic carbonates (MDAC) were also selected for mineralogical determinations. Diverse samples were strategically selected. MDAC concretion was first sub-sampled at the most superficial part of the piece (422Gr-cost). Afterwards, the concretion was cleaned in an ultrasonic bath in distilled water. Once dried and free of fine sediments, the concretion was again sub-sampled (422Gr-carb). The MDAC chimney was likewise cleaned in an ultrasonic bath in distilled water, air dried, and sub-sampled for mineralogical determinations.

3.4. Methods

Bulk and clay mineral composition were determined by X-ray diffraction (XRD). Mud breccia samples were carefully sampled, removing clasts and rock fragments over ~0.5 cm in order to have relative homogeneous portions of mud breccia matrices. For bulk mineralogy determinations, all samples (mud breccia, MV-related sediments

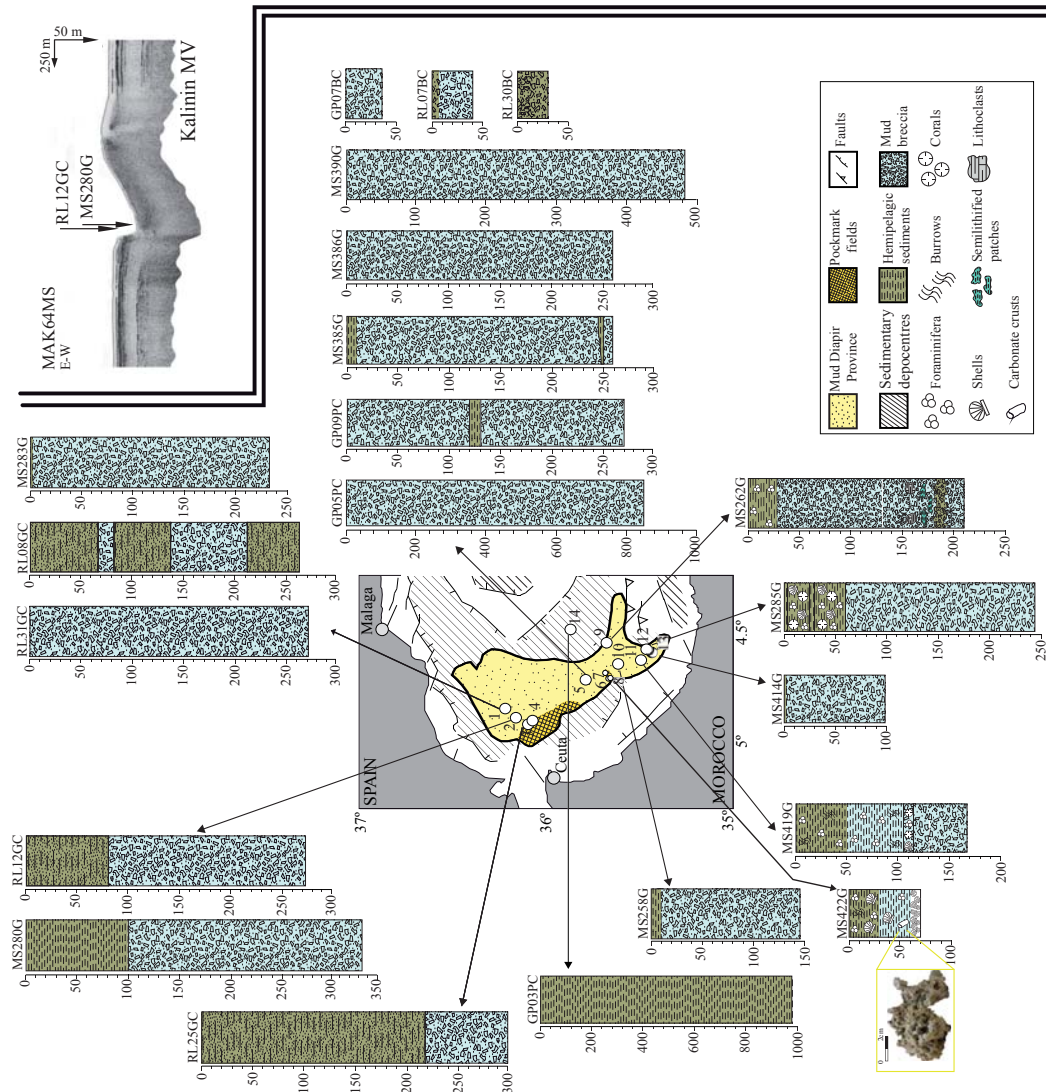
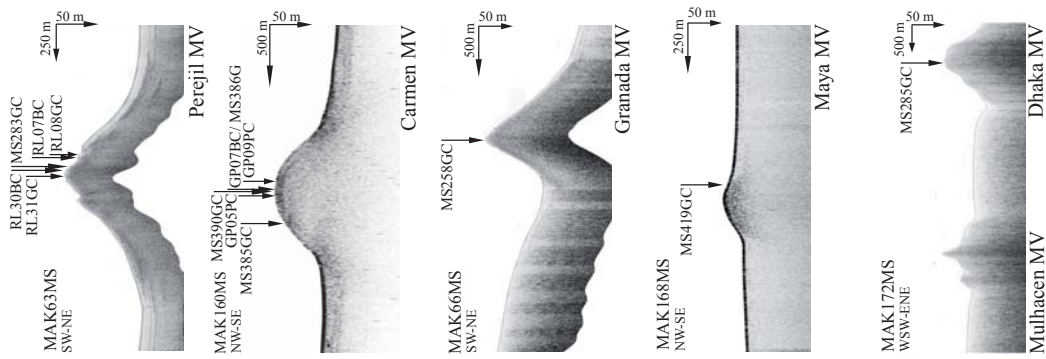


Figure 3.1. Map location of all core sediments used for this study. Core logs show main lithologies found at the investigated MVs and total lengths. MAK sub-bottom profilers indicate the position of recovery at Kalinin, Perejil, Carmen, Granada, Dhaka and Maya MVs. Line positions in figure 2.4

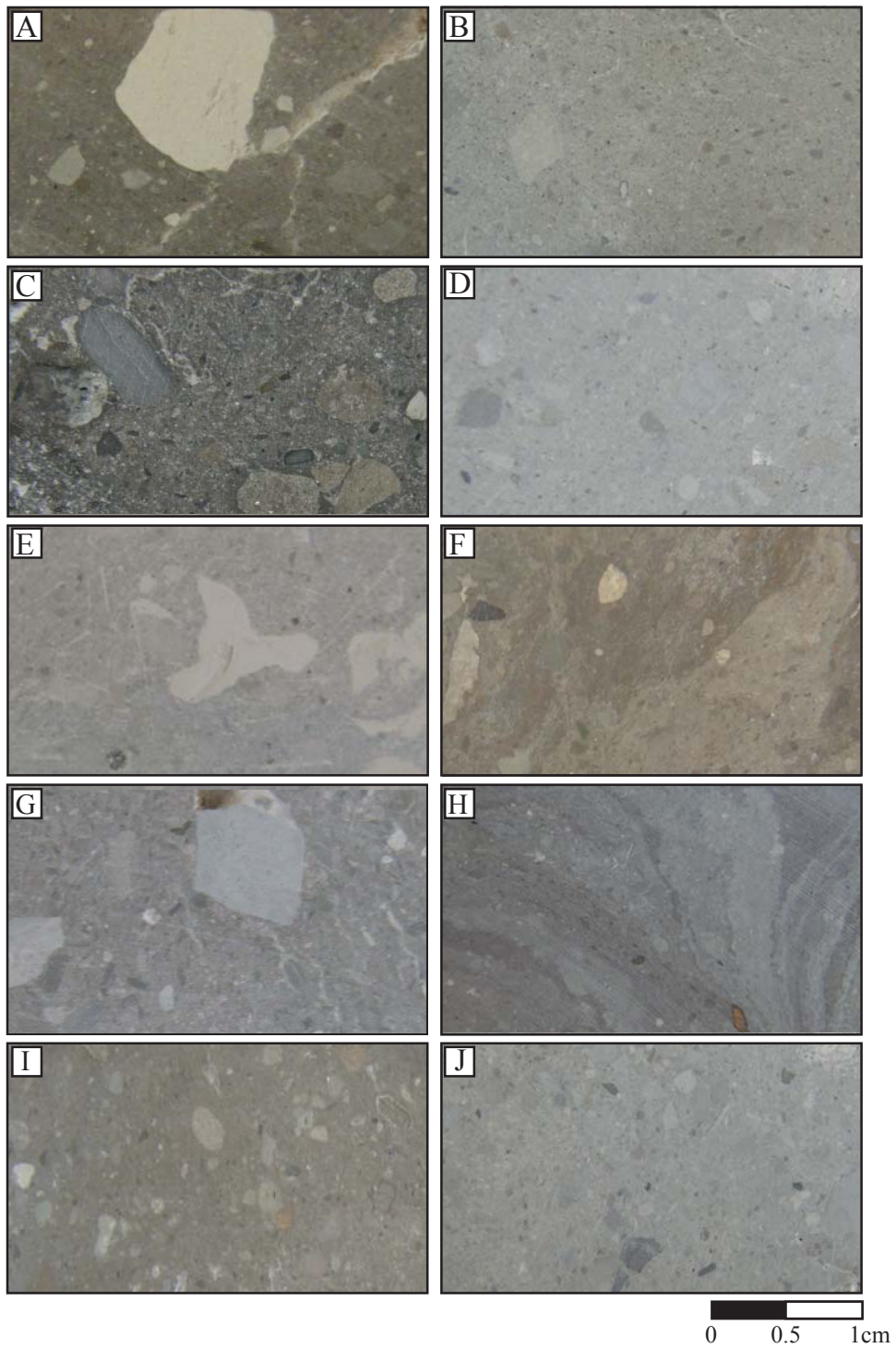


Figure 3.2. Polished hand samples showing clast content of mud breccias from a) Perejil, b) Kalinin, c) Carmen flank d-e) Carmen crater, f) Marrakech, g) Granada, h) Maya, i) Dhaka and j) Mulhacen MVs.

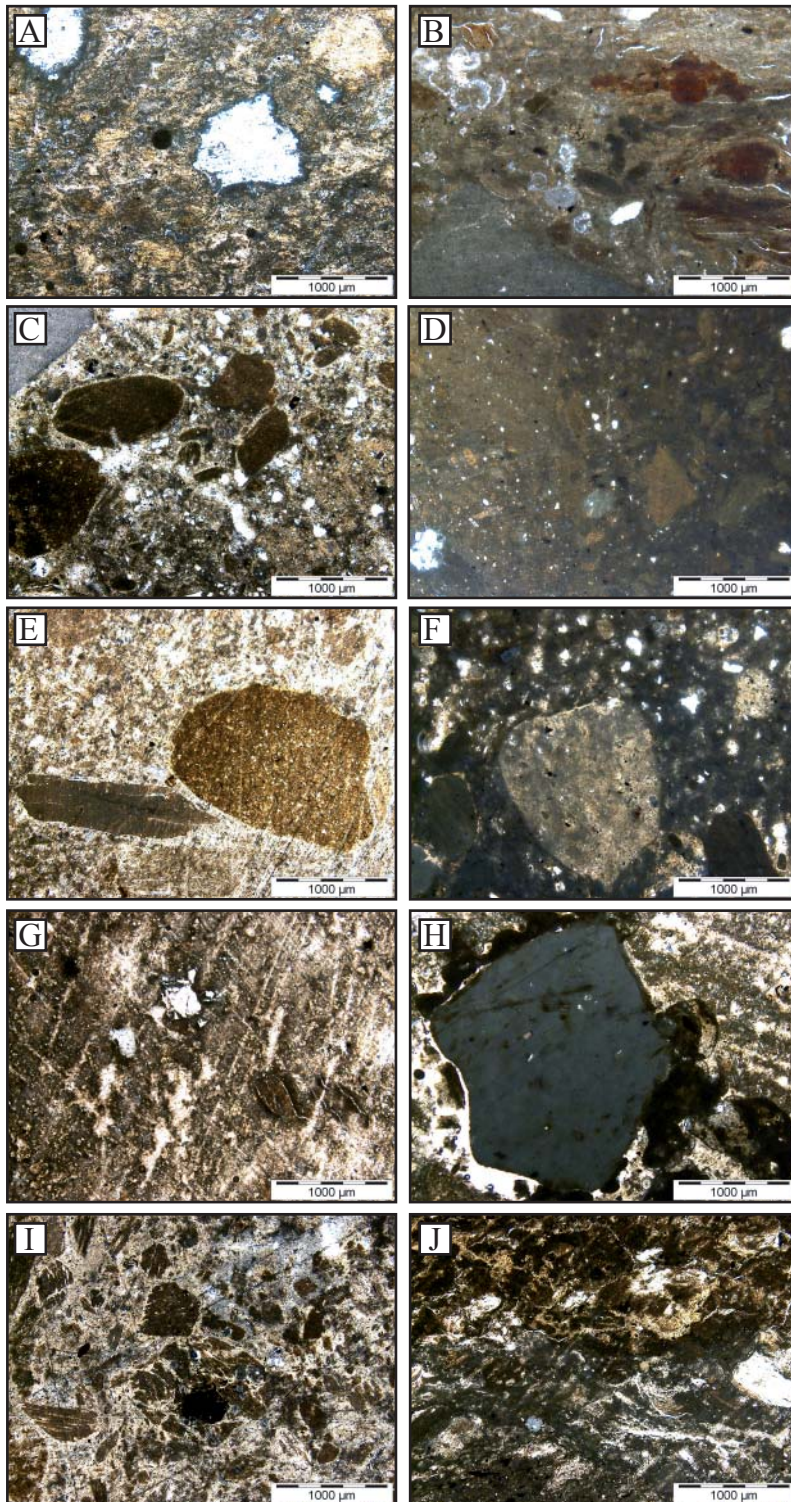


Figure 3.3. Thin sections of air-dried and polished mud breccias from a) Perejil, b) Kalinin, c) Carmen flank d-e) Carmen crater, f) Marrakech, g) Granada, h) Maya, i) Dhaka and j) Mulhacen MVs. Note micro-clasts of different lithologies embedded in mud breccias matrices.

and MDAC sub-samples) were air-dried and homogenized first using an agate mortar, and then ground in a mechanical mortar to finer size. Separation of the clay fraction and preparation of the samples for XRD were performed following the international recommendations compiled by Kirsch (1991). Thus, for clay mineral analyses, the carbonate fraction was removed using acetic acid and successive washing to deflocculate clays. The $< 2 \mu\text{m}$ fraction was separated by centrifugation at 900 rpm for 1.3 minutes, at least four times, and was smeared onto glass slides in order to allow orientation of clay minerals (with crystallographic axis perpendicular to the glass slide).

X-ray diffractograms were obtained using a PANalytical X'Pert PRO diffractometer with Cu-K α radiation and an automatic slit (CSIC-University of Granada). Scans were run from 4-70° 2 θ for bulk-sample diffractograms and untreated clay preparations, and from 3-30° 2 θ for glycolated clay-fraction samples. Resulting diffractograms were interpreted using X Powder 12 software (Martin, 2004 .www.xpowder.com). Peak areas were measured in order to estimate semi-quantitative mineral content. The clay mineral proportions were estimated from the glycolated diffractograms. The 10 Å peak was used for detrital mica and the 17 Å peak for smectite, and in turn the 7 Å peak for the total amount of chlorite + kaolinite, using the respective peak ratios at 3.54 Å and 3.58 Å to differentiate the two minerals. The estimated semi-quantitative analysis error for bulk mineralogy values is 5%, whereas error ranges from 5% to 10% for clay mineral proportions. Nevertheless, semi-quantitative analysis aimed to show changes or gradients in mineral abundances rather than absolute values.

The Illite-smectite (IS) mixed-layers clays were analyzed using specific software MacDiff 4.2.5. The 14 Å peak was used to differentiate expandable mixed-layer minerals, which expands to 15-17 Å after ethylene glycol saturation, as well as the second-order 5 Å to 6.5 Å peak (Moore and

Reynolds, 1997). IS ordering was determined by deconvolution of XRD peaks on $< 2 \mu\text{m}$ glycolated fractions allowing the determination of the percentage of illite (%) and giving the stacking order (Reichweite; R) values used for inter-layering illite-smectite and smectite (Moore and Reynolds, 1997).

Additionally, morphological and textural analyses from selected mud breccia samples were obtained by Field Emission Scanning Electron Microscopy (Auriga FIB-FESEM; Carl Zeiss-SMT), equipped with an EDAX microanalysis system (CIC, University of Granada). The analyses were performed on dried samples deposited onto an aluminum base and metallized with a thin carbon layer. For MDAC concretion samples, electron microscopy analyses (SEM) were performed at the facilities of Aveiro University (Portugal). SEM observations were carried out coupled with energy dispersive spectrometer X-ray elemental analysis (EDS), in fresh fractured surfaces and in samples etched with HCl 1% during 1-4 minutes before the SEM observations.

Transmission and Analytical Electron Microscopy (TEM-AEM) was used to obtain the composition of selected clay particles. TEM-AEM analyses allowed the determination of the chemical composition of clay minerals. These were performed on dispersed samples deposited onto a Cu-grid. Individual mineral particles were chemically analyzed in situ with a Philips CM20 scanning transmission electron microscope (STEM) device with a BaLa filament, providing a maximum resolution of 2 Å under STEM mode. An attached EDX (Energy Dispersive X-ray fluorescence) detector was used for microanalyses and a CCD camera for image capturing. Atomic proportions calculated from peak intensity were transformed into atomic concentrations using natural standards (Cliff and Lorimer, 1975). In order to avoid alkali loss, a short counting time (30 s) was selected, thus providing better reproducibility for alkali contents (Nieto et al., 1996).

Seven ^{14}C -AMS radiocarbon ages (Accelerator Mass Spectrometry, AMS) were selected to date hemipelagic drapes. Approximately 15 mg of monospecific planktonic foraminifera *Globigerina bulloides* from the size fraction $>125\ \mu\text{m}$ were measured in the Poznan Radiocarbon Laboratory (Poland). In order to compare our data with other marine records, all ^{14}C -AMS ages were calibrated to calendar years using the specific software Calib 7.0 (Stuiver and Reimer, 1993) and the Marine13 calibration curve, with a correction for ocean surface reservoir effects of 400 yr (Reimer et al., 2009). The obtained dates are given in reference to calibrated years before present (yr cal. BP), BP being equivalent to AD 1950.

3.5. Results

3.5.1. Hemipelagic sediments and mud breccias

Hemipelagic drapes and alternations of hemipelagic sediments between mud breccia intervals generally lacked sedimentary structures and were mostly oxidized at the uppermost intervals. These sediments showed similar characteristics, texture and fabric at all the studied sites (Fig. 3.1).

Mud breccias were always poorly sorted and had clast-rich to clast-poor matrix-supported fabrics, somewhat comparable to those shown by debris flow deposits. Generally, the matrices of mud breccias were structureless and dark grey in color; and only cores from Maya and Marrakech MVs (respectively MS262G and MS419G) presented some laminations in the fine-grained matrix (Fig. 3.2 and Fig. 3.3). No significant down core variation in clast contents or clast lithology was recognized (Kenyon et al., 2000, 2003; Ivanov et al., 2010).

Mud breccia matrices were similar in all cores, consisting of matrix-supported fabrics with largely to finely comminute rock fragments (grain-sized sand, silt, and clay), representing finer grained equivalents of clast lithologies, embedded in a clayed material. The common color of the

matrix was dark gray. Polarized microscope observations of thin sections revealed evidence of 1) unresolvable fine-grained clay and mud; 2) weakly consolidated clay and mud compositionally similar to poorly consolidated clay-stone and mudstone clasts; and 3) well-lithified micro-lithoclasts that could be correlated with the compositions of coarser clasts (Fig. 3.3).

The clasts in the mud breccias were very heterogeneous, with highly variable size at least up to 0.5 cm, as demonstrated by grab sampling (Kenyon et al., 2003; Ivanov et al., 2010). The clasts had an average size of $< 2\ \text{mm}$, randomly distributed, and accounting for 25%-30% of total volume. The largest clasts were up to some centimeters. Clasts were mostly angular in shape, and presented different degrees of roundness according to the hardness of their lithology. Hard rocks showed higher angularity (Fig. 3.2 and Fig. 3.3) and presented different types of sandstone fragments, mainly subfeldspathic lithic wackes and lithic sandstones. Laminated silstones and schistose silstone and marlstone were less frequent, being encountered only in the Carmen MV core. Hand samples showed massive matrices in all cores except those from Maya and Marrakech MVs, where the matrix was mixed with unconsolidated clasts, tracing a slight lamination (Fig. 3.2 and Fig. 3.3). Soft and friable lithoclasts were dominant in core breccias. Among them, pieces of dark-gray, dark-green, and dark-red claystone to calcareous mudstones (marls) were dominant. Incipient schistosity, laminations, organic-matter spots and burrows were observed at these soft lithoclasts. Light marly limestones and marlstone existed in minor quantities, represented by dark clasts that were mostly observed in Carmen MV and Dhaka MV, but it was in Maya mud breccia where the major quantities were found. Hard rock lithoclasts also showed original sedimentary structures (parallel- and cross-lamination, graded bedding, soft-hard alternating laminations, burrows) denoting an origin from older and very different stratigraphic sequences.

3.5.2. Core lithologies.

Kalinin MV

Gravity core MS280G was taken from the top of the crater of Kalinin MV (Fig. 3.1; Kenyon et al., 2003). It recovered 334 cm of sediments, containing both hemipelagic sediments and mud breccia. Hemipelagic sediments consisted of up to 150 cm thick brownish marls, moderately bioturbated and featuring the presence of Pogonophora tubeworms (Siboglinidae, Frenulata) in the uppermost part. The lower interval consisted of 184 cm of stiff dark grey mud breccia.

Perejil MV

Gravity core MS283G was retrieved from the crater of Perejil MV (Fig. 3.1; Kenyon et al., 2003). The core comprised 233 cm of stiff dark grey mud breccia overlain by a thin layer (~ 2 cm) of brownish and water-saturated hemipelagic marls. At this site, no chemosynthetic fauna was recognized, though the core had a distinct and intensive smell of H₂S.

Granada MV

Gravity core MS258G was taken from the crater of Granada MV (Fig. 3.1; Kenyon et al., 2000). It recovered 144 cm of sediments, containing both hemipelagic sediments and mud breccia. The hemipelagic sediments consisted of 20 cm of light olive brown pelagic marls very enriched in planktonic foraminifera content. The mud breccia interval contained coarse clast fragments of different lithologies, with a prevalence of marlstones and claystones. The upper part of the mud breccia interval was oxidized and bioturbated.

Marrakech MV

Gravity core MS262G was taken from the flank of the Marrakech MV (Fig. 3.1; Kenyon et al., 2000). The uppermost 30 cm were represented by structureless, olive grey hemipelagic marls rich in foraminifera. The lower boundary of the interval was very transitional. Whereas the lower interval was composed of fine grey mud breccia clayed matrix

with abundant foraminifera and numerous clasts of semi-lithified claystones varying from 0.05 to 1 mm in size, its lowermost part (up to 150 cm) consisted of reworked and intensively deformed fine mud breccia.

Dhaka MV

Gravity core MS285G was taken from the crater of Dhaka MV (Fig. 3.1; Kenyon et al., 2003). It cored 244 cm of stiff dark grey mud breccia overlain by 70 cm of olive brown hemipelagic marls. The first 3 cm consisted of siliciclastic-rich water saturated marls, followed by a unit (down to 75 cm) containing shell fragments and abundant pieces of cold-water corals (*Lopheliapertusa*). Above this interval, a coarse mud breccia interval containing clasts of semi-lithified rocks was observed.

Carmen MV

Three gravity cores and one piston core from the Carmen MV were investigated. Cores GP05PC, MS386G and MS390G were recovered from the crater of this structure and core MS385G was taken from the flank (Fig. 3.1; Ivanov et al., 2010). The “flank” core MS385G recovered 258 cm of stiff dark grey mud breccia containing clasts of different lithologies and sizes (-3 cm in diameter). The mud breccia interval was covered by 5 cm of hemipelagic sediments. This core contained thin alternations of hemipelagic sediments and mud breccia (Fig. 3.1), extending from 245 to 250 cm depth. Thus, two mud breccia layers could be distinguished, the upper boundary being irregular and not fully distinctive, while the lower boundaries were sharp and very distinctive. At this core, an intensive smell of H₂S was also clearly detected in the lower part of the mud breccia interval.

In contrast to the sediment from the flank, the 259 cm of crater sediments in core MS386G and the 480 cm of sediments in core MS390G were both characterized by a typical structureless and porous greenish grey mousse-like mud

breccia. Moreover, Pogonophora tubeworms were observed in the upper centimetres of core MS386G. No hemipelagic marls were recovered at this site, and a strong smell of H₂S was detected. Piston core GP05PC contained 855 cm of typical structureless and dark greyish mousse-like mud breccia, with millimeter-to centimeter-sized rock clasts of claystones and mudstones. At this site, no hemipelagic drape was present and a noticeable smell of H₂S was detected along the whole core.

Mulhacen MV

Gravity core MS414G was taken from the crater of Mulhacen MV (Fig. 3.1) and was composed of 97 cm of stiff dark grey mud breccia, oxidized at the upper part (Ivanov et al., 2010). Abundant rock clasts of diverse lithologies and of variable sizes (up to 10 cm) were found within the mud breccia interval. At this site no hemipelagic drape was observed (Fig. 3.1).

Maya MV

Gravity core MS419G was taken from Maya MV (Fig. 3.1; Ivanov et al., 2010). This core presented a thick hemipelagic sediment drape of up to 100 cm of brown marls rich in foraminifera and containing shell fragments. The lower boundary was moderately bioturbated. At 105 to 115 cm depth a coral-debris interval was observed containing cold-water corals (CWC; *Lopheliapertusa*, *Madrepora Oculata* and solitary species) (Margreth et al., 2011), shell fragments and abundant foraminifera contents (Gennari et al., 2013). The mud breccia unit extended from 115 to 169 cm depth. It consisted of a very stiff mud breccia containing striking lamination of semi-lithified and friable rock clasts resulting in a layered light-grey and grey to brownish-grey matrix.

3.5.3. Mineral composition

Hemipelagic drapes

The mineral composition of hemipelagic intervals associated with mud breccias is similar to the regular marine sediments described in the Alboran

Sea off the MV provinces (e.g., Jimenez-Espejo et al., 2007; Rodrigo-Gámiz et al., 2011). The bulk mineral composition comprises clay minerals, quartz and calcite as main minerals, ranging from 55%-85%, <10%-20% and <5%-25%, respectively. Low quantities of dolomite and feldspar were also present in very low proportions (<5%) (Table 3.2). Smectite and illite were the more abundant clays, with variable proportions ranging from 20% to of 70%. Additionally, kaolinite and chlorite were found in proportions ranging from 5% to 30% (Table 3.2).

Mud breccia

Mud breccia sediments had a comparable bulk mineral composition, with substantial clay minerals (60%-90%), quartz (<5%-25%) and calcite (<5%-25%), along with lower proportions of dolomite and feldspar (<5%) (Table 3.2). Clay mineral assemblages were dominated by smectite and illite in variable proportions, respectively ranging from 10% to 80% and from <5% to 65%. Kaolinite and chlorite were also present, varying from <5% to 35% (Table 3.2).

The down-core mineral distribution showed some differences in the abundance of mineral phases at the different MVs (Fig. 3.4). Regarding bulk mineral composition, studied sediments from Granada MV (MS258G), Mulhacen MV (MS414G), Perejil MV (MS283G), Kalinin MV (MS280G), and Carmen MV (MS385G, MS386G and MS390G) showed relatively constant and continuous mineral distribution down core (Fig. 3.3 a and b). In contrast, records from Maya (MS419G), Dhaka (MS285G) and Marrakech (MS262G) MVs showed some bulk mineral variation down core. Clay mineral content increased down core at Maya (MS419G) and Dhaka MVs (MS285G) whereas it decreased at Marrakech MV (MS262G) (Fig. 3.4 a and b). All cores showed same calcite content. Nevertheless, some variations were seen for Dhaka MV (MS285G) and Marrakech MV (MS262G), respectively decreasing and increasing down core (Fig. 3.4a and b).

Table 3.2. Bulk and clay mineral range abundances in a) hemipelagic sediments and b) mud breccia matrices from the studied MVs. Dash numeric entry (-) denotes no available data.

a)	BULK MINERALOGY					CLAY MINERAL ASSEMBLAGE		
	Core Code	Mud Volcano	Quartz (%)	Calcite (%)	Clay Minerals (%)	Smectite (%)	Illite (%)	Kaolinite+Chlorite (%)
Hemipelagic Sediments	MS258G	Granada	10-15	<10	70-80	40-70	20-50	5-10
	MS262G	Marrakech	<10-15	<10	70-80	30-60	30-50	15-20
	MS280G	Kalinin	10-15	<10-20	60-75	25-40	45-60	<5-20
	MS283G	Perejil	10	5	85	>60	>25	>10
	MS285G	Dhaka	10-20	15-25	55-70	20-40	50-70	5-20
	MS385G	Carmen	10-15	<10	70-75	30-35	50-55	10-15
	MS386G	Carmen	-	-	-	-	-	-
	MS390G	Carmen	-	-	-	-	-	-
	MS414G	Mulhacen	10-15	<5	80	35	40	25
	MS419G	Maya	10-15	<10-15	65-75	20-40	40-70	<5-30
	GP05PC	Carmen	-	-	-	-	-	-
	b)	BULK MINERALOGY					CLAY MINERAL ASSEMBLAGE	
Core Code		Mud Volcano	Quartz (%)	Calcite (%)	Clay Minerals (%)	Smectite (%)	Illite (%)	Kaolinite+Chlorite (%)
Mud breccia	MS258G	Granada	10	5-10	80-85	60-80	<5-30	<5-10
	MS262G	Marrakech	<5-10	<5-20	65-90	40-65	10-30	10-25
	MS280G	Kalinin	10-25	5-15	60-75	30-60	25-55	10-20
	MS283G	Perejil	5-15	<5	80-90	50-70	20-35	10-15
	MS285G	Dhaka	10-15	<5-15	70-80	10-40	20-50	10-25
	MS385G	Carmen	10-20	10-15	60-75	30-40	40-55	5-15
	MS386G	Carmen	10-20	10-15	60-75	25-40	35-45	20-30
	MS390G	Carmen	10-15	10-15	65-70	20-50	20-50	10-35
	MS414G	Mulhacen	<5-15	<5	75-90	25-50	30-50	20-30
	MS419G	Maya	<5-10	<5-10	70-90	45-70	10-40	10-20
	GP05PC	Carmen	10-15	5-10	65-75	20-45	35-65	<5-10

Clay mineral content showed a regular down-core trend. Some minor fluctuations of smectite were observed at the bottom of Maya MV (MS419G), Kalinin MV (MS280G), Marrakech MV (MS262G) and Carmen MV (MS390G) cores (Fig. 3.4c and d).

Figure 3.5 shows bulk and clay mineral assemblage distributions in ternary diagrams. The bulk ternary plot (quartz – calcite (%) + dolomite (%) – clay minerals (%)) (Fig. 3.5a) showed very similar mineralogy for all mud breccia matrices. In general, the data set plotted in a well-defined

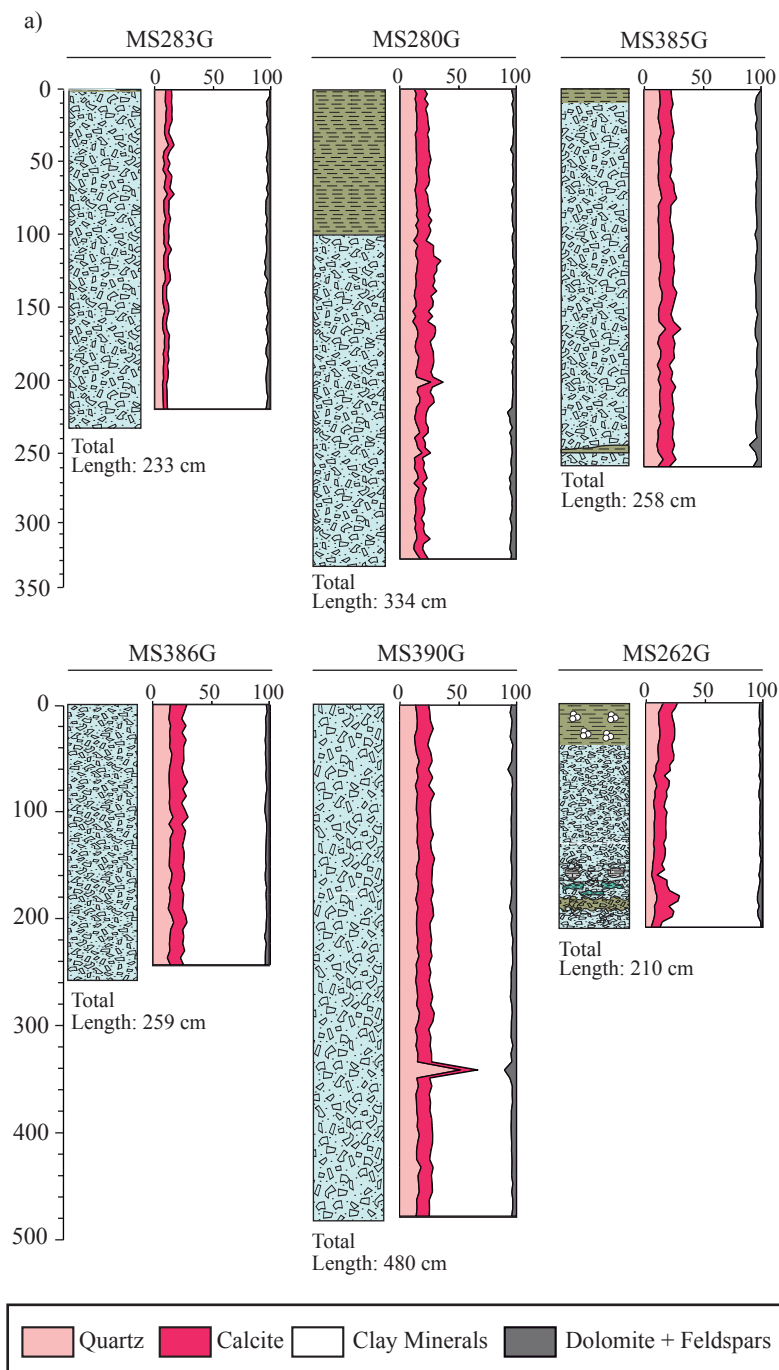


Figure 3.4. Depth distribution of a-b) bulk minerals and lithology column Perejil (MS283G), Kalinin (MS280G), Carmen flank (MS385G) and crater (MS386 and MS390G) and Marrakech (MS262G), Granada (MS258G), Maya (MS419G), Dhaka (MS285G) and Mulhacen (MS414G) MVs

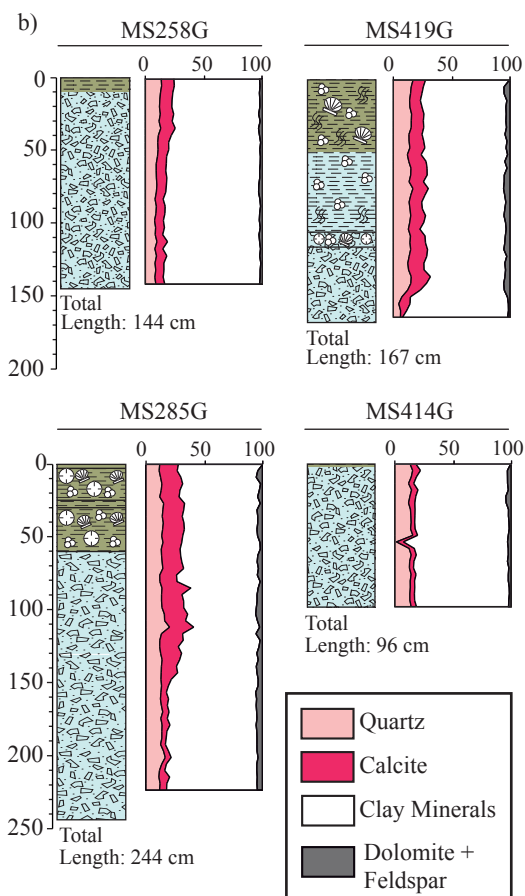


Figure 3.4. (cont.)

cluster characterized by low quartz (10%-20%) and calcite + dolomite content (5%-20%) with high contents of clay minerals, varying between 65% and 90% (Fig. 3.5a). The ternary diagram of the clay mineral assemblage- (Fig. 3.5b) showed data plotted in a well defined elongated cluster characterized by high proportions of smectite (25%-80%) as well as illite + chlorite (10%-70%) and low kaolinite content (<5%-25%) (Fig. 3.5b). According to Figure 3.5b, smectite and illite + chlorite contents differed slightly among structures, allowing three main groups to be discerned. The first group comprised the samples from MV cores Perejil, Kalinin, Marrakech, Carmen and Maya (MS283G, MS280G, MS262G, GP05PC and MS419G, respectively). The distribution smectite - illite + chlorite - kaolinite revealed very low

kaolinite variation (<5%-15%) and variable smectite (25%-70%) and illite + chlorite (15%-70%) contents. Samples from Dhaka MV and Carmen MV flank (MS385G) and crater (MS386G) showed variable proportions of clay minerals. Thus, in the case of Dhaka MV (MS285G) smectite - illite+chlorite - kaolinite respectively varied from 25%-40%, 50%-60% and 10%-20% (Fig. 3.5b). At the core flank of Carmen MV (MS385G) smectite, illite+chlorite and kaolinite reported values of 25%-40%, 50%-60% and 5%-15% (Fig. 3.5b), correspondingly. In contrast, samples from the crater of Carmen MV (MS386G) showed smectite, illite+chlorite and kaolinite values of 10%-20%, 70%-75% and 10%-15%, respectively (Fig. 3.5b).

Meanwhile, the distribution of the samples from the craters of Mulhacen (MS414G), Granada (MS258G) and Carmen (MS390G) are more dispersed, giving values ranging from 25% to 60% for smectite, from 30% to 60% for illite + chlorite content and from 15% to 25% for kaolinite contents (Fig. 3.5b).

Figure 3.6 shows the smectite and illite proportions from different MV structures (Fig. 3.6). Although all samples displayed over the line 1:1, some differences were noted when comparing the MVs: illite exceeded smectite at samples from Dhaka MV (MS285G) and Carmen MV flank and crater (MS385G and MS386G); smectite exceeded illite at Granada MV (MS258G); and variable proportions of smectite-illite were detected at Marrakech MV (MS262G), Kalinin MV (MS280G), Perejil MV (MS283G), Maya MV (MS419G), Carmen crater (MS390G) and Mulhacen (MS414G) MVs (Table 3.1; Fig. 3.6).

SEM observations revealed an abundance of smectite of a webby flake-like shape as well as carbonate derived from bioclasts (e.g. coccoliths) (Fig. 3.7a and b). Authigenic minerals were also observed, pyrite being very abundant as framboid aggregates, and in some cases filling foraminifera chambers (Fig. 3.7c). Minor amounts of gypsum and rhomboidal dolomite were also observed (Fig. 3.7d and e).

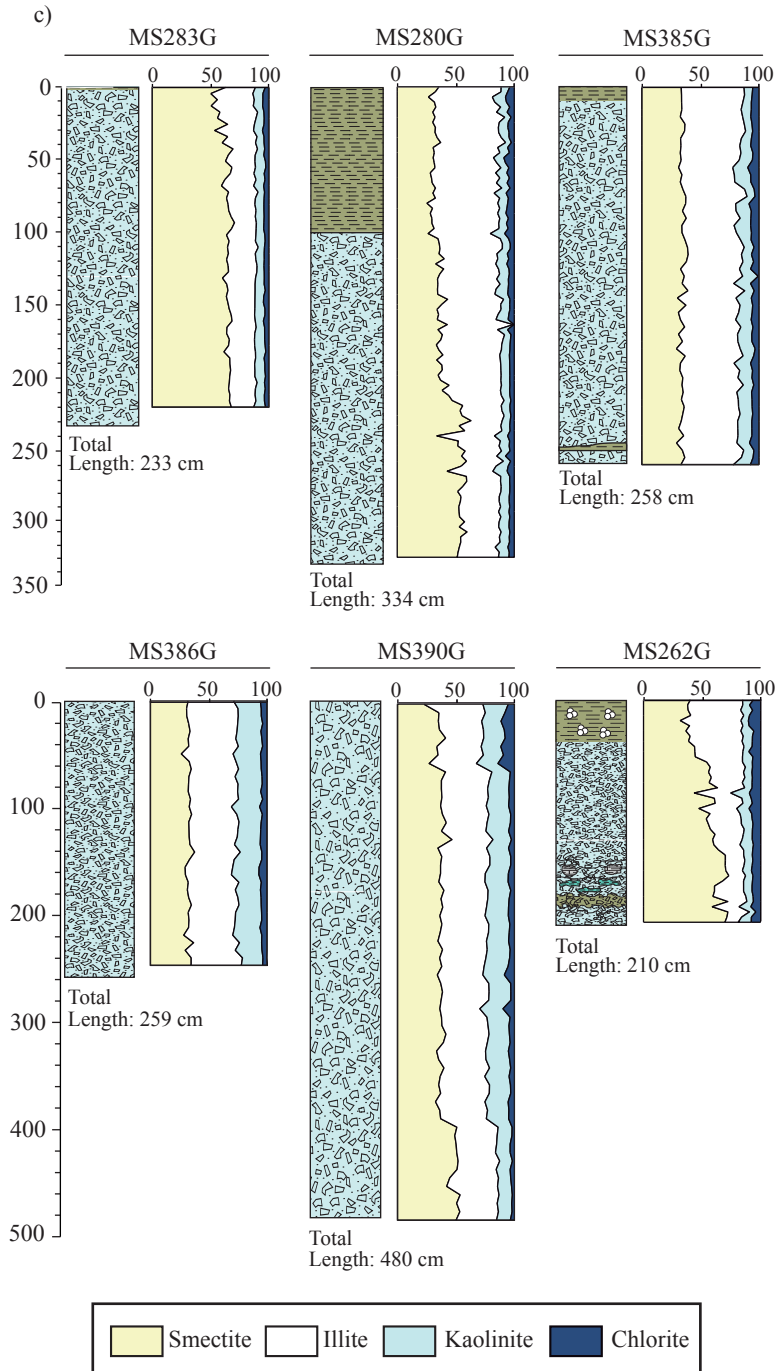


Figure 3.4. (cont.)

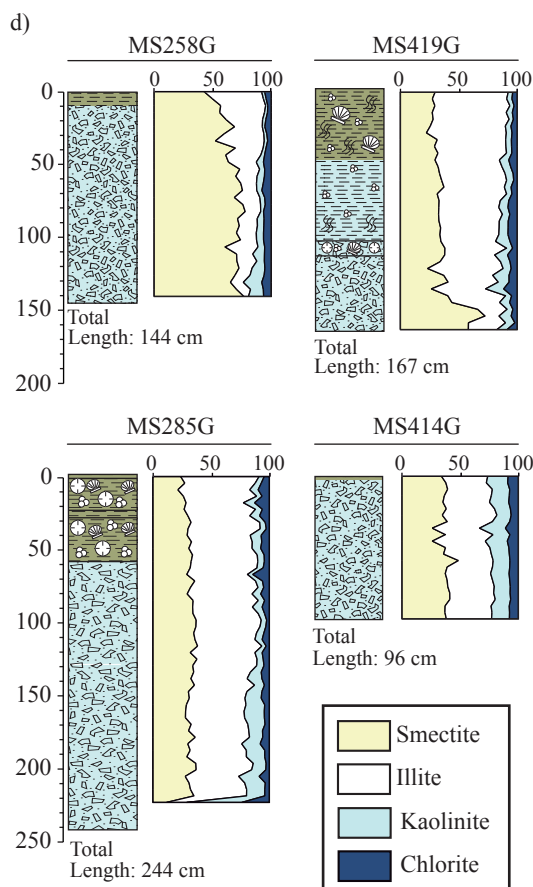
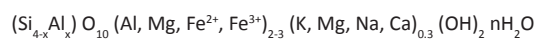


Figure 3.4. (cont.)

Similarly, TEM-AES showed abundant smectite aggregates with irregular flaky shapes (Fig. 3.8). In most of the samples, K^+ was the dominant interlayer cation, varying from 0.07 to 0.54 (Table 3.3). Minor amounts of Na^+ , Ca^{2+} and Mg^{2+} , with average values of 0.04, 0.10 and 0.04, respectively, were also detected (Table 3.2).

We consider the structural formula for the studied smectite particles as follows:



Although preliminary XRD data showed that all samples were mainly composed by smectite and illite, the deconvolution (using MacDiff 4.2.6) of selected mud breccia samples obtained from the oriented fraction after glycolation revealed that detrital smectite and mixed-layer IS phases were also present within the extruded materials (Fig.

3.9).

Regarding the illite percentage in IS and the stacking order R, XRD patterns of the glycolated samples showed the occurrence of the ordered R0-R3 IS mixed layers in all the studied mud breccias, the percentage of illite ranging between 10% and 95% (Table 3.4 and 3.5; Fig. 3.10)

MDAC concretion & chimney

The selected MDAC concretion was characterized to have variable color, from grey to light yellowish, presenting an irregular shape (Fig. 3.11). MDAC concretion contained important proportions of semi-consolidated sediments filling holes and cavities. Occasionally, sessile organisms, especially cold-water corals (e.g. *Lophelia Pertusa*) were also found attached to the hard surface of the concretion (Fig. 3.11a).

The bulk mineral composition of the MDAC concretion sub-samples consisted of clay minerals, quartz, calcite, Mg-calcite, feldspar and aragonite as major minerals (Table 3.3).

In sample 422Gr-cost, clay minerals, quartz, calcite, Mg-calcite and aragonite were present in respective proportions of 45%, 10%, 15%, 10% and 15%, along with minor feldspars and dolomite (<5%). At sample 422Gr-carb, the proportions of clay minerals, quartz, calcite, feldspars and aragonite were 25%, 15%, 15%, 15% and 20%, respectively, together with minor Mg-calcite and dolomite (<5%).

Bulk mineral composition of the MDAC-chimney showed strong similarities to the concretion. X-ray diffraction revealed predominant aragonite (35%) clay minerals (20%), feldspars (20%), quartz (10%), and calcite (10%). Dolomite and Mg-calcite were present in minor proportions (<5%).

SEM images from MDAC concretion showed abundant clay minerals of flake-like shape encompassing aragonite. Aragonite was present as needle crystals, or aggregates of twinning crystals (Fig. 3.11b). Biogenic components such as shell fragments, coccoliths and planktonic foraminifera

were also observed in SEM images.

3.5.4. Dating

The mud breccia intervals from the studied cores are associated with hemipelagic sediments which allow dating period of mud volcanic quiescence by ^{14}C -AMS on planktonic foraminifera. Marrakech MV show the most recent extrusion of mud breccias occurring at 718 ± 98 cal. yr BP, followed by Granada MV (1321 ± 67 cal. yr BP), Kalinin MV (2330 ± 145 cal. yr. BP), Dhaka MV (5368 ± 88 cal. yr. BP), Maya MV (5601 ± 84 cal. yr. BP) and Carmen MV, where the older mud flow occurred later than 10890 ± 172 cal. yr. BP

materials, as well as about diagenetic processes related to mud volcanism.

3.6.1. On the activity of mud volcano from pelagic drapes

The variable thickness of the hemipelagic sediments encountered within the studied cores strongly depends on their position within the volcano structure, according to the variability of the volcanic or sedimentological processes. Volcano flanks, especially those with gentle slopes, and tops of inactive volcanoes present a better preservation of “normal” marine deposition (i.e., Maya or Kalinin MVs (Fig. 3.1). Nevertheless, sig-

Table 3.1. Results of AMS ^{14}C carbon dating of single planktonic foraminifera *G. bulloides* ($>125 \mu\text{m}$) taken at hemipelagic drapes from Granada, Marrakech, Kalinin, Dhaka, Carmen and Maya MVs. Calibration was done using Calib 7.0 software. We used Marine13 calibration curve with standard marine correction of 400 years (data from two sigma probability interval)

Mud Volcano	Sample code	Core depth (cm)	Laboratory code	^{14}C AMS age (BP)	Calibrated age (yr cal. BP) (range 2σ)
Granada	MS258G 01 8-10	9	Poz-47278	1080 ± 30	1321 ± 67
Marrakech	MS262G 01 0-2	1	Poz-47279	2180 ± 35	173 ± 97
Marrakech	MS262G 01 22-24	23	Poz-47280	2910 ± 35	718 ± 98
Kalinin	MS280G 02 36-38	97	Poz-47281	4200 ± 50	2330 ± 145
Dhaka	MS285G 01 27-29	28	Poz-30692	6780 ± 40	5368 ± 88
Carmen	MS385G 05 24-26	247	Poz-47284	11370 ± 70	10890 ± 172
Maya	MS419G 02 18-20	79	Poz-30694	7070 ± 40	5601 ± 84

3.6. Discussion

Obtained data regarding the mineral composition of MV sediments have provided new insights as to the activity of the Alboran MVs and the nature, source areas and provenance of the mud breccia

nificant differences in the thickness of the hemipelagic sediments draping mud breccias beneath the seafloor were encountered at the studied sites (Fig. 3.1). Such differences in the thickness of hemipelagic drapes provide information about the times of mud volcanic activity: the thicker the

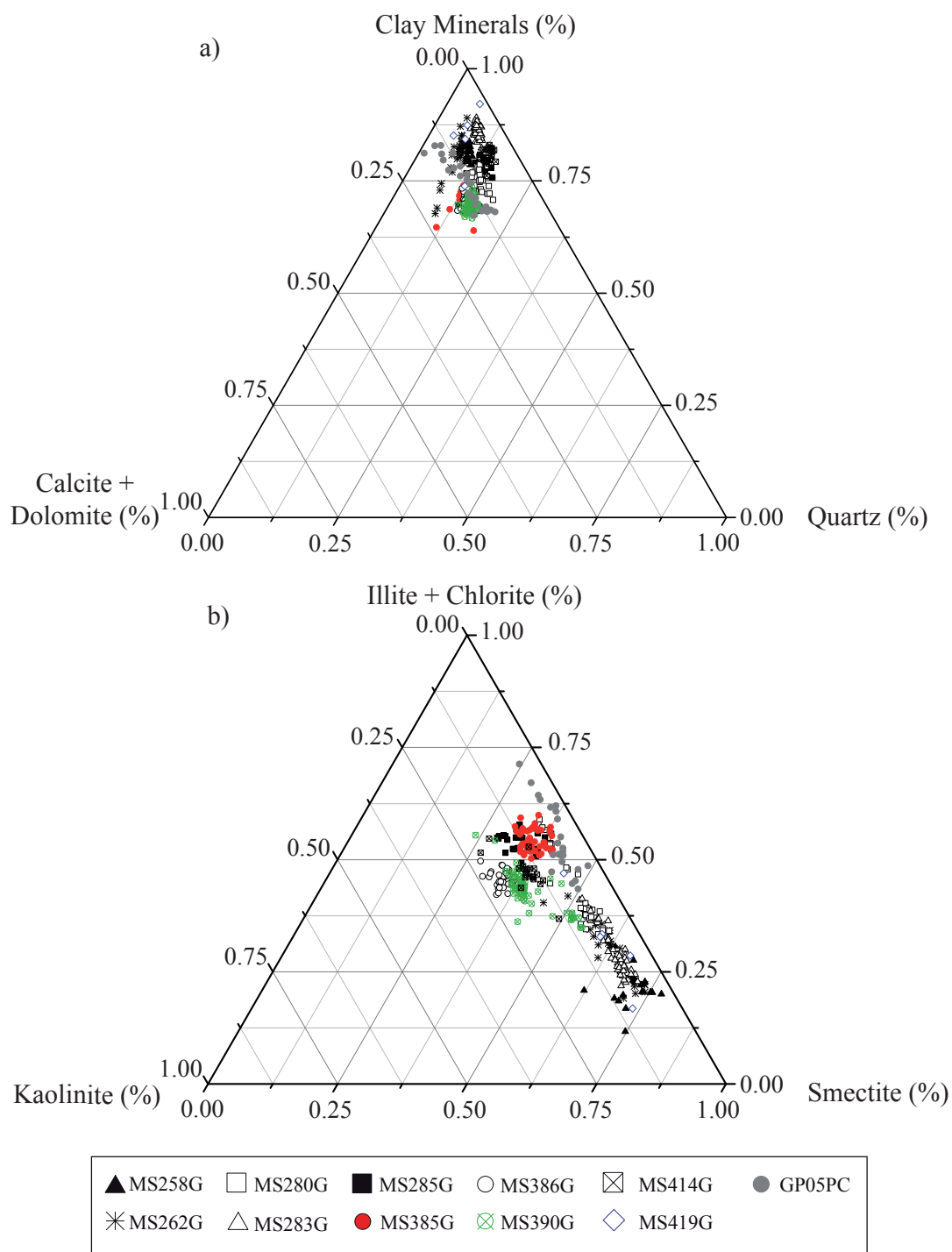


Figure 3.5. Ternary plots of a) quartz (%) – calcite + dolomite (%) – clay minerals (%) and b) smectite (%) – kaolinite (%) - illite + chlorite (%) distribution in mud breccias from Granada (MS258G), Marrakech (MS262G), Kalinin (MS280G), Perejil (MS283G), Dhaka (MS285G), Carmen (MS385G, MS386G, MS390G and GP05PC), Mulhacen (MS414G) and Maya (MS419G) MVs.

Table 3.3. TEM-AES analyses of smectites found in mud breccias from Perejil, Dhaka and Carmen MVs. Data express averaged values

Structural formulae based on 11 oxygens

Depth cm b.s.f.	Tetrahedral cations		Octahedral cations					Interlayer cations				
	Si	Al (VI)	Al (IV)	Mg	Fe	Ti	$\Sigma_{\text{Oct. cat.}}$	K	Na	Ca	Mg	$\Sigma_{\text{Int. cat.}}$
MS283G Perejil Mud Volcano												
7	3.62	0.38	1.52	0.29	0.28	0.00	2.09	0.20	0.02	0.10	0.04	0.36
41	3.65	0.35	1.43	0.29	0.35	0.00	2.07	0.13	0.01	0.16	0.05	0.35
68	3.60	0.40	1.45	0.28	0.33	0.00	2.06	0.26	0.02	0.16	0.02	0.46
131	3.59	0.41	1.42	0.28	0.38	0.00	2.08	0.22	0.08	0.00	0.04	0.33
161	3.59	0.41	1.52	0.25	0.29	0.01	2.06	0.25	0.03	0.03	0.04	0.35
181	3.58	0.42	1.50	0.28	0.28	0.00	2.06	0.17	0.05	0.19	0.04	0.44
211	3.51	0.49	1.38	0.32	0.40	0.00	2.10	0.26	0.02	0.16	0.03	0.47
MS285G Dhaka Mud Volcano												
3	3.38	0.62	1.71	0.12	0.2	0.00	2.04	0.28	0.05	0.04	0.10	0.46
41	3.46	0.54	1.46	0.30	0.33	0.00	2.09	0.34	0.05	0.10	0.02	0.51
67	3.41	0.59	1.46	0.32	0.3	0.00	2.10	0.31	0.08	0.06	0.05	0.49
112	3.51	0.49	1.49	0.30	0.30	0.00	2.09	0.32	0.02	0.12	0.02	0.49
138	3.55	0.45	1.60	0.20	0.25	0.00	2.05	0.22	0.04	0.06	0.07	0.39
168	3.51	0.49	1.47	0.31	0.32	0.00	2.10	0.19	0.01	0.10	0.09	0.40
204	3.50	0.50	1.53	0.23	0.31	0.00	2.06	0.19	0.04	0.11	0.08	0.42
MS385G Carmen Mud Volcano												
35	3.88	0.12	1.47	0.28	0.20	0.00	1.95	0.25	0.08	0.14	0.00	0.47
65	3.60	0.40	1.49	0.32	0.25	0.00	2.06	0.26	0.04	0.16	0.03	0.48
95	3.85	0.15	1.44	0.35	0.22	0.00	2.00	0.21	0.04	0.19	0.00	0.45
140	3.46	0.54	1.44	0.32	0.33	0.00	2.09	0.25	0.02	0.16	0.06	0.50
178	3.70	0.30	1.56	0.22	0.26	0.00	2.05	0.14	0.06	0.00	0.06	0.26
208	3.71	0.29	1.49	0.31	0.30	0.00	2.10	0.16	0.04	0.00	0.03	0.23
240	3.52	0.48	1.36	0.35	0.40	0.00	2.11	0.30	0.04	0.00	0.06	0.40

hemipelagic drape interval, the older the activity was. Thus, the general continuity and homogeneity of the hemipelagic drapes and lack of interruptions (e.g. absence of mud breccia interlayering) also suggest that once mud volcanism stopped,

these sites were dominated by a normal marine sedimentation covering the volcanic edifices. For cores retrieved at volcano rims or upper slopes, the possibility that hemipelagic drapes could be formed by slumps of hemipelagic layers must be

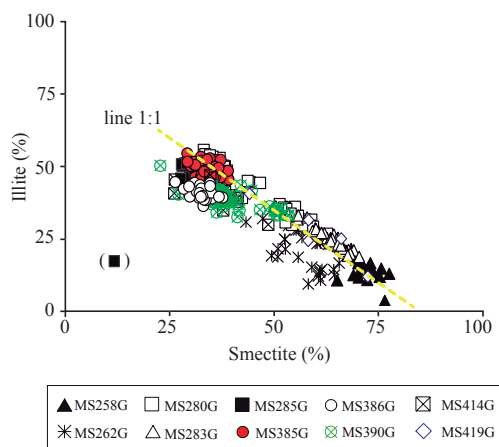


Figure 3.6. Smectite vs illite proportion quantified at the studied MVs. Yellow dashed-line corresponds to proportions 1:1 from Granada (MS258G), Marrakech (MS262G), Kalinin (MS280G), Perejil (MS283G), Dhaka (MS285G), Carmen (MS385G, MS386G, and MS390G), Mulhacen (MS414G) and Maya (MS419G) MVs

checked, and the underlying mud breccia dated (if possible), to ensure accurate activity timing.

The recent activity of the studied MV from the Alboran Sea, where the sedimentary rate seems relatively constant during the Late Pleistocene and the Holocene (e.g. Masqué et al., 2003), must be assessed taking into account the position of each specific core. For instance, the Perejil MV core, recovered from the top of the crater, contained 3 cm thick of hemipelagic drape, suggesting very recent volcanic activity (Fig. 3.1). Thicker hemipelagic drapes at Kalinin, Marrakech, Granada, Maya and Dhaka MVs cores (150, 30, 20, 100 and 70 cm, respectively) suggest comparatively older volcanic activity (Fig. 3.1). Radiocarbon dating supports this assessment, indicating that the duration of the MV activity in the Alboran is highly variable from site to site (Table 3.1). According to our core data, the older eruption started earlier than 10.8 ka BP at Carmen MV, whereas the most recent episode of mud extrusion occurred before 0.7 ka BP at Marrakech MV. This finding is in line with specific micropaleontological studies in the area by Margreth et al. (2011) and Gennari et al. (2013), which reported a difference of thousands of years between extrusive episodes. Neverthe-

less, this assumption has to be taken with caution since significant sediment reworking is known to occur between hemipelagic sediments and mud breccia intervals (Gennari et al., 2013; López-Rodríguez et al., 2014), thereby obscuring the true location of the boundary and consequently impeding accurate timing of the activity.

Compared to normal marine deposits, hemipelagic sediments covering MVs show similar clay mineral proportions. Still, subtle differences were encountered at boundaries between drapes and mud breccia intervals. This fact may suggest that the mineralogy of “hemipelagic” drapes, at least toward their lower part, can be traced to a different origin than off-volcano cores from other areas in the Alboran Sea (Martínez-Ruiz, et al., 2003; Jimenez-Espejo et al., 2008; Rodrigo-Gámiz et al., 2011). This would indicate that the sediment mineralogy reflects blends, supporting the above hypothesis of sedimentary reworking at boundaries between hemipelagic drapes and mud breccia intervals.

Cases of active MVs have also been documented in the Alboran Sea. Such is the case of Carmen MV, proved to be active nowadays, as methane emission to the seafloor and chemosynthetic living fauna (Pogonophora tube worms) were encountered in the volcano crater during TTR-17 cruise (Comas et al., 2010; Ivanov et al., 2010; Hilário et al., 2011). Moreover, cases of mud breccias interbedded with layers of hemipelagic sediments (e.g. flank of Carmen MV or at the flank of Kalinin MV, cores MS385G and RL08CG, respectively, Fig. 3.1) indicate that pelagic sedimentation processes can also alternate with episodes of mud breccia or mud flow accumulation (Gennari et al., 2013; López-Rodríguez et al., 2014; Fig. 3.1).

3.6.2. On the nature and source of mud breccias

Mud breccia matrices constitute the most reliable fraction that can provide information about

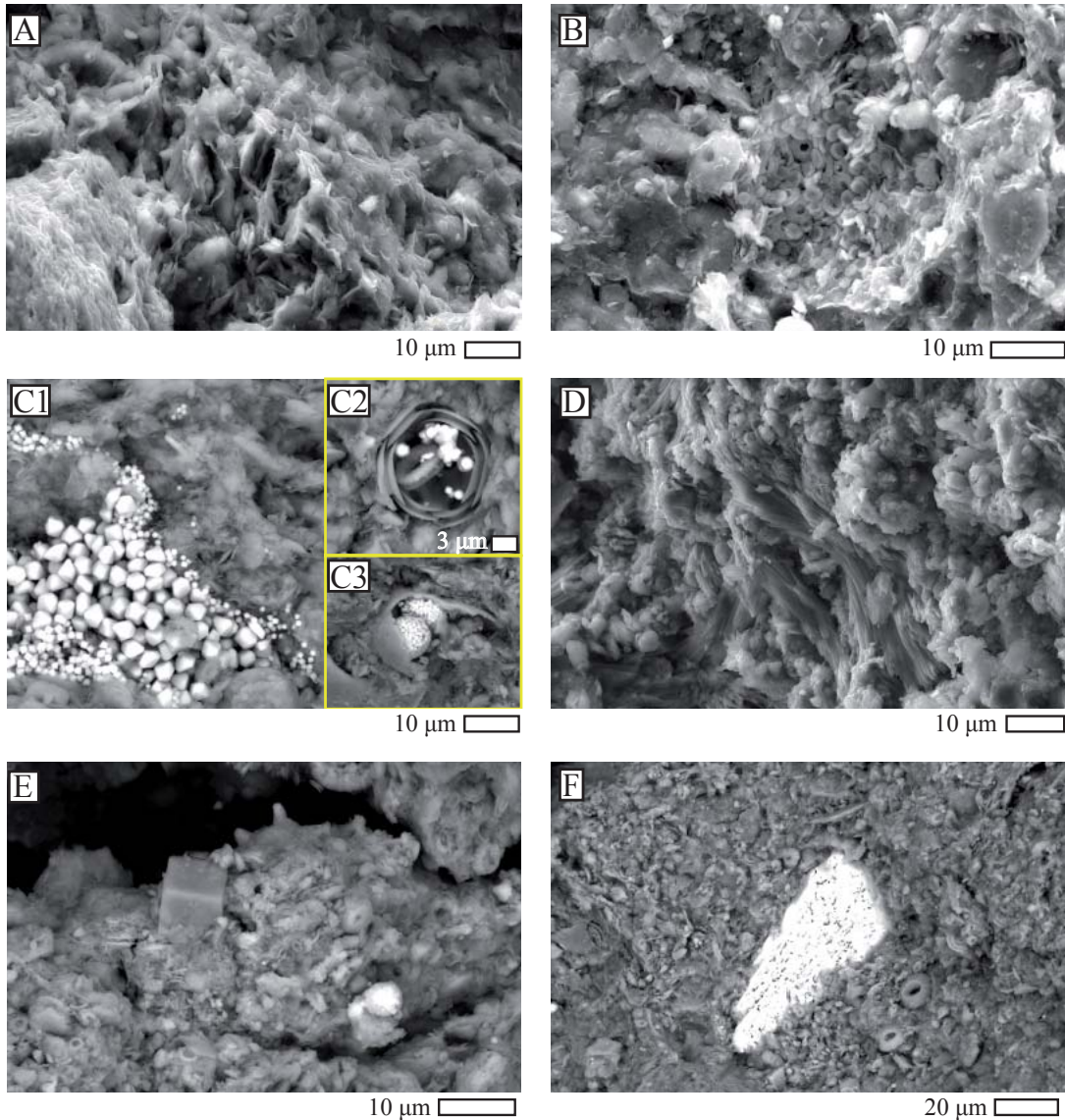


Figure 3.7. SEM images of mud breccia matrices showing a) smectite from Granada MV, b) accumulation of coccoliths found in Carmen MV, c) 1-Pyrites found in Kalinin MV; 2-detail of pyrite inside coccolithophorids observed at mud breccia from Marrakech MV and 3-framboids aggregates of pyrite from Kalinin MV, d) gypsum found at Kalinin MV, e) rhomboidal dolomite and f) barite found at Marrakech MV.

the nature and provenance from parental layers of the extruded material. Some authors who address the abundance or absence of rock clasts in extruded breccias evoke differences in the transport competence of the expelled fluids, induced by physical factors such as density, viscosity, plasticity, or friction coefficient (Flecker and Kopf, 1996). Gas content plays a particularly

important role in the fluid transport competence, since gas-rich mud breccias are less able to maintain clasts and rock fragments in suspension as compared with gas-poor mud breccias. Large sedimentary rock clasts are found in most MVs from the Alboran Sea. For instance, the presence of relatively big polymictic blocks boulders at the crater of Granada MV, in some cases larger than

1-2 meters (Fig.1.9; Sautkin et al., 2003), suggests that violent eruptions of stiff muds may have mechanically forced the triggering of the sedimentary sequence during their ascent, giving rise to the presence of such huge blocks embedded in the mud breccias. The low amount and small size of clasts in mud breccias from the cores recovered at the summit of Perejil and Carmen MVs (Fig. 3.3) and the occurrence of mousse-like mud breccia at these sites may, in turn, reveal that the extruded materials in those MVs contain greater concentrations of gases, at least at the sampled

Table 3.4. Positions (CuK α) of detected reflections and estimating percent of illite layer in illite/EG-smectite from selected mud breccia samples. R denotes the Reichweite number

% illite	R	<u>001/002</u>		<u>002/003</u>		$\Delta 2\theta$
		d(Å)	2θ	d(Å)	2θ	
Granada MV MS258G						
20	0	-	-	5.57	15.90	-
50	0	-	-	5.46	16.19	-
60	1	-	-	5.36	16.52	-
85	1	9.77	9.03	-	-	-
95	3	9.90	8.91	-	-	-
Marrakech MV MS262G						
10	0	-	-	5.62	15.73	-
40	0	-	-	5.50	16.09	-
60	1	-	-	5.36	16.52	-
75	1	-	-	5.24	16.88	-
85	1	9.73	9.06	-	-	-
95	3	9.89	8.93	-	-	-
Perejil MV MS283G						
25	0	8.74	10.0	5.55	15.92	-
50	0	-	-	5.44	16.25	-
55	0	9.16	9.59	-	-	-
60	1	-	-	5.33	16.62	-
75	1	9.33	9.46	-	-	-
85	1	9.73	9.06	-	-	-
Dhaka MV MS285G						
25	0	-	-	5.55	15.92	-
65	1	9.31	9.49	-	-	-
75	1	9.57	9.23	5.32	16.65	7.42
85	1	9.76	9.03	5.13	17.24	8.21
Carmen MV MS385G						
10	0	-	-	5.61	15.76	-
55	0	-	-	5.39	16.42	-
75	1	9.46	9.33	5.24	16.88	7.55
85	1	9.75	9.07	5.12	17.28	-
95	3	9.92	8.90	-	-	-

% illite	R	001/002		002/003		$\Delta 2\theta$
		d(Å)	2 θ	d(Å)	2 θ	
<i>Carmen MV MS386G</i>						
20	0	-	-	5.58	15.88	-
60	1	-	-	5.34	16.60	-
80	1	9.64	9.17	-	-	-
85	1	-	-	5.17	17.13	-
90	3	9.83	8.98	-	-	-
<i>Carmen MV MS390G</i>						
20	0	-	-	5.59	15.83	-
45	0	8.98	9.83	-	-	-
55	0	-	-	5.41	16.36	-
70	1	-	-	5.29	16.72	-
75	1	9.58	9.20	-	-	-
85	1	9.69	9.11	5.15	17.19	-
<i>Carmen MV GP05PC</i>						
20	0	-	-	5.57	15.90	-
60	1	-	-	5.35	16.56	-
80	1	9.64	9.17	-	-	-
85	1	9.77	9.04	5.18	17.09	8.05
<i>Mulhacen MV MS414G</i>						
75	1	9.43	9.36	-	-	-
85	1	9.75	9.07	-	-	-
90	3	9.80	9.00	-	-	-
<i>Maya MV MS419G</i>						
30	0	-	-	5.53	15.99	-
60	1	-	-	5.34	16.60	-
85	1	9.71	9.10	-	-	-
90	3	9.83	8.98	-	-	-

locations (on their craters).

Moreover, specific studies performed on mud breccia matrices from the Gulf of Cadiz (i.e., Ginsburg and Meknes MVs; Martín-Puertas et al., 2007; Mhammedi et al., 2008; Mhammedi et al., 2010) have revealed that significant differences in clay mineral assemblages as well as in clay abundances—especially in smectite and illite content—are indicative of differences in the source of mud breccias.

In the Gulf of Cadiz region, abundant smectites in MVs materials have also been described at Tasyo field (Martin-Puertas et al., 2007), and similarly cited in several MVs from the eastern Mediterranean (e.g., Jurado-Rodriguez and Martinez-Ruiz, 1998). Analysis of fluid geochemistry of different MVs suggests that the MV fluids derive, at least partially, from dehydration due to the transformation of smectite to illite at several km depth (e.g., Dählmann and de Lange, 2003; Hensen et

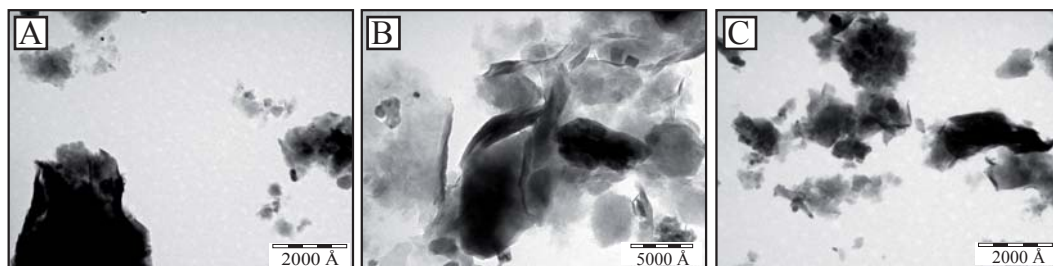


Figure 3.8. TEM images from a) Mulhacen, b) Carmen crater and c) Marrakech mud breccia matrices showing smectites

al., 2007). However, differences in smectite abundance in source feeding materials must also be taken into account in order to explain clay mineral abundances in the mud breccia. Indeed, smectites are especially abundant in Mediterranean Messinian sediments, as also reported in marine cores from the Alboran Sea (e.g., ODP Site 976, Martínez-ruíz et al., 1999). Such differences in smectites/illite abundances of mud breccias may therefore be the result of differences 1) in the nature of the source of mud breccias, 2) in the depth of the source of such materials, or 3) a combination of both.

The similarities in mineral contents that we encountered in all mud breccia matrices come to indicate that all the material expelled by the Alboran MVs shares a common or nearby source area. This assumption is in good agreement with previously reported data derived from mud breccia matrices (Gennari et al., 2013) and demonstrated by seismic reflection data (i.e. Talukder et al., 2003; Comas et al., 2012; Soto et al., 2010), which identified the parental beds of the extruded muds at the basal Unit VI (including overpressured olistostrome or megabreccia strata, dated as late Early to Middle Miocene (Burdigalian) and lower overpressured Unit Va (Langhian in age) (Jurado and Comas, 1992; Diaz-Merino et al., 2003). Specific organic geochemistry studies performed on selected rock fragments (Poludetkina and Kozlova, 2003; Sautkin et al., 2003) and mud breccia matrices (López-Rodríguez et al., 2014) confirm this hypothesis and have corroborated a deep source for the upward mud fluids.

Nonetheless, materials extruded by MVs may suffer enormous trituration during the mud ascents, triggering clasts and sediments from other sedimentary horizons throughout the stratigraphic sequence that are also eventually incorporated into the matrix (Cita et al., 1981; Dimitrov, 2002; Kopf, 2002) must also be taken into consideration as an influence on the mineralogy content of mud breccias.

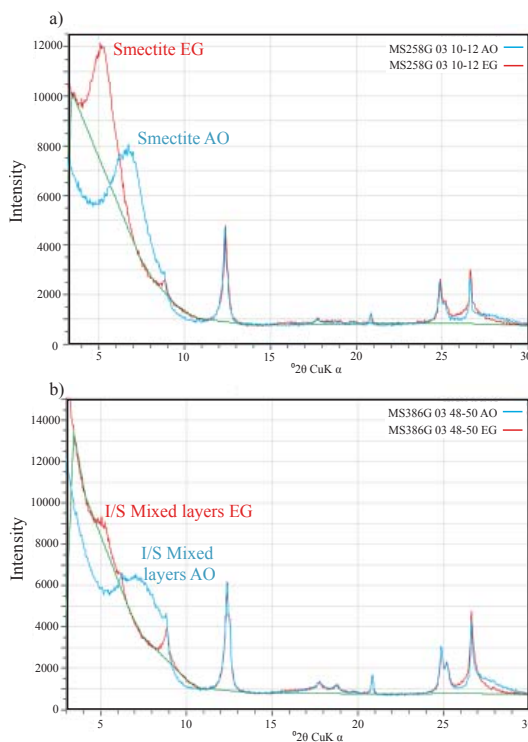


Figure 3.9. X-Ray diffractograms of untreated clays (AO) and glycolated clay-fractions (EG) at selected mud breccia from a) Granada showing occurrence of smectite and b) Carmen crater showing presence of illite/smectite mixed-layers (IS)

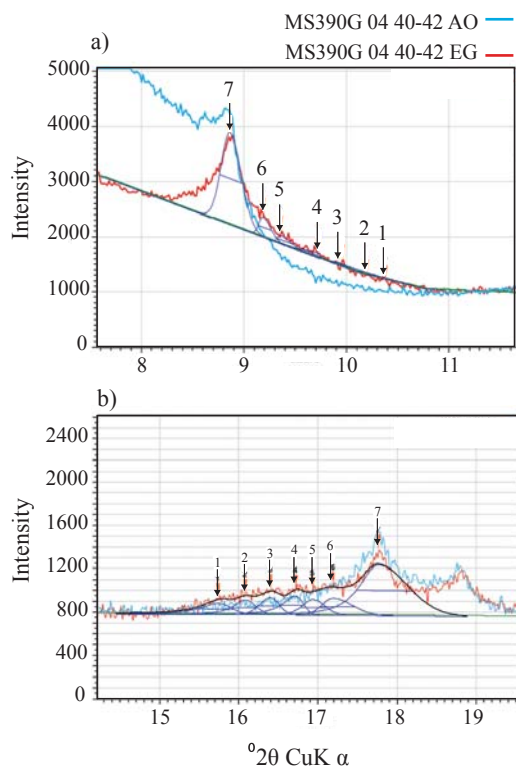


Figure 3.10. Diffraction pattern of selected mud breccia samples from Carmen crater mud breccia. Arrows denote reflection peaks for a) 001/002 $d(\text{\AA})$ 8.58–9.83 and b) 002/003 $d(\text{\AA})$ 5.62–5.10. Navy-blue line corresponds with calculated peaks obtained by deconvolution. Light blue line shows background

3.6.3. Role of clay dehydration on fluid flow

Clay mineral composition from sedimentary rocks can be used to understand the role that burial diagenesis plays in mineral transformations over time, their implication in fluid generation, and the thermal evolution of a sedimentary succession. Several authors have described the smectite-to-illite transformation as a progressive process that requires burial, heat and time (Meunier and Velde, 2004; Vaughan and Wogeluis, 2013); this is a potential source of fluids since smectites can host significant water and hydrocarbon-rich fluid mineral structures that can be released when transformed into illites (Martos-Villa et al., 2014).

In the mud breccias from the Alboran volcanoes, the 1:1 ratio between smectite (S) and illite (I)

Table 3.5. Example of positions ($\text{CuK}\alpha$) of detected reflection peaks and estimating percent of illite layer in illite/EG-smectite from mud breccia from Carmen MV. R denotes the Reichweite number. N^o peaks correspond with arrows from Figure 3.10

a)		001/002		
N ^o Peak	% illite	R	$d(\text{\AA})$	2θ
Carmen MV MS390G 04 40-42				
1	5	0	8.56	10.33
2	40	0	8.90	9.94
3	55	0	9.19	9.63
4	70	1	9.41	9.38
5	80	1	9.65	9.17
6	95	3	9.85	8.98
7	> 95	3	9.99	8.85
b)		002/003		
N ^o Peak	% illite	R	$d(\text{\AA})$	2θ
Carmen MV MS390G 04 40-42				
1	5	0	5.63	15.74
2	35	0	5.51	16.09
3	55	0	5.40	16.43
4	70	1	5.29	16.74
5	80	1	5.21	17.00
6	95	3	5.12	17.32
7	> 95	3	4.98	17.79

at all MVs sites (Fig. 3.6; Table 3.2) signals the progressive increase in illite content compared to smectite, and furthermore indicates the occurrence of diagenetic processes affecting clay mineral transformation at depth.

During smectite illitization, a steady increase of the illite content in mixed-layer IS occurs simultaneously with the enhancement of the grade of stacking order. This entails the progressive variation from randomly interstratified (R0) illite-smectite minerals (IS) to more illitic ordered ones (R1-R3) (Reynolds, 1980; Drits and Tchoubar, 1990; Moore and Reynolds, 1997; Lanson et al., 2009).

Similar situations have been described in mud breccias from the Gulf of Cadiz, where specific

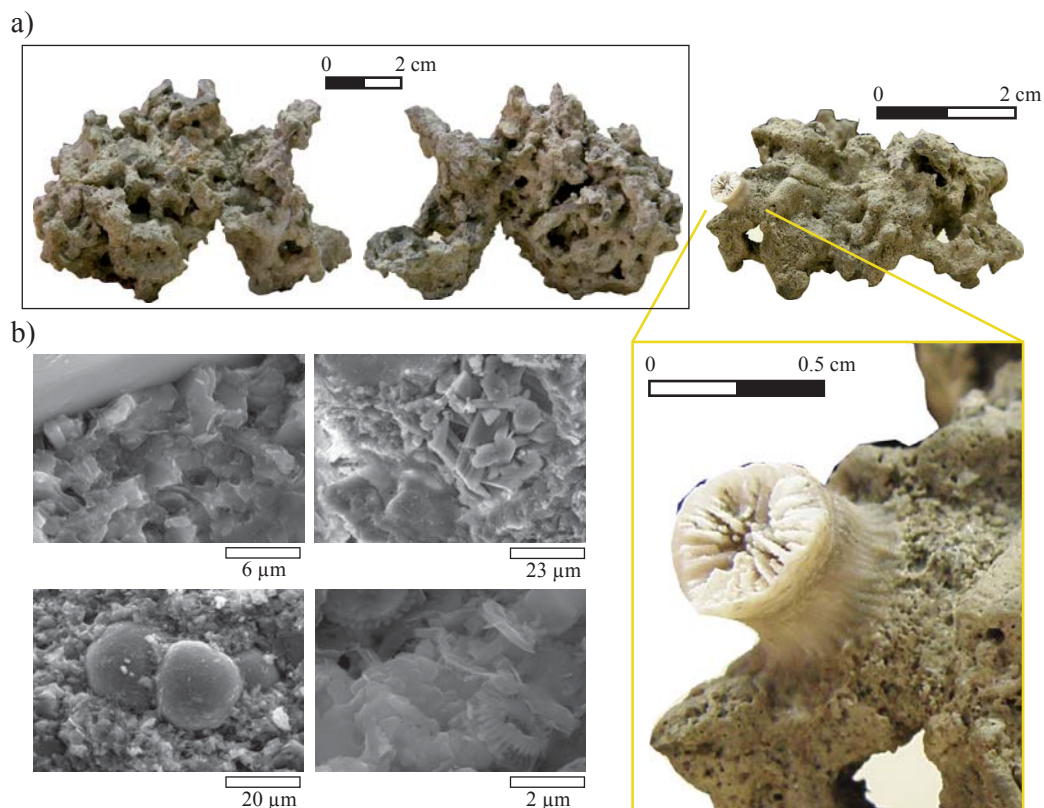


Figure 3.11. a) a sediment concretion of methane-derived authigenic carbonates (MDACs) sample recovered at the Crow's foot pockmark and b) SEM images of the MDAC concretion showing smectites, aragonite crystals, and biogenic content (i.e., foraminifera and coccoliths). Close up from (a) showing coral attached to crusts.

mineralogical studies on MV samples underline the coexistence of both low- and high-illite-layer IS (up to 75%) and subsequently low (R0) and high stacking illite order (R3), implying diagenetic changes at depth that gave rise to a progressive illitization of smectite (Martos-Villa et al., 2014; Mata et al., 2012).

According to our mineralogical characterization, the wide range of illite percentage in IS mixed layers would evidence the complex nature and burial evolution of mud breccias (Fig. 3.6; Table 3.4). Transformation of smectite to illite is supported by the presence of ordered interstratified expandable layers R0 to R3 in the studied samples. Hence, mud breccia may involve an admixture of sediments from shallow strata formed at lower diagenetic grades (IS with R0) together with sediments from deeper sources affected by high

diagenetic grades (IS with R3), reaching, under these severe conditions, maximum temperatures ranging from 120°C to 160°C.

Our results are in line with seismic and tectonic data. In view of the regional thermal gradient of about 25 °C/km for the West Alboran Basin (Torre and Fernández, 2000) we might expect that the source of the mud breccias is located at a maximum depth of 4-6 km beneath the MVs. Considering a prograding burial sequence at this depth, the mud breccia matrices from the Alboran MVs may have suffered severe diagenetic conditions, or at least moderate to late stages of diagenesis (Bethke et al., 1986; Lanson et al., 2009, among others) affecting the mineralogy and leading to the release of fluids. This assumption is compatible with the close relationship previously demonstrated between MVs and mud diapirs in the

WAB (i.e., Talukder et al., 2003; Soto et al., 2010; Comas et al., 2012). The proposed origin for the extruded mud breccias from a deep source (in the lowermost strata of the basin infill; Talukder et al., 2003; Soto et al., 2010; Comas et al., 2012), together with the sedimentary lithology of these lowermost units (pressurized olistostromic deposits embedded in an under-compacted shale-rich matrix; Talukder, 2003; Comas et al., 2010, 2012; Soto et al., 2012), constitute favorable conditions for the processes of clay mineral dehydration and the subsequent generation of fluids (Dählmann and de Lange, 2003) under a relatively well defined range of temperatures ($\sim 80^{\circ}$ to $\sim 150^{\circ}$ C) close to oil generation (Kastner et al., 1991).

Consequently, our findings constitute mineralogical evidence of a progressive smectite illitization process that takes place at depth within the source strata feeding MVs. The data corroborate the occurrence of important mineral transformation under severe conditions of late diagenesis, and demonstrate the presence of IS mixed layers having high illite content.

3.7 Conclusions

Though most of the MVs described to date in the WAB are dormant, one active volcano (Carmen, cruise TTR-17) and several pockmarks have been recognized. There is diverse evidence their recent activity, including the absence of hemipelagic drapes and gas bubbling. At the same time, the presence of interbedded hemipelagic sediments between mud breccia indicate periods of quiescence between events of mud expulsion. Thus, hemipelagic sediments and drapes allowed us to date eruptions from 0.7 to 10.8 ka BP, at Marrakech at Carmen MVs, respectively). Past and presently active hydrocarbon-rich fluid venting is further evidenced by the precipitation of authigenic carbonates as crust and chimneys.

The relative homogeneity and similar mineralogical composition of mud breccia at different MVs suggest a common source feeding these structures, which

corroborates that Units Va and VI, Early to Middle Miocene in age, fed mud diapirs and volcanoes in the WAB. Clay mineral assemblages from mud breccia are particularly rich in smectite and illite, while illite-smectite mixed layers are also recognized, and show a wide range of ordering (from 10% to 95% illite layers). Regular mixed-layers evidencing smectite dehydration suggest that it played a major role in the generation of deep fluids within this basin.

4

**Major and trace elements in
mud-volcano solid phases and
involved sediments from the
West Alboran Basin**

Chapter 4

Major and trace elements in mud – volcano solid phases and involved sediments from the West Alboran Basin

Abstract

The inorganic geochemical composition of mud breccias and other volcanic-related sediments provides relevant information about the nature of source units feeding and about fluids discharged to the seafloor. In the mud volcano province of the West Alboran Sea, major the distribution of trace elements and rare earth elements in mud breccia show considerable homogeneity, which suggests a common source and comparable material feeding the diverse volcanoes within this province. Volcanic activity does not significantly impact the composition of hemipelagic sediments covering or intercalated in mud breccia except for sediment mixing at the boundaries between hemipelagic and extruded sediments. Redox sensitive elements (i.e, Mo, S) and those associated with authigenic carbonates (i.e. Sr and Mg) serve as proxies elucidating past activity so as to reconstruct ancient pulses of methane seepage and paleo-sulfate-methane transition zones. Extremely $\delta^{13}\text{C}$ -depleted values (-38.21‰ VPDB) of authigenic carbonates from a chimney encountered at one core in the Crow pockmark field confirm microbial sulfate reduction and anaerobic oxidation of methane. The correlations between $\text{Ce}_{\text{anomaly}}$ and LaN/SmN , $\text{Ce}_{\text{anomaly}}$ and DyN/SmN , $\text{Ce}_{\text{anomaly}}$ and $\sum\text{REE}$ moreover reveal that the REE signatures are preserved, while those from authigenic carbonates reflect the original signature of fluids.

4.1 Introduction

The geochemical composition of extruded mud breccias from mud volcanoes (MVs) results from complex interactions of sediments, rocks and fluids. Ascending muds can also incorporate sediments and rock fragments from feeder channels (e.g., Akhmanov and Woodside, 1998), thereby masking the original geochemical signature of source units. Diverse geochemical proxies can be used, however, to infer source and provenance, and detect the contribution of sediment successions pierced by ascending muds (Akhmanov, 1996; Kopf et al., 2000; Akhmanov et al., 2003; Sautkin et al., 2003; Lykousis et al., 2009).

At the seafloor, the discharge of fluids also involves significant reactions that determine the geochemical signature of MV-related sediments. When hydrocarbon-rich fluids reach the seafloor and encounter seawater sulfate, authigenic minerals precipitate (Hinrichs et al., 1999; Boetius et al., 2000; Michaelis et al., 2002), forming crusts, chimneys or concretions (i.e., Magalhães et al., 2012 and references therein), and even mineral fronts (i.e., Aloisi et al., 2000; Dickens, 2001; Peckmann and Thiel, 2004; Riedinger et al., 2006; Peketi et al., 2012; Pierre et al., 2014; among others).

In the western Mediterranean, studies based on the organic content of clasts and rock fragments approach the origin of mud flows in the Alboran MVs (Poludetkina and Kozlova, 2003; Poludetkina et al., 2008). The provenance of mud breccia matrices is addressed by specific micropalaeontological studies (Gennari et al., 2013) and organic geochemical determinations based on lipid biomarkers (López-Rodríguez et al., 2014). Yet there is less documentation regarding MV sediments in the Alboran Sea, whose geochemistry is also essential for an understanding of the complex interactions of fluid and solid phases in volcano settings. This research therefore focuses on the inorganic geochemistry (major and trace elements, rare earth elements, isotopes) of core

sediments and associated authigenic carbonates recovered from the mud volcano province of the West Alboran Basin (WAB). Geochemical investigations complement previous studies based on sedimentological and mineralogical studies to shed new light on mud/fluid ejection activity and the biogeochemical processes underlying authigenic carbonate formation. In addition to discerning the nature and origin of mud breccias, this information will help to constrain recent and ancient pulses of mud activity.

4.2 Geological Background

The Alboran Sea is a marginal basin placed in the westernmost Mediterranean Sea, in the inner part of the Gibraltar Arc. Several ridges and seamounts on the Alboran seafloor contribute to the complex configuration of the seabed morphology, dividing Alboran in three sub-basins: Western (WAB), Southern (SAB) and Eastern Alboran Basin (EAB) (Fig. 4.1).

Geological and geophysical data have constrained the complex geodynamic evolution of the Alboran Basin, and the timing and tectonic regime of Basin evolution (Fig. 1.6) (Comas et al., 1992, 1999; Soto et al., 1996; Rodríguez-Fernandez et al., 1999). Multichannel seismic profiles from well-logging indicate an irregular sedimentary infill in Alboran Basin; the thickest sedimentary depocentre is in the WAB, where more than 7-8 km of sediments from the Early Miocene to Present accumulated on top of the metamorphic basement (Fig.1.6 and Fig.1.8; Jurado and Comas, 1992; Comas et al., 1996,1999; De la Linde et al., 1996; Soto et al., 1996; and references therein).

Comprehensive lithology, biostratigraphy and logging data from the basement and sedimentary sequence beneath the Alboran Sea are known from commercial wells Andalucía-G1 and Alboran-A1, and ODP Leg 161 drilling (Fig.1.7; Comas et al., 1996, 1999 and references therein). These data allow one to distinguish six major seismo-

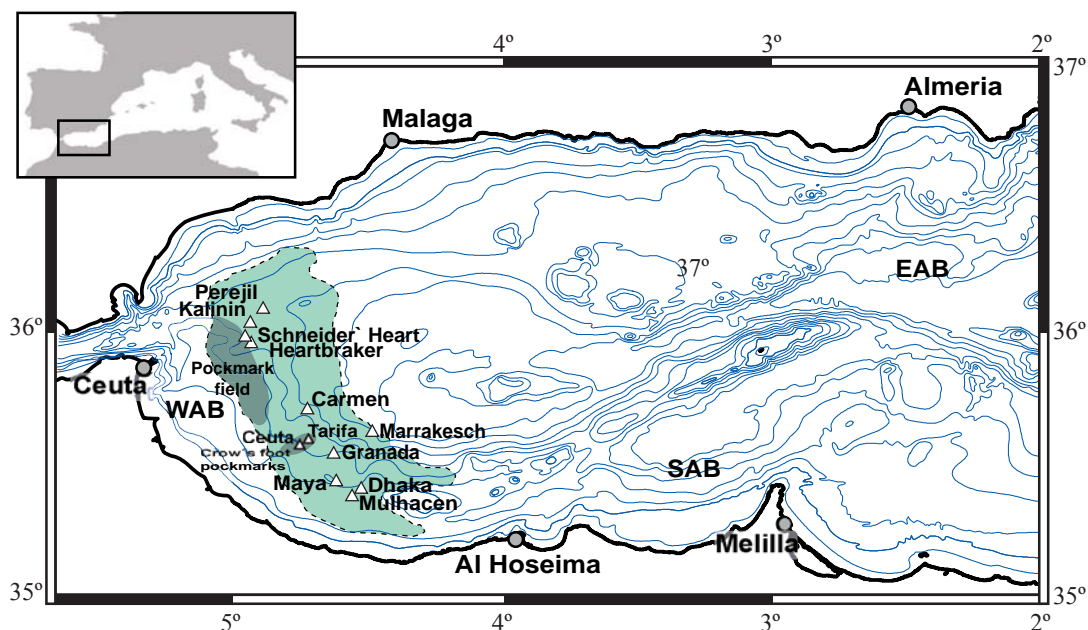


Figure 4.1. The Alboran Sea Basin showing the location of the Mud Diapir Province, the West, South and Eastern Alboran Basins. White triangles correspond with MVs; green areas refer to pockmark fields. Modified after Comas et al., (1999)

stratigraphic units within the WAB sedimentary infill (Fig. 1.7; Comas et al., 1992; Jurado and Comas, 1992). Borehole sampling indicates that the basal units (Unit VI and lowermost Unit V) overlie a metamorphic basement. Unit VI (Burdigalian in age) mainly consists of undercompacted (pressurized) shales and olistostromic/brecciated lithologies containing heterogeneous rock fragments (blocks, boulders and clasts) of different ages, whereas Unit Va (Langhian in age) contains under-compacted green clays. Sonic logging demonstrated that both units encompass significant gas and fluid content, implying major overpressure at depth (Jurado and Comas, 1992; Diaz-Merino et al., 2003).

In the WAB, significant shale diapirism affects the undercompacted materials from Unit VI and Unit Va. It extends from the Iberian peninsula to the Moroccan margins as a huge Mud Diapir Province (MDP; Fig.1.8), where mud volcanoes and pockmarks develop (i.e. Comas et al., 1999, 2012; Soto et al., 2010).

Seismic profiles show that volcano feeder-channels connected to deeper shale-diapirs bring up to the seafloor over-pressured shales and olistostromes/megabreccias from Unit VI and/or over-pressured green clays from Unit Va, at a depth of over 5 km (Fig. 4.2; Talukder et al., 2003; Comas et al., 2012).

Episodes of mud volcanism in the WAB are associated with recent stages of shale mobilization from the underlying diapiric structures; compressive tectonics conditioned pierced diapirs and subsequent mud volcanism at the seafloor (Comas et al., 2010; and references therein). Furthermore, Somoza et al. (2012) associate some mud volcanism stages to erosional episodes during major sea-level falls (Plio-Quaternary, from 4-5 Ma onwards).

4.3. Core sediment and sampling

The sediment cores selected for geochemical determinations were collected during three oceanographic cruises performed within the framework of the UNESCO/IOC Training Through Re-

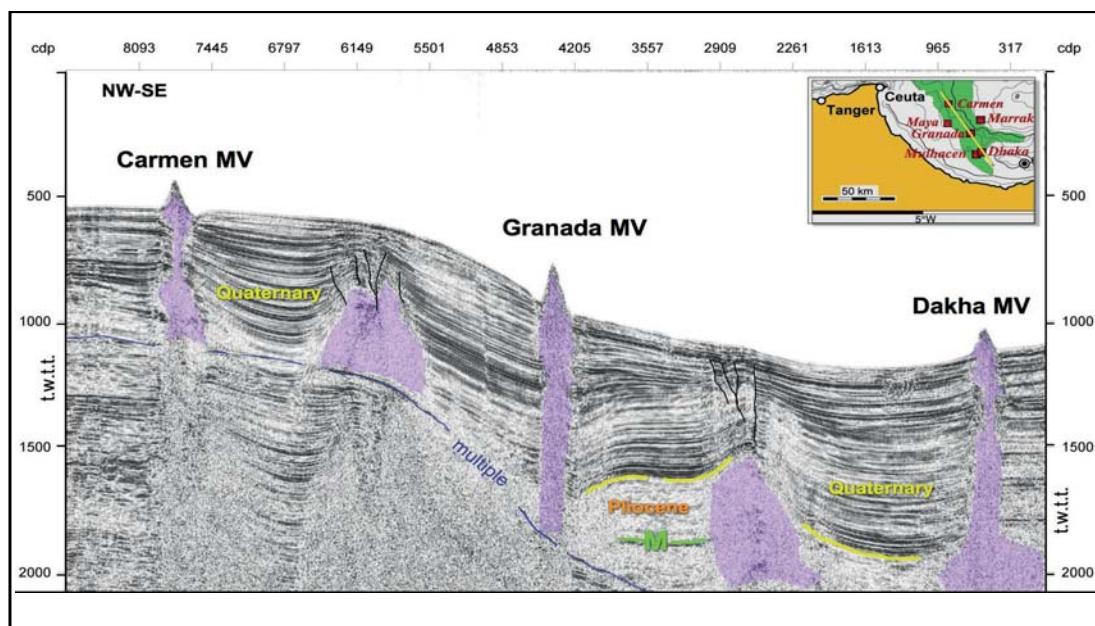


Figure 4.2. Single-channel seismic profile across Carmen, Granada and Dhaka MVs showing seismic stratigraphic units, major regional reflectors and main sedimentary sequence documented in the Betic Neogene basins (modified after Jurado and Comas, 1992; Rodríguez-Fernández et al., 1999); M-Messinian unconformity. Reflectors correspond to major unconformities within sediments; Purple shadow corresponds with overpressure shales and megabreccia. From Comas et al., 2012.

search Programme (TTR). The expeditions TTR-9 BASACALB Cruise (Kenyon et al., 2000), TTR-12 Leg 3, MARSIBAL-1 Cruise (Kenyon et al., 2003) and TTR-17 Leg 1 cruise SAGAS-08 (Ivanov et al., 2010) respectively in 1999, 2002, and 2008, were on board RV Professor Logachev (Fig. 2.1). A total of ten cores were selected, and at least one at each volcano structure. One gravity core was studied at Perejil, Kalinin, Marrakech, Granada, Maya, Dhaka, and Mulhacen MVs, whereas three gravity cores were analyzed at Carmen MV, given its current activity (Table 2.1; Fig. 3.1). Additionally, methane-derived authigenic carbonates (MDAC) recovered from “Crow’s foot” pockmark were also analyzed (Fig. 3.1). For further details about technical specifications and sampling operations during TTR-cruises see *Chapter 3, section 3.3* (Ivanov et al., 1992a, b; Kenyon et al., 2003). Geochemical determinations were performed on the same sediment samples as mineralogical and sedimentological analyses. Thus, the sampling procedure for hemipelagic sediments and mud

breccia matrices determinations was accomplished in the same way for specific geochemical and for mineralogical and sedimentological analyses. Specific details are provided in *Chapter 3.3, section 3.4*.

Geochemical determinations and isotopic composition of MDACs were also determined. Samples were obtained from a seepage chimney and from a carbonate concretion.

4.4. Methods

Major element measurements (Al, Si, Ca, Mg, Fe, K) were obtained by X-Ray Fluorescence (XRF). Powdered sediment samples were prepared as pressed pellets using 5 gr of ground bulk sediment in a briquette with boric acid backing and homogenized in an agate mortar. The pellets were pressed at 130 bars in a Nannetti hydraulic press for 30 s. Samples were analyzed using a commercial wavelength dispersive X-ray fluorescence instrument (Bruker AXS S4 Pioneer) with an analytical error of 2% and equipped with a Rh

anode X-ray tube (60 Kv and 150 mA).

Trace and rare earth elements (REEs) were analyzed using Inductively Coupled Plasma-Mass Spectrometry (ICP-MS). Samples were prepared by sequential acid digestion with HNO₃ and HF. First, 100 mg of the powder sample was dissolved in 2 ml of HNO₃, and after reaction, 3 ml of HF. The resultant dilution was heated until total evaporation and then re-dissolved in 1 ml of HNO₃ two times. The final residue was dissolved in 4 ml of HNO₃+ 96 ml of ultrapure water; 1 ml of this dissolution was mixed with 0.5 ml of a 200 ppb Rh dilution (internal standard) and 8.5 ml of ultrapure water. Measurements were taken in triplicates via Perkin-Elmer Sciex Elan 5000 spectrometry at the Analytical Facilities of the University of Granada (CIC-UGR). A blank standard prepared with the same sample procedure was intercalated to monitor analytical quality. The instrumental error is $\pm 2\%$ and $\pm 5\%$ for elemental concentrations of 50 ppm and 5 ppm, respectively (Bea, 1996).

Additionally, selected core sediments from Carmen MV were analyzed using the ITRAX Core Scanner. The analytical procedure was based on the standard guidelines for ITRAX studies defined by Rodríguez-Germade et al., (2015) for typical mud volcanic deposits; thus, 2 cm diameter U-channel cores were extracted from each core and analyzed at the University of Vigo. For XFR determinations, u-channel cores were covered with protective film transparent in order to avoid desiccation during X-ray analysis. The analyses were performed with Mo-tubes using an exposure time of 20 s, voltage 45 kv, and current of 55 mA. Preliminary results were evaluated applying the criteria of Cuven et al. (2007), which consider the percentage of XRF values as equal to zero, and fitting a normal distribution of XRF values (Rodríguez-Germade et al., 2015).

On selected samples, Total Carbon (TC), Total Inorganic Carbon (TIC) and Total Nitrogen (TN) were measured by means of a CHN analyzer in separate portions of air-dried sediment samples

using a LECO CNS-Tru Spec analyzer. Total Organic Carbon (TOC) was calculated by subtracting the amount of inorganic carbon from the total carbon content.

Isotopic carbon and oxygen composition of MDAC samples were analyzed at the stable isotope laboratory of the Marine Geology group (Marum, Bremen University) and also at the Leibniz-Laboratory for Radiometric Dating and Isotope Research (Kiel University). Samples for stable isotopic analyses were prepared by reacting at 90°C with 100% phosphoric acid on an automated carbonate device connected to a VG-PRISM mass spectrometer calibrated with NBS19, NBS 18 and NBS 20. The results are reported in the conventional δ ‰-notation with reference to VPDB (Vienna Peedee Belemnite). Analytical reproducibility of the method, based on repeated standards, is better than $\pm 0.1\%$ for both carbon and oxygen.

4.5. Elemental ratios

In this work major and trace element concentrations were normalized to Al. As bulk elemental concentrations may be subjected to large fluctuations caused by variable proportions of biogenic versus detrital minerals, instead normalized concentrations are normally considered in geochemical investigations of marine sediments. Diverse refractory elements were used for normalization (e.g., Calvert and Pedersen, 2007), though this calls for caution when the detrital fraction content is very low (e.g., van der Weijden, 2002; Tribouillard et al., 2006). Yet when the detrital contribution is high, as in the Mediterranean, Al may be considered as a good indicator of the terrigenous aluminosilicate sediment fraction and it generally behaves conservatively. Al-normalized concentrations are therefore considered here as a useful tool to illustrate geochemical variations in element concentrations.

The amount of CaCO₃ (%) was calculated from

the total Ca concentration (Ca_{tot}) with a correction for the Ca inventory supported by the detrital component:

$$CaCO_3 (\%) = 2.5 [Ca_{tot} - (Al_{tot} * Ca / Al_{average\ shale})]$$

Where $Ca / Al_{average\ shale}$ values is 0.276.

REEs were also normalized to the Post Archean Australian Shales (PAAS) as reference standards (Taylor and McLennan, 1985). This eliminates the abundance variation between lanthanides of odd and even atomic numbers, producing curves or REE patterns where subtle REE enrichments or depletions are readily apparent. The method is also useful because Post Archean Australian Shales are thought to be compositionally similar to the upper continental crust (Taylor and McLennan, 1985). Diverse REE-ratios were additionally considered in order to assess environmental redox conditions during carbonate precipitation (Feng et al., 2009, 2013; Himmler et al., 2010; Hu et al., 2014; Wang et al., 2014; among others).

The Ce anomalies were derived from calculation of the logarithm of the ratio of shale-normalized Ce contents with respect to the value obtained by interpolation between shale-normalized La and Pr, as follows:

$$Ce/Ce^* = Ce_n / (La_n^{1/2} \times Pr_n^{1/2}) \quad (1)$$

Eu anomalies were calculated using the equation suggested by Taylor and McLennan (1985), calculating the logarithm of the ratio of shale-normalized Eu content with respect to the value obtained by interpolation between shale-normalized Sm and Gd.

$$Eu/Eu^* = Eu_n / (Sm_n \times Gd_n)^{1/2} \quad (2)$$

The subscript "n" represents shale-normalized REEs

4.6. Results

4.6.1. Geochemical composition

Hemipelagic drapes

Major and trace element ratios from hemipelagic sediments are listed in Table 4.1. Sediments were

characterized by high amounts of SiO_2 varying between 39% as the average value at Marrakech (MS262G) to 47% at Mulhacen MV (MS414G) (Table 4.1). Sediments showed moderate carbonate content: from 10% to 31% on average, respectively at drapes from Mulhacen (MS414G) and Dhaka (MS285G) MVs. Similar mean values for selected detrital/Al ratios (Mg/Al, K/Al, Rb/Al, Ti/Al and Zr/Al) were observed at all sites (Table 4.1).

Mud breccia

As a general estimate of mud breccia matrix composition and possible differences, Al, Si and Ti contents are represented in ternary diagrams. The detrital ternary plot ($Al_2O_3+TiO_2 - SiO_2 - Fe_2O_3$) revealed very similar compositions for all the extruded samples (Fig.4.3a). Data are plotted in a well-defined cluster, characterized by moderate values of $Al_2O_3+TiO_2$ (30%), high SiO_2 values (65%), and very low Fe_2O_3 content (5%).

The $MgO+CaO - SiO_2 - Al_2O_3+Fe_2O_3$ ternary plot (Fig. 4.3b) showed high SiO_2 content (55%), and moderate $MgO+CaO$ (15%) and $Al_2O_3+Fe_2O_3$ (25%) values, correspondingly. Nevertheless, slight variations in $MgO+CaO$ content point to two different tendencies. The mud breccia matrices from Carmen (MS385G, MS386G and MS390G), Perejil (MS283G), Granada (MS258G) and Mulhacen (MS414G) MVs showed constant values, describing a well-defined cluster data. In turn, the carbonate content of the mud breccia samples from Marrakech (MS262G), Kalinin (MS280G), Dhaka (MS285G) and Maya (MS419G) MVs displays significant $MgO+CaO$ variations, the mud breccias from Marrakech MV (MS262G) showing the highest $MgO+CaO$ content (15% on average), whereas those from Mulhacen MV (MS414G) gave the lowest content (6% on average).

Regarding depth profiles (Fig.4.4a), mud breccia intervals from Maya, Carmen and Marrakech MVs show fluctuations in the Ca distribution —it decreases in Maya MV, is relatively constant in Carmen MV, and increases at Marrakesh MV (Fig. 4.4a).

Table 4.1. Mean values and variation range of geochemical proxies for hemipelagic and mud breccia samples at the studied cores. Major elements are given in wt% and trace elements are given in mg kg⁻¹. Reference Site MS293G data from Rodrigo-Gámiz et al., (2011). Hemipelagic sediments

	Perejil MV (MS283G)			Kalinin MV (MS280G)			Carmen MV (MS385G)			Carmen MV (MS386G)			Carmen MV (MS390G)		
	Mean	Max	Min	Mean	Max	Min	Mean	Max	Min	Mean	Max	Min	Mean	Max	Min
Al ₂ O ₃ (%)	16.3	17.3	13.2	15.7	16.5	14.5	14.2	15.3	13.5	14.6	15.0	14.2	14.8	15.1	14.5
SiO ₂ (%)	44.0	47.0	34.8	43.4	45.4	39.5	42.0	43.5	38.2	44.1	45.0	43.0	44.4	45.2	43.7
CaO (%)	5.3	6.7	4.1	10.3	13.5	8.1	12.3	15.1	10.6	12.0	12.7	11.5	12.2	12.7	11.7
TOC	0.50	0.58	0.43	0.57	0.77	0.38	0.67	0.90	0.38	0.57	0.73	0.44	0.53	0.71	0.35
TN	0.06	0.09	0.04	0.08	0.13	0.04	0.09	0.12	0.06	0.09	0.11	0.08	0.09	0.12	0.06
C/N	8.7	12.2	6.1	7.8	10.9	4.2	7.8	11.9	5.2	6.7	9.6	4.9	5.8	8.0	3.1
Si/Al	2.38	2.42	2.32	2.43	2.47	2.38	2.62	2.76	2.41	2.67	2.70	2.64	2.66	2.70	2.62
Ti/Al	0.053	0.058	0.050	0.053	0.056	0.050	0.053	0.055	0.051	0.053	0.054	0.051	0.054	0.056	0.052
Zr/Al	16.6	19.2	15.0	17.2	18.5	16.1	19.3	22.2	18.3	17.2	18.0	16.6	18.1	19.7	17.2
Mg/Al	0.16	0.16	0.14	0.18	0.19	0.17	0.18	0.20	0.17	0.16	0.20	0.16	0.16	0.17	0.15
K/Al	0.24	0.26	0.22	0.24	0.27	0.22	0.26	0.29	0.25	0.24	0.25	0.23	0.24	0.25	0.23
Fe/Al	0.51	0.56	0.47	0.49	0.54	0.47	0.48	0.52	0.46	0.48	0.49	0.46	0.48	0.51	0.47
Ba/Al x10e-3	27.33	36.97	23.37	24.87	30.04	17.91	34.95	64.25	26.20	33.69	45.62	22.37	31.94	37.73	27.36
Mn/Al x10e-3	98.05	230.90	66.54	63.73	101.63	49.51	57.82	89.92	36.27	91.24	113.02	80.64	87.00	108.20	75.16
Mo/Al x10e-4	0.26	0.51	0.12	0.24	0.43	0.08	0.73	2.27	0.11	0.39	1.57	0.24	0.32	0.44	0.27
U/Al x10e-4	0.26	0.34	0.21	0.26	0.30	0.22	0.48	0.73	0.30	0.30	0.63	0.21	0.26	0.31	0.24
V/Al x10e-4	18.1	22.0	16.5	15.4	17.0	14.2	13.0	15.7	10.9	15.1	17.6	11.8	14.7	16.3	13.6
Ni/V	0.28	0.82	0.10	0.40	0.58	0.32	0.41	0.57	0.36	0.35	0.37	0.32	0.35	0.44	0.31
Ce/Ce*	1.03	1.06	1.00	1.00	1.02	0.97	0.98	1.01	0.96	0.99	1.05	0.97	0.99	1.01	0.96
Ce anomaly	-0.13	-0.16	-0.10	-0.16	-0.19	-0.14	-0.18	-0.20	-0.15	-0.17	-0.19	-0.11	-0.17	-0.20	-0.15
Rb/Al x10e-4	11	15	10	10	13	9	11	13	10	10	11	8	10	12	10
ΣREE/Al x10e-4	18.8	22.9	17.4	16.5	17.7	15.7	19.8	21.7	18.0	17.8	20.1	13.6	17.4	19.7	16.5
Eu/Eu*	0.72	0.77	0.63	0.70	0.74	0.65	0.72	0.81	0.66	0.71	0.79	0.67	0.71	0.77	0.67
La/Sc	3.3	10.2	2.1	2.0	2.2	1.7	3.1	4.1	2.4	2.0	2.4	1.3	2.3	2.9	1.9
Th/Sc	0.91	2.90	0.57	0.58	0.64	0.49	0.92	1.23	0.66	0.59	0.72	0.39	0.66	0.81	0.54
LaN/YbN	9.8	10.8	8.1	10.1	11.0	9.1	9.6	10.7	8.0	9.7	11.4	8.4	10.3	11.1	9.1
LaN/SmN	3.6	3.9	3.3	3.4	3.8	3.2	3.3	3.5	3.1	3.4	3.7	3.2	3.5	3.7	3.2

Table 4.1. Hemipelagic sediments (cont.)

	Marrakech MV (MS262G)			Granada MV (MS258G)			Maya MV (MS419G)			Dhaka MV (MS285G)			Mulhacen MV (MS414G)		
	Mean	Max	Min	Mean	Max	Min	Mean	Max	Min	Mean	Max	Min	Mean	Max	Min
Al ₂ O ₃ (%)	15.4	18.5	11.7	16.0	16.4	15.7	16.9	18.5	15.1	16.4	17.6	11.9	18.0	19.1	16.8
SiO ₂ (%)	39.1	44.3	34.7	44.5	45.8	43.7	41.6	44.9	39.3	45.9	48.8	35.9	48.5	51.2	45.9
CaO (%)	12.6	19.2	6.5	8.3	9.0	7.6	5.5	9.5	2.0	7.7	17.7	5.1	4.8	5.9	3.4
TOC	0.63	0.70	0.56	0.45	0.50	0.41	0.60	0.64	0.54	0.50	0.67	0.41	0.49	0.55	0.41
TN	0.07	0.10	0.06	0.06	0.08	0.04	0.05	0.07	0.04	0.07	0.10	0.06	0.08	0.09	0.07
C/N	9.0	10.7	6.9	7.7	11.1	6.6	12.2	14.4	8.3	7.4	10.4	3.9	6.1	7.3	4.7
Si/Al	2.26	2.61	2.05	2.45	2.49	2.41	2.25	2.52	2.04	2.47	2.66	2.42	2.39	2.47	2.34
Ti/Al	0.051	0.054	0.048	0.058	0.060	0.055	0.055	0.059	0.048	0.055	0.057	0.053	0.055	0.056	0.054
Zr/Al	15.3	18.9	13.8	15.4	16.3	14.5	15.2	17.2	12.9	16.2	21.5	14.9	14.2	15.2	13.7
Mg/Al	0.19	0.26	0.14	0.17	0.18	0.17	0.14	0.18	0.10	0.16	0.23	0.15	0.14	0.15	0.13
K/Al	0.22	0.26	0.18	0.20	0.22	0.19	0.19	0.21	0.18	0.21	0.26	0.20	0.19	0.21	0.19
Fe/Al	0.50	0.55	0.48	0.53	0.56	0.51	0.52	0.64	0.46	0.50	0.61	0.45	0.50	0.54	0.47
Ba/Al x10e-3	16.93	27.32	11.87	20.45	24.60	16.88	48.19	81.03	33.88	29.44	107.36	15.04	17.14	29.94	13.13
Mn/Al x10e-3	63.65	135.52	40.59	61.85	81.08	46.64	58.10	83.75	40.35	49.84	60.37	44.69	57.51	89.70	49.11
Mo/Al x10e-4	2.61	6.14	0.22	1.06	1.35	0.46	0.65	2.11	0.20	0.38	1.56	0.16	0.81	1.09	0.38
U/Al x10e-4	0.77	1.52	0.30	0.44	0.57	0.32	0.34	0.53	0.25	0.25	0.45	0.16	0.35	0.50	0.23
V/Al x10e-4	17.2	19.5	15.4	19.1	20.8	18.1	16.0	17.0	14.7	18.7	20.0	17.0	17.2	18.3	16.2
Ni/V	0.30	0.37	0.25	0.26	0.27	0.25	0.30	0.39	0.25	0.29	0.54	0.24	0.26	0.42	0.24
Ce/Ce*	1.00	1.02	0.98	0.99	1.00	0.97	1.00	1.01	0.99	1.00	1.02	0.98	1.01	1.02	1.00
Ce anomaly	-0.16	-0.18	-0.14	-0.17	-0.19	-0.16	-0.16	-0.17	-0.15	-0.16	-0.18	-0.14	-0.15	-0.16	-0.14
Rb/Al x10e-4	9	12	8	8	9	8	9	10	7	9	11	8	8	9	8
ΣREE/Al x10e-4	17.2	20.6	15.3	17.0	17.6	16.5	19.2	21.3	17.0	16.3	17.2	14.5	16.8	18.2	15.7
Eu/Eu*	0.72	0.76	0.68	0.74	0.77	0.69	0.76	0.80	0.70	0.70	0.78	0.63	0.75	0.78	0.71
La/Sc	2.1	2.3	1.8	2.3	2.4	2.2	2.6	2.8	2.3	1.8	2.0	1.6	2.2	2.5	2.1
Th/Sc	0.60	0.69	0.54	0.58	0.61	0.54	0.80	0.86	0.70	0.50	0.54	0.41	0.60	0.66	0.56
La/YbN	10.5	11.1	9.8	11.1	11.6	10.5	10.5	11.2	10.3	11.6	12.9	9.7	11.4	13.0	9.5
LaN/SmN	3.4	3.6	3.3	3.6	3.8	3.3	3.2	3.3	3.1	3.6	3.7	3.4	3.5	3.7	3.2

Table 4.1. Mud breccia (cont.)

	Reference Site (MS293G)				Pereiji MV (MS283G)				Kalinin MV (MS280G)				Carmen MV (MS385G)			
	Mean	Max	Min		Mean	Max	Min		Mean	Max	Min		Mean	Max	Min	
Al ₂ O ₃ (%)	12.5	13.7	10.7		16.6	16.6	16.6		15.7	17.0	13.9		14.3	15.2	13.1	
SiO ₂ (%)	34.1	36.8	30.6		44.1	44.1	44.1		41.0	43.6	37.4		40.9	41.8	39.8	
CaO (%)	16.6	20.5	13.1		6.3	6.3	6.3		11.2	15.0	8.3		11.3	12.8	10.1	
TOC	-	-	-		-	-	-		0.75	0.91	0.48		0.56	0.66	0.48	
TN	-	-	-		-	-	-		0.10	0.13	0.08		0.10	0.11	0.09	
C/N	-	-	-		-	-	-		7.2	9.4	5.2		5.9	6.0	5.6	
Si/Al	2.42	2.53	2.31		2.35	2.35	2.35		2.32	2.40	2.25		2.53	2.72	2.40	
Ti/Al	0.046	0.048	0.044		0.059	0.059	0.059		0.050	0.052	0.049		0.053	0.054	0.051	
Zr/Al					19.8	19.8	19.8		16.5	17.8	15.6		18.9	19.4	18.4	
Mg/Al	0.24	0.27	0.22		0.15	0.15	0.15		0.17	0.19	0.15		0.18	0.19	0.17	
K/Al	0.31	0.32	0.29		0.26	0.26	0.26		0.27	0.28	0.26		0.27	0.27	0.26	
Fe/Al	0.50	0.57	0.47		0.58	0.58	0.58		0.48	0.51	0.47		0.49	0.50	0.48	
Ba/Al x10e-3	39.88	41.90	37.91		29.03	29.03	29.03		30.46	32.26	28.26		32.51	36.11	26.52	
Mn/Al x10e-3	136.19	1192.28	55.43		89.93	89.93	89.93		49.32	199.50	36.40		58.13	75.56	42.01	
Mo/Al x10e-4	0.13	1.08	0.06		0.15	0.15	0.15		0.09	0.20	0.06		0.22	0.39	0.12	
U/Al x10e-4	0.34	0.49	0.22		0.23	0.23	0.23		0.25	0.35	0.20		0.30	0.32	0.28	
V/Al x10e-4	15.0	15.7	14.2		17.3	17.3	17.3		14.7	16.1	13.4		13.5	15.9	11.4	
Ni/V	0.56	0.81	0.48		0.30	0.30	0.30		0.51	0.64	0.44		0.39	0.40	0.36	
Ce/Ce*	0.97	1.00	0.94		1.01	1.01	1.01		0.98	1.02	0.96		0.99	0.99	0.98	
Ce anomaly	-0.19	-0.22	-0.16		-0.15	-0.15	-0.15		-0.18	-0.20	-0.14		-0.17	-0.18	-0.17	
Rb/Al x10e-4	15	16	14		12	12	12		12	13	10		11	12	11	
ΣREE/Al x10e-4	18.5	19.2	17.3		18.2	18.2	18.2		15.8	17.1	14.1		19.8	20.5	19.2	
Eu/Eu*	0.68	0.72	0.61		0.76	0.76	0.76		0.71	0.76	0.66		0.70	0.72	0.68	
La/Sc	2.3	2.5	2.2		2.6	2.6	2.6		2.0	2.2	1.8		3.0	3.3	2.5	
Th/Sc	0.75	0.82	0.71		0.75	0.75	0.75		0.58	0.64	0.52		0.87	1.02	0.68	
LaN/YbN	11.2	12.1	9.3		10.1	10.1	10.1		10.5	11.6	9.3		9.6	10.2	9.4	
LaN/SmN	3.4	3.6	3.2		3.6	3.6	3.6		3.6	3.8	3.4		3.3	3.4	3.2	

Table 4.1. Mud breccia (cont.)

	Marrakech MV (MS262G)			Granada MV (MS258G)			Maya MV (MS419G)			Dhaka MV (MS285G)			Mulhacen MV (MS414G)		
	Mean	Max	Min	Mean	Max	Min	Mean	Max	Min	Mean	Max	Min	Mean	Max	Min
Al ₂ O ₃ (%)	15.5	15.8	15.0	16.0	16.4	15.7	14.6	16.3	11.6	12.2	13.5	10.9	17.3	17.3	17.3
SiO ₂ (%)	39.0	40.0	38.0	42.3	42.5	41.9	40.6	42.7	38.2	34.8	36.7	32.6	47.3	47.3	47.3
CaO (%)	11.9	12.9	10.6	10.1	10.4	9.7	12.2	15.0	8.9	17.8	21.0	15.1	5.8	5.8	5.8
TOC	0.68	0.80	0.54	0.50	0.63	0.34	0.80	0.90	0.62	0.60	0.79	0.31	-	-	-
TN	0.09	0.11	0.06	0.08	0.11	0.05	0.10	0.13	0.06	0.09	0.13	0.05	-	-	-
C/N	7.7	8.3	6.6	6.2	6.7	5.7	8.4	10.6	5.8	6.6	9.9	4.9	-	-	-
Si/Al	2.23	2.24	2.21	2.33	2.38	2.26	2.46	2.99	2.29	2.53	2.69	2.32	2.41	2.41	2.41
Ti/Al	0.050	0.051	0.049	0.055	0.058	0.053	0.053	0.059	0.049	0.053	0.056	0.050	0.056	0.056	0.056
Zr/Al	15.2	16.1	14.7	15.8	16.7	15.3	17.9	22.5	16.0	21.2	24.0	16.5	15.2	15.2	15.2
Mg/Al	0.18	0.18	0.17	0.16	0.17	0.16	0.19	0.24	0.16	0.22	0.25	0.17	0.15	0.15	0.15
K/Al	0.25	0.27	0.23	0.24	0.26	0.23	0.28	0.30	0.26	0.28	0.29	0.26	0.21	0.21	0.21
Fe/Al	0.48	0.50	0.44	0.55	0.60	0.52	0.54	0.82	0.49	0.54	0.68	0.47	0.53	0.53	0.53
Ba/Al x10e-3	23.27	33.21	15.87	23.83	28.14	20.58	35.30	52.12	31.04	43.54	234.88	28.93	18.42	18.42	18.42
Mn/Al x10e-3	47.96	64.75	37.84	48.38	55.46	33.14	44.79	73.55	34.85	38.43	63.77	29.11	60.05	60.05	60.05
Mo/Al x10e-4	0.85	2.20	0.19	0.16	0.20	0.12	0.21	1.74	0.09	0.09	0.16	0.06	0.59	0.59	0.59
U/Al x10e-4	0.50	0.72	0.30	0.22	0.27	0.19	0.34	0.52	0.24	0.35	0.47	0.24	0.33	0.33	0.33
V/Al x10e-4	17.4	19.5	15.7	17.4	18.6	15.7	13.3	14.4	10.5	14.8	17.0	13.4	17.3	17.3	17.3
Ni/V	0.33	0.37	0.28	0.29	0.34	0.27	0.55	0.69	0.48	0.65	0.80	0.47	0.26	0.26	0.26
Ce/Ce*	0.99	1.01	0.95	0.99	1.01	0.97	0.98	1.00	0.96	0.97	1.00	0.96	1.00	1.00	1.00
Ce anomaly	-0.17	-0.21	-0.15	-0.17	-0.19	-0.15	-0.18	-0.20	-0.16	-0.19	-0.20	-0.16	-0.16	-0.16	-0.16
Rb/Al x10e-4	11	13	9	10	11	9	12	13	10	12	13	10	9	9	9
ΣREE/Al x10e-4	17.4	20.5	16.3	16.3	16.9	15.7	16.9	18.2	13.9	16.2	17.5	15.3	16.9	16.9	16.9
Eu/Eu*	0.71	0.73	0.68	0.74	0.78	0.69	0.72	0.77	0.67	0.71	0.87	0.66	0.72	0.72	0.72
La/Sc	2.0	2.4	1.9	2.1	2.3	2.0	2.3	2.4	2.0	2.0	2.2	1.7	2.1	2.1	2.1
Th/Sc	0.59	0.67	0.55	0.58	0.60	0.54	0.70	0.74	0.59	0.54	0.63	0.45	0.58	0.58	0.58
LaN/YbN	10.9	11.9	10.1	11.2	12.1	9.8	10.9	11.6	10.0	10.7	11.6	9.5	11.1	11.1	11.1
LaN/SmN	3.5	3.7	3.3	3.5	3.6	3.4	3.3	3.5	3.1	3.5	3.7	3.3	3.5	3.5	3.5

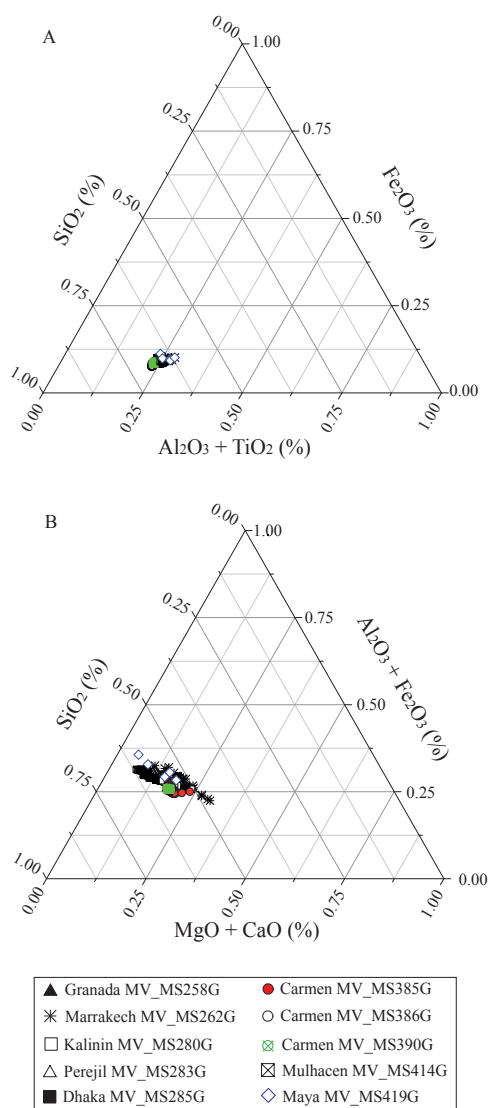


Figure 4.3. Ternary plots showing (a) major element composition $\text{SiO}_2 - \text{Al}_2\text{O}_3 + \text{Fe}_2\text{O}_3 - \text{MgO}$ and (b) detrital composition $\text{SiO}_2 - \text{Fe}_2\text{O}_3 - \text{Al}_2\text{O}_3 + \text{TiO}_2$ in mud breccias from the studied cores

Considering the estimation of calcium carbonate content calculated from the CaO (%) content, three main groups are distinguished. Mud breccias with up to 20% in average CaCO_3 (Marrakech and Carmen MVs MS262G, MS385G, MS386G and MS390G); between 15% and 20% average CaCO_3 content (Granada and Kalinin MVs; MS258G and MS280G); and mud breccias with less than 15% CaCO_3 content (Perejil, Mulhacen,

Maya, Dhaka; MS283G, MS414G, MS419G and MS285G) (Table 4.2).

Ancient pulses of methane fluxes can lead to authigenic carbonate precipitation within the sediments during AOM processes (e.g., Boetius et al., 2000). To trace the presence of disseminated authigenic carbonate phases within mud breccias we applied the relationship between Mg/Ca vs. Sr/Ca since they are used to distinguish aragonite, high-Mg carbonates, low-Mg calcite and terrigenous fractions in cold seep sediments (Bayon et al., 2007).

Mg/Ca vs. Sr/Ca diagram defined by Bayon et al., (2007) revealed a mixing model between four end-members (aragonite, high Mg-calcite, biogenic calcite and the detrital fraction). In general, Alboran mud breccia samples had comparable Sr/Ca and Mg/Ca values to the high-Mg calcite end-member, with low Sr/Ca and high Mg/Ca ratio values (Table 4.2; Fig. 4.4b). A different trend was described by mud breccia from Maya MV (MS419G), which followed the mixing line between high-Mg calcite and the detrital end-member (Table 4.2; Fig. 4.4b).

Total organic carbon content (TOC) showed relatively similar values at all the analyzed mud breccia samples, varying from 0.45 wt % at Granada MV (MS285G) to 0.67 wt % at Carmen MV flank (MS385G; Table 4.1).

Diagenetic barite (BaSO_4) typically forms at the sulfate-methane transition (SMT; Dickens, 2001), where upward diffusing Barium (Ba^{2+}) from the methane zone meets downward diffusing sulfate. When situated above the present SMT, a barite front from the past will be preserved under the high sulfate concentration. Below the SMT, depletion of sulfate by microbial activity leads to an undersaturation of the pore water with respect to barite, thereby driving its dissolution and remobilization (Torres et al., 1996; Dickens, 2001; Contreras et al., 2013).

Ba/Al enrichment peaks inform about barite

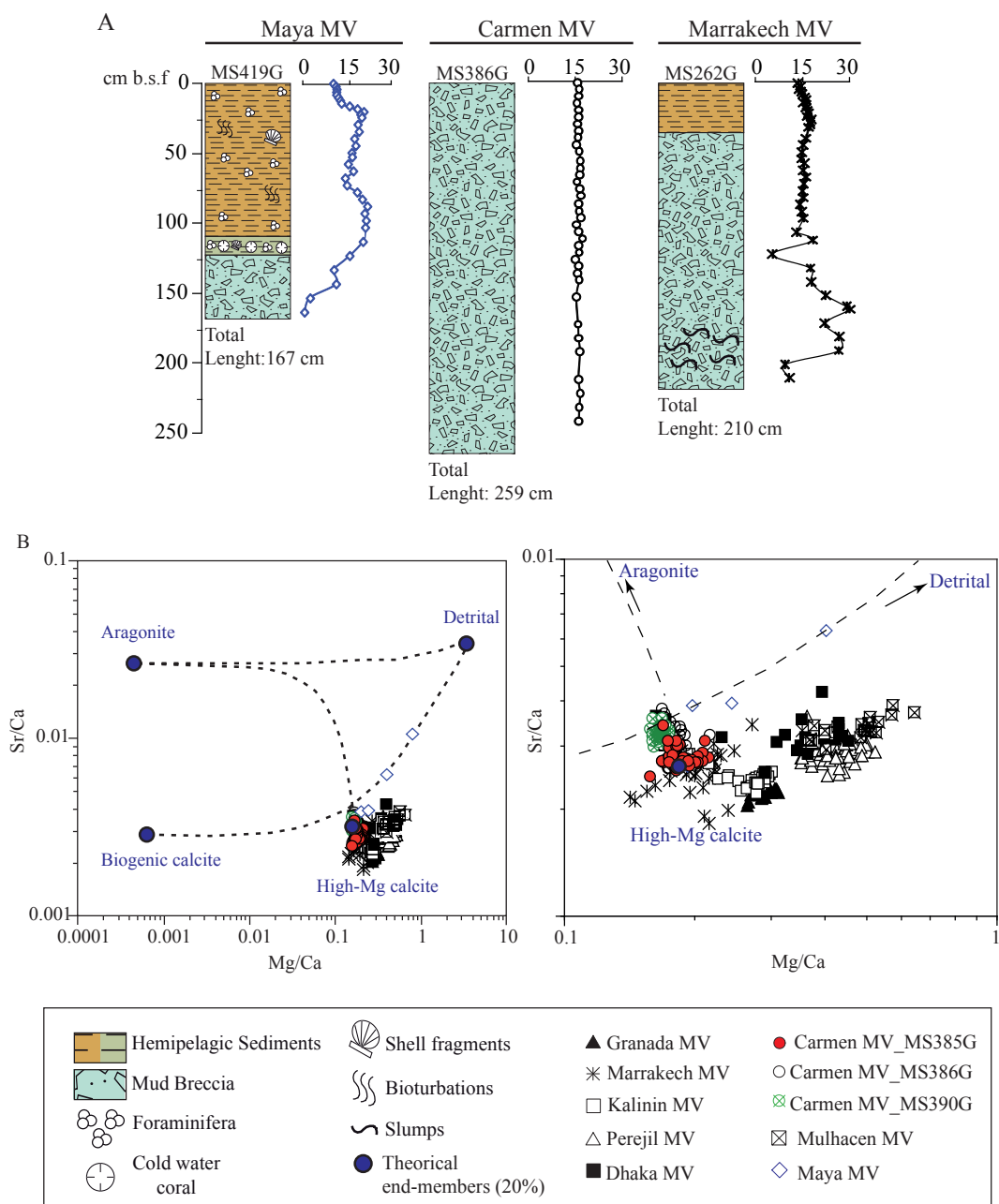


Figure 4.4. (A) Downcore profiles of CaCO_3 at Maya, Carmen and Marrakech MVs, as example of the typical carbonate variations. CaCO_3 is expressed in wt%. (B) End-member carbonate diagram adopted from Bayon et al., (2007) showing the relationship between Sr/Ca and Mg/Ca (wt ratio) at mud breccias. Dashed lines correspond to mixing lines between hypothetical end-members (aragonite, high-Mg calcite, biogenic calcite and detrital)

precipitation within sediments, and are used as paleo-tracers for ancient methane seepage events (Dickens, 2001; Peketi et al., 2012). Our results show that the Ba/Al ratio ranged between 16.9 at Marrakech MV (MS262G) to 48.2 at

Maya MV (MS419G), and only mud breccia from Dhaka MV (MS285G) showed an increase in Ba/Al of almost one order of magnitude (>100 ; Fig. 4.5). Moreover, Mo enrichments in sediments evidence seepage of hydrogen sulphide directly

Table 4.2. Mean values and variation range of CaCO₃ content (wt%) and Mg/Ca and Sr/Ca (wt%) ratios at hemipelagic sediments and mud breccias from the studied MVs

HEMIPELAGIC SEDIMENTS						
Core Code	Mud Volcano	CaCO ₃ (%)			Mg/Ca	Sr/Ca
		Mean	Max	Min		
MS258G	Granada	18.0	18.7	17.2	0.19	0.0034
MS262G	Marrakech	21.2	23.0	18.9	0.29	0.0039
MS280G	Kalinin	11.2	15.0	8.3	0.18	0.0044
MS283G	Perejil	11.3	11.3	11.3	0.30	0.0039
MS285G	Dhaka	31.7	37.5	26.9	0.11	0.0064
MS385G	Carmen	20.2	22.8	18.0	0.17	0.0041
MS386G	Carmen	-	-	-	-	-
MS390G	Carmen	-	-	-	-	-
MS414G	Mulhacen	10.3	10.3	10.3	0.33	0.0045
MS419G	Maya	22.0	26.9	16.0	0.17	0.0044

MUD BRECCIA						
Core Code	Mud Volcano	CaCO ₃ (%)			Mean	Mean
		Mean	Max	Min		
MS258G	Granada	14.8	16.1	13.6	0.24	0.0031
MS262G	Marrakech	22.6	34.2	11.6	0.30	0.0036
MS280G	Kalinin	10.3	13.5	8.1	0.21	0.0036
MS283G	Perejil	9.4	12.0	7.3	0.36	0.0040
MS285G	Dhaka	13.7	31.6	9.2	0.29	0.0045
MS385G	Carmen	22.0	26.9	19.0	0.16	0.0039
MS386G	Carmen	21.5	22.8	20.6	0.15	0.0045
MS390G	Carmen	21.7	22.7	20.9	0.14	0.0045
MS414G	Mulhacen	8.5	10.5	6.0	0.40	0.0050
MS419G	Maya	13.2	21.1	3.6	0.31	0.0060

linked to the discharge of methane fluxes (Peketi et al., 2012). Our data indicate several Mo enhancements in mud breccia intervals from Carmen flank (MS385G) and crater (MS386G), Dhaka (MS285G), Granada (MS258G), Marrakech (MS262G), Mulhacen (MS414G) and Maya (MS419G) (Table 4.1; Fig.4.5).

XFR data from ITRAX Core Scanner correspond to elemental composition based on the integration of the peak areas expressed in count per second rather than in absolute concentrations. Ongoing work focuses on data re-evaluation using the Cox proprietary software Q-Spec 6.5.2. for optimal data quality. In this regard, preliminary data from ITRAX Core Scanner performed at Carmen MV flank (MS385G) revealed significant increases in Ba/Ti and Sr/Ca ratios, which are related to

methane-related authigenic carbonates, at 50-60 cm depth. Moreover, significant sulfur enhancement has been detected down core, at 225 and 235 cm depth (Fig. 4.6).

In terms of REE composition, all the analyzed mud breccias samples display shale-normalized REE patterns describing typical REE distribution with a negative Eu anomaly (Fig. 4.7).

Methane-derived authigenic carbonates (MDAC).

The diverse carbonate facies from the studied concretion and chimney samples showed different major element composition, as revealed by bulk major and detrital element ratios (Table 4.3). Chimney MDAC samples were depleted in Al₂O₃ (0.69) and enriched in CaO (61.47) compared to concretion MDAC sample, which revealed close values to mud breccia matrices (Table 4.3). No large negative Ce anomalies were detected (0.94 < Ce/Ce* < 0.95) (Table 4.3)

There were depleted δ¹³C values varying from -33.20 to -38.21 ‰ VPDB and δ¹⁸O ranged from 2.51 to 3.98 ‰ VPDB (Table 4.4).

4.7. Discussion

4.7.1. Control of fluid venting in hemipelagic drapes

Dormant MVs are characterized by drapes of hemipelagic sediments covering the mud breccias. In the WAB the composition of this pelagic cover is not significantly affected by fluid diffusion, and geochemical compositions are generally similar to those reported from marine pelagic cores recovered in the Alboran Sea (e.g., Martínez-Ruiz et al., 2003; Jimenez-Espejo et al., 2007; Rodrigo-Gámiz et al., 2011). Moreover, the Pb enrichment recognized in all the analyzed drapes (Table 4.1) indicates that they correspond to very similar sediment deposition. Some mixing is evidenced at the transitions between hemipelagic and mud breccia facies. Detrital and redox sensitive element concentrations at these boundaries have slightly different concentrations from those of

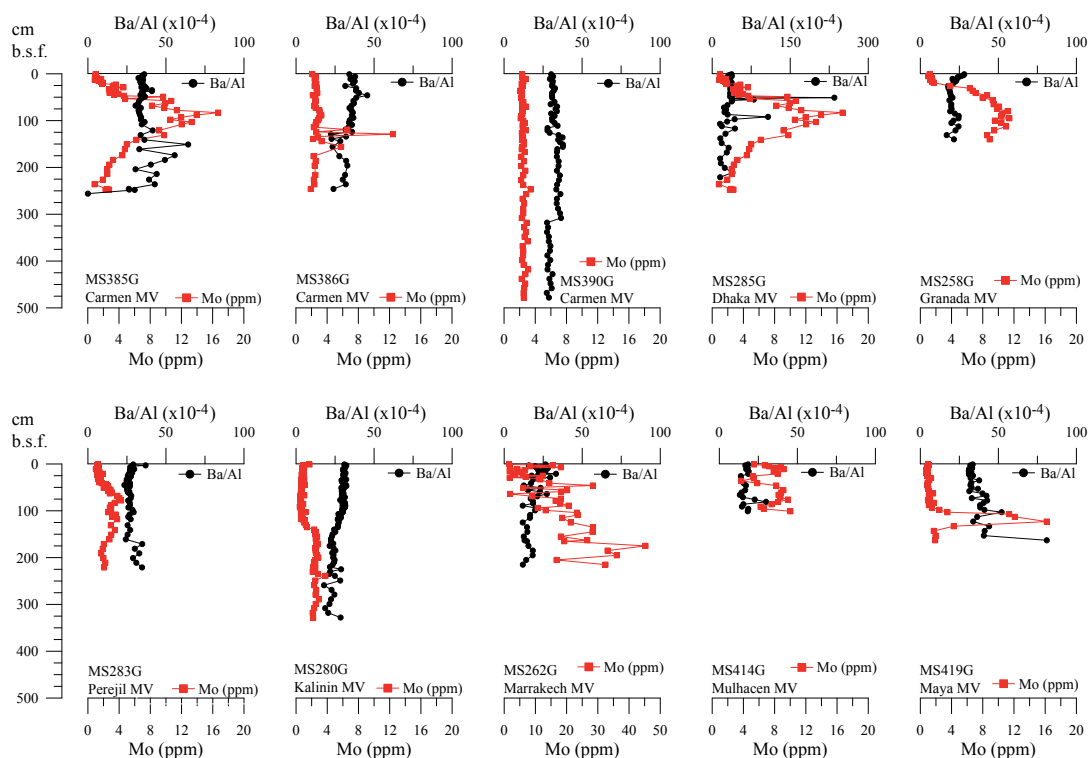


Figure 4.5. Vertical profiles showing the Mo concentrations and Ba/Al ratio at the studied cores.

the typical pelagic sediments. Such differences most likely derive from sediment reworking involving the top of mud breccia intervals. Previous studies based on micropalaeontological data and specific organic compounds report the admixture of microfauna (Gennari et al., 2013) and significant variations of some lipid biomarkers (López-Rodríguez et al., 2014) at the mud breccia drape transitions. This further suggests bioturbation processes affecting the top of MVs structures, giving rise to variations of the original geochemical signatures of the sedimentary drapes.

4.7.2. Geochemical constrains on the nature of mud breccias from the Alboran mud volcanoes

The geochemical signature of MVs provided new insights into the potential source strata that feed mud volcanism in the WAB, as well as into fluid flow and diagenetic processes.

The typical detrital element ratios (i.e., Si/Al, K/

Al, Mg/Al, Rb/Al, and REE/Al) of on mud breccias generally show the element distribution of the source rocks (e.g., McLennan et al., 1993). Previous research on the inorganic geochemistry of mud breccias from the Gulf of Cadiz (Mata and López-González, 2012) and Malta Plateau (Cangemi et al., 2010) supports this assumption, revealing that the expulsion of mud-rich fluids from depth does not necessarily mean a change in the sediment geochemistry. Our findings are in line with this hypothesis, revealing similar major (Fig 4.3) and detrital-element contents (Table 4.1) within the studied mud breccia intervals. This finding further supports that all MVs are fed by the same source strata, which may have lateral continuity proceeding from a similar depth within the MDP. Shale-normalized REE patterns and REE element ratios similarly point to similarities between mud breccia matrices. Comparable studies performed in MVs from the Gulf of Cadiz allowed for the identification and characterization of sha-

flow biogenic vs. deep detrital sources (Mata and López-González, 2012); the similar shale-normalized REE trends encountered for all the Alboran mud breccias (Fig.4.6) indicate that all expelled muds proceed from the same source-layer.

At Maya MV, however, slight differences in the geochemical signature as compared with the mud breccias from the other studied MVs are recognized (Fig. 4.4).

Hence, we conclude that, in general, the matrices of mud breccias from all the studied Alboran MVs contain similar geochemical signatures. The geochemical composition of these matrices would therefore represent the average geoche-

mical composition of the mobilized original source layer feeding the MVs, or at least the average geochemical composition of the finer grain-size solid phase from the upward migrated source materials. It is important to stress that the feeder channels of the volcano are rooted in the mixed overpressured layer formed of undercompacted clays and heterogeneous olistostrome/mega-breccia breccias corresponding to Units Va and VI of the Mud Diapir Province in the WAB (Comas et al., 2010; Somoza et al., 2012 and references therein). Some dissimilarity in the geochemical composition—as encountered in the Maya MV—are attributed to particular differentiation of the upward migrated fluxes within the plumbing systems feeding the MVs.

Table 4.3. Major and trace element composition of selected samples from authigenic methane-derived carbonates (MDAC) concretion and chimney from the “Crow’s foot pockmark” field. Major elements are expressed in wt

	Concretion	Chimney
	422Gr-Tot	r-2
Al ₂ O ₃ (%)	14.03	0.69
SiO ₂ (%)	5.09	nd
CaO (%)	39.08	61.47
Si/Al	0.32	nd
Mg/Ca	0.0253	0.011
Sr/Ca	0.0173	15.39
Ti/Al	0.02	nd
Zr/Al x 10e-4	33.27	36.32
Mg/Al	0.10	1.09
K/Al	0.10	4.44
Fe/Al	0.22	2.09
Ba/Al x10e-4	11.71	24.31
Mn/Al x10e-4	14.60	0.02
Mo/Al x10e-4	1.65	1.12
U/Al x10e-4	0.90	1.90
V/Al x10e-4	8.87	23.89
Ni/V	0.46	0.69
Ce/Ce*	0.95	0.94
Ce anomaly	-0.02	-0.03
Rb/Al x10e-4	5.06	7.34
ΣREE/Al x10e-4	6.55	10.09

4.7.3. Influence of fluid venting on sediment geochemistry

Paleo-tracer of SMZT and AOM occurrence

The occurrence of active fluid venting at MVs is generally associated with the occurrence of a sulfate methane transition zone (SMTZ). The SMTZ represents the redox interface within anoxic sediments where sulfate and methane interact as a consequence of the anaerobic oxidation of methane (AOM) leading to the precipitation of authigenic carbonates (e.g., Reeburgh, 2007; Knittel and Boetius, 2009; and references therein). Thus, MDAC fronts within sediments are used as paleo-tracers to discern manifestations of ancient seep vents and the occurrence of ancient AOM (e.g., Cangemi et al., 2010; Peketi et al., 2012; Pierre et al., 2014).

Redox-sensitive element ratios (i.e., Mo/Al U/Al, V/Al, Cr/Al, Ni/Al, Pb/Al) are potentially more influenced by fluids and diagenetic processes (Table 4.1; Fig. 4.5). For instance, enrichments in Mo in marine sediments constitute a proxy to determine the occurrence of redox transformations. Mo behaves conservatively in oxic waters and exists as molybdate (Mo(VI)O₄²⁻); but under

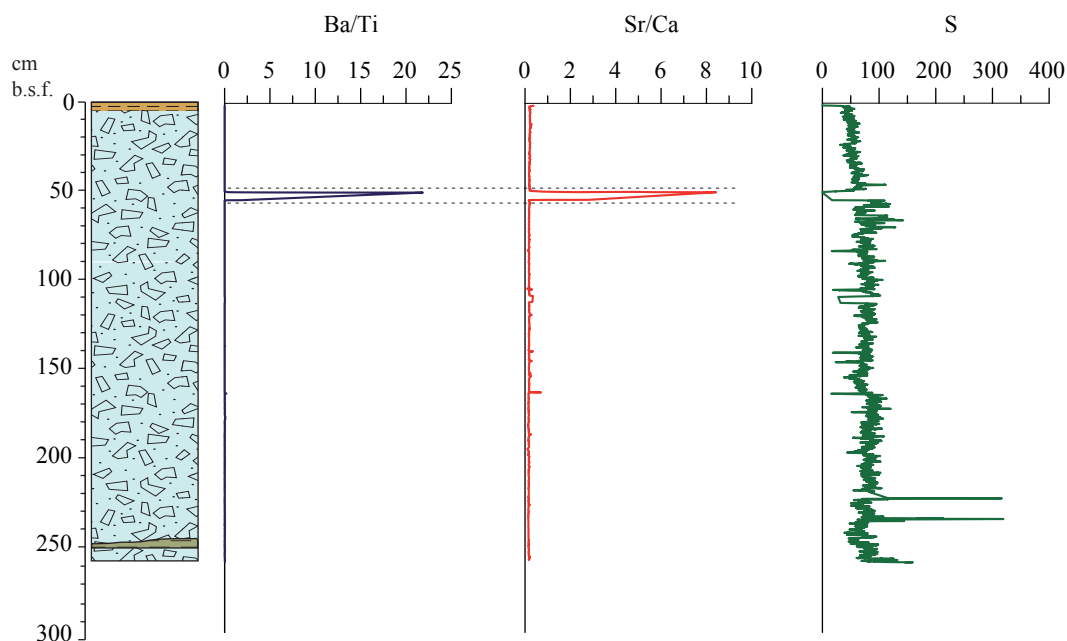


Figure 4.6. Geochemical profiles of Ba/Ti, Sr/Ca ratios and S obtained with Mo-tube with ITRAX Core Scanner at core MS385G from Carmen MV flank. The intensity of the signal is expressed as a peak area for each element and ratio

sulfidic conditions Mo is eventually scavenged as tetrathiomolubdate (Mo(IV)S_4^{2-}) from seawater by FeS (Helz et al., 2004). Accordingly, the coprecipitation of Mo(IV)S_4^{2-} and FeS usually occurs when H_2S exceeds $10 \mu\text{M}$ (Erickson and Helz, 2000). Under such conditions Mo enhancements can be used to assess subsequent paleo-sulfidic conditions (e.g., Crusius et al., 1996; Helz et al., 2004; Peketi et al., 2012).

Barium enrichments can also be used as paleo-tracers of SMTZ. Dissolved Ba^{2+} reacts with sulfate just above this zone and barite (BaSO_4) precipitates, generating Ba-enriched fronts within the sediments (Dickens, 2001; Riedinger et al.,

Table 4.4. C and O stable isotopic composition of selected samples from authigenic methane-derived carbonates (MDAC) concretion and chimney from the “Crow’s foot pockmark” field. $\delta^{13}\text{C}$ and $\delta^{18}\text{O}$ are expressed in ‰ VPDB.

	$\delta^{13}\text{C}$ (VPDB)	$\delta^{18}\text{O}$ (VPDB)
MDAC Concretion		
422Gr-cost	-33.20	2.51
422Gr-carb	-36.57	2.72
MDAC Chimney		
r-2	-38.21	3.98

2006; Peketi et al., 2012; Contreras et al., 2013). Overall, the rather constant values of most of the redox-sensitive element ratios as well as the regular Ba/Al ratio we found at the mud breccia matrices (Table 4.1; Fig. 4.5) may indicate that barite fronts are not preserved within these sediments. Nevertheless, the enrichment peaks of Mo (Fig. 4.5) we encountered in most of the sediment cores —i.e., Carmen MV crater and flank (MS386G and MS385G), Dhaka (MS285G), Granada (MS258G), Marrakech (MS262G), Mulhacen (MS414G) and Maya (MS419G)— appear to reflect H_2S pulses at these intervals, revealing that ancient AOM may have occurred at these intervals (Peketi et al., 2012). Geochemical results of pore waters carried out on active seep vents at Carmen MV (Chapter 4) are in line with this assumption and demonstrate that intense and current pulses of methane develop as addressed events of HS^- up to 10 mM at SMTZ. Regarding the solid phases, some peaks (e.g., Sr/Ca or Mg/Ca ratios and S) were reported within the mud breccia from Maya MV (MS419G; Rodríguez-

Germade et al., 2015) as well as in mud breccia from Carmen MV flank (MS385G, Fig. 4.6). This most likely reveals intervals of high-Mg calcite and aragonite enriched fronts, confirming that ancient methane seepages together with sulfate reduction must have occurred in these mud breccia (e.g., Calvert and Fontugne, 2001; Rodríguez-Germade et al., 2015).

Current discharge and sources of MDAC-related fluids

In the Alboran Sea no extensive areas of MDAC deposits have been documented; in this sense, it is significantly different from the Gulf of Cadiz MV region (Díaz-del-Río, 2003; Pinheiro et al., 2003; Magalhães, 2007; González et al., 2009; Magalhães et al., 2012). Several authors demonstrated that when hydrocarbon-rich fluids discharge into the seafloor, massive MDAC pieces can be generated along with finely dispersed fronts

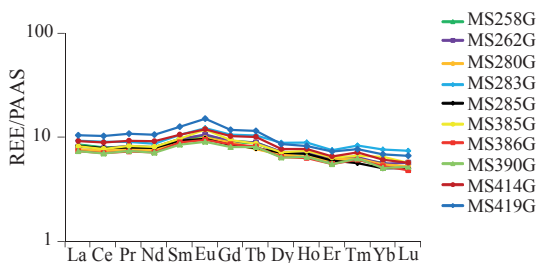


Figure 4.7. Shale-normalized REE patterns of representative samples of mud breccias from the studied MVs.

of authigenic carbonates, which may precipitate during AOM within the sediments (e.g., Luff and Wallmann, 2003; Bayon et al., 2007; Nöthen and Kasten, 2011; Pierre et al., 2012, among others). In active seepages, a limited occurrence of authigenic carbonate fronts can be explained by particular factors or a combination of them: 1) Low activity or lack of methane venting; 2) Fluids depleted in dissolved methane; 3) Very high rates of fluid flow; 4) Severe bioturbation; and/or 5) High sedimentation rates (Bayon et al., 2007). In the Alboran Sea, scarce discrete MDAC pieces at the studied MV cores and the limited occurrence of

MDAC concretion and chimneys, only recovered at “Crow’s foot” pockmark, can be interpreted as differences in the rates of hydrocarbon emission and seepage activity among structures (Blinova et al., 2011). Accordingly, the presence of MDAC pieces at “Crow’s foot” pockmark matches the occurrence of moderate seepage activity at this site (Blinova et al., 2011). The scarce accumulations of authigenic carbonates (i.e., disseminate MDAC fronts, barite, Mo enrichments) at the crater of Carmen MV (core MS390G) would be in line with the extremely high methane concentrations measured here (Blinova et al., 2011; López-Rodríguez et al., in preparation, Chapter 5). This fact strongly supports that Carmen MV is characterized by very high rates of hydrocarbon emissions as well as strong and current mud volcanic activity, which may impede any geochemical indicator of paleo-SMTZ within the mud breccias. Moreover, the lack of enhanced fronts of paleo-SMTZ proxies at Perejil MV is compatible the occurrence of medium hydrocarbon rates ($\sim 230 \mu\text{M}$ /wet sediment) and the relative activity of this MV (López-Rodríguez et al., 2014). This contrasts with the rest of the studied MVs, where extremely low concentrations of hydrocarbons — together with the occurrence of well-developed hemipelagic cover at most, i.e., Kalinin or Maya MVs; Fig.3.1 — indicate these structures are inactive and dormant at present (Blinova et al., 2011; López-Rodríguez et al., 2014).

MDAC usually preserve the original REE signatures and are indicative of the chemical environment during carbonate precipitation (Feng et al., 2013). At the Alboran Sea, REEs patterns of MDAC reveal that trace elements have not suffered alteration and preserve the original geochemical signatures (Table 4.3). Particularly, Ceanomaly constitutes a redox-sensitive proxy for carbonate precipitation conditions in marine sediments (German and Elderfield, 1990), and according to Wright et al. (1987) its values inform about oxidizing or anoxic conditions (Ceanomaly < -0.1 or

Ce anomaly > -0.1, respectively). Nevertheless, this proxy can suffer alteration during late diagenesis and has to be used with caution (Shields and Stille, 2001; Feng et al., 2013). Specific REE ratios are used to discern the applicability of Ce anomaly. Thus, if LaN/SmN exceeds 0.35 and if no correlation occurs between LaN/SmN and Ce anomaly, late diagenesis does not affect REE. According to Shields and Stille (2001), late diagenesis also causes a negative correlation between Ce anomaly and DyN/SmN and a positive correlation between Ce anomaly and REE contents. Such correlations are not obvious in the studied carbonates (Fig. 4.8). Further investigation of MDAC would be needed to confirm whether the REE content of these samples preserves the original redox conditions during precipitation, and therefore no later diagenesis affected the REE content of MDACs.

The carbon isotopic composition of the MDAC can reveal the origin of carbon incorporated during carbonate precipitation or the source of fluids. Thus, biogenic methane is characterized by strongly depleted $\delta^{13}\text{C}$ (-40 to -110‰ VPDB); thermogenic methane (-20 and -60‰ VPDB); petroleum (-25 to -35‰ VPDB), sedimentary organic carbon (-20‰ VPDB), and marine carbonate $\delta^{13}\text{C}$ (~0‰ VPDB) (Whiticar, 1999). The carbon isotopic determinations performed on MDACs from “Crow’s foot” pockmark (Table. 4.4) show typical values of carbonates formed at methane seep environments (e.g., Wiedicke and Weiss, 2006; Magãlhaes et al., 2012; Pierre et al., 2014). Extremely ^{13}C -depleted values (up to -38.21‰; Table 4.4) show that an important part of the carbon fraction of MDAC comes from the oxidation of isotopically light methane, which is in good agreement with the data reported by Blinova et al. (2011), who indicated this carbonate signature generated during AOM processes. This result is also in line with the presence of hydrocarbons (mainly methane) together with all sets of homologues up to pentanes at Carmen MV (Blinova et

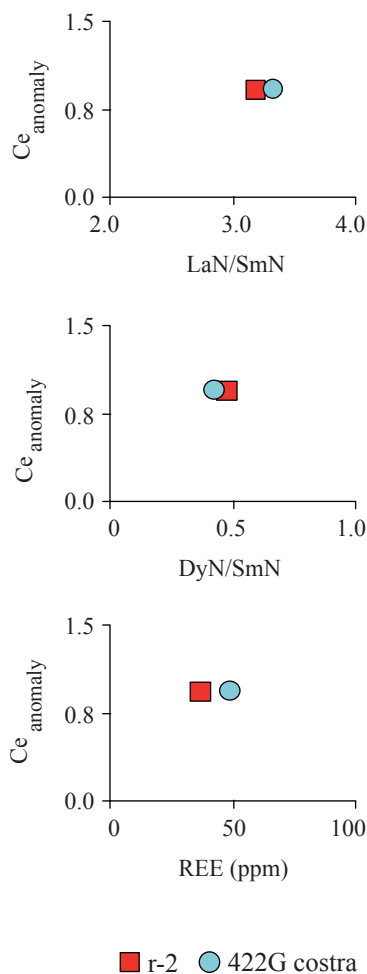


Figure 4.8. Diagenetic influence on $\text{Ce}_{\text{anomaly}}$ within the studied MDAC samples; a) $\text{Ce}_{\text{anomaly}}$ vs. LaN/SmN; b) $\text{Ce}_{\text{anomaly}}$ vs. DyN/SmN; and c) $\text{Ce}_{\text{anomaly}}$ vs. ΣREE . Color squares correspond with sub-samples of the MDAC chimney

al., 2011); and also supported by carbon isotopic values of methane (-59‰; Chapter 5), revealing that the source of the carbonate carbon is hydrocarbon-rich fluids thermogenic in origin.

4.8. Conclusions

Major and trace element composition of MV expelled materials and related sediments from the Alboran Sea show considerable homogeneity. Mud breccia would therefore derive from a single source: geophysical data show feeder channels of the volcano rooted in the mixed overpressured

layer formed of undercompacted clays and heterogeneous olistostrome/megabreccias corresponding to the Units Va and VI described in the Mud Diapir Province of the WAB. Composition of the matrices of mud breccia mostly represents the average geochemical composition of the mobilized original source-layer feeding the MVs, although sediments from ascending conduits could also become assimilated. The composition of hemipelagic sediments is not significantly affected by discharging fluids. Nonetheless, considerable sediment mixing is recognized at the boundaries between these sediments and mud breccia. At dormant MVs, paleo-AOM and ancient pulses of methane fluid venting can be assessed through enhanced intervals of redox-sensitive elements (i.e., Mo, S), and the precipitation of authigenic carbonates, high-Mg calcite and aragonite. The extremely $\delta^{13}\text{C}$ -depleted (-38.21‰ VPDB) isotopic values of methane-derived authigenic carbonates at “Crow’s foot” pockmark confirm fossil AOM and suggest the fluid source is thermogenic methane.



5

Fluid venting and methane seep
in active mud volcanoes
from the Alboran Sea

Chapter 5

Fluid venting and methane seep in active mud volcanoes from the Alboran Sea*.

Abstract

The occurrence of recent active mud volcanism is documented in the West Alboran Basin. Though most of the recognized mud volcanoes to date in this region are dormant, a few structures evidence hydrocarbon-rich fluid venting. This is the case of the Carmen mud volcano, which is a cone-shaped structure 89 m high and 1.3 km in basal diameter. Vigorous active methane-rich seepage occurring at its crater is evidenced by intense gas bubbling and presence of living chemosynthetic fauna. The enhanced methane concentration in mud breccias (~1.5 mmol/wet sediment) and the observed CH_4 and SO_4^{2-} concentrations in pore waters from recovered cores also support current methane seepage. This is also reinforced by the depletion of major elements (i.e., Ca^{2+} and Mg^{2+}) and enrichment of trace species (i.e., Li^+ and B) at depth. Geochemical composition of pore waters indicates a deep thermogenic source and pore fluid freshening at depth. Isotopic $\delta^{18}\text{O}$ and δD compositions of pore waters support smectite dehydration as main pore water freshening mechanism at the Alboran MVs. Calculated water formation temperatures throughout the application of the empirical geo-thermometers (K-Na, K-Mg and K-Ca) reveal that fluids generate at temperature up to 200 °C. This temperature suggests a fluid source from deep zones (about 8 Km depth) associated with underlying sedimentary units Early to Middle Miocene in age. Stable carbon isotopic composition of methane ($\delta^{13}\text{C}_{\text{methane}} \sim -59.42\text{‰}$ VPDB) confirms its thermogenic origin. The anomalous seawater-like composition of the pore fluids in the upper part of mud breccia intervals from cores suggests that certain zones of the MV are also affected by gas outburst, which leads to the downward advection of seawater after each episode of fluid expulsion. Distinctive concave-shape pore water SO_4^{2-} - CH_4 profiles confirms a sulfate-methane transition zone (SMT) coinciding with the enhancement of HS^- concentrations, suggesting the occurrence of active anaerobic oxidation of methane.

* To be submitted to *Chemical Geology*

5.1 Introduction

Mud volcanoes (MVs) have been the target for intensive geochemical studies worldwide, aiming and understanding provenance and pathways of their expelled pore fluids. MVs are usually associated to active seepage fields, often dominated by methane venting (Hovland et al., 1997; Hensen et al., 2003; Haese et al., 2006; Mastalerz et al., 2007; Blinova et al., 2011). They generally develop in basins with thick sedimentary infill. The upward migration of hydrocarbon-rich fluids is conditioned by over-pressurized material from deeper sedimentary layers. The venting activity in a seepage field is not always homogeneous in time, space, and intensity, and can vary from site to site (Haese et al., 2006). In the same field of MVs, individual and neighboring structures can have different scales and intensities of fluid discharge, which not only controls the level of seepage activity but also affects the composition of the expelled fluids. In some cases, such differences can also be noticed between individual seep vents inside the crater of a single MV (Mazzini, 2009a).

Consequently, the geochemical signature of discharged fluid is firstly related to the geological and structural setting of the MV field, as well as to the composition and maturity of the organic matter of the source rocks. In addition, it is also the result of a complex geochemical history that usually includes a number of diagenetic processes which take place simultaneously beneath the MVs (Hensen et al., 2007; Scholz-böttcher et al., 2009; Hensen et al., 2015). Thus, the understanding of the geochemical and isotopic compositions of the expelled fluids contributes to elucidate their origin and provide useful information about diagenetic processes that can occur in the MV system.

In the western Mediterranean, the presently known occurrence of fluid discharge from MVs and seepages is confined to the West Alboran Basin where a MV field developed associated

with a major sedimentary depocentre and under a compressive tectonic regime (Jurado and Comas, 1992; Comas et al., 1996). Geophysical and geochemical studies performed in the area have revealed that most of the Alboran MVs are dormant at present, nonetheless detectable venting of methane/hydrocarbon occurs at a few volcanoes. The most active structure is the Carmen MV (Blinova et al., 2011; Somoza et al., 2012). In this study, we investigate the geochemical and isotopic composition of pore water fluids from three different sites located in the crater of Carmen MV, to better understand fluid origin at this cold seep. We also evaluate the main diagenetic processes that may have affected the fluid composition through its ascending transport by using integrated data of pore water analyses, in combination with sediment data from the mud breccia

5.2. Geological background and site description

The Alboran Sea Basin is located in the westernmost part of the Mediterranean Sea, within the inner part of the Gibraltar Arc (Fig. 1.6). The actual Alboran Sea Basin represent the back-arc basin of the Gibraltar Arc System (GAS), which has evolved under a prevalent north to south convergence between the Eurasian and African plates since the Late Oligocene (Dewey et al., 1989). Geological and geophysical data have demonstrated that the Alboran Sea has suffered variable tectonic conditions, from extensional (Middle to Upper Miocene) to contractive tectonics (Late Miocene to onwards). The major tectonic reorganization in the basin was during Pliocene to Quaternary times under contractive tectonics, which resulted in the north to south shortening of the marine realm and coetaneous uplift and emersion of the surrounding Betic and Riff chains (Comas et al., 1999, and reference therein). This tectonic reorganization conditioned the basin architecture and the actual seafloor morphology (Fig. 1.6) (Comas et al., 1992; Ballesteros et al., 2008; Muñoz et al., 2008).

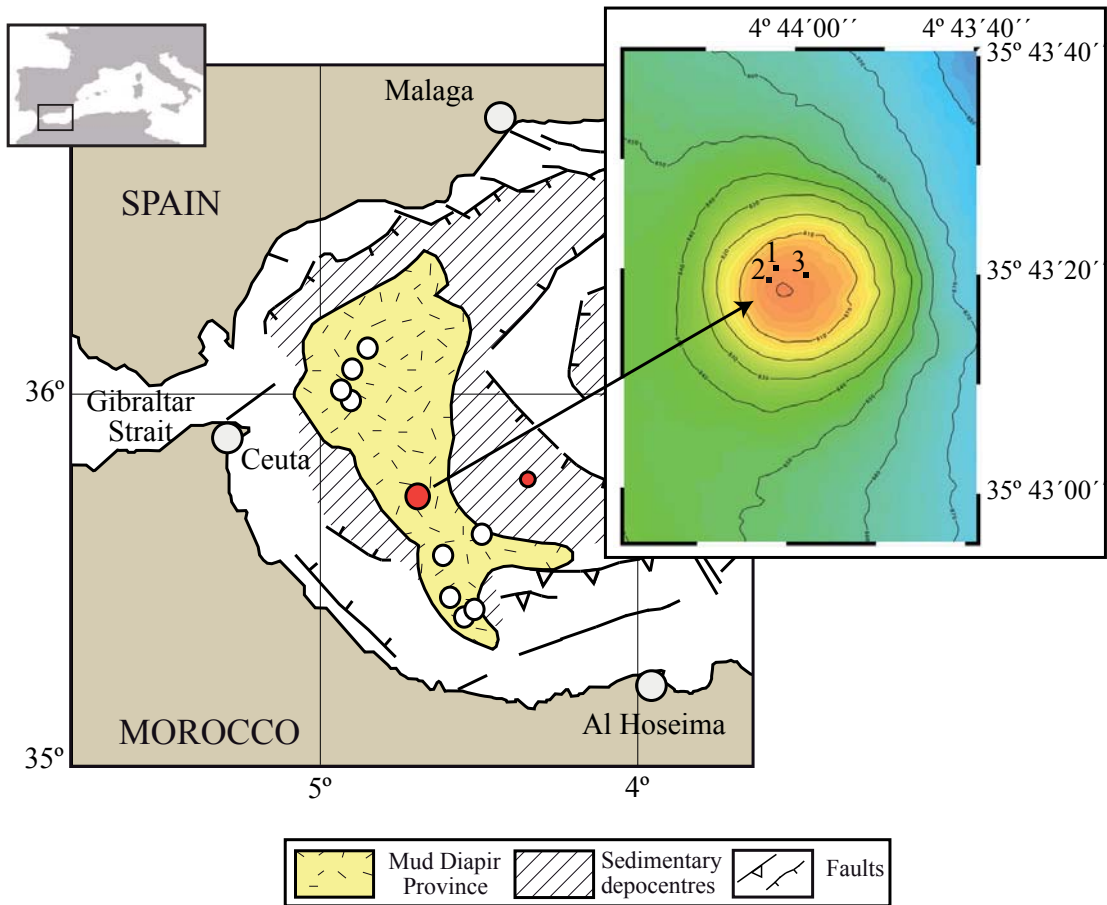


Figure 5.1. The West Alboran basin showing the location of the Mud Diapir Province. White dots correspond with non-studied MVs whereas red dot and square corresponds to Carmen MV and the reference site, respectively. Close up show multibeam image of the crater of Carmen MV. Black squares show position of the studied cores 1) GP05PC, 2) GP07BC and 3) GP09PC from GASALB-Pelagia cruise.

ODP Leg 161 scientific drilling got significant information on the basement and sedimentary infill underneath the Alboran Sea. Geophysical data indicate that the West Alboran Basin (WAB) contains the major sedimentary depocentre in the basin (Fig. 1.7), containing Miocene to Quaternary sedimentary sequences (up to 8 km in thickness) on top of a metamorphic basement (Fig. 1.7; Comas et al., 1996). The WAB is characterized by widespread shale diapirism conditioned by the existence of under-compacted units at depth affected by the tectonic processes (Comas et al., 1999, 2012; Soto et al., 2010). Offshore commer-

cial well (Andalucia-G1 and Alboran-A1) logging data have revealed that this under-compaction is due to important fluid pressure present at the basal sedimentary units of the WAB (Units VI and Unit Va from Jurado and Comas, 1992, Fig. 1.7).

5.2.1. Mud volcanism in the West Alboran Basin

Shale (mud-rocks) diapirism extends N-S in the WAB from the Iberian to the Moroccan margins, forming the Mud Diapir Province (MDP; Fig. 5.1). Above the MDP MV fields occur associated to the shale diapirism, and constrained by the diapiric province. Seismic profiles indicate that deep-fee-

der channels of Alboran MVs connect with the oldest and deepest sediments of the basin (Unit VI - Unit Va- Early Miocene and Middle Miocene), bringing up to the surface material from over-pressured shales and olistostromes (Fig. 5.2; Talukder et al., 2003, Comas et al., 2012). Previous geochemical data on pore waters and mud breccia (Blinova et al., 2011; López-Rodríguez et al., 2014) as well as specific studies on chemosynthetic fauna (Hilário et al., 2011) all have indicated that recent active methane/hydrocarbon cold seeps occur at some Alboran MVs.

Carmen mud volcano

Carmen MV is located in the center of the MDP (Fig. 5.1). TTR-17 Cruise Leg 1 (2008) recognized this MV by sediment coring (Comas et al., 2010). Morphologically, it corresponds with a single edifice with a sub-circular coned shape of 89 m height, 1130 m of diameter at the base and 70 m at the summit. The volcano had gentle slopes of 7° on average, although somewhat steeper slopes were observed on the eastern flank with maximum values of 12° (Fig. 5.3). Seismic images have revealed that the summit of this volcano contains seismic features related to recent ex-

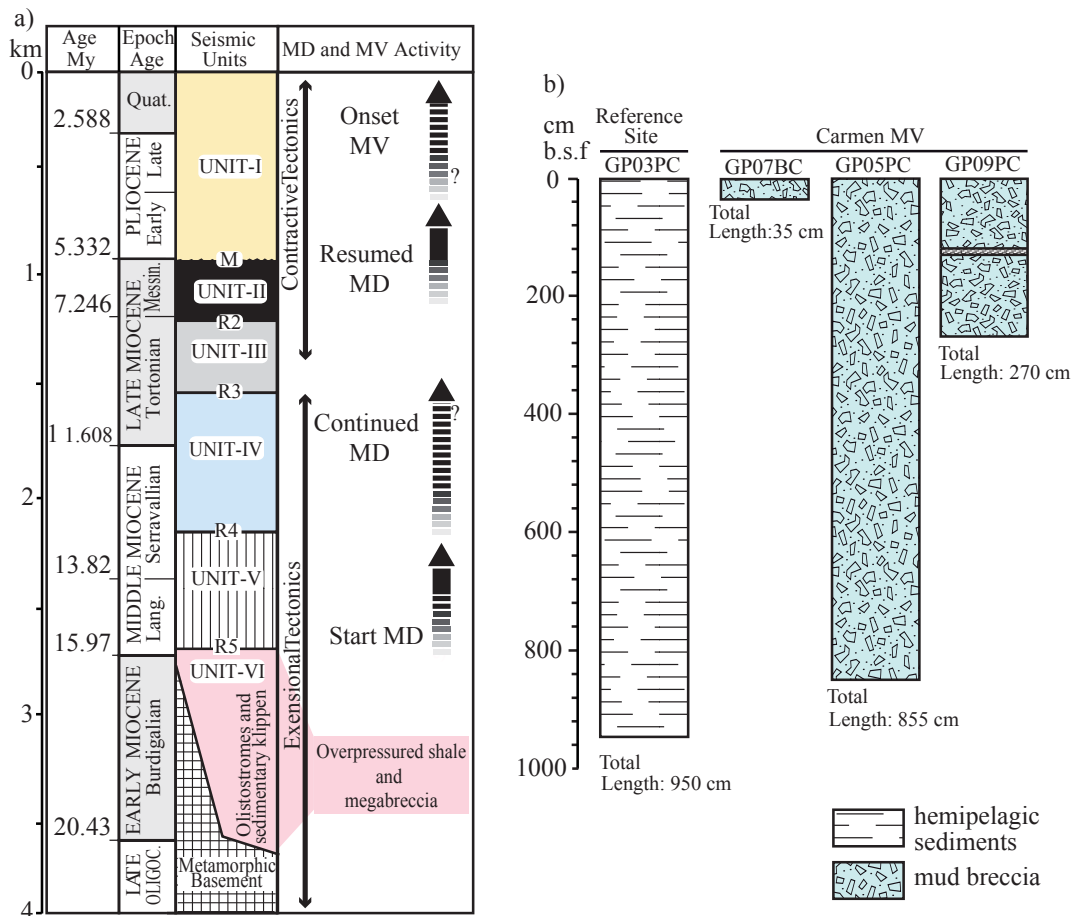


Figure 5.2. a) Seismic stratigraphic units, major regional reflectors and main sedimentary sequence documented in the Betic Neogene basins (modified after Comas et al., 1999); M-Messinian unconformity. R1-5-reflectors correspond to major unconformities within sediments; MD refers to mud diapirism; MV corresponds to mud volcanism; b) schematic core logs showing the main sediment facies from the studied cores.

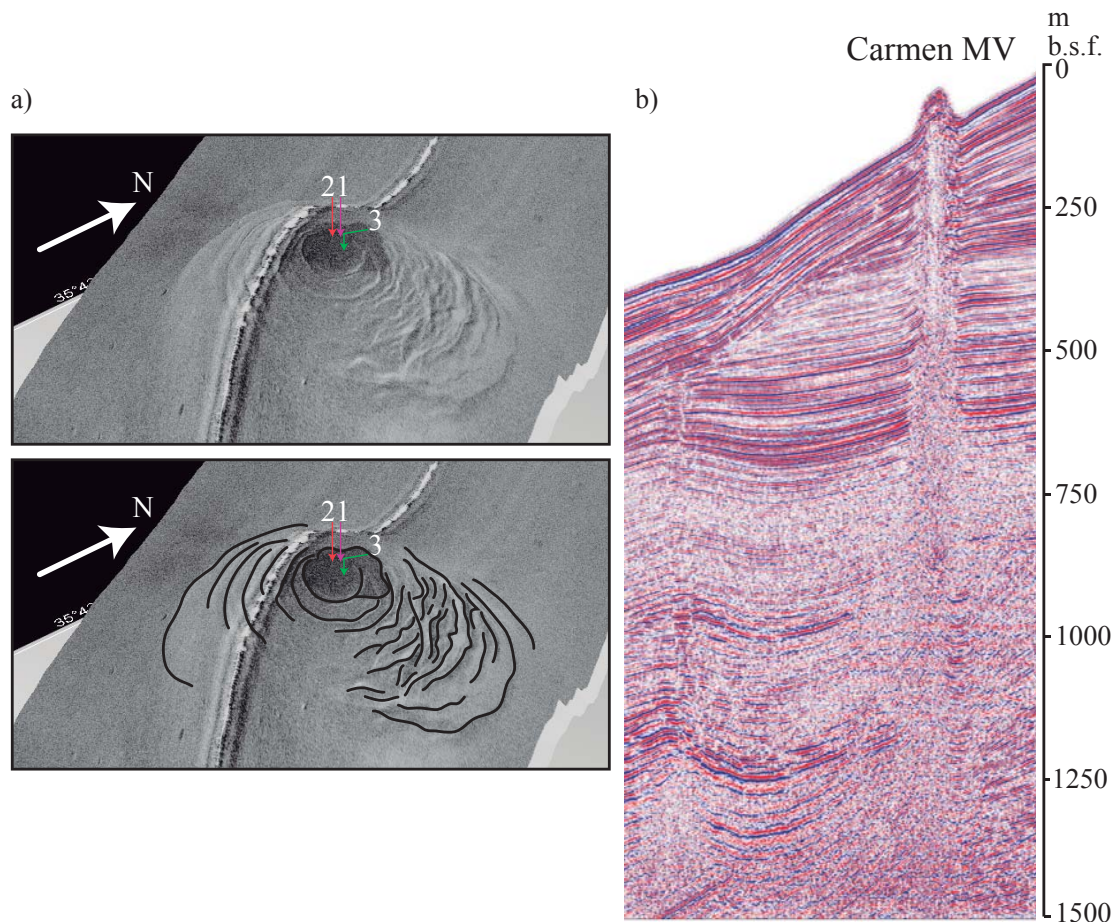


Figure 5.3. a) MAK160MS sonograph uninterpreted (up) and interpreted (below) showing the morphology of Carmen MV. Coloured arrows and numbers refer to the studied cores 1) GP05PC, 2) GP07BC and 3) GP09PC. Note concentric mud breccia flows forming the volcano edifice; b) Multichannel seismic line GPS01 across Carmen MV.

pulsion of mud-rich fluids (Somoza et al., 2012). Several semi-circular depressions were also detected in the southwestern sector (Fig. 5.3), revealing relatively recent seepage activity (Comas et al., 2010; Somoza et al., 2012).

During sample retrievals evidences for actual seepage activity was found surface of a box –core, (hydrocarbon smell, frenulate tubeworms and gas bubbling) indicating the occurrence of current methane seepage. Underwater TV-survey from cruise TTR-17 also revealed free gas bubbling from the seafloor at the central part of the crater (Comas et al., 2010; Blinova et al., 2011).

5.3. Sampling and analytical procedures

5.3.1. Sediment sampling and core lithology

The sediment cores for this study were recovered during the GASALB-Pelagia cruise with RV Pelagia in November 2011. Two piston cores (GP05PC and GP09PC) and one box core (GP07BC) were taken from the crater of Carmen MV and one piston core was retrieved from a reference site for comparison (GP03PC) (Fig. 5.1, Table 5.1). The sampling operations accomplished on board RV Pelagia were performed using a 1200 kg piston corer with maximum tubing of 24 m long and with an internal diameter of 11 cm. The round-

Table 5.1. General information about sampling and positioning of the studied cores

Core Code	Site	Cruise	Location	Sampling Site	Water depth (m)	Recovery (cm)
GP03PC	Reference Site	Gasalb-Pelagia	35° 47.261' N 04° 32.089' W	Hemipelagic	1306	950
GP05PC	Carmen MV	Gasalb-Pelagia	35° 43.333' N 04° 44.046' W	Crater	795	820
GP07BC	Carmen MV	Gasalb-Pelagia	35° 43.319' N 04° 44.050' W	Crater	795	35
GP09PC	Carmen MV	Gasalb-Pelagia	35° 43.332' N 04° 43.975' W	Crater	795	260
MS386G	Carmen MV	TTR-17	35° 43.309' N 04° 44.008' W	Crater	809	259
MS390G	Carmen MV	TTR-17	35° 43.306' N 04° 44.017' W	Crater	809	250

shaped box corer (ca. 1350 kg) had an internal diameter of 50 cm and a height of 55 cm. Immediately after recovery the piston cores were cut into sediment segments of 30 or 50 cm. Upon cutting on deck, each section was sampled immediately for gas and pore water. Sediments from the box core were sampled from sub-cores using pvc tubes of ca. 50 cm length and 9 cm inner diameter which were pushed vertically into the sediments. Afterwards, all sediment sections were stored at + 4 °C for further analysis on land.

The box core GP07BC recovered 35 cm of typical structureless dark-gray mousse-like mud breccia with clear degassing texture, where the topmost part (<1 cm) was oxidized (Fig. 5.2; Table 5.1). At this site, some methane bubbling was discernible across the oxidized sediments as well as the presence of Pogonophora tube worms. The existence of chemosynthetic fauna such as living Acharax shells and white crabs were also detected at 7 and 13 cm depth, respectively.

Piston core GP05PC contained 855 cm of typical structureless and dark-greyish mousse-like mud breccia, with millimetre-to centimetre- sized rock clasts of claystones and mudstones. At this site, no hemipelagic cover was present and a noticeable smell of H₂S was detected along the whole core.

Piston core GP09PC contained 270 cm of alterna-

tions of hemipelagic sediments and mud breccia. At this site, two distinct mud breccia intervals were distinguished. The uppermost mud breccia interval consisted of soft dark-grey mousse-like mud breccia, highly porous due to degassing processes. A strong smell of H₂S was noticed along the whole upper interval as well as presence of Pogonophora tube worms. Additionally, a small fragment of carbonate centimetric size and white in color was found at c.a. 10 cm depth. From 121-131 cm inter-layered hemipelagic sediments consisting of black marls with some foraminifera appeared separating the two mud breccia intervals. This layer reported a sharp upper boundary whereas the lower limit was irregular and no well-expressed. The lower mud breccia interval extended from 132 to 270 cm depth. It consisted in mud breccia with its upper part intensively bioturbated and oxidized. Down core, relatively stiff and laminated dark-grey mud breccia occurred with lack of H₂S odor from 132 to the bottom.

Reference piston core GP03PC recovered hemipelagic sediments and was used for comparison with the MV sediments recovered at Carmen MV. It consisted of 950 cm of olive-gray marl, homogeneous and structureless with some foraminifera. Within the whole core black spots were identified throughout the sediments.

5.3.2. Pore waters and hydrocarbon gases

Samples for the extraction of gas and pore water of piston cores were taken directly from the cut-sides of the 30 or 50 cm sections. For gas samples, decapped 10 ml syringes were used whereas for pore water two 60 ml decapped syringes were used on deck. Subsequently in the onboard laboratory maintained at in-situ temperature, additional pore water samples were extracted using rhizons (Seeberg-Elverfeldt et al., 2005)

Samples for the extraction of gas and pore water of the box core were taken from the dedicated predrilled sub-cores. For gases, after cutting the tape a decapped syringe was gently pushed in to recover 10 ml of sediment whereas rhizons or cut-off slices were used for pore water extractions (for more detail see section below).

Gas extraction and analysis

For gas analysis, the 10 ml of fresh sediment sample recovered with the decapped syringe was immediately transferred into a 65 ml glass vial pre-filled with a saturated NaCl solution. The vials were immediately closed with a thick gas-tight rubber stopper while excluding air, and subsequently well-mixed. After approximate 1 hour, 5 ml headspace was made with nitrogen gas (purity 5.0) while 5 ml of saltwater was simultaneously removed using a second needle. Afterwards, the bottles were shaken a mixed again to make a homogeneous suspension and were equilibrated upside down for at least 24 h at room temperature prior to gas analysis (following procedures by Mastalerz et al., 2007). The methane concentration in the headspace was routinely determined on board, injecting 1 ml gas sample into a Shimadzu Gas Chromatograph GC-14B with a flame ionization detector and equipped with a packed stainless steel Porapack Q (6 ft, 2mm i.d., 80/100 mesh, Alltech).

The isotopic signatures of methane were measured with continuous flow isotope ratio mass spectrometry systems at the Royal Holloway Uni-

versity of London (RHUL) for $\delta^{13}\text{C}$.

Subsamples were extracted from the headspace present in the sealed flasks and injected to the sample loop of each system to be mixed with a carrier gas (Helium). High precision measurements of $\delta^{13}\text{C}$ were obtained by sample preconcentration and subsequent pyrolysis to H_2 or combustion to CO_2 for measurement of either stable isotope, before entering the mass spectrometers: a Trace Gas and Isoprime mass spectrometer (Isoprime Ltd) for $\delta^{13}\text{C}$ (Fisher et al., 2006; Brass and Röckmann, 2010; Sapart et al., 2011).

Pore water extraction

The two cut-off 60 ml-syringes were pushed into the bottom of each 30 or 50 cm section of the piston cores, and the recovered sediment was transferred into 50 ml plastic centrifuge tubes with screw caps. These were centrifuged for 15-60 min at 2800-3500 rpm in a cooled laboratory at in situ temperature of + 14 °C (De Lange et al., 1992). Furthermore, additional pore water extractions were done on these sections while being stored at + 14 °C. This was done using rhizons (Seeberg-elverfeldt et al., 2005) pushed into the top of each 30 or 50 cm piston core section. For water-saturated sediment samples, rhizons were left with negative pressure for at least 30 min, whereas for relatively dry samples, rhizons remained operational overnight. For the box core, pore water extractions were done at high resolution pushing rhizons into the sediment every 2 cm throughout pre-drilled holes in the pvc tube. Additional pore waters from box core were extracted by sediment sampling into an anoxic glove-box, pushing the sediment up with a core pusher. Samples were taken every 2 cm, being transferred into 50 ml plastic centrifuge tubes with screw caps and centrifuged for 15-60 min at 2800-3500 rpm in a cooled laboratory at in situ temperature of + 14 °C (De Lange et al., 1992). After centrifugation, all aliquots were filtered and subsampled for onboard analyses and/or stored at + 4 °C.

For piston core GP05PC most of the mud breccia sediment was dry and little pore water was recovered using centrifugation. Additional pore water was then extracted from these centrifuged sediments, pushing the rhizons into the sediment within the centrifuge tubes. After centrifugation or rhizon extraction, the pore waters were transferred into an anoxic glove-box under N_2 -atmosphere where it was filtered through 0.2 μm cellulose-acetate membrane filters. Subsequently, samples were split into sub-samples for shipboard analyses or stored at + 4 °C prior to shore-based pore water analyses.

Pore water analyses

After pore water extraction and filtration, the most-sensitive parameters were immediately measured on board. Thus, total alkalinity (TA) was determined by titration with HCl following the procedure of Grasshoff et al. (1983). Dissolved inorganic carbon (DIC) was analyzed spectrophotometrically by a continuous flow set-up (Stoll et al., 2001). Concentrations of sulfide were also determined immediately, using standard photometric procedures adapted for pore waters with relatively high concentrations (~ mM) of dissolved sulfide (after Grasshoff et al., 1969). For ammonia and phosphates, all analyses were carried out on board with continuous flow analyzer, applying auto-analyzer colorimetric methods (Grasshoff et al., 1983).

Total dissolved anions (Cl^- , SO_4^{2-} and Br^-), cations (Na^+ , Ca^{2+} , Mg^{2+} , K^+ , Ba^{2+} , Li^+ , Sr^{2+}) and H_3BO_3 (boric acid) concentrations in the pore water samples were measured by inductively coupled plasma atomic emission spectrometer (ICP-AES, Perkin Elmer Optima 3000) and inductively coupled plasma mass spectrometer (ICP-MS, ThermoFisher Scientific Element2-XR) in the shore-based laboratory at the department of Earth Sciences, Geochemistry (Utrecht University). The ICP-MS sample triplicate measurements had a relative error < 1.5 %. Replicate analyses indicated that the relative error for ICP-OES analyses were

<5%.

The stable carbon ($\delta^{13}C$) isotope values of dissolved inorganic carbon (DIC) in pore waters were performed by elemental analyzer-continuous flow isotope ratio-mass spectrometry using a Fisons 1500 NCS elemental analyzer coupled to a Finnigan Mat Delta Plus mass spectrometer. The accuracy of the internal standards was ± 0.06 ‰. The $\delta^{13}C$ -DIC was reported in standard delta notation (‰) relative to VPDB standard. Average analytical precision based on routine analysis of internal laboratory reference material demonstrated a standard deviation of 0.15 ‰.

Stable oxygen ($\delta^{18}O$) and hydrogen (δD) isotope values were determined by the H_2O - CO_2 equilibration method using a continuous flow technology with helium carrier gas performed in a GasBench II interfaced with a Finnigan Mat-253 with a Kiel-device coupled online to a Finnigan MAT-253 mass spectrometer. The accuracy of the internal standards was ± 0.1 ‰ for $\delta^{18}O$ and ± 1 ‰ for δD . The $\delta^{18}O$ and δD of pore water were reported using the standard delta notation (‰) relative to the SMOW standard. Average analytical precision based on routine analysis of internal laboratory reference material demonstrated a standard deviation of 0.08 and 2.3 ‰, respectively (Nelson, 2000).

Radiogenic strontium isotope analyses were measured by MC-ICP-MS (Thermo Scientific Neptune Plus multi-collector ICP-MS) after chromatographic strontium separation using Sr-Spec resin (©Eichrom) at the Institute for Chemistry and Biology of the Marine Environment (ICBM), University of Oldenburg (Germany).

Chemical separation of Sr and analyses of $^{87}Sr/^{86}Sr$ isotope ratios were examined by repeated analyses of the Strontium Carbonate isotopic standard SRM 987 from the NIST (National Institute of Standards and Technology) and IAPSO seawater standard; the average of the external reproducibility of the NIST SRM 987 is $\pm 4.5E-06$ (2σ , $n=16$). Sr-isotope ratios were normalized to

NIST SRM 987 standard (0.710248; Howarth and McArthur, 1997)

Geo-thermometer calculations

The empirical geo-thermometer based on the temperature-dependant equilibrium between fluids composition and major minerals (K^+ , Na^+ , Ca^{2+} and Mg^{2+}) use diagnostic ratios based on pore water elements to estimate such potential temperature (Kharaka and Mariner, 1989). In cold seeps and MVs at compressive margins this calculation can be applied in order to assess the reservoir temperature of the fluids expelled to the surface (Giggenbach, 1988). The concentration of K^+ , Na^+ , Ca^{2+} and Mg^{2+} from the pore water samples from gravity and box cores were used to calculate the equilibrium temperature according to the following formulae (Giggenbach, 1988; Haese et al., 2006)

$$T\text{ }^{\circ}\text{C} = (1390 / (1.75 - \log (K^+ / Na^+)) - 273.15 \quad (1)$$

$$T\text{ }^{\circ}\text{C} = (4410 / (14.0 - \log ((K^+)^2 / Mg^{2+})) - 273.15(2)$$

$$T\text{ }^{\circ}\text{C} = (\log ((K^+)^2 / Ca^{2+}) + 0.78) / 0.0168 \quad (3)$$

Where, T is temperature ($^{\circ}\text{C}$) and K^+ , Na^+ , Ca^{2+} and Mg^{2+} concentrations given in mg/l.

5.4. Results

5.4.1. Fluid composition

Dissolved major and trace elements

Pore waters from the reference core showed SO_4^{2-} concentrations decreasing gradually from typical bottom water value of 31 to 7.4 mM at 945 cm depth in the sediment. The concentration of TA, DIC, NH_4^+ and PO_4^{3-} increased with depth (Fig. 5.4). Salinity and related dissolved salts (Cl^- and Na/Cl ratio) showed constant values with depth. The same was observed for B/Cl, Li/Cl, Ba/Cl and Br/Cl ratios (Fig. 5.5). In contrast, Ca/Cl, Sr/Cl, K/Cl and Mg/Cl ratios decreased with depth (Fig. 5.5).

In contrast to the reference core, the analyzed

pore waters at the different cores from Carmen MV reported different geochemical patterns. At all sites the pore water are SO_4^{2-} depleted within the interval from 20 to 240 cm below the sediment surface (Fig. 5.4). From this depth downward, an increase in the concentration of CH_4 to maximum values of 1526 μM was detected, especially in core GP05PC (Fig. 5.4). Total alkalinity (TA) and dissolved inorganic carbon (DIC) run parallel, increasing with depth to 41.8 mM and 39.8 mM values, respectively. Strong enrichment in ammonium (NH_4^+) and phosphate (PO_4^{3-}) concentrations were detected at all sites at depth. In GP05PC, sulfide (HS^-) increased significantly between 75 to 225 cm b.s.f. (below sea floor) reaching maximum values of 917 μM (Fig. 5.4).

All the investigated pore waters from Carmen MV were strongly depleted in Cl^- and Na^+ , varying from typical seawater values at the most superficial sediments to minimum concentrations of 143 mM and 168 mM, respectively. At the surface, the Na/Cl ratio was similar to that in the bottom water (0.86). However, in the deepest sediments this ratio increased to values up to 1.15 (Fig. 5.5). Similarly to dissolved salts, salinity significantly decreased in depth with more than 70 % compared with the most superficial pore water salinity reported (Table 5.2). Deep fluids were strongly depleted in Ca/Cl, Mg/Cl and K/Cl ratios and considerably enriched in Sr/Cl, B/Cl, Li/Cl, Ba/Cl, and Br/Cl ratios (Fig. 5.5).

Stable and radiogenic isotopes ($\delta^{13}\text{C}$, δD , $\delta^{18}\text{O}$ and $^{87}\text{Sr}/^{86}\text{Sr}$)

Pore waters from core GP05PC showed δD values that are lower than those reported in seawater, varying from -10.1 ‰ to 12.4 ‰ values, with a general decreasing trend with depth. In contrast, the $\delta^{18}\text{O}$ values increase down core, ranging from 0.99 ‰ to 5.72 ‰ (Fig. 5.6); accordingly, a pronounced negative correlation is observed between $\delta^{18}\text{O}$ and δD (Fig. 5.6). The carbon isotopic signature ($\delta^{13}\text{C}$) from the investigated pore fluids

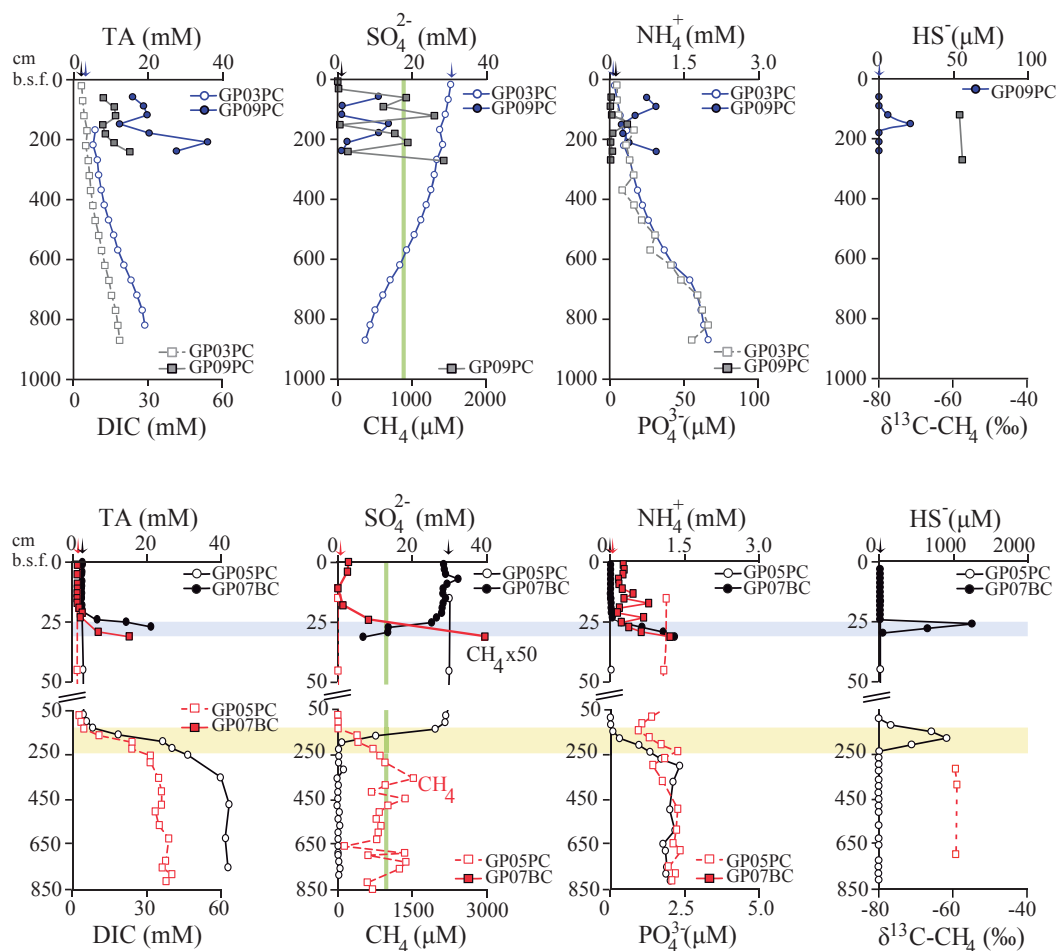


Figure 5.4. Pore water profiles showing the most sensitive parameters (TA, DIC, SO_4^{2-} , NH_4^+ , PO_4^{3-} and HS^-) and methane (CH_4) concentrations measured at the studied sites. Values expressed in mM kg^{-1} and $\mu\text{M kg}^{-1}$. For a better understanding, an interruption on the vertical scale at GP05PC was done at 50 cm depth. Vertical green lines mark the level of methane saturation for seawater. Methane concentration values from GP07BC were increased using a factor of X50. Horizontal blue and yellow lines show the SMZ at cores GP07BC and GP05PC, respectively. At GP03PC sulfide values were below detection limit. Vertical arrows position the sea water values. Deviating samples were denoted into brackets

revealed depleted values that tend to be more negative at depth, varying from -8.40‰ in the uppermost sediments to -21.13‰ at 165 cm b.s.f. (Fig. 5.6).

Two down core samples GP05PC were analyzed for radiogenic strontium isotopes. The isotopic values showed similar $^{87}\text{Sr}/^{86}\text{Sr}$ ratios at both samples, with a ratio value of 0.70899 for the shallowest sample at 595 cm below seafloor and 0.70902 for the deepest one at 755 cm below seafloor.

5.4.2 Methane isotopic composition

The stable carbon composition ($\delta^{13}\text{C}$) of methane was only analyzed at core GP05PC and GP09PC. Results showed very similar values between sites, varying from -59.42 to -59.01‰ VPDB at GP05PC and from -58.75 to -58.06‰ VPDB at GP09PC (Fig. 5.4).

Table 5.2. Element-based ratios calculated at the selected cores at Carmen MV

Depth (cm)	pH	Salinity (‰)	N/P
Reference Site GP03PC			
20	-	37	18.31
70	7.90	37	28.17
120	-	37	33.27
170	8.07	37	20.51
220	7.99	37	24.72
270	8.14	37	29.49
320	8.06	37	28.79
370	7.90	37	64.58
420	7.99	37	39.54
470	7.99	37	35.59
520	8.22	37	30.06
570	8.12	37	39.84
620	8.28	37	30.72
670	8.22	37	33.37
720	8.35	37	29.46
770	8.29	37	29.31
820	8.26	37	28.35
870	-	37	35.61
Carmen Mud Volcano GP05PC			
15	6.99	-	8.30
45	7.51	35	10.22
75	7.59	35	19.68
105	7.75	36	31.02
135	7.91	35	81.30
165	8.13	34	159.15
195	8.34	26	345.074
225	8.54	26	355.92
255	8.59	18	559.79
285	-	17	972.71
315	-	14	-
355	8.86	14	722.06
385	-	12	-

5.5. Discussion

5.5.1. Geochemical evidences of seawater intrusion

Active zones of MVs usually report characteristic pore water concentration profiles (i.e. SO_4^{2-} , CH_4) which reflect upward fluid advection of methane and/or the occurrence of sulfate reduction processes (Reeburgh, 1982; Hensen et al., 2003). Shapes of pore water profiles, especially the-

sultant from sulfate decline in depth, are well known and most likely inform about geochemical conditions of the system and interactions among dissolved species, mainly between sulfate and methane, which are strongly reactive. Nevertheless, the occurrence of anomalous seawater-like composition of pore waters recently encountered at craters and active parts of MVs have suggested that sedimentary events or volcanic episodes of mud expulsion may affect to the geochemistry of pore fluids (Zabel and Schulz, 2001; Hensen et al., 2007; Mastalerz et al., 2007; Feseker et al., 2010; Reitz et al., 2011).

Our data have revealed that the processes affecting pore water compositions at reference core GP03PC and flank core GP09PC from Carmen MV are different from those encountered at the crater cores GP07BC and GP05PC from the same structure (Fig. 5.4). More details about the biogeochemical processes operating at reference site GP03PC and flank-core GP09PC will be addressed in *section 5.5.3*.

In the case of the crater cores (GP07BC and GP05PC), deep fluids show tendencies that are fully in line with the typical pore water patterns found in anoxic MVs sediments (Haese et al., 2006; Hensen et al., 2007; Reitz et al., 2011; Scholz, 2009). Nevertheless, the unusual and rather constant pore water profiles reported at these both summit cores (GP07BC and GP05PC, Fig. 5.2b) differ significantly from the observed at the reference core GP03PC suggesting a lack of sulfate consumption. This fact clearly point to the absence of both microbial mediated processes (i.e. AOM) and degradation of organic matter at these sites, which may lead to characteristic SO_4^{2-} profiles of kink-type or linearly decreasing with depth, respectively (Borowski et al., 1996; Hensen et al., 2003). This assumption is especially evident at core GP05PC where the consistent seawater-like concentrations and elemental ratios comparable to marine seawater values above the sulfate-reduction zone (Fig. 5.2b) strongly

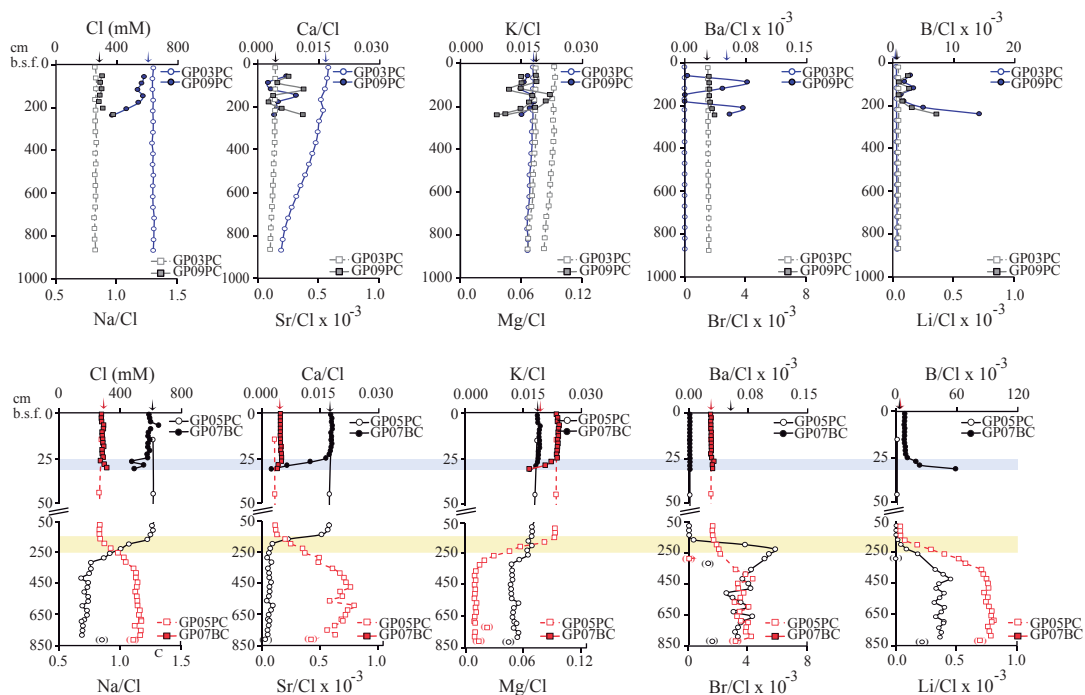


Figure 5.5. Pore water profiles showing the major and trace dissolved elements at all the investigated cores. Vertical arrows indicate seawater values. Concentrations of Cl, Na/Cl, Ca/Cl, Sr/Cl, K/Cl, Mg/Cl, Br/Cl, B/Cl and Li/Cl were obtained by ICP-OES whereas Fe/Cl, Mn/Cl, Ba/Cl values were acquired by ICP-MS and expressed in mM kg^{-1} . For GP05PC major and trace element concentrations correspond to averaged-values of pore waters taken by rhizons directly on sediments and additional pore waters extracted by rhizons on sediment remainders after-centrifugation (for more details see section 3.2.2). Horizontal blue and yellow lines show the SMZ at cores GP07BC and GP05PC, respectively. Vertical arrows position the sea water values. Deviating samples were denoted into brackets

suggest the downward intrusion and mixing with bottom seawater.

Similar geochemical patterns have been previously described in others MVs from the Eastern Mediterranean (Mastalerz et al., 2007; Feseker et al., 2010) or the Black Sea (Reitz et al., 2011) where hydrocarbon gas ebullition or bioirrigation by tube dwelling organisms have been addressed as potential factors for such constant seawater-like compositions (Emerson et al., 1984; Wallmann et al., 1997; Fossing et al., 2000; Haeckel et al., 2007).

Although bio-ventilation of deep sediments caused by the activity of tubeworms can contribute to the exchange between deep pore fluids with underlying seawater-like fluids and can extend several meters into the sediments (Weaver and Schultheiss, 1983; Emerson et al., 1984; Wall-

mann et al., 1997; Fossing et al., 2000), in Carmen MV this process may only affect to the uppermost sediments, since specific chemosynthetic epifauna have been only encountered above 10 cm depth (Fig. 5.3). Mastalerz et al., (2007) described at the center of Isis MV (eastern Mediterranean) similar tendencies for pore waters concentrations. In such case, they suggested these conspicuous seawater-like compositions due to recent mud flows or by downward advection followed by a recent gas expulsion. In this case, the occurrence of mud flows is very likely. All summit cores are susceptible to be affected by abrupt mud eruption events due to their locations at the crater of Carmen MV, and consequently at the most active part of the structure (Fig. 5.1). After sediment deposition the pore water compositions would lead to kink-type profiles since a steady-state in-

duced by diffusive stabilization is expected to be reached. However, this hypothesis does not explain the abrupt change to deep-fluid signatures that occur at 200 cm depth at core GP05PC (Fig. 5.4 and Fig. 5.5) and neither the typical and continuous marine stable isotopic δD and $\delta^{18}O$ values reported along this interval (Fig. 5.6).

These observations are comparable with the previously reported by Mastalerz et al., (2007) which explained the sea-like compositions of pore waters by the entrance of seawater caused by recent gas expulsion. At Carmen MV such constant seawater-like pore water composition within the mud breccia interval is unlikely reached under a stable situation and most likely indicate the occurrence of a very recent injection of bottom seawater and mixing after bubble release by recent hydrocarbon gas ebullition. This assumption is strongly supported by the typical concave-down pore water profiles (SO_4^{2-} , CH_4 , TA, DIC, NH_4^+ , PO_4^{3-}) that cores GP07BC and GP05PC report at depth (Fig. 5.4), and is fully in line with the recent vent activity documented at this structure (Ivanov et al., 2010; Blinova et al., 2011). Moreover, the relative light $\delta^{13}C$ for methane reported by us (Fig 5.4) as well as the rather constant values throughout the mud breccia interval match well with previous $\delta^{13}C$ for methane measured at core MS390G (Blinova et al., 2011). These data imply that the methane of these sediments are not-in situ generated and derive from deep and thermogenic sources. In consequence, we strongly suggest that the injection of seawater after episodes of gas outburst and the release of rich-gas fluids are the most likely mechanism affecting to the uppermost part of cores GP05PC and GP07BC at Carmen MV.

5.5.2. Relative rates of fluid venting activity

Pore water composition and resultant profile shape is largely controlled by changes in depositional conditions and strongly dependant on the concentration of the methane fluxes, varying from concave profiles during transient stages to linear

profiles once the pore water concentration re-equilibrates and a new steady state is reached (Hensen et al., 2003). Compared to other investigated seep sites and MVs such as the Black Sea (Reitz et al., 2011) or the Gulf of Cadiz (Haese et al., 2003; Hensen et al., 2007; Niemann et al., 2006), the summit cores of Carmen MV (GP07BC and GP05PC, Fig. 5.2) have shown similar rapid transition to underlying pore water signatures typical for active MVs (Haese et al., 2006; Hensen et al., 2007; Scholz et al., 2009; Reitz et al., 2011). Furthermore, the concave-down concentration depth profiles of e.g. SO_4^{2-} and CH_4 , encountered at Carmen pore water profiles and the sharp boundary reported at these crater cores (e.g. below 200 cm depth at GP05PC; Fig. 5.4) not have only revealed changes in the methane flux from below and also have suggested that current pulses of methane are recently occurring at this structure. Moreover, the rapid depletion of methane and sulfate at Carmen MV is comparable to the reported at the Captain Arutyunov MV at the Gulf of Cadiz (Niemann et al., 2006). This trend clearly point out to high rates of AOM and SR occurring within the SMT zone at Carmen MV. This assumption is also in good agreement with both geological and geochemical data reported by Blinova et al., (2011) designating Carmen MV as the most active structure at the Alboran Sea Basin.

Despite of these similarities, we would expect to find parallel tendencies for SO_4^{2-} and CH_4 occurring in a 1:1 ratio similarly to the reported at MVs from the Gulf of Cadiz (e.g. Haese et al., 2003; Hensen et al., 2007; Niemann et al., 2006). However, our pore water data, particularly those from core GP05PC, have shown significant differences in at least one order of magnitude between these gradients (e.g. SO_4^{2-}/CH_4) but also with DIC and TA (Fig. 5.4). In addition, with the observed SO_4^{2-} -tendency, a 10-time large peak in HS^- is expected that is not reached at core GP05PC (Fig. 5.4). Thus overall, our data suggest that there is an apparent total mismatch/disequilibrium between fluxes of oxidants and those of products at Carmen MV.

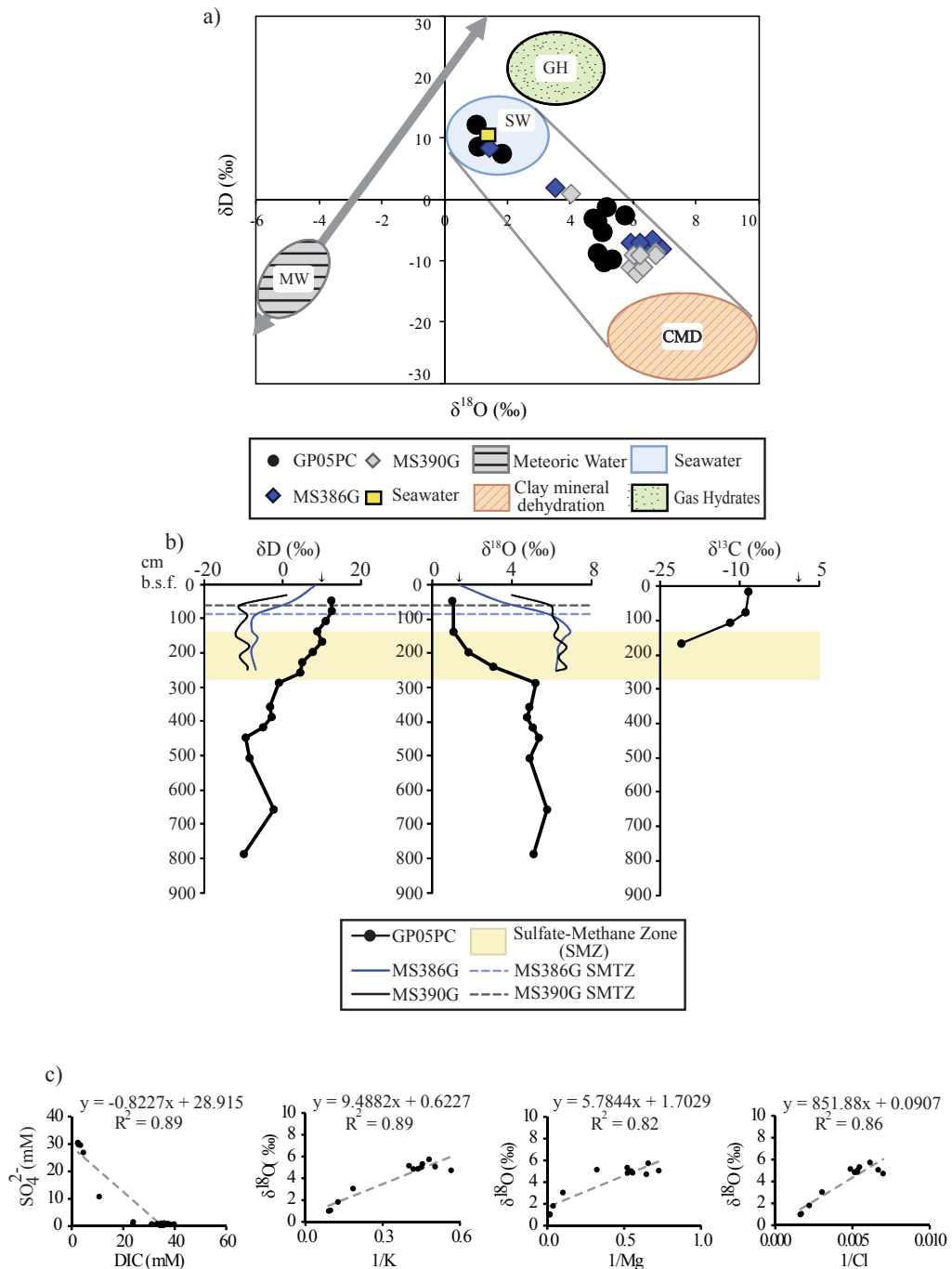


Figure 5.6. a) δD vs $\delta^{18}O$ values from GP05PC at Carmen MV. Additional δD vs $\delta^{18}O$ values from Blinova et al., (2011) as well as from a Mediterranean seawater sample from a CTD station taken above Carmen MV are also included for comparison. Main sourced-fields affecting the δD vs $\delta^{18}O$ composition of pore waters are presented as colored circles and adapted from Dählmann and De Lange (2003); b) δD and $\delta^{18}O$ of pore waters $\delta^{13}C$ -DIC along the core depth at GP05PC from Carmen MV. Additional δD and $\delta^{18}O$ composition are also included for comparison. Grey and blue dashed horizontal lines correspond to AOM depths detected at cores MS390G and MS386G (data from Blinova et al., 2011), respectively; c) SO_4^{2-} vs DIC showing negative correlation and $\delta^{18}O$ vs $1/K$, $1/Mg$ and $1/Cl$ showing positive correlations. Green dashed lines correspond to lineal regression lines

5.5.3 Potential associated processes

In marine sediments, the distribution of sulfate can be regulated by physical factors, such as seawater diffusion, advection, sediment permeability (Jørgensen and Kasten, 2006) and/or biological factors such as bioturbation or bioirrigation (Fossing et al., 2000; Jørgensen and Parkes, 2010). The decline of sulfate in marine sediments is usually controlled by one of the two dominant processes of 1) organoclastic sulfate reduction (OSR) fueled by degradation of organic matter (OM) or 2) by anaerobic oxidation of methane (AOM) (Malinverno and Pohlman, 2011, and references therein), giving as a result linear SO_4^{2-} profiles and SO_4^{2-} kink-type, respectively.

The reference core GP03PC constitutes a non-seepage affected site, where no evidence of AOM is expected. At this site the decline of sulfate and the linear DIC trend (Fig. 5.4), together with the N/P ratio values (Table 5.2 and Fig. 5.4) indicate that the degradation of OM via OSR constitutes the main process consuming sulfate at this site. This finding is in accordance with the results previously reported by Bernasconi et al., (1994) and Böttcher et al., (1998) at hemipelagic sites in the Alboran Sea, where they stated OSR process as main sink of sulfate.

Above the sharp boundary generated by the entrance of marine seawater, pore fluids from the active cores GP05PC and GP07BC showed a rapid depletion of sulfate (Fig. 5.4). Although occurring at different depth levels, it indicates that important sulfate-reduction processes take place at these sites.

At GP05PC the transition boundary between seawater composition and deep fluid signatures is located below 200 cm depth. It clearly indicates that sulfate is being consumed above this depth and that most, if not all, the sulfate reduction is driven by AOM processes (Fig. 5.4). The enhanced concentration of HS^- between 105 and 165 cm depth (Fig. 5.4), i.e. the depth interval where the sulfate-methane transition zone (SMTZ) oc-

cur, as well as the sharply increase of methane concentrations below the SMTZ to values above the sea level saturation concentration at up to 300 cm (up to 900 μM ; Fig. 5.4), are fully in line with this assumption. In the case of GP07BC, the SO_4^{2-} , CH_4 and HS^- profiles also indicate that AOM also occurs at this site.

Consequently, pore water profiles may suggest the consumption of dissolved sulfate through anaerobic methane oxidation at ~ 135 cm for GP05PC and at 25 cm depth for GP07BC (Fig. 5.4).

AOM processes can also induce authigenic carbonate formation, consuming simultaneously calcium and bicarbonate in a ratio of 1:2, and reducing the pore water Ca^{2+} and DIC content in a 1:2 ratio (Luff and Wallmann, 2003; Hensen et al., 2007; Reitz et al., 2011). The deepest pore fluids from piston GP05PC are strongly depleted in dissolved Ca^{2+} and Mg^{2+} , as indicated by Ca/Cl and Mg/Cl ratios below the SMTZ (Fig. 5.5) and leading to the occurrence of authigenic carbonates precipitation at this site. Nevertheless, during this process, not only dissolved Ca^{2+} and Mg^{2+} are consumed but also bicarbonates, producing a sink of DIC in pore waters. Our results showed that deep pore fluids from core GP05PC had high DIC values suggesting likely the occurrence of an additional source of DIC, such as methanogenesis resulting from anaerobic organic matter degradation rather than authigenic carbonate precipitation via AOM.

This hypothesis is also supported by our results in NH_4^+ and PO_4^{3-} encountered at GP05PC. Compared to the reference core GP03PC and to the uppermost part of the mud breccia interval, deep fluids from core GP05PC show extremely high N/P values (N/P ~ 1000 ; Table 5.2). Desorption of clay minerals could explain a strong increase in ammonium in the surrounding fluids (Williams et al., 1991) without affecting phosphate concentration in pore waters and explaining the relationship between these two species in our expelled

fluids. However, this ion exchange constitutes a minor process at Carmen MV and discarded as source of NH_4^+ . Consequently, we consider the large increase in the ammonium concentration in depth as consequence of thermal maturation of organic matter (Martin et al., 1996) rather than by clay mineral transformations that have not been observed. Our $\delta^{13}\text{C}_{\text{DIC}}$ results ($\sim -21\text{‰}$; Fig. 5.6) are in line with this assumption, together with previously reported data on gas composition (Blinova et al., 2011) and lipid biomarkers (López-Rodríguez et al., 2014) which have revealed a deep source for the expelled fluids from Carmen MV and consequently an important influence of thermal degradation of organic matter in deep rather than in-situ production via OSR processes.

5.5.4. Deep-source signature for deep sediments

The pore water profiles reveal the presence of deep fluids strongly depleted in Cl^- values at GP05PC and GP07BC (Fig. 5.5). Such decrease can be due by methane clathrates dissociation, meteoric water input, clay membrane ion exchange, clay mineral dehydration processes (De Lange, 1983; Dählmann and de Lange, 2003). The determination on stable isotopes $\delta^{18}\text{O}$ and δD of pore waters constitutes a useful tool to constrain the mechanism that affect the freshening of fluids (Dählmann and de Lange, 2003). Thus, the deepest pore fluid samples from GP05PC showed strong depletion in δD and enrichment in $\delta^{18}\text{O}$ (Fig. 5.6a and b) revealing a clear negative correlation between them (Fig 5.6a). It suggests the occurrence of deep-fluid freshening processes, which not only may alter the salinity but also affect its isotopic signature (Dählmann and de Lange 2003) e.g., clay mineral transformations of smectite to illite. Our δD and $\delta^{18}\text{O}$ isotopic composition points to the occurrence of smectite to illite transformation releasing water of this signature (e.g., Dählmann and de Lange, 2003). Clay mineral assemblages from three different cores recovered from the Carmen MV summit (see *Chapter 3*) show similar smectite and illite

content as well as an increase of the illite layers in mixed illite/smectite layers and the enhance of stacking order at the selected mud breccias (Reynolds, 1980; Drits and Tchoubar, 1990; Moore and Reynolds, 1997; Lanson et al., 2009). This finding is consistent with the clay mineral transformation which vary to randomly interstratified (R0) illite-smectite minerals (IS) to more illitic ordered (R1-R3) (Hower et al., 1976; Velde and Vasseur, 1992) and suggested to occur at greater depth under a range of temperature of about ~ 50 (Freed and Peacor, 1989; Kastner et al., 1991; Martin et al., 1996; Chan and Kastner, 2000; Haese et al., 2006) to ~ 160 °C (Kastner et al., 1991; Dählmann and de Lange, 2003). Moreover, indicators for enhanced temperatures for fluid-rock interaction can be derived from the pore water composition of the deep-fluids. Using the equations based on empirical K-Na, K-Mg and K-Ca geo-thermometer (Giggenbach, 1988; Haese et al., 2006) and applying these to the derived elemental values for the deepest samples we have estimated that deep fluids for Carmen MV has an average geo-temperature of ~ 130 , ~ 100 and ~ 215 °C, respectively.

Other indicators for such enhanced temperature are the significantly enriched concentrations of B and Li^+ compared to seawater (Kopf and Deyhle, 2002; Haese et al., 2003; You et al., 2004; Martin et al., 2006; Hensen et al., 2007; Scholz et al., 2009; Vanneste et al., 2011). Both elements are present in clay minerals that form at low temperature, where B and Li^+ act as exchangeable elements that can enter into the interlayer and replace cations (Bergaya et al., 2006). Under specific conditions, such as hydrothermal alteration of marine sediments at relatively low temperature (~ 50 °C; Chan et al., 1994; You et al., 1996b; James et al., 2003) or mineral dehydration reactions during burial (Brumsack and Zuleger, 1992; James and Palmer, 2000; Aloisi et al., 2004a; Hensen et al., 2007; Scholz et al., 2010), clay-rich sediments may release significant volumes of fluids, which in cases have high concentrations of dissolved B and Li^+ .

Several studies based on hydrothermal alteration of sediments have demonstrated that, under experimental conditions, clay-rich sediments expel fluids enriched preferentially in Li⁺ over B when temperatures rise 150 °C (You et al., 1995; Chan et al., 1999; You and Geiskes, 2001). Fluids from core GP05PC show enrichment of B (~ 9.6 mM) and Li (~ 135 µM), relatively to non-seepage affected sediments (Fig. 5.5). Also, the B/Li ratio in Carmen MV is relatively high, reporting steady values of ~ 60 (Table 5.2). In comparison with the reported values in the Gulf of Cadiz (Hensen et al., 2007; Scholz et al., 2009; Vanneste et al., 2011), deep fluids from Carmen MV show strong similarities (high B/Li value; > 50 and low concentration of Li; < 200 µM), which likely suggest the alteration of sediments at relatively low temperatures rather than the hypothesis of a source strata affected by hydrothermal processes as origin for the fluids in Alboran.

Radiogenic strontium isotope ratios measured at deepest pore fluids from GP05PC have shown that the ⁸⁷Sr/⁸⁶Sr ratio values distinctly differ from that present day Mediterranean seawater values (~ 0.709165; De Lange et al., 1990b), suggesting that these mud fluids may proceed from a different ambient rather than from sea water as well as from a carbonated-source. In comparison with the averaged Messinian ⁸⁷Sr/⁸⁶Sr ratios our strontium isotope ratios have relatively similar values, which apparently can suggest an evaporitic source for the expelled fluids. Nevertheless, no Messinian salts have been identified in the West Alboran, neither by sediment drilling nor by seismic profiles (Comas et al., 1999). Accordingly, the occurrence of leaching processes of cortical material seems more likely, suggesting the existence of a deep source that may influence the deep fluids in Carmen MV.

5.6. Conclusions


Geochemical and isotopic composition of pore waters and methane from Carmen MV has provided new insights into the biogeochemical processes oc-

curred at this MV as well as into the mechanisms of fluid discharge to the subsurface.

- Active gas venting at the crater of Carmen MV is confirmed by gas bubbling and presence of living chemosynthetic fauna (i.e., frenulate tubeworms) as well as by current pulses of methane discharge.
- Occurrence of downward advection and mixing with bottom seawater at this volcano is supported by the typical marine water signature of pore waters as well as by the constant stable carbon isotopic values of methane we have found in the uppermost breccias of GP05PC supporting the intrusion of seawater after episodes of gas outburst.
- Pore water composition, in particular SO₄²⁻-CH₄ depth profiles and enhancement of HS⁻ concentrations suggest that methane oxidation is mediated under anaerobic conditions with sulfate as the electron acceptor as well as high rates of anaerobic oxidation of methane (AOM) and sulfate reduction.
- Isotopic δ¹⁸O and δD compositions of pore waters evidence that smectite dehydration constitute a fluid origin mechanism that contribute to the pore water freshening at this MV.
- Empirical geo-thermometers (K-Na, K-Mg and K-Ca) reveal that fluids generate at temperature up to 200 °C. This temperature reaches at depth where locates the source Unit VI and Unit Va (Early to Middle Miocene in age), and endorses that this strata are under severe diagenetic conditions favorable for transformation of smectite to illite as well as hydrocarbon generation.
- Stable carbon isotopic compositions δ¹³C reveal that methane at Carmen MV proceeds from a deep thermogenic source.
- Radiogenic strontium isotopes (⁸⁷Sr/⁸⁶Sr) of Carmen MV fluids most likely suggest the occurrence of leaching processes of crustal rocks and sediments, supporting the existence of secondary processes that affect to the geochemical signature of pore waters.



6



Origin of lipid biomarkers
in mud volcanos from the
Alboran Sea, western
Mediterranean

Chapter 6

Origin of lipid biomarkers in mud volcanoes from the Alboran Sea, western Mediterranean

C. López-Rodríguez¹, A. Stadnitskaia², G.J. De Lange³, F. Martínez-Ruiz¹, M. Comas¹ and J.S. Sinninghe Damsté^{2,3}

[1] {Instituto Andaluz de Ciencias de la Tierra (CSIC-Granada University), Armilla, Spain}

[2] {NIOZ Royal Netherland Institute for Sea Research, Department of Marine Organic Biogeochemistry, Texel, the Netherlands}

[3] {Faculty of Geosciences, Utrecht University, Utrecht, the Netherlands}

Correspondence to: C. López-Rodríguez (carmina@ugr.es)

*Published in Biogeosciences 11, 3187-3204. DOI: 10.5194/bg-11-3187-2014

Abstract

Mud volcanoes (MVs) are the most prominent indicators of active methane/hydrocarbon venting at the seafloor on both passive and active continental margins. Their occurrence in the Western Mediterranean is patent at the West Alboran Basin, where numerous MVs develop overlaying a major sedimentary depocenter containing overpressured shales. Although some of these MVs have been studied, the detailed biogeochemistry of expelled mud so far has not been examined in detail. This work provides the first results on the composition and origin of organic matter, Anaerobic Oxidation of Methane (AOM) processes and general characteristics on MV dynamics using lipid biomarkers as the main tool. Lipid biomarker analysis was performed on MV expelled material (mud breccias) and interbedded hemipelagic sediments from Perejil, Kalinin and Schneider's Heart MVs located in the northwest margin of the Alboran Sea. The n-alkane distributions and n-alkane-derived indices (CPI and ACL), in combination with the epimerization degree of hopanes (22S/(22S+22R)) indicate that all studied mud breccia have a similar biomarker composition consisting of mainly thermally immature organic matter with an admixture of petroleum-derived compounds. This concordant composition indicates that common source strata must feed all three studied MVs.

The past or present AOM activity was established using lipid biomarkers specific for anaerobic methanotropic archaea (irregular isoprenoids and DGDs) and the depleted carbon isotope composition ($\delta^{13}\text{C}$) of crocetane/phytane. The presence of these lipid biomarkers, together with the low amounts of detected GDGTs, is consistent with the dominance of anaerobic methanotrophs of the ANME-2 over ANME-1, at least in mud breccia from Perejil MVs. In contrast, the scarce presence or lack of these AOM-related lipid biomarkers in sediments from Kalinin and Schneider's Heart MVs, suggest no recent active methane seepage has occurred at these sites. Moreover, the observed methane concentrations support the current activity of Perejil MV, and the very low methane seepage activity in Kalinin and Schneider's Heart MVs.

6.1 Introduction

Mud volcanoes (MVs) are mainly formed due to an extensive discharge of hydrocarbon-rich fluids from deeper sedimentary units. This phenomenon, commonly occurring in petroliferous regions, results from upward transport of deep-generated water and hydrocarbons to the subsurface (e.g. Guliyev and Feizullaev, 1997). The emitted fluids consist of a mixture of mud, water, and gases, mainly methane, together with an admixture of carbon dioxide, hydrogen sulphide, heavier methane homologues and other petroleum components (Dimitrov, 2002; Milkov et al., 2003). The origin of hydrocarbon gases at MVs can be either thermogenic (formed by maturation of buried organic matter in the subsurface as a consequence of increasing temperature and pressure) or biogenic (produced by anaerobic microorganisms from organic matter at low temperatures), or a mixture of both (Milkov et al., 2003; Stadnitskaia et al., 2007, 2008; Mastalerz et al., 2007; 2009; Etiope et al., 2009).

In addition to hydrocarbon-rich fluids, MVs expel large volumes of clastic volcanic material called “mud breccia” (Cita et al., 1981; Akhmanov, 1996). It is a complex mixture of matrix and rock fragments, mechanically incorporated into the eruption deposit by the powerful upward transport of fluids (Akhmanov, 1996; Akhmanov and Woodside, 1998). Mud breccias, rock clasts and matrix contain important information regarding the composition and genesis of sediments in the subsurface, their maturity and hydrocarbon potential of the area (Akhmanov, 1996; Ovsyannikov et al., 2003; Wheeler and Stadnitskaia, 2011 and references therein).

Ascending fluids radically affect sedimentary environments at and below the sea floor. Due to the supply of organic and inorganic components (methane, hydrogen sulfide, carbon dioxide), MVs and cold seeps in general support a unique niche of microbes and other organisms, establishing their survival through chemosyn-

thesis (e.g. Olu et al., 1996; Corselli and Basso, 1996; Vanreusel et al., 2009). Microbial anaerobic oxidation of methane (AOM) is performed by a consortium of anaerobic methane-oxidizing archaea (ANME) and sulfate reducing bacteria (SRB) (Reeburgh 1976, 1996; Boetius et al., 2000, Knittel and Boetius, 2009) and is considered to be one of the main processes occurring at MVs and methane seepage environments. The methanotrophic archaea (falling in the ANME-1, -2 and -3 phylogenetic clusters; Knittel et al., 2005) that mediate this process contain a variety of ¹³C-depleted diagnostic lipid biomarkers such as glycerol dialkyl glycerol tetraethers (GDGTs), isoprenoidal dialkyl glycerol diethers (DGDs) or irregular isoprenoids (Niemann and Elvert, 2008 and references therein). Thus, their presence in sediments provides information on the presence of AOM processes, and therefore the availability of methane.

Here we report the lipid biomarker composition of Alboran MVs, i.e. Perejil, Kalinin and Schneider’s Heart (Fig. 6.1). We use these data to assess the source-strata for the expelled materials and to determine the thermal maturity level of the organic matter present in the mud breccia matrices. We use lipid biomarkers related to methanotrophic archaea, and the measured methane content to evaluate the recent activity of these MVs. In addition, we apply the relative contribution of methanotrophic Euryarchaeota vs. planktonic Thaumarchaeota, to determine the AOM active zone. Furthermore, on the basis of lipid biomarker distribution and compound-specific stable carbon isotope composition, we also discuss the AOM microbial community.

6.2 Geological background

The Alboran Sea is a marginal basin located in the westernmost Mediterranean Sea. Differences in structural architecture, sedimentary infill and seafloor morphology within allow to differentiate the Western, Eastern and Southern Alboran Ba-

sins (Fig. 1). The Alboran Sea Basin is a remnant of the Miocene back-arc basin from the Gibraltar Arc System. The Gibraltar Arc System comprises the Betics (Spain) and Rif (Morocco) orogenic arc, the Alboran and Algerian back-arc basins, and the forearc accretionary prism in the Atlantic side. Within the Gibraltar Arc System, the Alboran Basin evolved since the Late Oligocene in a geodynamic setting characterized by a pervasive N-S convergence between the Eurasian and African plates (Dewey et al., 1989).

Geological and geophysical data demonstrate that the Alboran Sea originated in the Early Miocene, and evolved first by extensional tectonics (from Middle to Upper Miocene) and later has undergone significant contractive tectonics (from Late Miocene onwards). Post-Miocene contractive tectonics caused a major reorganization of the basin, which resulted in prominent N-S shortening of the marine realm and uplifting and emersions on the surrounding Betics and Riff chains. The recent and actual active tectonics conditioned the present coastal line position, as well as the current seafloor morphology (Comas et al., 1999, and references therein).

Basement and sedimentary cover beneath the Alboran Sea are known from commercial wells and ODP Leg 161 drilling. The thicker sedimentary depocenter is located in the West Alboran basin (Fig. 6.1) where more than 7 km of sediments exist on top of the metamorphic basement (Fig. 6.2) (Jurado and Comas, 1992; Soto et al., 1996; Comas et al., 1996)

The West Alboran basin is characterized by the presence of extensive shale (mud-rocks) diapirism and shale tectonics conditioned by the existence of overpressured units at depth (Comas et al., 1999, 2012; Soto et al., 2010). Overpressure is conditioned by significant gas and fluids contents in the basal units of the West Alboran Basin (Unit VI and Unit V from Jurado and Comas, 1992; Fig. 6.2), as it has been reported by logging (sonic velocity, density and resistivity) data from

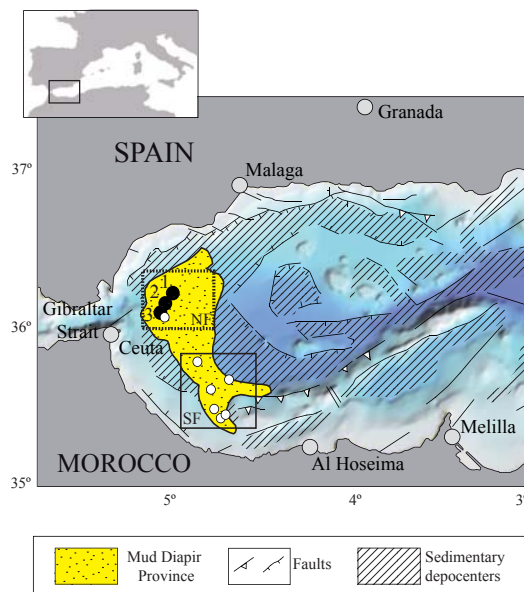


Figure 6.1. The Alboran Sea showing the location of the Mud Diapir Province and the Northern (NF) and Southern (SF) MV fields. Black dots correspond to the studied 1) Perejil, 2) Kalinin and 3) Schneider's Heart MVs; white dots refer to other MVs. Modified after Comas et al., 1999.

Andalucia-G1 and Alboran-A1 boreholes drilled in the West Alboran basin. Furthermore, borehole sampling indicate that Unit VI (Burdigalian in age) is formed of under-compacted (pressurized) olistostromic or brecciated materials made of heterogeneous rock-fragments (blocks, boulders and clasts) of different ages embedded in a shale matrix intercalated to clayed, marly and sandy intervals, and that Unit Va (Langhian in age) also contains under-compacted green clays (Jurado and Comas, 1992, Diaz-Merino et al, 2003) (Fig.6.2).

Mud volcanism and pockmarks occurring in the West Alboran basin lie on top of the huge Mud Diapir Province that extends from the Iberian to the Moroccan margins (Fig. 6.1). As evidenced by previous works, the mud volcanism is linked to recent stages of shale diapirism happened during compressive tectonics (Plio-Quaternary, from 4-5 Ma onwards), which conditioned pierced diapirs and lend subsequently to mud volcanism at the seafloor (Comas et al, 2010, and references the-

rein). Seismic profiles show that volcano feeder-channels connect to deeper shale-diapir structures proving that volcanic processes bring up to the seafloor over-pressured shales and olistostromes from Unit VI (Fig. 6.2) laying at more than 5 km deep (Talukder et al., 2003; Comas et al., 2012).

The extruded mud breccias contain exotic rocks from different sedimentary units. Micropaleontological data from core sampling indicate that MVs bring up to the seafloor sedimentary rocks of different ages but ranging from the Late Cretaceous to the Late Miocene (Sautkin et al., 2003; Gennari et al., 2013). A deep thermogenic source of fluids expelled by the Alboran MVs has been suggested on the basis of ^{13}C isotope determinations in authigenic carbonates, pore-water analyses and gas composition (Blinova et al., 2011; López-Rodríguez et al., 2014). Abundance of chemosynthetic habitats (bivalves, tubeworms) on the top of some MVs concludes current methane/hydrocarbon seeping in some of them (Hilário et al., 2011). However, the majority of the Alboran MVs seem to be inactive, or maybe just dormant (Comas et al., 2010).

6.3 Materials and methods

6.3.1 Samples

The studied sediment cores were collected during the first leg of Ristretto e Lungo expedition in December 2010 on board R/V Meteor. In total, sediments from four gravity cores and two box-cores (Fig. 6.2, Table 6.1) were chosen for this study on the basis of changes in lithology, gas manifestation and gas saturation. The sampling operations were performed using a 1200 kg gravity corer with a 6 m barrel and 11 cm inner diameter tubings. The 900 kg box-corer had a round box with an internal diameter of 30 cm and a height of 55 cm. The recovered gravity cores were cut in 1 m sections, split open lengthwise and lithologically described. Box-cores were sub-sampled using

pvc tubes of 50 cm length and 9 cm inner diameter which were pushed vertically in the sediment. Subsequently, these sampling tubes were split open lengthwise and lithologically described. The sub-sampling for lipid biomarkers was done on board in a + $^{\circ}\text{C}$ container as soon as possible after recovery. The sediment was sampled every 2 to 5 cm taking into consideration lithological variations. Samples were stored and transported at -20 $^{\circ}\text{C}$ for on-land laboratory studies.

6.3.2. Extraction and separation

A total of 20-50 g of freeze-dried sediments were crushed to a fine powder, and extracted with an automatic Accelerated Solvent Extractor (ASE 200/DIONEX) using a solvent mixture of dichloromethane: methanol (9:1, v/v) at 1000 psi and 100 $^{\circ}\text{C}$. The obtained total lipid extracts were rotary evaporated to near dryness and elemental sulfur was removed by adding ca. 10 mg of activated copper and stirring the sample overnight. An aliquot of the total lipid extract was used for analysis of total lipid distribution. To this end, fatty acids were methylated by adding CH_2N_2 and alcohol groups were silylated by adding 25 μl pyridine and 25 μl of N, O-bis(trimethylsilyl)-trifluoroacetamid (BSTFA) and heating at 60 $^{\circ}\text{C}$ for 20 min. Another part of the total lipid extract was chromatographically separated into apolar and polar fractions using a column with Al_2O_3 (activated for 2 h at 150 $^{\circ}\text{C}$) as stationary phase. Apolar compounds were eluted using hexane: dichloromethane (9:1, v/v), and polar compounds, including glycerol diethers and glycerol dialkyl glycerol tetraethers (GDGTs) core membrane lipids, were obtained with methanol: dichloromethane (1:1, v/v) as eluent. To calculate absolute concentration of biomarkers in mud breccia matrixes, a known amount of anteiso-C22 hydrocarbon was added to each fraction as internal standard (Stadnitskaia et al., 2007; 2008).

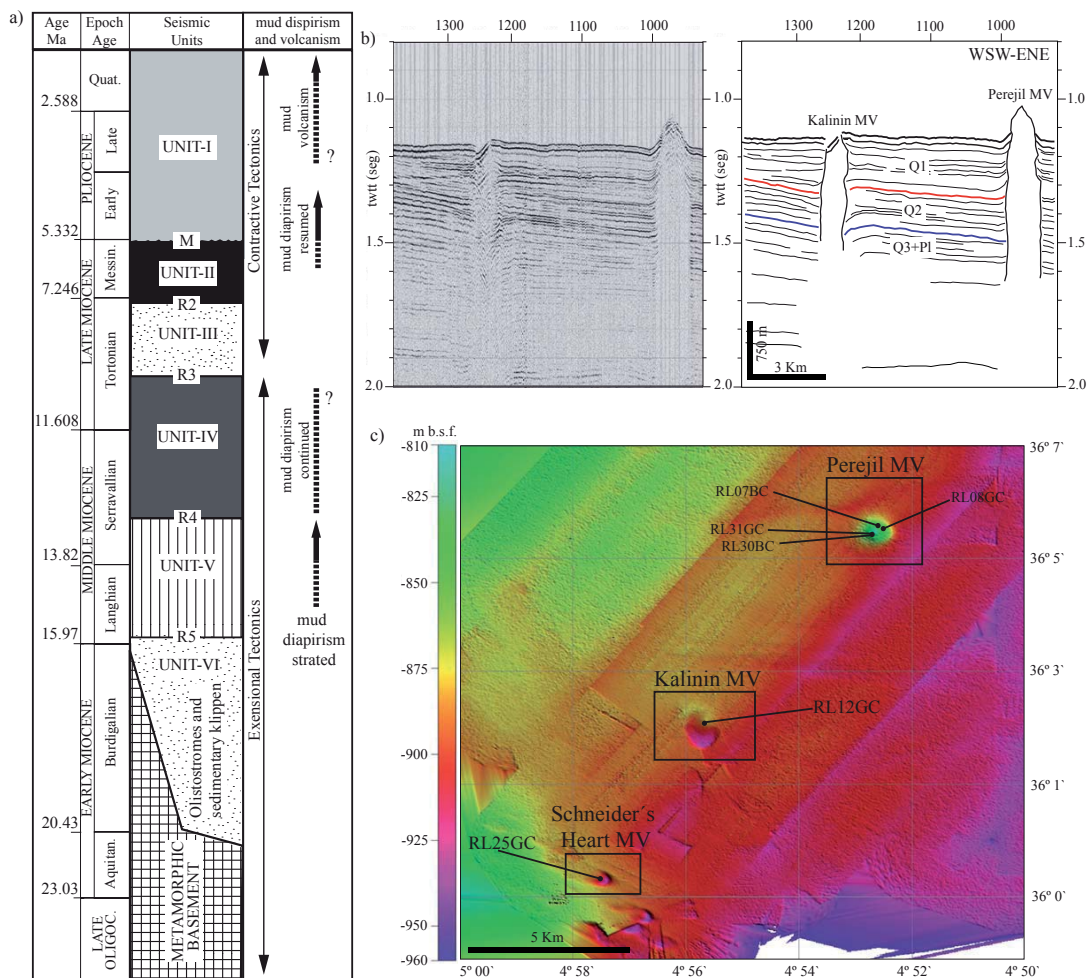


Figure 6.2. a) Seismic stratigraphic units, major regional reflectors and main sedimentary sequence documented in the Betic Neogene basins (modified after Jurado and Comas, 1992; Rodríguez-Fernández et al., 1999); M-Messinian unconformity. R-reflectors correspond to major unconformities within sediments. b) High-resolution seismic line PS200MS across Perejil and Kalinin MVs (Talukder, 2003); Blue and red lines refer to seismic reflectors within the Plio-Quaternary sequence (Unit I) (Jurado and Comas, 1992; Comas et al., 1999) c) Multibeam swath bathymetry of the Northern MV field showing Perejil, Kalinin and Schneider's Heart MVs. Numbers referred to studied sites (gravity and box-cores).

6.3.3 Analysis and identification of lipid biomarkers

Gas Chromatography (GC) was performed with a Thermo Finnigan TRACE instrument equipped with a fused silica capillary column (CP Sil-5, 25m x 0.32 mm, df = 0.12 μ m), with a flame ionization detector and helium as a carrier gas. Samples were injected at 70°C. The GC oven temperature was subsequently raised to 130°C at a rate of 20°C min⁻¹, and then to 320°C at 4°C min⁻¹. The temperature was then held constant for 15 min.

All fractions were analyzed by gas chromatography-mass spectrometry (GC-MS) for compound identification. The gas chromatograph was coupled to a Thermo Finnigan TRACE DSQ quadrupole mass spectrometer with ionization energy of 70 eV, with a mass range of m/z 50-800. GC conditions of GC-MS were the same as those described for GC.

To determine the distribution of intact glycerol dialkyl glycerol tetraethers (GDGTs), the polar fractions of the sediment extracts were analyzed using high performance liquid chromatography-

Table 6.1. General sampling information on the studied sites: location, water depth and length of the studied cores.

Core Code	Structure	Location	Sampling Site	Depth (m)	Recovery (cm)
RL07BC	Perejil Mud Volcano	36° 6.11' N; 04° 53.08' W	Flank	818.9	40.0
RL08GC	Perejil Mud Volcano	36° 6.11' N; 04° 53.08' W	Flank	822.4	262.5
RL30BC	Perejil Mud Volcano	36° 6.07' N; 04° 53.11' W	Crater	807.8	30.0
RL31GC	Perejil Mud Volcano	36° 6.07' N; 04° 53.11' W	Crater	807.8	270.5
RL12GC	Kalinin Mud Volcano	36° 3.00' N; 04° 55.90' W	Flank	872.6	280.0
RL25GC	Schneider's Heart Mud Volcano	36° 0.28' N; 04° 57.57' W	Flank	924.0	310.0

mass spectrometry (HPLC-MS) (Hopmans et al., 2000) using an Agilent 1100 series/1100 MSD series instrument, with auto-injection system and HP Chemstation software. An Alltech Prevail Cyano column (150 mm x 2.1 mm, 3 μ m) was used with hexane: propanol (99:1, 13v) as mobile phase (0.2 ml min⁻¹). After 5 min, a linear gradient to 1.8% propanol was used (45 min). MS analysis and quantification of both isoprenoidal and branched GDGTs followed methods reported by Weijers et al. (2006). The GDGT-based ratios (Methane Index, MI; GDGT-0/Crenarchaeol and GDGT-2/Crenarchaeol) were applied to express the relative distribution of methanotrophic Euryarchaeota (presumably represented by GDGT-1, -2 and -3) vs. planktonic and possibly benthic Thaumarchaeota (represented by crenarchaeol and its regioisomer) (Sinninghe Damsté et al., 2002; Zhang et al., 2011; Weijers et al., 2011; Schouten et al., 2012).

Isotope-ratio-monitoring gas chromatography-mass spectrometry (IRM-GC-MS) was performed on a Finnigan MAT DELTA plus XL instrument used for determining compound-specific $\delta^{13}\text{C}$ values. The GC used was a Hewlett Packard 6890 A series, and the same analytical conditions were used as described for GC and GC-MS. For carbon isotopic correction of the added trimethylsilyl groups, the stable carbon isotope composition of the used BSTFA was determined. Obtained

values were reported in per mil relative to the VPDB standard. In order to monitor the accuracy of the measurements, the analyses were carried out with co-injection of two standards, C20 and C24 n-alkanes, with a known stable carbon isotope composition.

6.3.4 Methane and sulfate analyses

Methane concentrations in hemipelagic sediments and mud breccia from Perejil, Kalinin and Schneider's Heart MVs were routinely measured on board. Decapped 10 ml syringes were used to sample the fresh sediment immediately upon recovery. The volume of sediment was rapidly put into a 65 ml glass vial prefilled with a saturated NaCl solution. The vial was immediately closed and mixed. Subsequently, a 5 ml headspace was made (for full procedure, see Mastalerz et al., 2007). The methane concentration in the headspace was determined on-board with a Shimadzu gas chromatograph with a Flame Ionization Detector.

For sulphate analyses, the pore water was extracted on board using rhizons, acidified, and analyzed on-land using ICP-AES (for details see Mastalerz et al., 2007).

6.4 Results

6.4.1 Core lithologies

Perejil MV

Two gravity-cores and two box-cores were taken at Perejil MV. Cores RL08GC and RL07BC were taken from the flank, RL31GC and RL30BC from the crater of the structure (Fig. 6.2). The “flank” box-core RL07BC contained 40 cm of typical structureless dark gray mud breccia, for which the top 10 cm were oxidized (Fig. 6.3a). At this site, methane bubbles were present as well as abundant Pogonophora tube worms at the top. Additionally, chemosynthetic fauna such as living Acharax bivalves were found at ~10 cm depth in the mud breccia. Core RL08GC, also taken at the flank, contained 263 cm of alternations of hemipelagic sediments and mud breccia (Fig. 3a). Although two mud breccia layers could be distinguished, the boundaries were not always fully distinct. The upper layer, from 65 to 79 cm, consisted of soft mousse-like mud breccia with occasional rock clasts, intensively bioturbated. The lower interval from 135 to 209 cm consisted of stiff mud breccia moderately bioturbated in the uppermost part. In both mud breccia intervals a few fragments of mudstone were found, and there was a distinct, moderate smell of H₂S. Hemipelagic sediments consisted of grayish brown marls with some foraminifera. The two sedimentary locations within the crater of Perejil MV showed different lithologies at their topmost sediments (hemipelagic and mud breccia, respectively) (Fig. 6.3a).

In contrast to the sediments on the flank of the MV, the 271 cm of crater sediments in core RL31GC were composed of a typical structureless dark gray mud breccia, with millimeter to centimeter-sized rock clasts of claystone, mudstone and carbonates (Fig. 6.3a). At this site, no hemipelagic cover was present and a strong scent of H₂S was noticed along the whole mud breccia section. The top 8 cm were visibly bioturbated. This is consistent with observations in the nearby box-core RL30BC

that contained 30 cm of oxidized mud breccia for which the top 10 cm were clearly bioturbated. Authigenic pyrite in the form of spherules of centimetric size and concretions were observed in the mud breccia matrix and rock clasts from this site.

Kalinin and Schneider’s Heart MVs

Gravity-cores taken from Kalinin and Schneider’s Heart MVs (RL12GC and RL25GC; Fig. 6.2) recovered 272 cm and 300 cm, respectively, containing both hemipelagic sediments and mud breccia. The lowermost part of the hemipelagic sediments at Schneider’s Heart MVs was moderately bioturbated (Fig. 6.3b), and at this site and at Kalinin MV the boundary with the mud breccia interval were irregular and not well expressed. In both structures the mud breccia intervals were covered with hemipelagic sediments: 78 cm and 217 cm at Kalinin and Schneider’s Heart MVs, respectively. MV deposits in both locations were represented by mousse-like mud breccia with a few millimeter sized rock clasts of sandstone and mudstone. At both MVs, the upper part of the mud breccia interval was moderately bioturbated.

6.4.2 Lipid biomarker distributions

The total lipid fractions of different sediment horizons from the MVs sedimentary cores showed similar lipid biomarker distribution patterns; apolar compounds significantly dominated over the polar. Hydrocarbons (within the analytical window of gas chromatography; i.e. up to a molecular weight of ca. 800 Da) were mainly represented by a series of C17-C37 n-alkanes with dominance of n-C23- n-C33, with a maximum at n-C29 or n-C31, and a moderate odd-over-even carbon number predominance (Fig. 6.3). The Carbon Preference Index (CPI) (19-36) (Bray and Evans, 1961) as well as the Average Chain Length (ACL) (Poynter, 1989) indices showed some variation along the sedimentary sections, mainly at the boundary between hemipelagic sediments and mud breccia intervals. In mud breccia inter-

vals the CPI values varied between 2.0 and 2.9 and ACL values ranged from 27.4 to 29.4 (Fig. 6.3; Table 6.2). Compared to mud breccia, hemipelagic sediments showed higher CPI (19-36) values, from 3.0 to 3.4, as well as higher ACL values, from 28.8 to 29.1 (Fig. 6.3; Table 6.2). As noted above, the boundaries between hemipelagic sediments and mud breccia were not always distinct. This seems also apparent for the CPI index, most notably for the lowermost mud interval at Perejil flank (RL08GC, Fig. 6.3a)

Pentacyclic triterpanes were identified at all studied MVs (Fig. 6.4, Table 3). For the apolar fractions the 17 α , 21 β (H)-hopane (C30) was the most dominant compound followed by 22R 17 α , 21 β (H)-homohopane (C31) and 17 α , 21 β (H)-30-norhopane (Fig. 6.4; Table 6.3). Hopanes with the 17 α , 21 β (H)-configuration in the range of C30–C32 were the main epimers. In this range, $\beta\alpha$ -epimeric series were not detected and the only hopane with 17 β , 21 β (H)-configuration found was homohopane. Unsaturated hopanoids were represented by neohop-13(18)-ene, and hop-22(29)-ene (diploptene; V see appendix A for structures) (Fig. 6.4; Tables 6.4). C32 benzohopane was only found in the mud breccia of Perejil and Kalinin MVs (Fig. 6.4; Table 6.3). Functionalized triterpenoids were represented by diploptero (17 β , 21 β (H)-hopan-22-ol; VI), which was detected only in Perejil and Kalinin MVs (Fig. 6.4; Tables 6.3-6.4).

Irregular isoprenoids diagnostic for methanotrophic archaea associated with AOM (e.g. Elvert et al, 2000; Pancost et al., 2000; Hinrichs et al., 2000) such as crocetane (2, 6, 11, 15-tetramethylhexadecane; I) and PMI (2, 6, 10, 15, 19-pentamethylcosane; II), were identified at all studied sites (Table 6.4). Crocetane was present in all the studied sites, whereas PMI was found only at few depths intervals at Perejil, Kalinin and Schneider's Heart MVs (Table 6.4). Sediments from the crater of Perejil MV were examined for the presence of crocetane relative to the more common and co-eluting acyclic isoprenoid phytane. This was done

using the examination of mass chromatograms for m/z 183 and m/z 169 - diagnostic fragment ions for phytane and crocetane, respectively (cf. Bian et al., 2001). This resulted in an estimated fractional abundance of crocetane of 0.4 to 0.8 at 80-110 cm (Fig. 6.5). Compound-specific stable carbon isotope measurements of the peak comprised of crocetane and phytane revealed a variation from -65 ‰ to -37 ‰, with the lowest values in the 80-110 cm interval (Fig. 6.5).

Archaea-derived isoprenoid dialkyl glycerol diethers (DGDs), such as archaeol (III) and hydroxyarchaeol (IV), were found at two MVs. Archaeol was detected in the mud breccia from Perejil, both at the crater and flank sites, and Kalinin MVs. Hydroxyarchaeol was only identified in the mud breccia from Perejil MV crater as well as in the uppermost sediments at the flank site (Table 6.4). Non-isoprenoidal DGDs (Pancost et al., 2001) were only identified at the mud breccia interval from Schneider's Heart MV (Table 6.4).

Specific glycerol dibiphytanyl glycerol tetraethers (GDGTs; Appendix) (Schouten et al., 2012 and reference therein) were detected in all cores. The GDGT distributions showed a clear dominance of isoprenoidal over branched GDGTs (Fig. 6.6). The isoprenoidal GDGTs were dominated by GDGT-0 (VII) and crenarchaeol (XI), with maximum abundances in average of 46 % and 51 %, respectively, in mud breccias and 35 % and 52 % in hemipelagic sediments. The average abundances of GDGT-1 (VIII) and GDGT-2 (IX) were much lower, i.e. 7.3 % and 7.6 % for hemipelagic sediments, and 8.1 % and 9.5 % for mud breccia.

At every site GDGT- based ratios (GDGT-0/crenarchaeol and GDGT-2/crenarchaeol) revealed substantial variations with depth, mainly matching with the boundary between hemipelagic sediments and mud breccia intervals (Table 6.2). In mud breccia from Perejil (crater and flank) and Kalinin MV, both GDGT-0/crenarchaeol and GDGT-2/crenarchaeol ratios were enhanced. In contrast, these ratios were different for mud breccia from

Perejil Mud Volcano

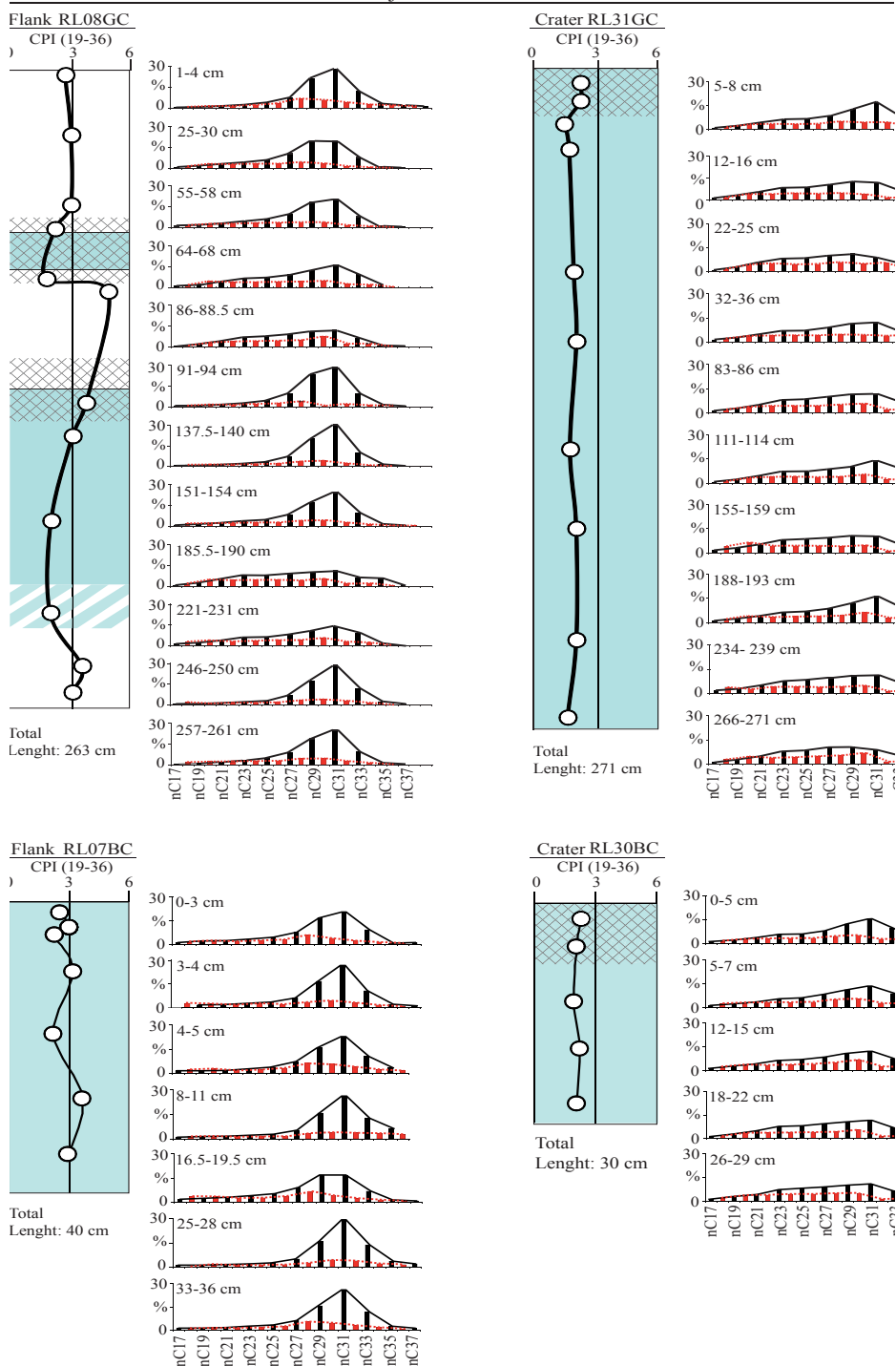


Figure 6.3. Distribution of n-alkanes and Carbon Preference Index (CPI) profiles along the sedimentary sections for a) Perejil MV flank and crater and b) Kalinin and Schneider's Heart MVs. Striped area correspond to hemipelagic sediments with lipid characteristics of mud breccia. Relative concentrations were calculated by normalization of peak areas obtained by gas chromatography.

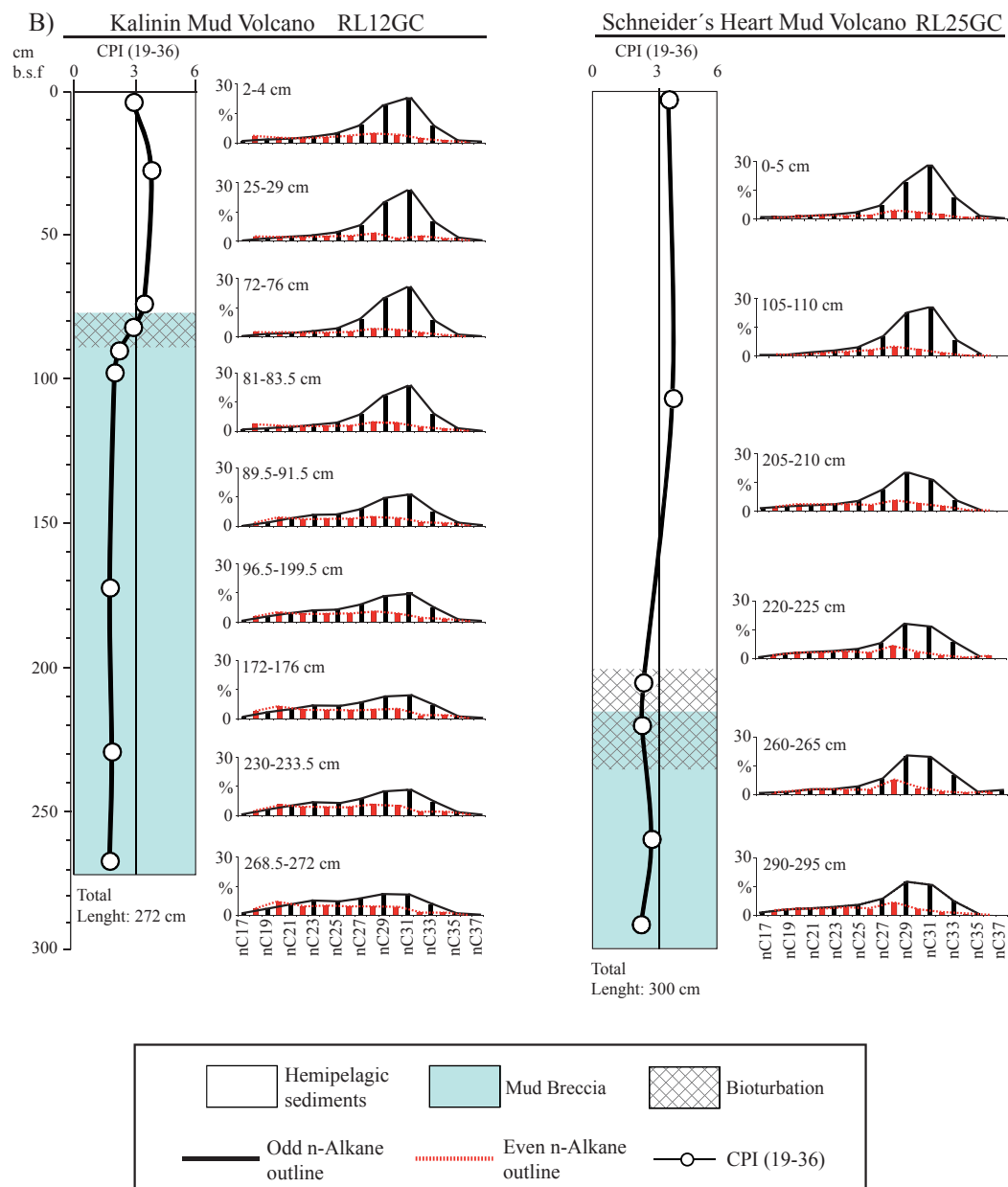


Figure 6.3. (cont.)

Table 6.2. Compound indexes related with n-alkanes (Carbon Preference Index, CPI and Average Chain Length, ACL), hopane and GDGTs-based ratios for the studied sites.

Lithology	intervals (cm b.s.f.)	n -Alkanes		CPI (C29-C32)	ACL (C19-C35)	Hopanoids		GDGTs Methane Index	GDGT-2/ Crenarch.	GDGT-0/ Crenarch.
		CPI (C19-C36)	C31 22S/(22S+22R)			C32 22S/(22S+22R)				
Perejil Mud Volcano Flank RL078C										
Mud Breccia	0-3	2.6	-	4.6	28.8	-	-	0.22	0.14	0.61
	3-4	3.0	-	5.5	29.4	-	-	0.20	0.13	0.56
	4-5	2.3	-	3.7	29.5	-	-	0.20	0.12	0.56
	8-11	3.2	-	5.6	30.1	-	-	0.23	0.15	0.68
	16.5-19.5	2.3	-	4.1	28.4	-	-	0.21	0.13	0.60
	25-28.5	3.7	-	5.9	30.0	-	-	0.21	0.13	0.58
	33-36	3.0	-	4.7	29.6	-	-	0.20	0.12	0.56
Hem. Sed. Av.		-	-	-	-	-	-	-	-	-
M.B. Average		2.9	-	2.9	29.4	-	-	0.21	0.13	0.59
Main Average		2.9	-	2.9	29.4	-	-	0.21	0.13	0.59
Perejil Mud Volcano Flank RL086C										
Hem. Sed.	1-4	2.7	-	4.4	29.7	-	-	0.20	0.12	0.59
	25-30	3.0	-	6.4	28.5	-	0.53	0.21	0.13	0.60
	55-58	3.0	-	5.8	28.5	0.51	0.39	0.20	0.13	0.55
Mud Breccia	64-68	2.2	-	3.6	28.1	0.31	0.57	0.21	0.13	0.58
Hem. Sed.	86-88.5	1.7	-	2.1	27.5	0.38	0.36	0.25	0.17	0.61
	91-94	5.0	-	14.7	29.4	0.43	0.31	0.22	0.14	0.60
	137.5-140	3.8	-	6.7	29.6	0.57	0.45	0.20	0.13	0.53
Mud Breccia	151-154	3.1	-	5.5	29.1	-	0.41	0.23	0.15	0.56
	185.5-190	1.2	-	2.5	27.8	0.45	0.50	0.34	0.27	1.00
	221-231	2.0	-	2.7	28.1	0.40	-	0.38	0.33	1.08
Hemi. Sed.	246-250	3.6	-	6.1	29.8	0.38	0.31	0.21	0.13	0.56
	257-261	3.1	-	5.6	29.2	0.56	0.38	0.21	0.13	0.58
Hem. Sed. Av.		3.0	-	3.1	28.8	0.44	0.38	0.31	0.21	0.86
M.B. Average		2.8	-	2.9	28.7	0.44	0.48	0.24	0.17	0.67
Main Average		3.0	-	3.1	28.8	0.44	0.42	0.29	0.20	0.78
Perejil Mud Volcano Crater RL308C										
Mud Breccia	0-5	2.3	-	3.2	28.3	-	-	0.22	0.14	0.59
	5-7	2.1	-	2.6	28.2	-	-	0.19	0.12	0.54
	12-15	1.9	-	2.2	27.7	-	-	0.25	0.17	0.72
	18-22	2.2	-	2.6	27.5	-	-	0.26	0.18	0.75
	26-29	2.1	-	2.7	27.6	-	-	0.31	0.24	0.86
Hem. Sed. Av.		-	-	-	-	-	-	-	-	-
M.B. Average		2.1	-	2.1	27.9	-	-	0.25	0.17	0.69
Main Average		2.1	-	2.1	27.9	-	-	0.25	0.17	0.69

Lithology	intervals (cm b.s.f.)	n-Alkanes		ACL (C19-C35)	Hopanoids		C32 22S/(22S+22R)	GDGTs		GDGT-2/ Crenarch.	GDGT-0/ Crenarch.
		CPI (C19-C36)	CPI (C29-C32)		C31 22S/(22S+22R)	Methane Index					
Perejil Mud Volcano Grater RL31GC											
Mud Breccia	5-8	2.3	3.3	28.2	-	0.46	0.23	0.15	0.61		
	12-16	2.3	3.9	27.2	0.38	-	0.21	0.13	0.62		
	22-25	1.6	1.8	26.8	0.30	0.55	0.21	0.13	0.59		
	32-36	1.7	2.6	27.4	0.50	0.47	0.22	0.13	0.61		
	83-86	2.0	2.6	27.2	0.41	0.52	0.30	0.22	0.79		
	111-114	2.1	2.8	27.8	-	-	0.29	0.22	0.84		
	155-159	1.8	2.9	26.9	-	-	0.38	0.33	1.02		
	188-193	2.1	2.9	28.0	0.46	0.52	0.33	0.26	0.94		
	234-239	2.1	2.9	27.1	0.60	0.33	0.33	0.26	0.97		
	266-271	1.7	1.7	26.9	0.35	0.51	0.45	0.48	1.28		
Hem. Sed. Av.		-	-	-	-	-	-	-	-		
M.B. Average		2.0	2.0	27.4	0.43	0.50	0.49	0.38	1.38		
Main Average		2.0	2.0	27.4	0.43	0.50	0.49	0.38	1.38		
Kalinin Mud Volcano RL12GC											
Hemipelagic	2-4	2.9	5.8	29.0	0.52	0.50	0.21	0.12	0.54		
Sediments	25-29	3.8	10.0	29.3	0.39	-	0.22	0.12	0.55		
	72-76	3.4	6.7	29.1	0.43	0.42	0.23	0.13	0.56		
Mud Breccia	81-83.5	2.9	5.6	29.0	0.32	0.43	0.23	0.15	0.54		
	89.5-91.5	2.2	4.1	28.2	0.45	0.53	0.26	0.16	0.66		
	96.5-100.5	2.0	3.6	27.8	0.44	0.43	0.28	0.16	0.72		
	172-176	1.7	2.9	27.5	0.55	0.47	0.35	0.22	0.86		
	230-233.5	1.8	3.0	27.6	0.44	0.49	0.31	0.19	0.74		
	268.5-272	1.7	3.0	27.1	0.42	0.45	0.35	0.22	0.85		
Hem. Sed. Av.		3.4	3.5	29.1	0.44	0.46	0.33	0.19	0.82		
M.B. Average		2.1	2.1	27.9	0.43	0.47	0.30	0.18	0.73		
Main Average		2.5	2.5	28.3	0.44	0.47	0.31	0.18	0.75		
Schneider's Heart Mud Volcano RL25GC											
Hemipelagic	0-5	3.7	6.7	29.6	0.43	0.57	0.19	0.11	0.55		
Sediments	105-110	3.9	7.1	29.2	0.35	0.42	0.26	0.17	0.69		
	205-210	2.4	4.5	28.2	0.44	0.48	0.19	0.10	0.66		
Mud Breccia	220-225	2.4	5.0	28.4	0.48	0.49	0.12	0.04	1.01		
	260-265	2.8	5.9	29.1	0.57	0.50	0.10	0.03	1.02		
	290-295	2.3	5.0	28.1	0.61	0.54	0.12	0.04	1.00		
Hem. Sed. Av.		3.3	3.4	29.0	0.41	0.49	0.22	0.13	0.63		
M.B. Average		2.5	2.6	28.5	0.55	0.51	0.11	0.04	1.01		
Main Average		3.0	3.1	28.7	0.48	0.50	0.16	0.08	0.82		

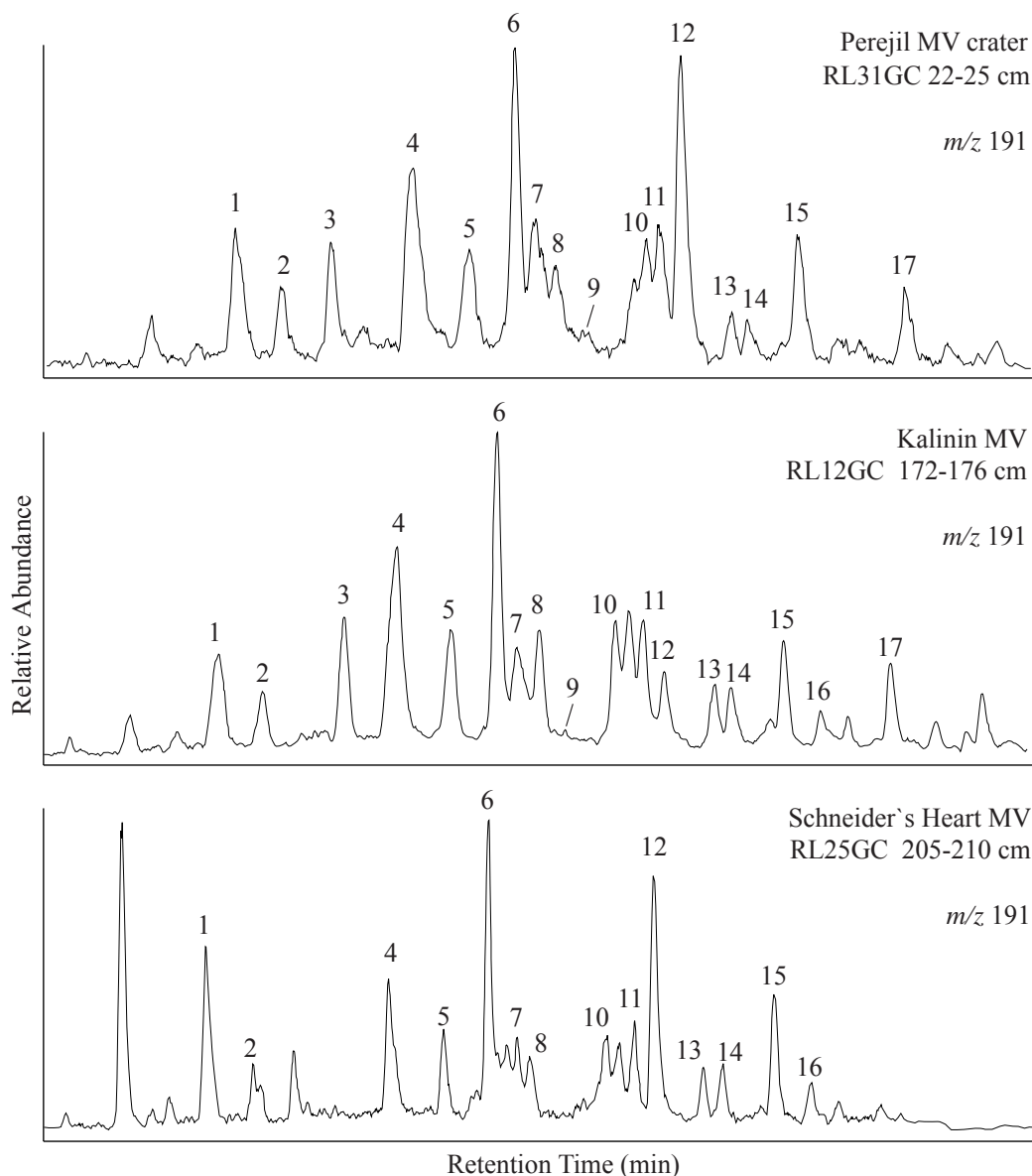


Figure 6.4. Typical m/z 191 mass chromatograms showing distributions of pentacyclic triterpenoids present in selected mud breccia samples of Perejil, Kalinin and Schneider's Heart MVs. Numbers refer to compounds listed in Table 3.

Schneider's Heart MV, the latter being similar to that at Perejil whereas the former was even lower than that for hemipelagic sediments, respectively (Table 6.2). The Methane Index (MI) defined by Zhang et al. (2011) was used to trace the presence of methanotrophic archaea. The MI ranged from 0.10, as the minimum value reported at Schneider's Heart mud breccia to a maximum of 0.45 at the

mud breccia interval from Perejil MV crater (Table 6.2). On average, MI ranged from 0.22 to 0.33 at the hemipelagic sedimentary drapes, while at mud breccia intervals the MI varied between 0.11 and 0.49, in average (Table 6.2).

Low amounts of branched GDGTs (i.e. <5% of total GDGTs) are present at all studied sites. In comparison with hemipelagic sediments, mud

Table 6.3. Pentacyclic triterpenoids identified in Perejil MV crater and flank, Kalinin and Schneider's Heart MVs.

Peak number	Compound name	Carbon number
1	17 α (H)-trisnorhopane	C27
2	17 β (H)-trisnorhopane	C28
3	17 α -bisnormoretane	C28
4	17 α 21 β (H)-30-norhopane	C29
5	17 β 21 α (H)-30-norhopane	C29
6	17 α 21 β (H)-hopane	C30
7	Isohop-13(18)-ene	C30
8	17 β 21 α (H)-hopane (moretane)	C30
9	Diplopterol (17 β 21 β (H)-hopan-22-ol)	C30
10	17 α 21 β (H)-homohopane 22S	C31
11	17 α 21 β (H)-homohopane 22R	C31
12	Diploptene (hop-22(29)-ene)	C30
13	17 α 21 β (H)-bishomohopane 22R	C32
14	17 α 21 β (H)-bishomohopane 22R	C32
15	17 β 21 β (H)-homohopane	C31
16	17 α 21 β (H)-trishomohopane	C33
17	20,32-cyclo-17 α -bishomohopane-20,22,32-triene	C32

breccia intervals showed slightly higher amount of branched GDGTs (Fig. 6.6).

6.4.3 Methane and sulphate

Methane concentrations for gravity cores taken at the centre of Kalinin and Schneider's Heart MVs were low, 0.21 and 0.17 μ M wet sed, respectively. The methane concentration for the gravity core taken at Perejil crater increased in the lower part; the highest concentration being 231 μ M wet sed (Fig. 6.5). The concentration of pore-water sulfate remained at seawater level for Kalinin and Schneider's Heart MVs (unpublished results), whereas it had a significant decrease in the lower part of the sediments recovered for Perejil crater (Fig.6.5).

6.5 Discussion

Within MV deposits, mud breccia rock clasts, matrix, fluid, and gas may not all be co-genetic (e.g., Stadnitskaia et al., 2008). In this regard, lipid biomarker distributions may provide key information on the

potential source strata that feed mud volcanism, on the sedimentary sequence pierced by mud/fluids during eruptive episodes, and on the origin of the gas fraction within the extruded material.

6.5.1 Source of organic matter in mud breccia and hemipelagic sediments

Lipid biomarkers have been demonstrated to be useful geochemical proxies to characterize the organic geochemical signature of sediments from different facies e.g. mud volcanic deposits and hemipelagic sediments. In addition, this capacity permits also to record the source of organic matter in mud breccia (Stadnitskaia et al., 2007, 2008).

Eglinton and Hamilton (1967) determined that terrestrial organic matter is typically characterized by relatively high CPI values (4 to 10) of the long-chain n-alkanes, derived of higher plant waxes. Meanwhile, the short-chain n-alkane distributions and low CPI values (close to 1) were reported to be typical for petroleum-derived compounds (Bray and Evans, 1961; Eglinton and Hamilton 1963; Peters et al., 2005). We assume these two cases to be end-members with different lipid biomarker signatures that may be useful to determine different sources for the organic matter present in sediments and mud breccias. We applied this interpretation of n-alkane distribution patterns to the mud breccia matrices from Perejil, Kalinin and Schneider's Heart MVs. Intermediate CPI (2.0-2.9) and ACL (27.4-29.4) values (Fig. 3, Table 2) suggest a mixed origin of the organic matter contained in the mud breccia.

For all MVs, the CPI and ACL values in the hemipelagic sediments are slightly higher than in the mud breccia intervals. This indicates that the contribution from higher plants relative to petroleum-derived compounds is more predominant in hemipelagic sediments than it is in mud breccia. However, mixed signatures with more petroleum-derived content have been also found

Table 6.4. Depth distributions of concentration of acyclic archaeal isoprenoids diagnostic for methanotrophic archaea and specific methanogen biomarkers such as diploptene and diplopterol for Perejil crater and flank, Kalinin, and Schneider's Heart MVs.

Lithology	intervals (cm b.s.f.)	Cr/(Cr+Ph)	PMI (µg/g)	Archaeol (µg/g)	Hydroxyarchaeol (µg/g)	Diplopterol (µg/g)	Diploptene (µg/g)	Non-isopren. DGD (µg/g)	
Perejil Mud Volcano RL07BC									
Mud	0-3	0.71	nd	0.72	nd	2.67	nd	nd	
Breccia	3-4	0.56	nd	nd	nd	1.13	nd	nd	
	4-5	0.29	nd	0.71	nd	0.85	nd	nd	
	8-11	0.65	nd	4.44	43.08	15.68	nd	nd	
	16.5-19.5	0.56	2.37	nd	nd	1.48	nd	nd	
	25-28.5	0.51	0.44	0.34	3.13	0.69	nd	nd	
	33-36	0.49	0.70	2.54	20.02	2.34	nd	nd	
Perejil Mud Volcano RL08GC									
Hem. Sed.	1-4	0.52	nd	nd	nd	3.89	0.56	nd	
	25-30	0.30	nd	nd	nd	nd	0.40	nd	
	55-58	0.35	nd	nd	nd	nd	0.14	nd	
M.B.	64-68	0.4	nd	nd	nd	0.90	1.11	nd	
Hem. Sed.	86-88.5	0.48	nd	nd	nd	nd	1.53	nd	
	91-94	nd	nd	nd	nd	nd	0.21	nd	
Mud	137.5-140	0.36	nd	nd	nd	nd	0.23	nd	
Breccia	151-154	0.19	nd	nd	nd	2.26	0.71	nd	
	185.5-190	0.36	nd	nd	nd	nd	1.34	nd	
Hem. Sed.	221-231	0.39	nd	nd	nd	0.07	0.90	nd	
	246-250	nd	nd	nd	nd	nd	nd	nd	
	257-261	nd	nd	nd	nd	nd	nd	nd	
Perejil Mud Volcano RL30BC									
Mud	0-5	0.40	nd	0.32	9.25	2.02	nd	nd	
Breccia	5-7	0.43	nd	0.24	6.16	0.71	nd	nd	
	12-15	0.61	0,06	0.16	nd	0.25	nd	nd	
	18-22	0.59	nd	nd	17.29	1.02	nd	nd	
	26-29	0.47	nd	1.26	nd	3.60	nd	nd	
Perejil Mud Volcano RL31GC									
Mud	5-8	0.55	nd	nd	2.62	2.91	1.02	nd	
Breccia	12-16	0.70	nd	nd	nd	1.24	0.63	nd	
	22-25	0.63	nd	nd	5.50	2.09	0.44	nd	
	32-36	0.52	nd	nd	0.53	0.29	0.98	nd	
	83-86	0.81	nd	nd	1.29	0.16	1.11	nd	
	111-114	0.76	nd	0.04	0.68	0.07	1.04	nd	
	155-159	0.40	nd	nd	nd	0.26	1.31	nd	
	188-193	0.45	nd	nd	nd	0.08	1.02	nd	
	234-239	0.43	nd	nd	nd	0.08	1.34	nd	
	266-271	0.41	nd	0.12	2.66	0.22	1.32	nd	
	Kalinin Mud Volcano RL12GC								
	Hem. Sed.	2-4	nd	nd	nd	nd	nd	nd	nd
25-29		nd	nd	nd	nd	11.31	nd	nd	
72-76		0.41	nd	nd	nd	2.45	nd	nd	
Mud	81-83.5	0.40	nd	nd	nd	4.73	0.71	nd	
	89.5-91.5	0.48	0.24	1.41	nd	4.31	1.09	nd	
	96.5-100.5	0.46	0.67	nd	nd	12.49	0.85	nd	
	172-176	0.38	nd	2.48	nd	5.93	1.58	nd	
	230-233.5	0.44	nd	0.56	nd	2.16	1.50	nd	
	268.5-272	0.36	nd	3.40	nd	4.89	1.49	nd	
Schneider's Heart Mud Volcano RL25GC									
Hem. Sed.	0-5	0.30	0.15	nd	nd	nd	nd	nd	
	105-110	nd	nd	nd	nd	nd	nd	nd	
	205-210	0.30	nd	nd	nd	nd	0.58	nd	
Mud	220-225	0.33	nd	nd	nd	nd	0.41	0.63	
	260-265	0.42	nd	nd	nd	nd	0.23	0.36	
	290-295	0.24	nd	nd	nd	nd	0.55	0.93	

in the hemipelagic sediments, especially near the boundary between hemipelagic and mud breccia intervals. This particular finding is interpreted as a result from significant sediment reworking at these boundaries, which may be due to local blends caused by physical (i.e., sediment mobilization) and/or biological processes (i.e., intensive bioturbation). These processes may not only lead to the geochemical exchange between contiguous sedimentary facies but also favour the mixture of microfaunas encountered in these facies (Gennari et al., 2013). Consequently, we conclude that such processes may obscure the true location of the boundary between hemipelagic sediments and mud breccia in our studied cores. This is particularly evident in the lowermost mud flow of the Perejil flank core (RL08GC) where all biomarker data suggest that the actual lower boundary is at ~230 cm rather than at the visually detected boundary at 209 cm depth (Figs. 3a). In the following discussions we will, therefore, tentatively adopt this lower mud breccia boundary to be at 230 cm (Fig. 3a).

6.5.2 Maturity of the organic matter

The suite of lipid biomarkers, and in particular hopanes, found in sediments can be used to assess the degree of thermal maturation of the organic matter. The suite of hopanes found in the mud breccia matrices and especially the 22S/(22S+22R) ratios for C31 and for C32 homohopane have a comparable distribution for all studied cores (Table 6.2). The average values for these two ratios are 0.49 ± 0.06 and 0.49 ± 0.02 , respectively. These values are relatively close to the thermodynamic equilibrium value (ca. 0.6; Seifert and Moldovan, 1980; van Duin et al., 1997), indicating that at least part of the organic matter present in the mud breccia matrices has moderate to high degree of thermal maturation. However, the occurrence of small amounts of 17 β ,21 β (H)-homohopane (Fig.6.4, Table 6.3) indicate the presence of immature organic mat-

ter also. The coincidence of these two groups of rather different thermal maturity must indicate the presence of two different sources of organic matter. The CPI values for n-alkanes confirm this hypothesis, having values that imply moderately mature organic matter or a contribution of petroleum-derived compounds (Fig. 6.3, Table 6.2). However, the abundance of n-alkanes in the range of C29-C31 indicates also the presence of immature organic matter (Fig.6.3, Table 6.2) (Bray and Evans, 1961; Eglinton and Hamilton 1963; Peters et al., 2005). The thermal maturation degree that we found for hemipelagic sediment (22S/(22S+22R) ratios for C31 and for C32 homohopanes) ranges between 0.41-0.44 and 0.38-0.49, respectively. This ratio is also much higher than commonly found for pelagic sediments, and suggests that part of the hopanes present in these sediments must come from a deeper source. This is in accordance with the interpretation that substantial mixing has occurred between hemipelagic and mud breccia sediments.

6.5.3 Probable source strata

The relatively high maturity degree that we report in mud breccia matrices from Perejil, Kalinin and Schneider's Heart MVs (Table 6.2) are in good agreement with the level of maturity found in other studies (Poludetkina and Kozlova, 2003; Kozlova et al., 2004; Poludetkina et al., 2008). In the same line, our maturity estimation for the mud breccia matrices from the three studied MVs are also in accordance with the previously reported data by Blinova et al. (2011), who found in Carmen MV a mixture of thermogenic and biogenic gases containing geochemical signatures typical of hydrocarbon generated during early stages of catagenesis. Therefore, all these suppositions support our hypothesis that part of the lipid biomarkers hosted in the mud breccia matrices of Perejil, Kalinin and Schneider's Heart MVs must originate from thermally matured or-

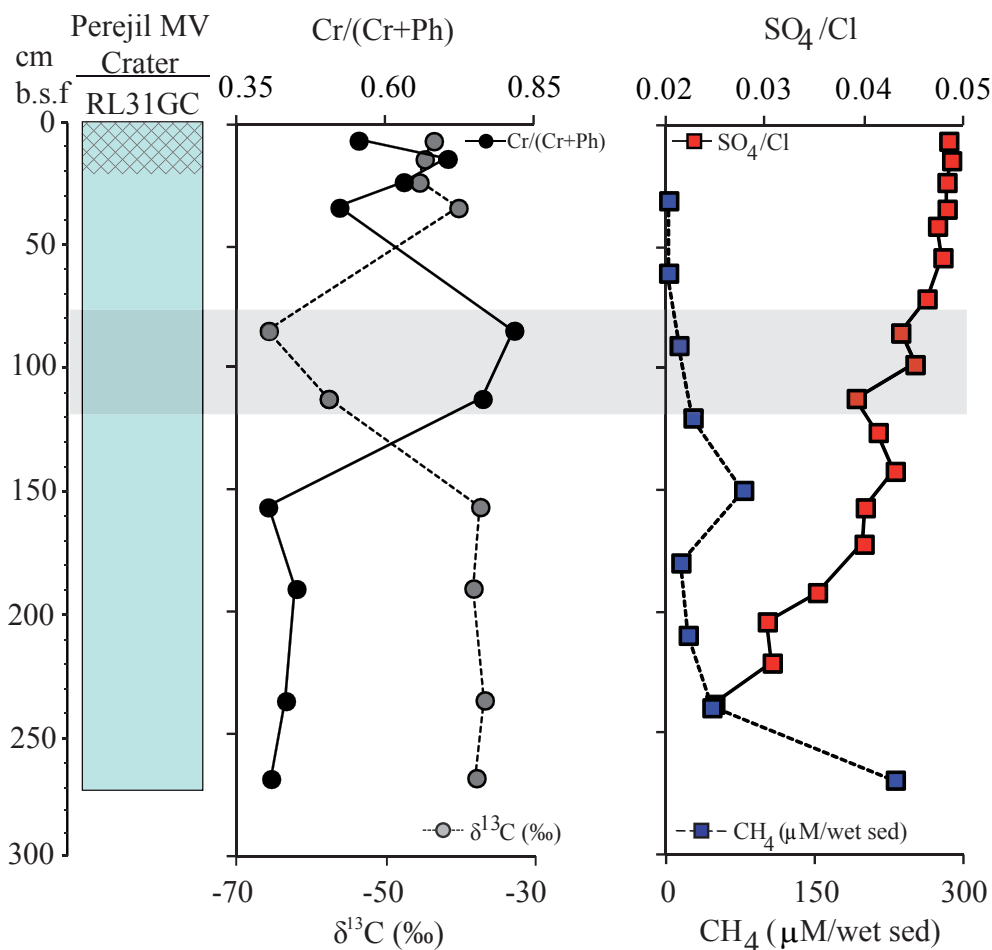


Figure 6.5. Fractional abundance of crocetane ($Cr/(Cr+Ph)$) and the stable carbon isotope composition of the phytane/crocetane peak vs. depth in mud breccia of the Perejil MV crater. Concentrations of methane and SO_4/Cl ratio from gases and pore fluids showing the zone of Anaerobic Oxidation of Methane (AOM).

ganic matter at depth, i.e. in the lowermost Unit VI of the infill basin (Early to Middle Miocene in age), indicating the potential occurrence of primary cracking processes able to generate some thermogenic hydrocarbons (including methane).

This assumption is supported by the presence of thick overpressured sedimentary units forming the Mud Diapir Province that extend beneath the MVs edifices (Fig. 6.1, Comas et al., 2010 and references therein). As demonstrated by reflexion seismic data, feeding conduits from mud volcano edifices are frequently rooted on pierced mud diapirs (i.e., Talukder et al., 2003; Comas et al., 2012; Soto et al., 2010). Overpressured units for-

ming the mud diapirs and subsequently leading to the mud volcanism correspond to the basal Unit VI and Unit V, Early to Middle Miocene (Fig. 2) (i.e., Comas et al., 1999, 2012; Talukder et al., 2003; Soto et al., 2003, 2010). Tectonic processes occurred since the Middle Miocene to nowadays have been reported to cause both the mud-diapirism and the subsequent mud volcanism that reaches the actual sea floor (see Geological Background above). Hence, they all identify the overpressured deeper strata laid down in the West Alboran Basin (Unit VI and the lower part of Unit V- Early to Middle Miocene in age, Fig. 6.2) as the most probable source strata of the mud-

volcanism products.

For the West Alboran Basin, temperatures of ~100-150 °C were suggested to be reached at 4-6 km sedimentary depths, under a geothermal gradient of 25 °C/Km, (Torné et al., 2000). According to these data and regarding the sedimentary lithology of the lowermost unit of the basin (under-compacted olistostromes embedded in a shale-rich matrix) (Fig. 6.2), the beginning of the “oil window” may be located at this depth, matching with the lower-to middle Miocene strata (Unit VI). This is in good agreement with our lipid biomarkers data, and is supported by the location at depth and sedimentary lithologies of units VI and Va (Fig. 6.2) as indicated by seismic data (i.e., Comas et al., 2012, Soto et al., 2010). Furthermore, this assumption is consistent with geochemical studies carried out on pore water and gases for other Alboran MVs, which reveal a thermogenic origin for the volcanic fluids (Blinova et al., 2011).

6.5.4 Recent microbial activity

At the Alboran MVs, GDGTs in hemipelagic sediments reflect the predominant marine pelagic thaumarchaeotal signature (Fig. 6.6; Schouten et al., 2012 and references therein). In contrast, mud breccia intervals show differences in GDGT distribution between individual MVs. Schneider’s Heart MV has a predominance of GDGT-0 and crenarchaeol, clearly revealing the influence of marine pelagic thaumarchaeotal and, consequently, inactive anaerobic oxidation of methane (AOM) at this site. This is also confirmed by the absence of irregular isoprenoids (crocetane and PMI) and isoprenoidal dialkyl glycerol diethers (archaeol and hydroxyarchaeol) (Table 6.4). This is in line with the observed methane content at Schneider’s Heart relative to Perejil MV, being respectively < 0.18 µM, relative to ~ 230 µM wet sediment. At Kalinin MV and more especially at Perejil MV, the GDGTs distribution and in particular the GDGTs-based ratios (MI > 0.4; elevated

GDGT-2/Crenarchaeol and GDGT-0/Crenarchaeol ratios; Table 6.2), document the occurrence of AOM performed by anaerobic methanotrophics archaea (ANME). However, some differences in GDGTs-based ratios and also in archaeal lipid biomarkers (mainly in crocetane contents; Table 6.2) indicate lower rate of anaerobic oxidation of methane (AOM) at Kalinin MV compared with Perejil MV (Table 6.2). In Perejil MV crater, the finding of authigenic pyrite in the mud breccia suggests that recent methane fluxes and concordant sulfate reducing processes occur at this site. This concurs with the observed profiles for methane and sulfate for Perejil MV crater (Fig. 6.5). Furthermore, microbial communities that are involved in AOM biosynthesize specific lipid biomarkers that are strongly depleted in $\delta^{13}\text{C}$ (Hinrichs et al., 1999; Pancost et al., 2000). Indeed, in Perejil MV crater, at ~100 cm depth there is evidence for strongly depleted crocetane (Fig. 6.5), confirming the consumption of hydrocarbons, mainly methane, by archaea of ANME-2 cluster for this MV (Niemann and Elvert, 2008). Moreover, at Perejil MV, the distribution of GDGTs also suggests that archaea belonging to the ANME -1 group also perform AOM in these mud breccia (Fig. 6.6, Table 6.4) (Blumenberg et al., 2004, Stadnitskaia et al., 2005).

6.5.5 MV dynamics

The lipid biomarker composition provides information about the dynamic processes at the MVs, such as discrete events of mud- flow expulsion. Furthermore, the presence or absence of hemipelagic intervals intercalated or draping mud breccia episodes help to determine volcanic pulses.

At the Perejil MV crater, the absence of hemipelagic sediments and the observed gas bubbling noticed during the core recovery, indicate that our sampled site correspond to a relatively very recent mud flow eruption. Where no clear lithological boundaries can be seen, some changes in

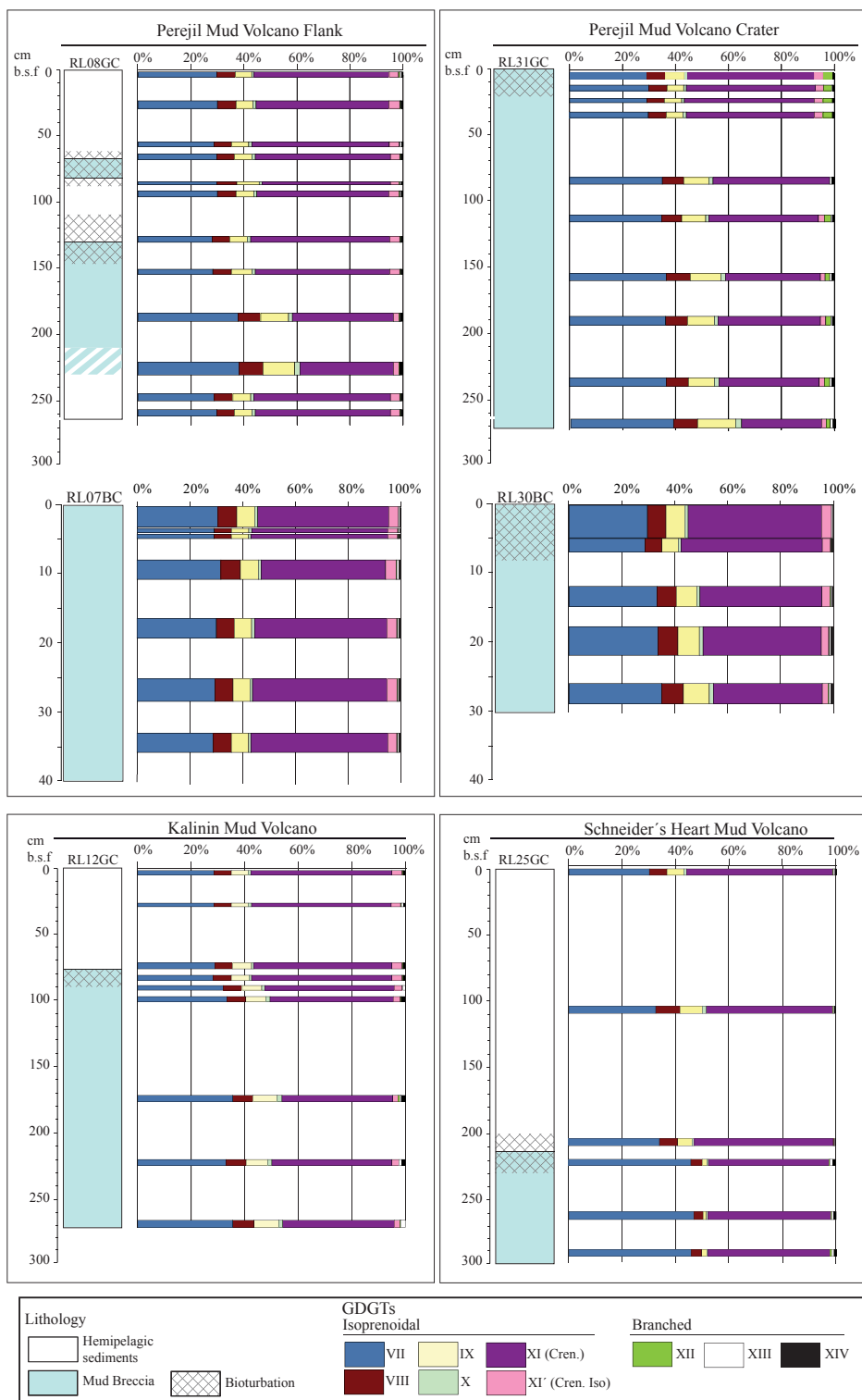


Figure 6.6. Fractional abundance (%) of isoprenoidal and branched GDGTs for Perejil MV crater and flank and Kalinin and Schneider's Heart MVs. For GDGTs structures see Appendix A.

the distributions of lipid biomarkers (Fig. 6.3, 6, Table 6.2) can be used to make a more precise lithology distinction between “real” hemipelagic and mud breccia intervals.

In accordance with our biomarker results, cases of boundary transitions between the two lithologies occur in Kalinin MV (core RL12GC) at ~ 80 cm and in Schneider’s Heart MVs (core RL25GC) at ~ 220 cm depth (Figs. 6.3b). At Perejil MV crater (core RL31GC), the more subtle but evident decrease in branched GDGTs, together with the variation on other lipid biomarkers such as CPI values and n-alkane distributions (Fig. 6.3a), are noted at ~110 and ~190 cm, which may represent (brief) interruptions of mud expulsion, whereas the change above 40 cm may reflect the ongoing bioturbation since the last eruptive event. In accordance with this interpretation, three consecutive mud expulsion events are detected at Perejil MV crater, i.e. below 190 cm, 110-190 cm, and above 110 cm. Compared to Perejil MV, Kalinin and Schneider’s Heart MVs are characterized by relatively thick hemipelagic draping, indicative of relatively old mud breccia flows (Fig. 6.3b). This fact, together with the absence of chemosynthetic macrofauna suggests that both MVs are currently inactive, at least at our sampling locations.

The observed reduced relative abundance of branched GDGTs and the interpretations given are consistent with the occurrence of some oxidative mixing between pelagic and mud breccia facies. As indicated above, mud fluid ejection and biological processes such as bioturbation may have influenced such mixing (Fig. 6.3, Table 6.2) at some boundaries between hemipelagic/ mud breccia intervals. Studies on the microfauna contained in mud breccia from some other Alboran MVs revealed significant mixture of foraminifera species from diverse ages, thus proving that mixing between hemipelagic sediments and mud breccia facies exists (Gennari et al., 2013). Consequently, and according with our findings, we propose that lipid biomarkers, can be used as reliable proxy to

discriminate between sedimentary and mud-volcano derived facies within mud volcano edifices.

The presence of AOM-related biomarkers, although at relatively low levels, is evident at the three studied MVs of the Alboran Sea (Table 6.4). This indicates that at least brief periods of methane emission must have occurred but that continuous fluxes of hydrocarbon-rich fluids at these MVs are unlikely. This interpretation is consistent with hydrocarbon gas data (Fig. 6.5) determined here and those reported by Blinova et al. (2011). Although our methane content for Perejil MV is much higher than those reported by Blinova et al. 2011 (230 $\mu\text{M}.\text{sed}$ vs. ~ 2 $\mu\text{M}.\text{sed}$), compared to actively seeping MVs: the methane concentrations observed at Perejil are rather low (230 $\mu\text{M}/\text{L}.\text{sed}$), compared to > 1000 $\mu\text{M}.\text{sed}$ for known active MV seepages, e.g. Mاستالزر et al., 2007).

Differences exist in the methane concentrations at Perejil MV that are reported here and those reported by Blinova et al. (2011) from neighboring sampling sites, which can be explained due to the dissimilar hydrocarbon contents of seeps via contiguous conduits within the volcano. Alternatively, such differences may result from changes in the composition and activity of seepages through time. However, further analyses and in situ MV-monitoring are needed to clearly discriminate between both options.

Furthermore, the presence of AOM-related biomarkers confirms that AOM-activity at Perejil MV is relatively recent (Fig. 6.5, Table 6.4). Also the absence of a hemipelagic drape supports that core RL31CG, recovered from the crater of the Perejil MV, sampled a recent mud-flow event that may occurred only some years ago. On the basis of all these findings we consider Perejil MV the currently most active MV at the northern margin of the West Alboran Basin.

6.6 Conclusions

Mud breccias sampled in three studied MVs from the northern West Alboran Basin present similar suites of lipid biomarker compositions and maturity properties of organic matter indicating a common source for the extruded mud breccia at the studied volcanic structures.

Our lipid biomarker results, in agreement with previous geophysical and stratigraphic data, confirm that the source strata of the organic matter in mud breccia belong to overpressured deep units occurring at depth in the West Alboran Basin (Unit VI and Unit Va, Early to Middle Miocene in age). The moderate mature-immature characteristics of the organic matter present in mud breccias corroborate a deep source for the upward fluids, at least at Perejil and Kalinin MVs.

Significant mixing may occur between hemipelagic sediment and mud-breccia facies at the interval boundaries, resulting in the significant variation of some lipid biomarkers, such as n-alkanes. Using this variability found in the lipid biomarker distributions, we suggest the occurrence of a very recent mud-flow eruption at Perejil MV and at least another two previous volcanic events.

The presence of specific AOM-related biomarkers together with direct evidence of recent activity (e.g. chemosynthetic fauna, gas bubbling, enhanced levels of methane and reduced level of sulfate), proves the occurrence of actual methane seepage at Perejil MV.

At Perejil MV, the presence of these AOM-related biomarkers indicates that active AOM is occurring at this structure. Additionally, the specific AOM-related biomarkers found at this MV have proved the co-occurrence of ANME-2 over ANME-1 group. To the contrary, the low occurrence or absence of specific lipid biomarkers related to methanotrophic archaea in the mud breccia at Kalinin and Schneider's Heart MVs suggests that very low or no AOM occurs at these sites, respectively.

7

Conclusions
Conclusiones

Chapter 7

Conclusions

Several mud volcanoes (MVs) from the Mud Volcano Province in the West Alboran Basin (WAB) (westernmost Mediterranean) were studied through a mineralogical, sedimentological, geochemical and biogeochemical multiproxy approach. Such investigations were accomplished on gravity core samples from several cruises. The analyses were performed on both fluids and solid phases from extruded volcanic material (mud breccia matrix) and hemipelagic sediments encountered within volcanic edifices. This study provides important insights about the nature and provenance of the volcanic extruded material and about the biogeochemical processes closely related with the discharge of hydrocarbon-rich fluids to the seafloor through the MVs. Furthermore, it also contributes to a better understanding of mud volcanism dynamics in the WAB and provides relevant information about recent and past mud volcano activity. Main conclusions of this PhD are listed below referred to the proposed objectives:

1. Mineralogical and geochemical characterization of hemipelagic sediments and extruded materials. Inferred diagenetic processes

- MVs contain Holocene hemipelagic sediments, both covering or interbedding intervals of extruded materials (mud breccia). These sediments correspond with “normal” marine sedimentation and have similar composition compared to contemporary marine records from other areas in the Alboran Basin.
- Events of mud extrusion that build up the mud edifices have not significantly affected the composition of the hemipelagic sediments covering the MVs. Nevertheless, some variations just occur at the mixed boundaries between hemipela-

gic and mud breccia intervals due to processes of syn-sedimentary remobilization.

- The relative similitude of mineralogical, geochemical and lipid biomarker composition from all studied mud breccias indicate that, despite of the eruptive upward migration of the volcanic fluxes, mud breccias matrices preserve the composition of the parent source strata.

- The materials that feed the mud breccia were affected by diagenetic processes resulting in smectite to illite transformation, as demonstrated by the presence of illite-smectite mixed layers with low- to high- illite-layer proportion (from 10% up to 95%) reveals.

- Smectite dehydration constitutes a fluid source mechanism that contributes to the pore water freshening being consistent with the isotopic $\delta^{18}\text{O}$ and δD compositions of pore waters.

- Diagenetic conditions suffered by materials feeding mud breccia matrices might have been suffered favorable conditions for transformation of smectite to illite as well as for hydrocarbon generation at the deep, as empirical geo-thermometers reveal (K-Na, K-Mg y K-Ca).

- Organic matter is mostly thermally immature with an admixture of petroleum-derived compounds and corroborates a deep source for the upward fluids at the studied MVs.

- Methane proceeds from a deep thermogenic source formed within the oil window range, as evidenced its stable carbon isotope composition and inorganic geochemical signatures of pore waters.

- Active AOM occurs at active MVs, Carmen and Perejil, and is corroborated by pore waters compositions and presence of specific AOM-related biomarkers.

- At active MVs existence of anaerobic methanotrophic archaeas (ANME), and more specifically the co-occurrence of ANME-2 over ANME-1 group, is confirmed by the presence of specific AOM-related biomarkers.

- At dormant MVs there is very low or no AOM, as support the low occurrence or absence of specific lipid biomarkers related to methanotrophic archaeas. The presence of methane-derived authigenic carbonates (MDACs) with extremely ^{13}C -depleted values confirms fossil AOM. Paleo- AOM reported in mud breccias from these inactive structures are assessed from enhanced intervals of redox-sensitive elements (Mo, S) and high-Mg calcite and aragonite enriched-fronts.

2. Dynamics of the mud volcanism in the area

- Hemipelagic deposits post-date periods of volcanic activity. This allows analyzing the mud volcano dynamic as well as determining the timing of volcanic events.

- The existence of hemipelagic covers overlaying craters of MVs indicates these are inactive. Moreover, interbedded hemipelagic intervals marks quiescence periods between events of mud expulsion.

- Hemipelagic drapes and intervals have allowed the dating of some volcanic eruptions at the studied cores: the older occurred at Marrakech MV whereas the most recent eruption happened 10.8 ka BP at Carmen and at 0.7 Ka BP at Marrakech MV.

- Only two MVs, Carmen and Perejil are active at present. This assumption is supported by methane and sulfate concentrations in pore waters as well as by direct evidence of volcanic activity, such as gas bubbling or living chemosynthetic fauna.

- Episodes of thermogenic gas outburst in MVs promote the mixture between extruded breccias and sea water. Some tops of breccia intervals present pore waters with sea-like water composition and constant stable carbon isotopes of methane.

- Maya MV has a particular flux dynamic. Differences in carbonate content and the finer grain sized breccias suggest segregated fluxes within the plumbing system that nourished this volcano.

- Extruded materials by MVs derive from common source strata, probably coming from a similar depth and from source strata with lateral continuity, as suggest the similar nature and compositions of extruded muds at studied MVs.

- Geochemical signature of certain pore fluids suggests existence of continental crust beneath the MV field.

- Active MVs, Carmen and Perejil corroborate the current discharge of methane rich fluids in the Alboran Sea.

- Concerning the origin of the extruded materials, the source strata that feed MVs correspond with the overpressured (undercompacted) clays and megabreccias that form the basal units from the sedimentary infill of the West Alboran Basin (Unit VI and Unit Va, Early to Middle Miocene in age). These units generate shale diapirism within the Mud Diapir Province (MDP) in the Alboran Sea, as previous geophysical, paleontological and geochemical studies have suggested.

Conclusiones

Varios volcanes de la Provincia Volcánica de Lodo de la Cuenca Oeste presente en el Mar de Alborán se han estudiado mediante la integración de datos y resultados mineralógicos, sedimentológicos, geoquímicos y biogeoquímicos. Los análisis pertinentes se han realizado sobre submuestras efectuados en los testigos de sondeos recuperados en diversas campañas oceanográficas. Estos análisis atañen tanto a la fases solidas (brechas de lodo) como fluidas (líquidos y gases intersticiales) de los materiales extruidos por esos volcanes. Adicionalmente se han investigado los sedimentos hemipelágicos involucrados en los edificios volcánicos. Este estudio aporta una valiosa información sobre la naturaleza y procedencia de los materiales extruidos, así como los procesos biogeoquímicos relacionados con la descarga de fluidos ricos en hidrocarburos a través de las estructuras volcánicas. Asimismo, contribuye a comprender mejor la dinámica del vulcanismo de lodo en la cuenca y la singularidad de la actividad volcánica actual y pasada. A continuación se detallan las conclusiones principales de esta Tesis, de acuerdo con los objetivos científicos planteados:

1. Caracterización mineralógica y geoquímica de los sedimentos hemipelágicos y materiales extruidos. Procesos diagenéticos inferidos

- Los edificios volcánicos contienen sedimentos hemipelágicos holocenos, que tapizan o se intercalan en los materiales extruidos (brechas de lodo). Dichos sedimentos representan la sedimentación "normal" en la cuenca y son similares en composición a los sedimentos hemipelágicos coetáneos que aparecen en otros ámbitos de la cuenca de Alborán.

- Las extrusiones de brechas de lodo que construyen los edificios volcánicos no afectan a la composición de los sedimentos hemipelágicos. No obstante, los límites entre intervalos de brechas

de lodo y hemipelagitas presentan ciertas variaciones en la composición mineralógica de estos sedimentos, atribuidas a mezclas entre ambas litologías por procesos de re-movilización sin-sedimentaria.

- La relativa homogeneidad mineralógica, geoquímica y de biomarcadores, que presentan los intervalos de brechas de lodo de todos los volcanes indican que la composición de la fuente originaria del material volcánico se preserva en los materiales extruidos (matrices de brechas de barro) a pesar de la migración ascendente de los flujos volcánicos.

- Los materiales que nutren las brechas de lodo han sufrido procesos diagenéticos resultantes en transformaciones de esmectita a illita, demostrado por la existencia de interestratificados illita-esmectita con un rango muy variable de capas de illita (desde 10% hasta 95%).

- La deshidratación de las esmectitas constituye un mecanismo de generación de fluidos incluidos en los flujos volcánicos, tal como indica la composición isotópica de oxígeno ($\delta^{18}\text{O}$) e hidrogeno (δD) de los fluidos intersticiales.

- Los materiales que nutren las brechas de lodo estuvieron sometidos a procesos diagenéticos que promovieron la generación de hidrocarburos en profundidad. Esto se deduce de la aplicación de fórmulas empíricas geo-termométricas (K-Na, K-Mg y K-Ca).

- La materia orgánica de las brechas de lodo es fundamentalmente inmadura y presenta mezcla con compuestos derivados del petróleo. Esto corrobora que los fluidos que ascienden en los volcanes estudiados proceden de una fuente profunda.

- El metano procede de una fuente termogénica profunda y se originó bajo condiciones favorables para la generación de petróleo (oil window), según demuestra la composición de isotopos estables de carbono y la composición geoquímica de los fluidos intersticiales.

- En los volcanes activos, Carmen y Perejil, se ha

detectado la presencia de una zona de oxidación anaeróbica del metano (OAM) activa según indica la composición de los fluidos intersticiales y la presencia de determinados biomarcadores lipídicos relacionados con arqueas anaeróbicas metanotróficas (ANME).

- En volcanes activos predominan los metanótrofos anaeróbicos del grupo ANME-2 sobre los del grupo ANME-1, tal y como han revelado la presencia determinados biomarcadores lipídicos relacionados con arqueas.

- En volcanes inactivos la OAM es muy débil o no existe, como sugiere la poca cantidad o ausencia de determinados biomarcadores relacionados con arqueas metanotróficas. La presencia de carbonatos autigénicos derivados del metano con una composición isotópica de carbono muy empobrecida indica una zona de oxidación anaeróbica del metano fósil. Paleo-OAM en las brechas de estos volcanes quedan también registrados como frentes enriquecidos en elementos sensibles a condiciones redox (Mo, S) y frentes ricos en calcita magnésica y aragonito.

2. Dinámica del vulcanismo de lodo en el área

- Los depósitos hemipelágicos post-datan los periodos de actividad volcánica, lo que permite analizar la dinámica del vulcanismo de lodo y determinar la edad de las extrusiones volcánicas.

- La existencia de coberteras hemipelágicas sobre los cráteres volcánicos indica que volcanes son inactivos. Asimismo, las intercalaciones de hemipelagitas entre intervalos de brechas marcan periodos de inactividad entre eventos de expulsión de lodo.

- Los intervalos y coberteras hemipelágicas de volcanes inactivos han permitido datar algunas erupciones en los testigos estudiados: la más antigua a 10.8 ka BP en el volcán Carmen y la más reciente a 0.7 ka BP en el volcán Marrakech.

- Únicamente dos volcanes, Carmen y Perejil, son actualmente activos tal y como indican las concentraciones de metano y sulfato en los fluidos inters-

ticiales, así como las observaciones de actividad volcánica actual: burbujeo de gas emitido al fondo marino y presencia de fauna quimiosintética viva.

- La expulsión de gas de origen termogénico en los volcanes promueve la mezcla entre brechas extruidas y agua marina. Algunos intervalos de brechas tienen a techo fluidos con una composición geoquímica similar a la del agua marina y valores constantes de los isotopos de metano.

- El volcán Maya presenta una particular dinámica de flujo. Las diferencias encontradas en el contenido en carbonato, y el menor tamaño de grano de las brechas, así como la ausencia de grandes clastos extruidos sugieren cierta segregación en los flujos volcánicos en este volcán (mayor fluidificación) respecto a los flujos (mayor competencia de transporte) de los materiales fuente que nutrieron el resto de los volcanes estudiados.

- Los materiales extruidos por los volcanes derivan de una misma formación fuente que es continua lateralmente en la Cuenca Oeste de Alborán, según demuestra la similitud entre la naturaleza y composición de los materiales extruidos por los distintos volcanes.

- La signatura geoquímica de ciertos fluidos intersticiales sugiere la existencia de una corteza continental bajo el campo de volcanes.

- Los volcanes activos Carmen y Perejil constatan que actualmente se están produciendo descargas de metano en el Mar de Alboran.

- Respecto al origen del material volcánico extruido, se asevera que la fuente que nutre los volcanes de lodo corresponde a las arcillas y megabrechas sobrepresurizadas (subcompactadas) que forman las unidades basales del relleno sedimentario de la cuenca (Unidad VI y Unidad Va; de edad Mioceno inferior y medio), que a su vez generan el diapirismo de lodo de la Provincia Diapirica de Lodo del Mar de Alboran, tal como ha sido propuesto por estudios geofísicos, paleontológicos y geoquímicos previos.



References

References

- Akhmanov, G. G.: Lithology of mud breccia clasts from the Mediterranean Ridge, *Mar. Geol.*, 132, 151–164, 1996.
- Akhmanov, G. G. and Woodside, J. M.: Mud volcanic samples in the context of the Mediterranean Ridge mud diapiric belt, *Proceeding Ocean Drill. Program, Sci. Results*, Vol. 160, 160, 597–605, 1998.
- Akhmanov, G. G., Premoli Silva, I., Erba, E. and Cita, M. B.: Sedimentary succession and evolution of the Mediterranean Ridge western sector as derived from lithology of mud breccia clasts, *Mar. Geol.*, 195(1-4), 277–299, doi:10.1016/S0025-3227(02)00693-X, 2003.
- Aloisi, G., Pierre, C., Rouchy, J. M., Foucher, J. P. and Woodside, J.: Methane-related authigenic carbonates of Eastern Mediterranean Sea mud volcanoes and their possible relation to gas hydrate destabilisation, *Earth Planet. Sci. Lett.*, 184(1), 321–338, doi:10.1016/S0012-821X(00)00322-8, 2000.
- Aloisi, G., Drews, M., Wallmann, K. and Bohrmann, G.: Fluid expulsion from the Dvurechenskii mud volcano (Black Sea) Part I. Fluid sources and relevance to Li, B, Sr, I and dissolved inorganic nitrogen cycles, *Earth Planet. Sci. Lett.*, 225, 347–363, doi:10.1016/j.epsl.2004.07.006, 2004.
- Ballesteros, M., Rivera, J., Muñoz, a., Muñoz-Martín, a., Acosta, J., Carbó, a. and Uchupi, E.: Alboran Basin, southern Spain—Part II: Neogene tectonic implications for the orogenic float model, *Mar. Pet. Geol.*, 25(1), 75–101, doi:10.1016/j.marpetgeo.2007.05.004, 2008.
- Barnes, R. O., and Goldberg, E. D.: Methane production and consumption in anoxic marine sediments, *Geology*, 4, 297–300, 1976.
- Bayon, G., Pierre, C., Etoubleau, J., Voisset, M., Cauquil, E., Marsset, T., Sultan, N., Le Drezen, E. and Fouquet, Y.: Sr/Ca and Mg/Ca ratios in Niger Delta sediments: Implications for authigenic carbonate genesis in cold seep environments, *Mar. Geol.*, 241(1-4), 93–109, doi:10.1016/j.margeo.2007.03.007, 2007.
- Bea, F.: Controls on the trace element composition of crustal melts, *Trans. R. Soc. Edinburgh, Earth Sci.*, 87(1-2), 33–41, 1996.
- Bergaya, F., Theng, B.K.G., and Lagaly, G.: *Handbook of Clay Science* (1st edition), Elsevier Publication, Amsterdam, 2006.
- Bethke CM, Vergo N, and Altaner, S.P.: Pathways of smectite illitization. *Clay Miner.*, 34,125-135, 1986.
- Bian, L., Hinrichs, K.-U., Xie, T., Brassell, S.C., Iversen, N., Fossing, H., Jørgensen, B.B., Hayes, J.M.: Algal and archaeal polyisoprenoids in a recent marine sediment: molecular isotopic evidence for anaerobic oxidation of methane, *Geochem. Geophys. Geosy*, 2, 1525-2027, doi: 10.1029/2000GC000112, 2001.
- Blinova, V. N., Comas, M. C., Ivanov, M. K., Poludetkina, E. N. and Matveeva, T. V.: Active mud volcanism in the West Alboran Basin: Geochemical evidence of hydrocarbon seepage, *Mar. Pet. Geol.*, 28(8), 1483–1504, doi:10.1016/j.marpetgeo.2011.06.001, 2011.
- Blumenberg, M., Seifert, R., Reichart, G.J., Pape, T., Michaelis, W.: Membrane lipid patterns typify distinct anaerobic methanotrophic consortia, *P. Natl. Acad. Sci.*, 101, 11111–11116, www.pnas.org/cgi/doi/10.1073_pnas.0401188101, 2004.
- Boetius, a, Ravensschlag, K., Schubert, C. J., Ricker, D., Widdel, F., Gieseke, a, Amann, R., Jørgensen, B. B., Witte, U. and Pfannkuche, O.: A marine microbial consortium apparently mediating anaerobic oxidation of methane., *Nature*,

- 407(6804), 623–6, doi:10.1038/35036572, 2000.
- Boetius, A. and Wenzhöfer, F.: Seafloor oxygen consumption fuelled by methane from cold seeps, *Nat. Geosci.*, 6(9), 725–734, doi:10.1038/ngeo1926, 2013.
- Borowski, W.S., Paull, C.K., and Ussler, W., III.: Marine pore-water sulfate profiles indicate in situ methane flux from underlying gas hydrate, *Geology*, 24,655–658, 1996.
- Brass, M. and Röckmann, T.: Continuous-flow isotope ratio mass spectrometry method for carbon and hydrogen isotope measurements on atmospheric methane, *Atmos. Meas. Tech.*, 3, 1707–1721, doi:10.5194/amt-3-1707-2010, 2010.
- Bray, E.E., and Evans, E.D.: Distributions of n-paraffins as a clue to recognition of source beds, *Geochim. Cosmochim. Ac.*, 22, 2-15, 1961.
- Brown, K. M., Sa, D. M. and Bekins, B. A.: Smectite diagenesis, pore-water freshening, and fluid flow at the toe of the Nankai wedge, *Earth Planet. Sci. Lett.*, 194, 97–109, 2001.
- Brumsack, H.-J. and Zuleger, E.: Boron and boron isotopes in pore waters from ODP Leg 127, Sea of Japan, *Earth Planet. Sci. Lett.*, 113(3), 427–433, doi:10.1016/0012-821X(92)90143-J, 1992.
- Calvert, S. E. and Fontugne, M. R.: On the late Pleistocene-Holocene sapropel record of climatic and oceanographic variability in the eastern Mediterranean, *Paleoceanography*, 16(1), 78–94, doi:10.1029/1999PA000488, 2001.
- Calvert, S. E. and Pedersen, T. F.: *Proxies in Late Cenozoic Paleoceanography*, Elsevier, 2007.
- Cangemi, M., Di Leonardo, R., Bellanca, A., Cundy, A., Neri, R. and Angelone, M.: Geochemistry and mineralogy of sediments and authigenic carbonates from the Malta Plateau, Strait of Sicily (Central Mediterranean): Relationships with mud/fluid release from a mud volcano system, *Chem. Geol.*, 276(3-4), 294–308, doi:10.1016/j.chemgeo.2010.06.014, 2010.
- Chamley, H., Giroud D'argoud, G. and Robert, C.: Clay mineralogy of Cretaceous and Cenozoic sediments off the Moroccan margin, Deep Sea Drilling Project sites 415 and 416., Initial reports Deep Sea Drill. Proj. Leg 50, Funchal, Maderia Islands, 1976, (U.S. GPO; U.K. Distrib. IPOD Committee, NERC, Swindon), 715–721 [online] Available from: <http://www.scopus.com/inward/record.url?eid=2-s2.0-0018915077&partnerID=tZOtx3y1>, 1980.
- Chan, L. and Kastner, M.: Lithium isotopic compositions of pore fluids and sediments in the Costa Rica subduction zone : implications for fluid processes and sediment contribution to the arc volcanoes, *Earth Planet. Sci. Lett.*, 183, 275–290, 2000.
- Cita, M.B., Ryan, W.B.F., Paggi, L.: Prometheus mud breccia. An example of shale diapirism in the Western Mediterranean Ridge, *Ann. Geo. Pa. Hélién.*, 30, 543-569, 1981.
- Cita, M. B., Woodside, J. M., Ivanov, M., Kidd, R. B. and Limonov, A. F.: Fluid venting, mud volcanoes and mud diapirs in the Mediterranean Ridge, *Rend. Lincei*, 5(2), 159–169, doi:10.1007/BF03001615, 1994.
- Collett, T. S., Lee, M. W., Agena, W. F., Miller, J. J., Lewis, K. a., Zyrianova, M. V., Boswell, R. and Inks, T. L.: Permafrost-associated natural gas hydrate occurrences on the Alaska North Slope, *Mar. Pet. Geol.*, 28(2), 279–294, doi:10.1016/j.marpetgeo.2009.12.001, 2011.
- Comas, M. C., García-Dueñas, V. and Jurado, M. J.: Neogene tectonic evolution of the Alboran Sea from MCS data, *Geo-Marine Lett.*, 12(2-3), 157–164, doi:10.1007/BF02084927, 1992.
- Comas, M.C., Zahn, R., and Klaus, A.: *Proceedings of the Ocean Drilling Program, Science Results*

- 161, college Station, TX, USA, 1996. doi:10.2973/odp.proc.ir.161.1996
- Comas, M. C., Platt, J. P., Soto, J. I., Watts, A. B.: The origin and tectonic history of the Alboran Basin: evidence from Leg 161, Proceedings of the Ocean Drilling Program, Science Results 161, college Station, TX, USA, 555-580, 1999.
- Comas, M.C., Pinheiro, L.M., Ivanov, M.K., and TTR-17 Scientific Party.: The Alboran Sea Leg-1: Look into mud volcanoes, carbonate mounds and climate changes, IOC Technical Series, 94, 8-64, 2010.
- Comas, M.C., Suades, E., Crespo-Blanc, A.: From mud diapirs to mud volcanoes: Shale tectonics within the structural evolution of the Alboran Sea basin. *Geotemas* 13, 138-141, 2012.
- Condie, K.C., Dengate, J., Robert, L., Cullers, L.: Behavior of rare earth elements in a paleoweathering profile on granodiorite in the Front Range, Colorado, USA. *Geochim Cosmochim Acta*, 59, 279-294, 1995.
- Contreras, S., Meister, P., Liu, B., Prieto-Mollar, X., Hinrichs, K.U., Khalili, A., Ferdelman, T., Kuypers, M.M.M., Jorgensen, B.B.: Cyclic 100-ka (glacial-interglacial) migration of subfloor redox zonation on the Peruvian shelf, *PNAS*, 110, 18098-18103, 2013.
- Corselli, C., and Basso, D.: First evidence of benthic communities based on chemosynthesis on the Napoli mud volcano (Eastern Mediterranean), *Mar. Geol.*, 132, 227-239, 1996.
- Crichton, G. and Condie, K. C.: Trace elements as source indicators in cratonic sediments: a case study from the early proterozoic libby creek group, Southeastern Wyoming, *Chicago Journals*, 101, 319-332, 1993.
- Crusius, J., Calvert, S., Pedersen, T. and Sage, D.: Rhenium and molybdenum enrichments in sediments as indicators of oxic, suboxic and sulfidic conditions of deposition, *Earth Planet. Sci. Lett.*, 145(1-4), 65-78 [online] Available from: <http://www.scopus.com/inward/record.url?eid=2-s2.0-0030434843&partnerID=tZOtx3y1>, 1996.
- Cui, M., Ma, A., Qi, H., Zhuang, X. and Zhuang, G.: Anaerobic oxidation of methane: an "active" microbial process, *Microbiologyopen*, 4(1), 1-11, doi:10.1002/mbo3.232, 2015.
- Cuven S., Francus P., Cremer, J.F.: Protocoles d'utilisation et essais de calibration du scanner de microfluorescence X de type "ITRAX Core Scanner". Rapport de recherché N° 954. ISBN: 978-2-89146-552-6, 2007.
- De Lange, G. J. and ten Haven, H. L.: Recent sapropel formation in the eastern Mediterranean, *Nature*, 305(5937), 797-798, doi:10.1038/305797a0, 1983.
- De Lange, G. ., Boelrijk, N. a. I. ., Catalano, G., Corselli, C., Klinkhammer, G. ., Middelburg, J. ., Müller, D. ., Ullman, W. ., Van Gaans, P. and Woititz, J. R. .: Sulphate-related equilibria in the hypersaline brines of the Tyro and Bannock Basins, eastern Mediterranean, *Mar. Chem.*, 31(1-3), 89-112, doi:10.1016/0304-4203(90)90032-8, 1990a.
- De Lange, G.J., Middelburg, J.J., Van der Weijden, C.H., Catalano, G., Luther, G.W., III, Hydes, D.J., Woititz, J.R.W., Klinkhammer, G.P.: Composition of anoxic hypersaline brines in the Tyro and Bannock Basins, eastern Mediterranean. *Marine Chem.*, 31,63-88, 1990b.
- De Lange, G. J.: Shipboard routine and pressure-filtration system for pore-water extraction from suboxic sediments, *Mar. Geol.*, 109(1-2), 77-81, doi:10.1016/0025-3227(92)90221-3, 1992.
- Dählmann, A. and de Lange, G.: Fluid-sediment interactions at Eastern Mediterranean mud volcanoes: a stable isotope study from ODP Leg 160, *Earth Planet. Sci. Lett.*, 212(3-4), 377-391, doi:10.1016/S0012-821X(03)00227-9, 2003.
- Deville, E., Battani, A., Griboulard, R., Guerlais, S., Herbin, J. P., Houzay, J. P., Muller, C. and Prin-

- zhofer, A.: The origin and processes of mud volcanism: new insights from Trinidad, *Geol. Soc. London, Spec. Publ.*, 216(1), 475–490, doi:10.1144/GSL.SP.2003.216.01.31, 2003.
- Deville, E., Guerlais, S. H., Callec, Y., Griboulard, R., Huyghe, P., Lallemand, S., Mascle, A., Noble, M. and Schmitz, J.: Liquefied vs stratified sediment mobilization processes: Insight from the South of the Barbados accretionary prism, *Tectonophysics*, 428(1-4), 33–47, doi:10.1016/j.tecto.2006.08.011, 2006.
- Dewey, J. F., Helman, M. L., Knott, S. D., Turco, E. and Hutton, D. H. W.: Kinematics of the western Mediterranean, *Geol. Soc. London, Spec. Publ.*, 45(1), 265–283, doi:10.1144/GSL.SP.1989.045.01.15, 1989.
- Díaz-del-Río, V.: Vast fields of hydrocarbon-derived carbonate chimneys related to the accretionary wedge/olistostrome of the Gulf of Cádiz, *Mar. Geol.*, 195(1-4), 177–200, doi:10.1016/S0025-3227(02)00687-4, 2003.
- Díaz-Merino, C., Comas, M. C. y Martínez del Olmo, W.: Secuencias de depósito neógenas del margen NO del mar de Alborán, *Cuenca de Málaga. Geotemas*, 61-65, 2003.
- Dickens, G. R.: Sulfate profiles and barium fronts in sediment on the Blake Ridge: Present and past methane fluxes through a large as hydrate reservoir, *Geochim. Cosmochim. Acta*, 65(4), 529–543, doi:10.1016/S0016-7037(00)00556-1, 2001.
- Dimitrov, L. I.: Mud volcanoes—the most important pathway for degassing deeply buried sediments, *Earth-Science Rev.*, 59(1-4), 49–76, doi:10.1016/S0012-8252(02)00069-7, 2002.
- Drits, V. A., and Tchoubar, C.: X-ray diffraction by disordered lamellar structures: Theory and applications to microdivided silicates and carbons: Berlin, Springer-Verlag, 371, 1990.
- Dupré, S., Berger, L., Le Bouffant, N., Scalabrin, C. and Bourillet, J.-F.: Fluid emissions at the Aquitaine Shelf (Bay of Biscay, France): A biogenic origin or the expression of hydrocarbon leakage?, *Cont. Shelf Res.*, 88, 24–33, doi:10.1016/j.csr.2014.07.004, 2014.
- Eglinton G., and Hamilton R. J., The distribution of n-alkanes, in: *Chemical Plant Taxonomy*, Academic Press, 187–217, 1963.
- Eglinton, G., and Hamilton, R.J.: Leaf epicuticular waxes, *Science*, 156, 1322-1335, 1967.
- Elvert M., Suess E., Greinert J., Whiticar M.J.: Archaea mediating anaerobic methane oxidation in deep-sea sediments at cold seeps of the eastern Aleutian subduction zone, *Org. Geochem.*, 31, 1175-1187, 2000.
- Emerson, S., R. Jahnke, and Heggie, D.: Sediment-water exchange in shallow water estuarine sediments. *J. Mar. Res.*, 42, 709–730, 1984.
- Erickson, B. E. and Helz, G. R.: Molybdenum(VI) speciation in sulfidic waters, *Geochim. Cosmochim. Acta*, 64(7), 1149–1158, doi:10.1016/S0016-7037(99)00423-8, 2000.
- Etiopie, G., Feyzullayev, A., Baciú, C.L.: Terrestrial methane seeps and mud volcanoes: A global perspective of gas origin, *Mar. Petrol. Geol.*, 26, 333-344, doi:10.1016/j.marpetgeo.2008.03.001, 2009.
- Etiopie, G.: Climate science: Methane uncovered, *Nat. Geosci.*, 5(6), 373–374, doi:10.1038/ngeo1483, 2012.
- Etiopie, G. and Klusman, R. W.: Geologic emissions of methane to the atmosphere. *Chemosphere*, 49, 777-789. 2002.
- Feng, D., Chen, D. and Peckmann, J.: Rare earth elements in seep carbonates as tracers of variable redox conditions at ancient hydrocarbon seeps, *Terra Nov.*, 21(1), 49–56, doi:10.1111/

- j.1365-3121.2008.00855.x, 2009.
- Feng, D., Lin, Z., Bian, Y., Chen, D., Peckmann, J., Bohrmann, G. and Roberts, H. H.: Rare earth elements of seep carbonates: Indication for redox variations and microbiological processes at modern seep sites, *J. Asian Earth Sci.*, 65, 27–33, doi:10.1016/j.jseaes.2012.09.002, 2013.
- Feseker, T., Brown, K. R., Blanchet, C., Scholz, F., Nuzzo, M., Reitz, A., Schmidt, M. and Hensen, C.: Active mud volcanoes on the upper slope of the western Nile deep-sea fan—first results from the P362/2 cruise of R/V Poseidon, *Geo-Marine Lett.*, 30(3-4), 169–186, doi:10.1007/s00367-010-0192-0, 2010.
- Feseker, T., Boetius, A., Wenzhöfer, F., Blandin, J., Olu, K., Yoerger, D. R., Camilli, R., German, C. R. and de Beer, D.: Eruption of a deep-sea mud volcano triggers rapid sediment movement, *Nat. Commun.*, 5, 5385, doi:10.1038/ncomms6385, 2014.
- Fischer, D., Sahling, H., Nöthen, K., Bohrmann, G., Zabel, M. and Kasten, S.: Interaction between hydrocarbon seepage, chemosynthetic communities, and bottom water redox at cold seeps of the Makran accretionary prism: Insights from habitat-specific pore water sampling and modeling, *Biogeosciences*, 9(6), 2013–2031, doi:10.5194/bg-9-2013-2012, 2012.
- Fisher, R., Lowry, D., Wilkin, O., Sriskantharajah, S. and Nisbet, E. G.: High-precision, automated stable isotope analysis of atmospheric methane and carbon dioxide using continuous-flow isotope-ratio mass spectrometry, *Rapid Commun. Mass Spectrom.*, 20(2), 200–8, doi:10.1002/rcm.2300, 2006.
- Flecker, R. y Kopf, A.: Clast and grain size of sediment recovered from the Napoli and Milano mud volcanoes. In: *Proceedings of the Ocean Drilling Program ODP, Initial Reports 160*, K.C. Emeis, A. H. F. Robertson, C. Richter, et al., (Eds). College Station, TX: Ocean Drilling Program, 529- 32, 1996.
- Fossing, H., Ferdelman, T. G. and Berg, P.: Sulfate reduction and methane oxidation in continental margin sediments influenced by irrigation (South-East Atlantic off Namibia), *Geochimical Cosmochim. Acta*, 64(5), 897–910, 2000.
- Freed, R.L., and Peacor, D.R.: Variability in temperature of the smectite/illite reaction in gulf coast sediments, *Clay Mine.*, 24, 171-180, 1989.
- Gennari, G., Spezzaferri, S., Comas, M. C., Rüggeberg, A., Lopez-Rodriguez, C. and Pinheiro, L. M.: Sedimentary sources of the mud-breccia and mud volcanic activity in the Western Alboran Basin, *Mar. Geol.*, doi:10.1016/j.margeo.2013.04.002, 2013.
- German, R. and Elderfield, H.: Application of the Ce anomaly as a paleoredox indicator: the ground rules, *Paleoceanography*, 5(5), 823–833, 1990.
- Giggenbach, W. F.: Geothermal solute equilibria. Derivation of Na-K-Mg-Ca geothermometers, *Geochim. Cosmochim. Acta*, 52(12), 2749–2765, doi:10.1016/0016-7037(88)90143-3, 1988.
- Ginsburg, G. D. and Soloviev, V. A.: Russian Research on Submarine Gas Hydrate Geology, *Ann. N. Y. Acad. Sci.*, 715(1 Natural Gas H), 484–486, doi:10.1111/j.1749-6632.1994.tb38862.x, 1994.
- Ginsburg, G. D. and Soloviev, V. A.: Accumulation of submarine gas hydrates, *ACS Div. Fuel Chem. Prepr.*, 42(2), 480–482 [online] Available from: <http://www.scopus.com/inward/record.url?eid=2-s2.0-3342882051&partnerID=tZOtx3y1>, 1997.
- Giresse, P., Loncke, L., Huguen, C., Muller, C. and Mascle, J.: Nature and origin of sedimentary clasts associated with mud volcanoes in the Nile deep-sea fan. Relationships with fluid venting, *Sediment. Geol.*, 228(3-4), 229–245, doi:10.1016/j.sedgeo.2010.04.014, 2010.
- Gontharet, S., Pierre, C., Blanc-Valleron, M.-M., Rouchy, J. M., Fouquet, Y., Bayon, G., Foucher, J. P., Woodside, J. and Mascle, J.: Nature and origin

- of diagenetic carbonate crusts and concretions from mud volcanoes and pockmarks of the Nile deep-sea fan (eastern Mediterranean Sea), *Deep Sea Res. Part II Top. Stud. Oceanogr.*, 54(11-13), 1292–1311, doi:10.1016/j.dsr2.2007.04.007, 2007.
- González, F. J., Somoza, L., Lunar, R., Martínez-Frías, J., Martín Rubí, J. a., Torres, T., Ortiz, J. E., Díaz del Río, V., Pinheiro, L. M. and Magalhães, V. H.: Hydrocarbon-derived ferromanganese nodules in carbonate-mud mounds from the Gulf of Cadiz: Mud-breccia sediments and clasts as nucleation sites, *Mar. Geol.*, 261(1-4), 64–81, doi:10.1016/j.margeo.2008.11.005, 2009.
- Grasshoff, K. and Kremlingl, K.: *Methods of Seawater Analysis.*, 1999.
- Graue, K.: Mud volcanoes in deepwater Nigeria. *Mar. Petrol. Geol.*, 17, 959-974, 2000.
- Guliev, I. S. and Feizullayev, A. A.: Geochemistry of hydrocarbon seepages in Azerbaijan, *AAPG Mem.*, (66), 63–70 [online] Available from: <http://www.scopus.com/inward/record.url?eid=2-s2.0-33745151498&partnerID=tZOtx3y1>, 1996.
- Guliyev, I.S., and Feizullaev, A.A.: *All about mud volcanoes*, Nafta Press, Baku, 1997.
- Gutscher, M. A., Dominguez, S., Westbrook, G. K., Le Roy, P., Rosas, F., Duarte, J. C., Terrinha, P., Miranda, J. M., Graindorge, D., Gailler, a., Sallares, V. and Bartolome, R.: The Gibraltar subduction: A decade of new geophysical data, *Tectonophysics*, 574-575, 72–91, doi:10.1016/j.tecto.2012.08.038, 2012.
- Haeckel, M., Boudreau, B.P., and Wallmann, K.: Bubble-induced por water mixing: A 3-D model for deep porewater irrigation, *Geochim. Cosmochim. Acta.*, 71, 5134-5154, doi:10.1016/j.gca.2007.08.011., 2007.
- Haese, R. R., Meile, C., Van Cappellen, P. and De Lange, G. J.: Carbon geochemistry of cold seeps: Methane fluxes and transformation in sediments from Kazan mud volcano, eastern Mediterranean Sea, *Earth Planet. Sci. Lett.*, 212(3-4), 361–375, doi:10.1016/S0012-821X(03)00226-7, 2003.
- Haese, R. R., Hensen, C. and de Lange, G. J.: Pore water geochemistry of eastern Mediterranean mud volcanoes: Implications for fluid transport and fluid origin, *Mar. Geol.*, 225(1-4), 191–208, doi:10.1016/j.margeo.2005.09.001, 2006.
- Heller, R. and Zoback, M.: Adsorption of methane and carbon dioxide on gas shale and pure mineral samples, *J. Unconv. Oil Gas Resour.*, 8(C), 14–24, doi:10.1016/j.juogr.2014.06.001, 2014.
- Helz, G. R., Vorlicek, T. P. and Kahn, M. D.: Molybdenum Scavenging by Iron Monosulfide, *Environ. Sci. Technol.*, 38(16), 4263–4268, doi:10.1021/es034969+, 2004.
- Hensen, C., Zabel, M., Pfeifer, K., Schwenk, T., Kasten, S., Riedinger, N., Schulz, H. D. and Boettius, A.: Control of sulfate pore-water profiles by sedimentary events and the significance of anaerobic oxidation of methane for the burial of sulfur in marine sediments, *Geochim. Cosmochim. Acta*, 67(14), 2631–2647, doi:10.1016/S0016-7037(03)00199-6, 2003.
- Hensen, C., Nuzzo, M., Hornibrook, E., Pinheiro, L. M., Bock, B., Magalhães, V. H. and Brückmann, W.: Sources of mud volcano fluids in the Gulf of Cadiz—indications for hydrothermal imprint, *Geochim. Cosmochim. Acta*, 71(5), 1232–1248, doi:10.1016/j.gca.2006.11.022, 2007.
- Hensen, C., Scholz, F., Nuzzo, M., Valadares, V., Gracia, E., Terrinha, P., Liebetrau, V., Kaul, N., Silva, S., Martinez-Loriente, S., Bartolome, R., Pinerro, E., Magalhaes, V. H., Schmidt, M., Weise, S. M., Cunha, M., Hilario, a., Perea, H., Rovelli, L. and Lackschewitz, K.: Strike-slip faults mediate the rise of crustal-derived fluids and mud volcanism in the deep sea, *Geology*, 43(4), 339–342, doi:10.1130/G36359.1, 2015.

- Hilário, A., Comas, M. C., Azevedo, L., Pinheiro, L., Ivanov, M. K. and Cunha, M. R.: First record of a Vestimentifera (Polychaeta: Siboglinidae) from chemosynthetic habitats in the western Mediterranean Sea—Biogeographical implications and future exploration, *Deep Sea Res. Part I Oceanogr. Res. Pap.*, 58(2), 200–207, doi:10.1016/j.dsr.2010.11.009, 2011.
- Hinrichs, K-U., Hayes, J.M., Sylva, S.P., Brewer, P.G., De Long, E.F.: Methane-consuming archaeobacteria in marine sediments, *Nature*, 398, 802-805, 1999.
- Hinrichs, K-U., Pancost, R.D., Summons, R.E., Sprott, G.D., Sylva, S.P., Sinninghe Damsté, J.S., Hayes, J.M.: Mass spectra of Sn-2-hydroxyarchaeol, a polar lipid biomarker for anaerobic methenotrophy, *Geochem. Geophys. Geosy.*, 1, 1525- 2027, doi: 10.1029/2000GC000118, 2000.
- Himmler, T., Bach, W., Bohrmann, G. and Peckmann, J.: Rare earth elements in authigenic methane-seep carbonates as tracers for fluid composition during early diagenesis, *Chem. Geol.*, 277(1-2), 126–136, doi:10.1016/j.chemgeo.2010.07.015, 2010.
- Hinrichs, K. U., Hayes, J. M., Sylva, S. P., Brewer, P. G. and DeLong, E. F.: Methane-consuming archaeobacteria in marine sediments., *Nature*, 398(6730), 802–5, doi:10.1038/19751, 1999.
- Hinrichs, K. and Boetius, A.: The Anaerobic Oxidation of Methane : New Insights in Microbial Ecology and Biogeochemistry, , 457–477, 2002.
- Holler, T., Widdel, F., Knittel, K., Amann, R., Kellermann, M. Y., Hinrichs, K.-U., Teske, A., Boetius, A. and Wegener, G.: Thermophilic anaerobic oxidation of methane by marine microbial consortia, *ISME J.*, 5(12), 1946–1956, doi:10.1038/ismej.2011.77, 2011.
- Hopmans, E.C., Schouten, S., Pancost, R.D., van der Meer, M.T.J., Sinninghe Damsté, J.S.: Analysis of intact tetraether lipids in archaeal cell material and sediments by high performance liquid chromatography/atmospheric pressure chemical ionization mass spectrometry, *Rapid Commun. Mass Sp.*, 14, 585–589, 2000.
- Hovland, M., Hill, A. and Stokes, D.: The structure and geomorphology of the Dashgil mud volcano, Azerbaijan, *Geomorphology*, 21(1), 1–15, doi:10.1016/S0169-555X(97)00034-2, 1997.
- Howarth, R. J. and McArthur, J. M.: Statistics for Strontium Isotope Stratigraphy: A Robust LOWESS Fit to Marine Sr-Isotope Curve for 0 to 206 Ma, with Look-up table for Derivation of Numeric Age. *J. Geol.*, 105, 441-456, 1997.
- Hower, J., Eslinger, E.V., Hower, M.E. and Perry, E.A.: Mechanism of burial metamorphism of argillaceous sediments: 1. Mineralogical and chemical evidence. *Bull. Geol. Soc. Am.*, 87, 725-737, 1976.
- Hu, Y., Feng, D., Peckmann, J., Roberts, H. H. and Chen, D.: New insights into cerium anomalies and mechanisms of trace metal enrichment in authigenic carbonate from hydrocarbon seeps, *Chem. Geol.*, 381, 55–66, doi:10.1016/j.chemgeo.2014.05.014, 2014.
- Huseynov, D. A. and Guliyev, I. S.: Mud volcanic natural phenomena in the South Caspian Basin: geology, fluid dynamics and environmental impact. *Environ. Geol.* 46, 1012-1023, 2004.
- Ivanov, M.K., van Weering, T.C.E., and Krugljakova, R.P.: Abstract. Mud volcanoes in the Black Sea. Second Conference on Gas in Marine Sediments, North Sea Centre, Hirshals, Denmark., 31–32, 1992a.
- Ivanov, M.K., A.F. Limonov and J.M. Woodside (Eds): Geological and geophysical investigations in the Mediterranean and Black Seas. Initial results of the “Training-through- Research” Cruise of R/V Gelendzhik in the Eastern Mediterranean and the Black Sea (June/July 1991). UNESCO Rep. *Mar. Sci.* 56, 208, 1992b.

- Ivanov, M.K., Limonov, A., and Wooside, J.M. Cronin, B.: Mud volcanism and fluid venting in the eastern part of the Mediterranean Ridge. In UNESCO reports Marine Science. UNESCO, Paris, 1996.
- Ivanov, M.K., Limonov, A.F., and Woodside, J.M.: Extensive fluid flux through the sea floor on the Crimean continental margin (Black Sea). In Gas hydrates: Relevance to World Margin Stability and Climatic Change. Ed. Henriot, J-P., and Mienert, J. The Geological Society, Special Publications No 137, London, 195-213, 1998.
- Ivanov, M. K., Kenyon, N. H., Laberg, J.-S. and Blinova, V. N.: Cold seeps, coral mounds and deep-water depositional systems of the Alboran Sea, Gulf of Cadiz and Norwegian continental margin., 2010.
- James, R.H., and Palmer, M. R.: Marine geochemical cycles of the alkali elements and boron: The role of sediments, *Geochim. Cosmochim. Acta*, 64(18), 3111–3122, 2000.
- James, R. H., Allen, D. E. and Seyfried, W. E.: An experimental study of alteration of oceanic crust and terrigenous sediments at moderate temperatures (51 to 350°C): insights as to chemical processes in near-shore ridge-flank hydrothermal systems, *Geochim. Cosmochim. Acta*, 67(4), 681–691, doi:10.1016/S0016-7037(02)01113-4, 2003.
- Jimenez-Espejo, F. J., Martinez-Ruiz, F., Sakamoto, T., Iijima, K., Gallego-Torres, D. and Harada, N.: Paleoenvironmental changes in the western Mediterranean since the last glacial maximum: High resolution multiproxy record from the Alge-ro-Balearic basin, *Palaeogeogr. Palaeoclimatol. Palaeoecol.*, 246(2-4), 292–306, doi:10.1016/j.palaeo.2006.10.005, 2007.
- Jorgensen, B.B., and Kasten, S.: Sulfur cycling and methane oxidation. In: Schulz HD, Zabel M (eds). *Marine Geochemistry*, 2nd edn. Springer: Berlin Heidelberg, 271-309, 2006.
- Judd, A. and Hovland, M.: *Seabed Fluid Flow*, Cambridge University Press, Cambridge., 2007.
- Jurado, M.J. and Comas, M. C.: Well Log interpretation and Seismic Character of the Cenozoic Sequence in the Northern Alboran Sea, *Geo-Marine Lett.*, 12, 129–136, 1992.
- Jurado-Rodriguez, M. J. and Martinez-Ruiz, F.: Some clues about the Napoli and Milano mud volcanoes from an integrated log-core approach, *Proc. Ocean Drill. Progr. Sci. Results*, 160, 607–624 [online] Available from: <http://www.scopus.com/inward/record.url?eid=2-s2.0-0032461576&partnerID=40&md5=2f963a4af5c7149d607e235aa2df0a67>, 1998.
- Kastner, M., Elderfield, H. and Martin, J. B.: Fluids in Convergent Margins: What do We Know about their Composition, Origin, Role in Diagenesis and Importance for Oceanic Chemical Fluxes?, *Philos. Trans. R. Soc. London A Math. Phys. Eng. Sci.*, 335(1638), 243–259 [online] Available from: <http://rsta.royalsocietypublishing.org/content/335/1638/243.abstract>, 1991.
- Kenyon, N. H., Ivanov, M. ., Akhmetzhanov, A. . and Akhmanov, G. G.: *Multidisciplinary Study of Geological Processes on the North East Atlantic and Western Mediterranean Margins.*, 2000.
- Kenyon, N. H., Ivanov, M. K., Akhmetzhanov, A. . and Akhmanov, G. G.: *Geological Processes in the Mediterranean and Black Seas and North East Atlantic*, *Intergov. Oceanogr. Comm. Tech. Ser.*, 62, 119, 2002.
- Kenyon, N. H., Ivanov, M. K., Akhmetzhanov, A. and Akhmanov, G. G.: *Interdisciplinary Geoscience Research on the North East Atlantic Margin, Mediterranean Sea and Mid-Atlantic Ridge*, Preliminary results of investigations during the TTR-12 cruise of RV Professor Logachev, June-August, 2002., 153, 2003.

- Kenyon, N.H., Ivanov, M.K., Akhmetzhanov, A.M. and Akhmanov, G.G. (Eds) Interdisciplinary Geoscience Studies of the Gulf of Cadiz and Western Mediterranean Basins. Preliminary Results of Investigations During the TTR-14 Cruise of RV Professor Logachev July-September, 2004. (Ed UNESCO), IOC Technical Series, 70. United Nations Educational, Scientific and Cultural Organization, Paris, 115, 2006.
- Kharaka, Y.K., and Mariner, R.H.: Chemical geothermometers and their application to formation waters from sedimentary basins. In: Naser, N.D., and McCollin, T.H.: Thermal History of Sedimentary Basin, Springer-Verlag, New York, 99-117, 1989.
- Kholodov, V. N.: Mud Volcanoes , Their Distribution Regularities and Genesis : Communication 1 . Mud Volcanic Provinces and Morphology of Mud Volcanoes , , 37(3), 197–209, 2002.
- Kirsch, H.J.: Illite crystallinity; recommendations on sample preparation, X-ray diffraction settings, and interlaboratory samples. *J. Metamorph. Geol.*, 9, 665-670, 1991.
- Knittel, K., Lösekann, T., Boetius, A., Kort, R., and Amann, R.: Diversity and distribution of methanotrophic archaea at cold seeps. *Appl. Environ. Microbiol.*, 71, 467-479, 2005
- Knittel, K. and Boetius, A.: Anaerobic oxidation of methane: progress with an unknown process., *Annu. Rev. Microbiol.*, 63, 311–34, doi:10.1146/annurev.micro.61.080706.093130, 2009.
- Kopf, A., Robertson, A. H. F. and Volkmann, N.: Origin of mud breccia from the Mediterranean Ridge accretionary complex based on evidence of the maturity of organic matter and related petrographic and regional tectonic evidence, *Mar. Geol.*, 166(1-4), 65–82, doi:10.1016/S0025-3227(00)00009-8, 2000.
- Kopf, A. J.: Significance of mud volcanism, *Rev. Geophys.*, 40(2), 1005, doi:10.1029/2000RG000093, 2002.
- Kopf, A. J. and Deyhle, A.: Back to the roots: boron geochemistry of mud volcanoes and its implications for mobilization depth and global B cycling, *Chem. Geol.*, 192(3-4), 195–210, doi:10.1016/S0009-2541(02)00221-8, 2002.
- Kopf, A. J.: Global methane emission through mud volcanoes and its past and present impact on the Earth's climate, *Int. J. Earth Sci.*, 92(5), 806–816, doi:10.1007/s00531-003-0341-z, 2003.
- Kopf, A.: Mud Volcano, *Encycl. Mar. Geosci.*, 1–14, doi:10.1007/978-94-007-6644-0, 2015.
- Kozlova, E., Ivanov, M.K., Baudin, F., Largeau, C., Derenne, S.: Composition and maturity of organic matter in the rock clasts of mud volcanic breccia. North Atlantic and Labrador Sea Margin Architecture and Sedimentary Process, in: International Conference and Twelfth Post-Cruise Meeting of the Training-Trough-Research programme, Copenhagen, Denmark, Intergovernmental Oceanographic Commission Workshop Report, 191, 24–25, 2004.
- Kuramoto, S.i., Ashi, J., Greinert, J., Gulick, S., Ishimura, T., Morita, S., Nakamura, K.-i., Okada, M., Okamoto, T., Rickert, D., Saito, S., Suess, E., Tsunogai, U. and Tomosugi, T. : Surface Observations of Subduction Related Mud Volcanoes and Large Thrust Sheets in the Nankai Subduction Margin; Report on YK00-10 and YK01-04 Cruises. *JAMSTEC J. Deep Sea Res.*, 19: 131-139, 2001.
- Lanson, B., Sakharov, B. A., Claret, F. and Drits, V. A.: Diagenetic smectite-to-illite transition in clay-rich sediments: A reappraisal of x-ray diffraction results using the multi-specimen method, *Am. J. Sci.*, 309(6), 476–516, doi:10.2475/06.2009.03, 2009.
- Lash, G. G.: Authigenic barite nodules and carbonate concretions in the Upper Devonian shale succession of western New York – A record of variable methane flux during burial, *Mar. Pet. Geol.*, 59, 305–319, doi:10.1016/j.marpetgeo.2014.09.009, 2015.

- Lazar, C. S., Parkes, R. J., Cragg, B. A., L'Haridon, S. and Toffin, L.: Methanogenic diversity and activity in hypersaline sediments of the centre of the Napoli mud volcano, Eastern Mediterranean Sea., *Environ. Microbiol.*, 13(8), 2078–91, doi:10.1111/j.1462-2920.2011.02425.x, 2011.
- León, R., Somoza, L., Medialdea, T., Maestro, A., Díaz-del-Río, V. and Fernández-Puga, M. D. C.: Classification of sea-floor features associated with methane seeps along the Gulf of Cádiz continental margin, *Deep Sea Res. Part II Top. Stud. Oceanogr.*, 53(11-13), 1464–1481, doi:10.1016/j.dsr2.2006.04.009, 2006.
- León, R., Somoza, L., Medialdea, T., González, F. J., Díaz-del-Río, V., Fernández-Puga, M. C., Maestro, a. and Mata, M. P.: Sea-floor features related to hydrocarbon seeps in deepwater carbonate-mud mounds of the Gulf of Cádiz: from mud flows to carbonate precipitates, *Geo-Marine Lett.*, 27(2-4), 237–247, doi:10.1007/s00367-007-0074-2, 2007.
- Li, N., Huang, H. and Chen, D.: Fluid sources and chemical processes inferred from geochemistry of pore fluids and sediments of mud volcanoes in the southern margin of the Junggar Basin, Xinjiang, northwestern China, *Appl. Geochemistry*, 46, 1–9, doi:10.1016/j.apgeochem.2014.04.007, 2014.
- Liu, C. C., Jean, J. S., Nath, B., Lee, M. K., Hor, L. I., Lin, K. H. and Maity, J. P.: Geochemical characteristics of the fluids and muds from two southern Taiwan mud volcanoes: Implications for water-sediment interaction and groundwater arsenic enrichment, *Appl. Geochemistry*, 24(9), 1793–1802, doi:10.1016/j.apgeochem.2009.06.002, 2009.
- Liu, C. C., Maity, J. P., Jean, J. S., Li, Z., Kar, S., Sraček, O., Yang, H. J., Chen, C. Y., Reza, a. H. M. S., Bundschuh, J. and Lee, C. Y.: The geochemical characteristics of the mud liquids in the Wushanting and Hsiaokunshui Mud Volcano region in southern Taiwan: Implications of humic substances for binding and mobilization of arsenic, *J. Geochemical Explor.*, 128, 62–71, doi:10.1016/j.gexplo.2013.01.006, 2013.
- López-Rodríguez, C., Stadnitskaia, A., De Lange, G. J., Martínez-Ruiz, F. and Comas, M.: Origin of lipid biomarkers in mud volcanoes from the Alboran Sea, western Mediterranean, *Biogeosciences*, 11(12), 3187–3204, doi:10.5194/bg-11-3187-2014, 2014.
- López-Rodríguez et al.: Fluid venting and methane seep activity in Carmen MV, West Alboran Basin, in preparation, 2016.
- Lösekann, T., Knittel, K., Nadalig, T., Fuchs, B., Niemann, H., Boetius, A. and Amann, R.: Diversity and abundance of aerobic and anaerobic methane oxidizers at the Haakon Mosby Mud Volcano, Barents Sea., *Appl. Environ. Microbiol.*, 73(10), 3348–62, doi:10.1128/AEM.00016-07, 2007.
- Luff, R. and Wallmann, K.: Fluid flow, methane fluxes, carbonate precipitation and biogeochemical turnover in gas hydrate-bearing sediments at Hydrate Ridge, Cascadia Margin: Numerical modeling and mass balances, *Geochim. Cosmochim. Acta*, 67(18), 3403–3421, doi:10.1016/S0016-7037(03)00127-3, 2003.
- Lui-Heung, C., Gieskes, J. M., Chen-Feng, Y. and Edmond, J. M.: Lithium isotope geochemistry of sediments and hydrothermal fluids of the Guaymas Basin, Gulf of California, *Geochim. Cosmochim. Acta*, 58(20), 4443–4454, doi:10.1016/0016-7037(94)90346-8, 1994.
- Lupi, M., Kenkel, J., Fuchs, F., Ricci, T., Suski, B. and Conventi, M.: Effects of remote earthquakes at the Nirano Mud Volcanic Field : insights from geophysical studies, , 16, 10918, 2014.
- Lykousis, V., Alexandri, S., Woodside, J., Nomikou, P., Perissoratis, C., Sakellariou, De Lange, G., Dahlmann, A., Casas, D., Rousakis, G., Ballas, D. and

- Ioakim, C.: New evidence of extensive active mud volcanism in the Anaximander mountains (Eastern Mediterranean): The "ATHINA" mud volcano, *Environ. Geol.*, 46(8), 1030–1037, doi:10.1007/s00254-004-1090-4, 2004.
- Lykousis, V., Alexandri, S., Woodside, J., de Lange, G., Dählmann, a., Perissoratis, C., Heeschen, K., Ioakim, C., Sakellariou, D., Nomikou, P., Rousakis, G., Casas, D., Ballas, D. and Ercilla, G.: Mud volcanoes and gas hydrates in the Anaximander mountains (Eastern Mediterranean Sea), *Mar. Pet. Geol.*, 26(6), 854–872, doi:10.1016/j.marpetgeo.2008.05.002, 2009.
- Magalhães, V. H.: Authigenic carbonates and fluid escape structures in the Gulf of Cadiz. PhD thesis, University of Aveiro, Portugal, 2007.
- Magalhães, V. H., Pinheiro, L. M., Ivanov, M. K., Kozlova, E., Blinova, V., Kolganova, J., Vasconcelos, C., McKenzie, J. a., Bernasconi, S. M., Kopf, A. J., Díaz-del-Río, V., González, F. J. and Somoza, L.: Formation processes of methane-derived authigenic carbonates from the Gulf of Cadiz, *Sediment. Geol.*, 243-244, 155–168, doi:10.1016/j.sedgeo.2011.10.013, 2012.
- Malinverno, a. and Pohlman, J. W.: Modeling sulfate reduction in methane hydrate-bearing continental margin sediments: Does a sulfate-methane transition require anaerobic oxidation of methane?, *Geochemistry, Geophys. Geosystems*, 12(7), 1–18, doi:10.1029/2011GC003501, 2011.
- Manga, M. and Brodsky, E.: Seismic triggering of Eruptions in the Far Field: Volcanoes and Geysers. *Annu. Rev. Earth Planet. Sci.*, 34, 263-291, 2006.
- Margreth, S., Gennari, G., Rüggeberg, a., Comas, M. C., Pinheiro, L. M. and Spezzaferri, S.: Growth and demise of cold-water coral ecosystems on mud volcanoes in the West Alboran Sea: The messages from the planktonic and benthic foraminifera, *Mar. Geol.*, 282(1-2), 26–39, doi:10.1016/j.margeo.2011.02.006, 2011.
- Martens, C.S., Berner, R.A.: Methane production in the interstitial waters of sulfate-depleted marine sediments. *Science*, 185, 1167-1169, 1974.
- Martin, B., Kastner, M., Henry, P., Pichon, X. Le and Lallement, S.: Chemical and isotopic evidence for sources of fluids in a mud volcano field seaward of the Barbados accretionary wedge, *J. Geophys. Res.*, 101, 20.325–20.345, 1996.
- Martin, D.: Using X Powder: A software package for Powder X-Ray diffraction analysis. <http://www.xpowder.com> D.L. GR 1001/04. ISBN 84-609-1497-6. 105 p. Spain. 2004.
- Martín-Puertas, C., Mata, M. P., Fernández-Puga, M. C., Díaz del Río, V., Vázquez, J. T. and Somoza, L.: A comparative mineralogical study of gas-related sediments of the Gulf of Cádiz, *Geo-Marine Lett.*, 27(2-4), 223–235, doi:10.1007/s00367-007-0075-1, 2007.
- Martinelli, G. and Panahi, B.: *Mud Volcanoes, Geodynamics and Seismicity*, edited by G. Martinelli and B. Panahi, Springer, 2005.
- Martinelli, G., Cremonini, S. and Samonati, E.: Geological and geochemical setting of natural hydrocarbon emissions in Italy, *Nat. Gas, InTech*, (September 2015), 43, 2012.
- Martínez-Ruiz, F., Comas, M. C. and Alonso, B.: Mineral Associations and Geochemical Indicators in Upper Miocene To Pleistocene Sediments in the Alboran Basin, *Proc. Ocean Drill. Program, Sci. Result*, 161, 21–36, doi:-, 1999.
- Martínez-Ruiz, F., Paytan, A., Kastner, M., González-Donoso, J. M., Linares, D., Bernasconi, S. M. and Jimenez-Espejo, F. J.: A comparative study of the geochemical and mineralogical characteristics of the S1 sapropel in the western and eastern Mediterranean, *Palaeogeogr. Palaeoclimatol. Palaeoecol.*, 190, 23–37, doi:10.1016/S0031-0182(02)00597-7, 2003.

- Martos-Villa, R., Mata, M. P. and Sainz-Díaz, C. I.: Characterization of CO₂ and mixed methane/CO₂ hydrates intercalated in smectites by means of atomistic calculations, *J. Mol. Graph. Model.*, 49, 80–90, doi:10.1016/j.jmgm.2014.01.008, 2014.
- Masclé, J., Zitter, T., Bellaiche, G., Droz, L., Gauthier, V., Loncke, L. and Party, P.S.: The Nile deep sea fan: preliminary results from a swath bathymetry survey. *Mar. Petrol. Geol.*, 18, 471-477, 2001.
- Masclé, J., Mary, F., Praeg, D., Brosolo, L., Camera, L., Ceramicola, S. and Dupré, S.: Distribution and geological control of mud volcanoes and other fluid/free gas seepage features in the Mediterranean Sea and nearby Gulf of Cadiz, *Geo-Marine Lett.*, 34(2-3), 89–110, doi:10.1007/s00367-014-0356-4, 2014.
- Masqué, P., Fabres, J., Canals, M., Sanchez-Cabeza, J., Sanchez-Vidal, A., Cacho, I., Calafat, A. and Bruch, J. : Accumulation rates of major constituents of hemipelagic sediments in the deep Alboran Sea: a centennial perspective of sedimentary dynamics, *Mar. Geol.*, 193(3-4), 207–233, doi:10.1016/S0025-3227(02)00593-5, 2003.
- Mastalerz, V., de Lange, G. J., Dähmann, A. and Feseker, T.: Active venting at the Isis mud volcano, offshore Egypt: Origin and migration of hydrocarbons, *Chem. Geol.*, 246(1-2), 87–106, doi:10.1016/j.chemgeo.2007.09.005, 2007.
- Mastalerz, V., de Lange, G.J., Dahlmann, A.: Differential aerobic and anaerobic oxidation of hydrocarbon gases discharged at mud volcanoes in the Nile deep-sea fan, *Geochim. Cosmochim. Ac.*, 73, 3849-3863, 2009.
- Mata, M. P. and López-González, N.: Geoquímica de Elementos TRaza y Tierras Raras en Sedimentos Marinos del Margen Marroquí del Golfo de Cádiz, *Macla*, 16, 102–103, doi:10.1007/s00367-012-0275-1, 2012.
- Mata, P., Williams, L. B., Nieto, F., Martos, R. and Sainz-díaz, C. I.: Preliminary B and Li Isotope Data of Illite / Smectite from Mud Volcano Sediments from the Gulf of Cádiz, , 100–101, 2012.
- Mazurenko, L. L. and Soloviev, V. A.: Worldwide distribution of deep-water fluid venting and potential occurrences of gas hydrate accumulations, *Geo-Marine Lett.*, 23(3-4), 162–176, doi:10.1007/s00367-003-0146-x, 2003.
- Mazzini, A.: Mud volcanism: Processes and implications, *Mar. Pet. Geol.*, 26(9), 1677–1680, doi:10.1016/j.marpetgeo.2009.05.003, 2009a.
- Mazzini, A., Svensen, H., Planke, S., Guliyev, I., Akhmanov, G. G., Fallik, T. and Banks, D.: When mud volcanoes sleep: Insight from seep geochemistry at the Dashgil mud volcano, Azerbaijan, *Mar. Pet. Geol.*, 26(9), 1704–1715, doi:10.1016/j.marpetgeo.2008.11.003, 2009b.
- McInerney, F. a. and Wing, S. L.: The Paleocene-Eocene Thermal Maximum: A Perturbation of Carbon Cycle, Climate, and Biosphere with Implications for the Future, *Annu. Rev. Earth Planet. Sci.*, 39(1), 489–516, doi:10.1146/annurev-earth-040610-133431, 2011.
- McLennan, S. M., Hemming, S., McDaniel, D. K. and Hanson, G. N.: Processes Controlling the Composition of Clastic Sediments, *Geological Society of America.*, 1993.
- Meunier, A., and Velde, B.: Illite: origins, evolution and metamorphism, Springer Science and Business Media, pp 288, 2013
- Mhammedi, N. A., Moumni, B. El, Hmaid, A. El, Raissouni, A. and Arrim, A. El: Mineralogical and geochemical study of mud volcanoes in north Moroccan atlantic margin, , 2(11), 387–396, 2008.
- Mhammedi, N. A., Martos-Villa, R., Falagán, C., Mata, M.P., Somoza, L., López-González, N., Casas, D., and Sánchez-Bellón, A.: Mineralogy of methane-related sediments of the Atlantic Moroccan Shelf, *Macla*, 13, 37-38, 2010.

- Michaelis, W., Seifert, R., Nauhaus, K., Treude, T., Thiel, V., Knittel, K., Gieseke, A., Peterknecht, K., Pape, T., Boetius, A., Amann, R., Jørgensen, B. B., Widdel, F., Peckmann, J. and Pimenov, N. V: Microbial Reefs in the Black Sea Fueled by Anaerobic Oxidation of Methane, *Sci. New Ser.*, 297(5583), 1013–1015 [online] Available from: <http://www.jstor.org/stable/3832051>, 2002.
- Milkov, A.: Worldwide distribution of submarine mud volcanoes and associated gas hydrates, *Mar. Geol.*, 167(1-2), 29–42, doi:10.1016/S0025-3227(00)00022-0, 2000.
- Milkov, A. V.: Global gas flux from mud volcanoes: A significant source of fossil methane in the atmosphere and the ocean, *Geophys. Res. Lett.*, 30(2), 1037, doi:10.1029/2002GL016358, 2003.
- Milucka, J., Ferdelman, T. G., Polerecky, L., Franzke, D., Wegener, G., Schmid, M., Lieberwirth, I., Wagner, M., Widdel, F. and Kuypers, M. M. M.: Zero-valent sulphur is a key intermediate in marine methane oxidation., *Nature*, 491(7425), 541–6, doi:10.1038/nature11656, 2012.
- Moore, D. M., and Reynolds, R. C., Jr.: X-ray Diffraction and the Identification and Analysis of Clay Minerals, United Kingdom, Oxford University Press, 378, 1997.
- Muñoz, A., Ballesteros, M., Montoya, I., Rivera, J., Acosta, J. and Uchupi, E.: Alborán Basin, southern Spain—Part I: Geomorphology, *Mar. Pet. Geol.*, 25(1), 59–73, doi:10.1016/j.marpetgeo.2007.05.003, 2008.
- Nelson, S.: Sample vial influences on the accuracy and precision of carbon and oxygen isotope ratio analysis in continuous flow mass spectrometric applications, *Rapid Commun. Mass Spectrom.*, 14(4), 293–7, doi:10.1002/(SICI)1097-0231(20000229)14:4<293::AID-RCM869>3.0.CO;2-L, 2000.
- Niemann, H.: Rates and signature of methane turnover in sediments of continental margins. PhD thesis, Bremen University, Germany. 2005.
- Niemann, H., Duarte, J., Hensen, C., Omoregie, E., Magalhães, V. H., Elvert, M., Pinheiro, L. M., Kopf, a. and Boetius, A.: Microbial methane turnover at mud volcanoes of the Gulf of Cadiz, *Geochim. Cosmochim. Acta*, 70(21), 5336–5355, doi:10.1016/j.gca.2006.08.010, 2006a.
- Niemann, H., Lösekann, T., de Beer, D., Elvert, M., Nadalig, T., Knittel, K., Amann, R., Sauter, E. J., Schlüter, M., Klages, M., Foucher, J. P. and Boetius, A.: Novel microbial communities of the Haakon Mosby mud volcano and their role as a methane sink., *Nature*, 443(7113), 854–858, doi:10.1038/nature05227, 2006b.
- Niemann, H., and Elvert, M.: Diagnostic lipid biomarker and stable carbon isotope signatures of microbial communities mediating the anaerobic oxidation of methane with sulphate, *Org. Geochem.*, 39, 1668-1677, doi:10.1016/j.orggeochem.2007.11.006, 2008.
- Nieto, F., Ortega-Huertas, M., Peacor, D. R. and Arostegui, J.: Evolution of illite/smectite from early diagenesis through incipient metamorphism in sediments of the Basque-Cantabrian Basin, *Clays Clay Miner.*, 44(3), 304–323 [online] Available from: <http://www.scopus.com/inward/record.url?eid=2-s2.0-0029750016&partnerID=tZ0tx3y1>, 1996.
- Nöthen, K. and Kasten, S.: Reconstructing changes in seep activity by means of pore water and solid phase Sr/Ca and Mg/Ca ratios in pockmark sediments of the Northern Congo Fan, *Mar. Geol.*, 287(1-4), 1–13, doi:10.1016/j.margeo.2011.06.008, 2011.
- Olu, K., Sibuet, M., Harmegnies, F., Foucher, J.P., Fiala-Médioni, A.: Spatial distribution of diverse cold seep communities living on various diapiric structures of the southern Barbados prism, *Prog. Oceanogr.*, 38, 347-376, 1996.
- Olu, K., Lance, S., Sibuet, M., Henry, P., Fiala-Médioni, A. and Dinét, A.: Cold seep commu-

- nities as indicators of fluid expulsion patterns through mud volcanoes seaward of the Barbados accretionary prism, *Deep. Res. Part I Oceanogr. Res. Pap.*, 44(5), 811–841, doi:10.1016/S0967-0637(96)00123-9, 1997.
- Oppo, D., Capozzi, R., Nigarov, A. and Esenov, P.: Mud volcanism and fluid geochemistry in the Cheleken peninsula, western Turkmenistan, *Mar. Pet. Geol.*, 57, 122–134, doi:10.1016/j.marpetgeo.2014.05.009, 2014.
- Orphan, V. J., Sylva, S. P., Hayes, J. M. and Delong, E. F.: Comparative Analysis of Methane-Oxidizing Archaea and Sulfate-Reducing Bacteria in Anoxic Marine Sediments Comparative Analysis of Methane-Oxidizing Archaea and Sulfate-Reducing Bacteria in Anoxic Marine Sediments, *Appl. Environ. Microbiol.*, 67(4), 1922 – 1934, doi:10.1128/AEM.67.4.1922, 2001a.
- Orphan, V. J., House, C. H., Hinrichs, K. U., McKeehan, K. D. and DeLong, E. F.: Methane-consuming archaea revealed by directly coupled isotopic and phylogenetic analysis., *Science*, 293(5529), 484–487, doi:10.1126/science.1061338, 2001b.
- Ovsyannikov, D.: Rock fragments from mud volcanic deposits of the Gulf of Cadiz: an insight into the Eocene–Pliocene sedimentary succession of the basin, *Mar. Geol.*, 195(1-4), 211–221, doi:10.1016/S0025-3227(02)00689-8, 2003.
- Pancost, R.D., Sinninghe Damsté, J.S., De Lint, S., Van der Maarel, M.J.E.C., Gottschal, J.C., and the Medinaut Shipboard Scientific Party.: Biomarker evidence for widespread anaerobic methane oxidation in Mediterranean sediments by a consortium of methanogenic archaea and bacteria, *Applied and Environ. Microbiol.*, 66, 1126–1132, 2000.
- Pancost, R.D., Bouloubassi, I., Aloisi, G., Sinninghe Damsté, J.S., and the Medinaut Shipboard Scientific Party: Three series of non-isoprenoidal Dialkyl glycerol diethers in cold-seeps carbonate crusts, *Org. Geochem.*, 32, 695-707, 2001.
- Pape, T., Feseker, T., Kasten, S., Fischer, D. and Bohrmann, G.: Distribution and abundance of gas hydrates in near-surface deposits of the Håkon Mosby Mud Volcano, SW Barents Sea, *Geochemistry, Geophys. Geosystems*, 12(9), n/a–n/a, doi:10.1029/2011GC003575, 2011.
- Peckmann, J. and Thiel, V.: Carbon cycling at ancient methane-seeps, *Chem. Geol.*, 205(3-4), 443–467, doi:10.1016/j.chemgeo.2003.12.025, 2004.
- Peckmann, J., Reimer, a., Luth, U., Luth, C., Hansen, B. T., Heinicke, C., Hoefs, J. and Reitner, J.: Methane-derived carbonates and authigenic pyrite from the northwestern Black Sea, *Mar. Geol.*, 177(1-2), 129–150, doi:10.1016/S0025-3227(01)00128-1, 2001.
- Peketi, A., Mazumdar, A., Joshi, R. K., Patil, D. J., Srinivas, P. L. and Dayal, A. M.: Tracing the Paleo sulfate-methane transition zones and H₂S seepage events in marine sediments: An application of C-S-Mo systematics, *Geochemistry, Geophys. Geosystems*, 13(10), 1–11, doi:10.1029/2012GC004288, 2012.
- Perez-Garcia, C., Feseker, T., Mienert, J. and Berndt, C.: The Håkon Mosby mud volcano: 330000 years of focused fluid flow activity at the SW Barents Sea slope, *Mar. Geol.*, 262(1-4), 105–115, doi:10.1016/j.margeo.2009.03.022, 2009.
- Perenthaler, A., Dekas, A. E., Brown, C. T., Goffredi, S. K., Embaye, T. and Orphan, V. J.: Diverse syntrophic partnerships from deep-sea methane vents revealed by direct cell capture and metagenomics., *Proc. Natl. Acad. Sci. U. S. A.*, 105(19), 7052–7, doi:10.1073/pnas.0711303105, 2008.
- Peters, E.K., Walters, C.C. and Moldovan, J.M.: *The Biomarker Guide*. 2nd Edition. Cambridge University Press, UK, 2005.
- Pierre, C., Blanc-Valleron, M.-M., Demange, J., Boudouma, O., Foucher, J.-P., Pape, T., Himmler, T., Fekete, N. and Spiess, V.: Authigenic carbonates from

- active methane seeps offshore southwest Africa, *Geo-Marine Lett.*, 32(5-6), 501–513, doi:10.1007/s00367-012-0295-x, 2012.
- Pierre, C., Bayon, G., Blanc-Valleron, M. M., Mascle, J. and Dupré, S.: Authigenic carbonates related to active seepage of methane-rich hot brines at the Cheops mud volcano, Menes caldera (Nile deep-sea fan, eastern Mediterranean Sea), *Geo-Marine Lett.*, 34(2-3), 253–267, doi:10.1007/s00367-014-0362-6, 2014a.
- Pierre, C., Blanc-Valleron, M. M., Caquineau, S., März, C., Ravelo, a. C., Takahashi, K. and Alvarez Zarikian, C.: Mineralogical, geochemical and isotopic characterization of authigenic carbonates from the methane-bearing sediments of the Bering Sea continental margin (IODP Expedition 323, Sites U1343-U1345), *Deep. Res. Part II Top. Stud. Oceanogr.*, 1–12, doi:10.1016/j.dsr2.2014.03.011, 2014b.
- Pinheiro, L., Ivanov, M. ., Sautkin, A., Akhmanov, G., Magalhães, V., Volkonskaya, A., Monteiro, J., Somoza, L., Gardner, J., Hamouni, N. and Cunha, M.: Mud volcanism in the Gulf of Cadiz: results from the TTR-10 cruise, *Mar. Geol.*, 195(1-4), 131–151, doi:10.1016/S0025-3227(02)00685-0, 2003.
- Planke, S., Svensen, H., Hovland, M., Banks, D. a. and Jamtveit, B.: Mud and fluid migration in active mud volcanoes in Azerbaijan, *Geo-Marine Lett.*, 23(3-4), 258–268, doi:10.1007/s00367-003-0152-z, 2003.
- Poludetkina, E. and Kozlova, E.: Geochemical Characteristics of Hydrocarbon Gases and Organic Matter from Mud Volcano Deposits of the Alboran Sea., *Int. Conf. Elev. Post-Cruise Meet. Training-Through-Research Program.*, 187, 5–7 [online] Available from: File:///C:/VHD/VHBiblio\MudVolcanism\VH04-1660.pdf, 2003.
- Poludetkina, E., Comas, M., Kozlova, E. and Ivanov, M.: Geochemical Preconditions of Oil-Gas-Bearing Capacity of the Alboran Basin, , 90074, 2008.
- Poynter, J.: *Molecular stratigraphy: The recognition of paleoclimate signals in organic geochemical data*, PhD Thesis, University of Bristol, 324 pp., 1989.
- Reeburgh, W.S.: Methane consumption in Cariaco Trench waters and sediments. *Earth Planet. Sci. Lett.*, 28, 337-344, 1976.
- Reeburgh, W.S.: Anaerobic methane oxidation rate depth distribution in Skan Bay sediments. *Earth Planet. Sci. Lett.*, 28, 337-344, 1980.
- Reeburgh, W.S.: “Soft spots” in the global methane budget. In *Microbial growth on C1 compounds*, Lidstrom, M.E. & Tabita, F.R. (Eds.), Kluwer Academic Publishers, 334-342, 1996.
- Reeburgh, W.S.: A major sink and flux control for methane in marine sediments: Anaerobic consumption, In (Eds) K. Fanning and F. Manheim. *Dynamic environment of the ocean floor*, Heath, Lexington, 203-217, 1982.
- Reeburgh, W. S., Ward, B. B., Whalen, S. C., Sandbeck, K. a., Kilpatrick, K. a. and Kerkhof, L. J.: Black Sea methane geochemistry, *Deep Sea Res. Part A. Oceanogr. Res. Pap.*, 38, S1189–S1210, doi:10.1016/S0198-0149(10)80030-5, 1991.
- Reeburgh, W.: Oceanic methane biogeochemistry, *Chem. Rev.*, 486–513, doi:10.1021/cr050362v, 2007.
- Reimer, P. J., Baillie, M. G. L., Bard, E., Bayliss, A., Beck, J. W., Blackwell, P. G., Ramsey, C. B., Buck, C. E., Burr, G. S., Edwards, R. L., Friedrich, M., Grootes, P. M., Guilderson, T. P., Hajdas, I., Heaton, T. J., Hogg, A. G., Hughen, K. A., Kaiser, K. F., Kromer, B., McCormac, F. G., Manning, S. W., Reimer, R. W., Richards, D. A., Southon, J. R., Talamo, S., Turney, C. S. M., van der Plicht, J. and Weyhenmeyer, C. E.: IntCal09 and Marine09 radiocarbon age calibration curves, 0-50,000 years CAL BP, *Radiocarbon*, 51(4), 1111–1150 [online] Available from: <http://www.scopus.com/inward/record.url?eid=2-s2.0-77950339815&partnerID=tZ0tx3y1>, 2009.

- Reitz, A., Pape, T., Haeckel, M., Schmidt, M., Berner, U., Scholz, F., Liebetrau, V., Aloisi, G., Weise, S. M. and Wallmann, K.: Sources of fluids and gases expelled at cold seeps offshore Georgia, eastern Black Sea, *Geochim. Cosmochim. Acta*, 75(11), 3250–3268, doi:10.1016/j.gca.2011.03.018, 2011.
- Reynolds, R.C.: Interstratified clay minerals, In Brindley, G.W., and Brown, G., Eds, *Crystal structures of clay mineral and their X-ray identification*: London, The Mineralogical Society, Monograph 5, 249-359, 1980.
- Riedinger, N., Kasten, S., Gröger, J., Franke, C. and Pfeifer, K.: Active and buried authigenic barite fronts in sediments from the Eastern Cape Basin, *Earth Planet. Sci. Lett.*, 241(3-4), 876–887, doi:10.1016/j.epsl.2005.10.032, 2006.
- Robertson, A. H. F. and Kopf, A.: Origen of clasts and matrix within the Milano and Napoli mud volcanoes, *Mediterranean Ridge accretionary complex 1*, 160, 1998.
- Rodrigo-Gámiz, M., Martínez-Ruiz, F., Jiménez-Espejo, F. J., Gallego-Torres, D., Nieto-Moreno, V., Romero, O. and Ariztegui, D.: Impact of climate variability in the western Mediterranean during the last 20,000 years: oceanic and atmospheric responses, *Quat. Sci. Rev.*, 30(15-16), 2018–2034, doi:10.1016/j.quascirev.2011.05.011, 2011.
- Rodríguez-Fernández, J., Comas, M.C., Soría, J., Martín-Pérez, J.A., Soto, J.I.: The sedimentary record of the Alboran Basin: An attempt at sedimentary sequence correlation and subsidence analysis, in: Zahn, R., Comas, M.C., Klaus, A. (Eds). *Proceedings ODP, Scientific Results 161*, College Station, TX (Ocean Drilling Program), 69-76, 1999.
- Rodríguez-Germade, I., Rubio, B., Rey, D., Vilas, F., López-Rodríguez, C., Comas, M. C. and Martínez-Ruiz, F.: Optimization of itrax core scanner measurement conditions for sediments from submarine mud volcanoes, in *Micro-XRF Studies of Sediment Cores*, vol. 17., 2015.
- Roberts, H.H.: Fluid and Gas Expulsion on the Northern Gulf of Mexico Continental Slope: Mud-Prone to Mineral-Prone Responses. In: *Natural Gas Hydrates: Occurrence, Distribution, and Detection* (Eds C.K. Paull and W.P. Dillon), *Geophysical Monograph*, 124, 145-161, American Geophysical Union, Washington, 2001.
- Ross, D. J. K. and Marc Bustin, R.: The importance of shale composition and pore structure upon gas storage potential of shale gas reservoirs, *Mar. Pet. Geol.*, 26(6), 916–927, doi:10.1016/j.marpetgeo.2008.06.004, 2009.
- Rovere, M., Gamberi, F., Mercorella, A., Rashed, H., Gallerani, A., and Leidi, E.: Venting and seepage systems associated with mud volcanoes and mud diapirs in the southern Tyrrhenian. *Mar. Geol.*, 347, 153-171, 2014. DOI: 10.1016/j.marpetgeo.2013.11.013.
- Sager, W.W., MacDonald, I.R. and Hou, R.: Geophysical signatures of mud mounds at hydrocarbon seeps on the Louisiana continental slope, northern Gulf of Mexico. *Mar. Geol.*, 198, 97-132, 2003.
- Sapart, C. J., van der Veen, C., Vigano, I., Brass, M., van de Wal, R. S. W., Bock, M., Fischer, H., Sowers, T., Buizert, C., Sperlich, P., Blunier, T., Behrens, M., Schmitt, J., Seth, B. and Röckmann, T.: Simultaneous stable isotope analysis of methane and nitrous oxide on ice core samples, *Atmos. Meas. Tech.*, 4(12), 2607–2618, doi:10.5194/amt-4-2607-2011, 2011.
- Sautkin, a., Talukder, a. R., Comas, M. C., Soto, J. I. and Alekseev, a.: Mud volcanoes in the Alboran Sea: evidence from micropaleontological and geophysical data, *Mar. Geol.*, 195(1-4), 237–261, doi:10.1016/S0025-3227(02)00691-6, 2003.
- Scholz, F.: Pore water expulsion at submarine cold seeps : geochemical evidence for short-cuts between crust, sediments and ocean. PhD thesis,

- GEOMAR Helmholtz Centre for Ocean Research and Kiel University, Germany, 2009.
- Scholz, F., Hensen, C., De Lange, G. J., Haeckel, M., Liebetrau, V., Meixner, A., Reitz, A. and Romer, R. L.: Lithium isotope geochemistry of marine pore waters – Insights from cold seep fluids, *Geochim. Cosmochim. Acta*, 74(12), 3459–3475, doi:10.1016/j.gca.2010.03.026, 2010.
- Scholz-Böttcher, B. M., Ahlf, S., Vázquez-Gutiérrez, F. and Rullkötter, J.: Natural vs. anthropogenic sources of hydrocarbons as revealed through biomarker analysis: A case study in the southern Gulf of Mexico, 47–56, 2009.
- Schouten, S., Hopmans, E. C. and Sinninghe Damsté, J. S.: The organic geochemistry of glycerol dialkyl glycerol tetraether lipids: A review, *Org. Geochem.*, 54, 19–61, doi:10.1016/j.orggeochem.2012.09.006, 2013.
- Seeberg-Elverfeldt, J., Schlüter, M., Feseker, T. and Martin, K.: Rhizon sampling of porewaters near the sediment-water interface of aquatic systems, *Limnol. Oceanogr.*, 3, 361–371, 2005.
- Seifert, W.K., and Moldovan, J.M.: The effect of thermal stress on source-rock quality as measured by hopane stereochemistry, in: Maxwell, J.R. (Eds). *Phys. Chem. Earth*, Pergamon, Oxford, 229–237, 1980.
- Schouten, S., Hopmans, E.C., Sinninghe Damsté, J.S.: The organic geochemistry of glycerol dialkyl glycerol tetraether lipids: a review, *Org. Geochem.*, 54, 19–61, <http://dx.doi.org/10.1016/j.orggeochem.2012.09.006>, 2012.
- Shields, G. and Stille, P.: Diagenetic constraints on the use of the cerium anomaly as a palaeoredox indicator: REE and isotopic data from basal Cambrian phosphorites., [online] Available from: <http://discovery.ucl.ac.uk/43791/>, 2001.
- Sibuet, M. and Olu, K.: Biogeography, biodiversity and fluid dependence of deep-sea cold-seeps communities at active and passive margins. *Deep-Sea Research* 45, 517–567, 1998.
- Somoza, L., Diaz-del-Rio, V., León, R., Ivanov, M., Fernández-Puga, M. C., Gadner, J. M., Hernández-Molina, F. J., Pinheiro, L. M., Rodero, J., Lobato, A., Maestro, A., Vázquez, J. T., Medialdea, T. and Fernández-Salas, L. M.: Seabed morphology and hydrocarbon seepage in the Gulf of Cádiz mud volcano area: Acoustic imagery, multibeam and ultra-high resolution seismic data, *Mar. Geol.*, 195(1-4), 153–176, doi:10.1016/S0025-3227(02)00686-2, 2003.
- Sinninghe Damsté, J.S., Schouten, S., Hopmans, E.C., van Duin, A.C.T., Geenevasen, J.A.J.: Crenarchaeol: the characteristic core glycerol dibiphytanyl glycerol tetraether membrane lipid of cosmopolitan pelagic crenarchaeota, *J. Lipid. Res.*, 43, 1641–1651, 2002.
- Somoza, L., Medialdea, T., León, R., Ercilla, G., Vázquez, J. T., Farran, M., Hernández-Molina, J., González, J., Juan, C. and Fernández-Puga, M. C.: Structure of mud volcano systems and pockmarks in the region of the Ceuta Contourite Depositional System (Western Alborán Sea), *Mar. Geol.*, 332–334, 4–26, doi:10.1016/j.mar-geo.2012.06.002, 2012.
- Soto, J.I., Comas, M.C. and de la Linde, J.: Espesor de sedimentos en la cuenca de Alborán mediante una consersión sísmica corregida, *Geogaceta*, 20(2), 382–385, 1996.
- Soto, J.I., Comas, M.C., Talukder, A.: Evolution of the mud diapirism in the Alboran Sea (Western Mediterranean), in: AAPG International Conference, Barcelona, Spain, 187, 1–6, 2003.
- Soto, J. I., Fernández-Ibáñez, F., Talukder, A. R. and Martínez-García, P.: Miocene shale tectonics in the northern Alboran Sea (Western Mediterranean), *AAPG Mem.*, (93), 119–144, doi:10.1306/13231312M933422, 2010.

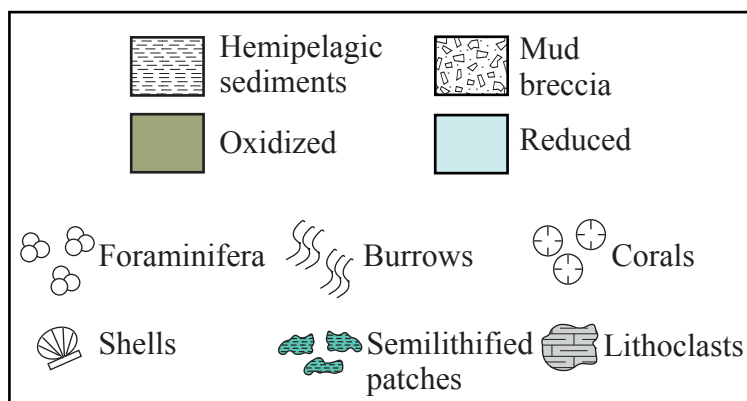
- Soto, J., Fernández-Ibáñez, F. and Talukder, A.: Recent shale tectonics and basin evolution of the NW Alboran Sea, *Soc. Explor. Geophys.*, 31(7), 768–775, doi:10.1190/tle31070768.1, 2012.
- Stadnitskaia, A., Muyzer, T.G., Abbas, B., Coolen, M.J.L., Hopmans, E.C., Baas, M., van Weering, T.C.E., Ivanov, M.K., Poludetkina, E., Sinninghe Damsté, J.S.: Biomarker and 16S rDNA evidence for anaerobic oxidation of methane and related carbonate precipitation in deep-sea mud volcanoes of the Sorokin Trough, Black Sea, *Mar. Geol.*, 217, 67–96, doi:10.1016/j.margeo.2005.02.023, 2005.
- Stadnitskaia, A.: Bio- and petroleum geochemistry of mud volcanoes in the Sorokin Trough (NE Black Sea) and in the Gulf of Cadiz (NE Atlantic): from fluid sources to microbial methane oxidation and carbonate formation. PhD thesis, Utrecht University, The Netherlands, 2007.
- Stadnitskaia A., Blinova, V., Ivanov, M.K., Baas, M., Hopmans, E., van Weering, T.C.E., and Sinninghe Damsté, J.S.: Lipid biomarkers in sediments of mud volcanoes from the Sorokin Trough, NE Black Sea: Probable source strata for the erupted material, *Org. Geochem.*, 38, 67–83, doi:10.1016/j.orggeochem.2006.08.012, 2007.
- Stadnitskaia, A., Ivanov, M. K., Poludetkina, E. N., Kreulen, R. and van Weering, T. C. E.: Sources of hydrocarbon gases in mud volcanoes from the Sorokin Trough, NE Black Sea, based on molecular and carbon isotopic compositions, *Mar. Pet. Geol.*, 25(10), 1040–1057, doi:10.1016/j.marpetgeo.2007.08.001, 2008.
- Stadnitskaia, A., Ivanov, M.K., Sinninghe Damsté, J.S.: Application of lipid biomarkers to detect sources of organic matter in mud volcano deposits and post-eruptional methanotrophic processes in the Gulf of Cadiz, NE Atlantic, *Mar. Geol.*, 255, 1–14, doi:10.1016/j.orggeochem.2008.04.019, 2008.
- Stuiver, M. and Reimer, P. J.: Extended 14C data base and revised CALIB 3.0 14C age calibration program, *Radiocarbon*, 35(1), 215–230 [online] Available from: <http://www.scopus.com/inward/record.url?eid=2-s2.0-0027464565&partnerID=tZotx3y1>, 1993.
- Talukder, M. A. R.: La Provincia Diapírica de lodo en la Cuenca Oeste del Mar de Alborán: Estructuras, Génesis y Evolución, PhD Thesis, Granada University, Granada, 251 pp., 2003.
- Talukder, a. R., Comas, M. C. and Soto, J. I.: Pliocene to Recent mud diapirism and related mud volcanoes in the Alboran Sea (Western Mediterranean), *Geol. Soc. London, Spec. Publ.*, 216(1), 443–459, doi:10.1144/GSL.SP.2003.216.01.29, 2003.
- Taylor, S. R. and McLennan, S. M.: The Continental Crust: its Composition and Evolution. An Examination of the Geochemical Record Preserved in Sedimentary Rocks., *Cont. Crust its Compos. Evol. An Exam. Geochemical Rec. Preserv. Sediment. Rocks.* [online] Available from: <http://www.scopus.com/inward/record.url?eid=2-s2.0-0022195502&partnerID=tZotx3y1>, 1985.
- Thomas, D.J., Zachos, J.C., Bralower, T.J., Thomas, E., and Bohaty, S.: Warming the fuel for the fire: Evidence for the thermal dissociation of methane hydrate during the Paleocene–Eocene thermal maximum: *Geology*, 30, 1067–1070, 2002, doi: 10.1130/0091-7613(2002)030<1067:WTF>2.0.CO;2.
- Tinivella, U. and Giustiniani, M.: An Overview of Mud Volcanoes Associated to Gas Hydrate System, *Updat. Volcanol. - New Adv. Underst. Volcan. Syst.*, 225–267, doi:10.5772/3390, 2013.
- Torne, M. and Fernández, M.: Lithospheric Structure Beneath the Alboran Basin: Results from 3D Gravity Modeling and Tectonic Relevance., *J. Geophys. Res.*, 105, 3209–3228, 2000.










- Torres, M. E., Brumsack, H. J., Bohrmann, G. and Emeis, K. C.: Barite fronts in continental margin sediments: a new look at barium remobilization in the zone of sulfate reduction and formation of heavy barites in diagenetic fronts, *Chem. Geol.*, 127(1-3), 125–139, doi:10.1016/0009-2541(95)00090-9, 1996.
- Torné, M., Fernández, M., Comas, M.C. and Soto, J.I.: Lithospheric structure beneath the Alboran Basin: results from 3D gravity modeling and tectonic relevance. *J. Geophys. Res.*, 105, 3209-3228, 2000.
- Treude, T., Boetius, a, Knittel, K., Wallmann, K. and Barker Jørgensen, B.: Anaerobic oxidation of methane above gas hydrates at Hydrate Ridge, NE Pacific Ocean, *Mar. Ecol. Prog. Ser.*, 264, 1–14, doi:10.3354/meps264001, 2003.
- Van Duin, A.C.T., Sinninghe Damsté, J.S., Koopmans, M.P., Van de Graaf, B., De Leeuw, J.W.: A kinetic calculation method of homohopanoide maturation: Applications in the reconstruction of burial histories of sedimentary basins. *Geochim. Cosmochim. Ac.*, 61, 2409-2429, 1997.
- Vanreusel, A., Andersen, A. C., Boetius, A., Connelly, D., Cunha, M. R., Decker, C., Hilario, A., Kormas, K. A., Maignien, L., Olu, K., Pachiadaki, M., Ritt, B., Rodrigues, C., Sarrazin, J., Tyler, P., van Gaever, S. and Vanneste, H.: Biodiversity of cold seep ecosystems along the European margins, *Oceanography*, 22(1), 110–127 [online] Available from: <http://www.scopus.com/inward/record.url?eid=2-s2.0-77952953907&partnerID=tZOtx3y1>, 2009.
- Vanneste, H., Kelly-Gerreyn, B. a., Connelly, D. P., James, R. H., Haeckel, M., Fisher, R. E., Heeschen, K. and Mills, R. a.: Spatial variation in fluid flow and geochemical fluxes across the sediment–seawater interface at the Carlos Ribeiro mud volcano (Gulf of Cadiz), *Geochim. Cosmochim. Acta*, 75(4), 1124–1144, doi:10.1016/j.gca.2010.11.017, 2011.
- Velde, B. and Vasseur, G.: A kinetic model of the smectite-to-illite transformation based on diagenetic mineral series. *Am. Miner.*, 77, 967-976, 1992.
- Vogt, P.R., Gardner, J. and Crane, K.: The Norwegian-Barents-Svalbard (NBS) continental margin: Introducing a natural laboratory of mass wasting, hydrates, and ascent of sediment, pore water, and methane. *Geo-Mar. Lett.*, 19, 2-21, 1999.
- Von Rad, U., Berner, U., Delisle, G., Dooze-Rolinski, H., Fechner, N., Linke, P., Luckge, A., Roeser, H.A., Schmaljohann, R., Wiedicke, M. and SONNE 122/130 Scientific Parties.: Gas and fluid venting at the Makran accretionary wedge off Pakistan. *Geo-Mar. Lett.*, 20,10-19, 2000.
- Wallmann, K., Linke, P., Suess, E., Bohrmann, G., Sahling, H., Schluter, M., Dahlmann, A., Lammers, S., Greinert, J., and von Mirbach, N.: Quantifying fluid flow, solute mixing, and biogeochemical turnover at cold vents of the eastern Aleutian subduction zone, *Geochim. Cosmochim. Ac.*, 61, 5209–5219, doi:10.1016/S0016-7037(97)00306-2, 1997.
- Wang, S., Yan, W., Chen, Z., Zhang, N. and Chen, H.: Rare earth elements in cold seep carbonates from the southwestern Dongsha area, northern South China Sea, *Mar. Pet. Geol.*, 57, 482–493, doi:10.1016/j.marpetgeo.2014.06.017, 2014.
- Wang, S., Magalhães, V. H., Pinheiro, L. M., Liu, J. and Yan, W.: Tracing the composition, fluid source and formation conditions of the methane-derived authigenic carbonates in the Gulf of Cadiz with rare earth elements and stable isotopes, *Mar. Pet. Geol.*, doi:10.1016/j.marpetgeo.2015.08.022, 2015.
- Van der Weijden, C. H.: Pitfalls of the normalization of marine geochemical data using a common deviator, *Mar. Geol.*, 184, 167–187, 2002.
- Weaver P. P. E. and Schultheiss P. J.: Vertical open burrows in deep-sea sediments 2 m in length. *Nature* 310, 329–331, 1983.
- Weijers, J. W. H., Schouten, S., Spaargaren, O. C. and Sinninghe Damsté, J. S.: Occurrence and distribution of tetraether membrane lipids in soils: Implications

- for the use of the TEX86 proxy and the BIT index, *Org. Geochem.*, 37(12), 1680–1693, doi:10.1016/j.orggeochem.2006.07.018, 2006.
- Weijers, J.W.H., Schouten, S., Hopmans, E.C., Geenevasen, J.A.J., David, O.R.P., Coleman, J.M., Pancost, R.D., Sinninghe Damsté, J.S.: Membrane lipids of mesophilic anaerobic bacteria thriving in peats have typical archaeal traits, *Environ. Microbiol.*, 8, 648–657, doi:10.1111/j.1462-2920.2005.00941.x, 2006.
- Weijers, J.W.H., Lim, K.L.H., Aquilina, A., Sinninghe Damsté, J.S., and Pancost, R.: Biogeochemical controls on glycerol dialkyl glycerol tetraether lipid distributions in sediments characterized by diffusive methane flux, *Geochem. Geophys. Geosy.*, 12, 1525–2027, doi:10.1029/2011GC003724, 2011.
- Wheeler, A.J., and Stadnitskaia, A.: Benthic deep-sea carbonates: reefs and seeps, in: Hüneke, H., Mulder, T. (Eds.), *Deep-Sea Sediments, Developments in Sedimentology*, Elsevier, Amsterdam, 63, 397–455, doi: 10.1016/S0070-4571(11)63006-9, 2011.
- Whelan, J., Eglinton, L., Cathles, L., Losh, S. and Roberts, H.: Surface and subsurface manifestations of gas movement through a N-S transect of the Gulf of Mexico, *Mar. Pet. Geol.*, 22(4 SPEC. ISS.), 479–497, doi:10.1016/j.marpetgeo.2004.08.008, 2005.
- Whiticar, M. J.: Carbon and hydrogen isotope systematics of bacterial formation and oxidation of methane, *Chem. Geol.*, 161(1), 291–314 [online] Available from: <http://www.scopus.com/inward/record.url?eid=2-s2.0-0034010663&partnerID=tZOtx3y1>, 1999.
- Wiedicke, M. and Weiss, W.: Stable carbon isotope records of carbonates tracing fossil seep activity off Indonesia, *Geochemistry, Geophys. Geosystems*, 7(11), doi:10.1029/2006GC001292, 2006.
- Wright, J., Schrader, H. and Holser, W. T.: Paleoredox variations in ancient oceans recorded by rare earth elements in fossil apatite, *Geochim. Cosmochim. Acta*, 51(3), 631–644, doi:10.1016/0016-7037(87)90075-5, 1987.
- You, C.-F., Castillo, P. R., Gieskes, J. M., Chan, L. H. and Spivack, A. J.: Trace element behavior in hydrothermal experiments: Implications for fluid processes at shallow depths in subduction zones, *Earth Planet. Sci. Lett.*, 140(1-4), 41–52, doi:10.1016/0012-821X(96)00049-0, 1996.
- You, C.-F. and Gieskes, J.M.: Hydrothermal alteration of hemi-pelagic sediments: experimental evaluation of geochemical processes in shallow subduction zones. *Appl. Geochem.*, 16, 1055–1066, 2001.
- Zabel, M. and Schulz, H. D.: Importance of submarine landslides for non-steady state conditions in pore water systems - Lower Zaire (Congo) deep-sea fan, *Mar. Geol.*, 176(1-4), 87–99, doi:10.1016/S0025-3227(01)00164-5, 2001.
- Zachos, J. C., Dickens, G. R. and Zeebe, R. E.: An early Cenozoic perspective on greenhouse warming and carbon-cycle dynamics., *Nature*, 451(7176), 279–283, doi:10.1038/nature06588, 2008.
- Zhang, Y.G., Zhang, C.L., Liu, X.L., Li, L., Hinrichs, K.U., Noakes, J.E.: Methane Index: A tetraether archaeal lipid biomarker indicator for detecting the instability of marine gas hydrates, *Earth Planet. Sc. Lett.*, 307, 525–534, doi:10.1016/j.epsl.2011.05.031, 2011.

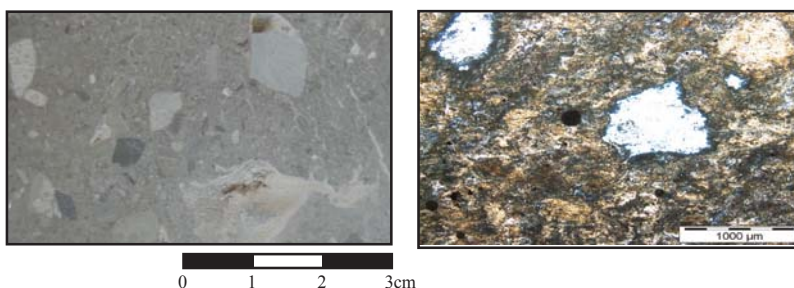
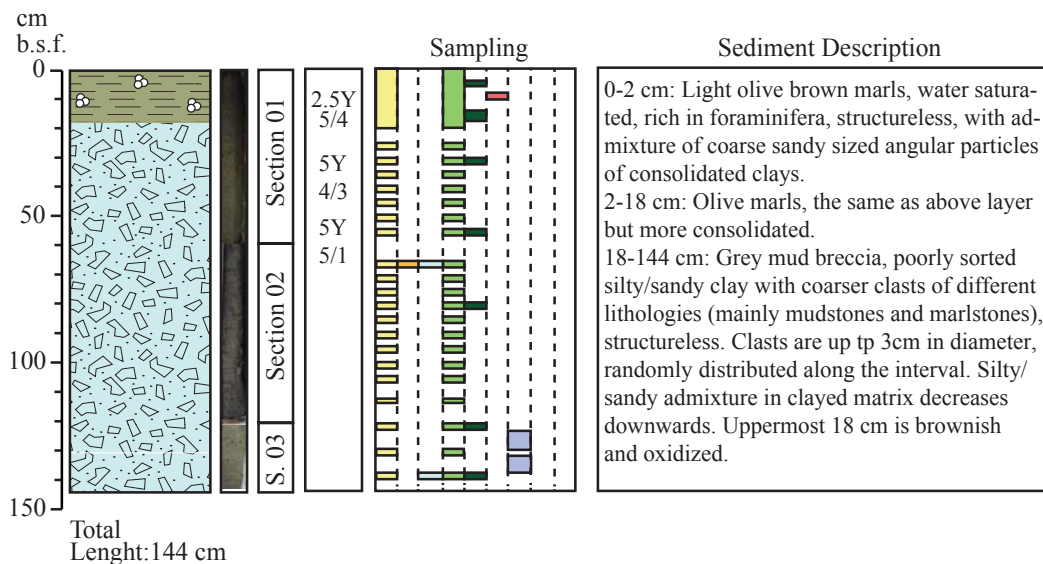


Appendix I

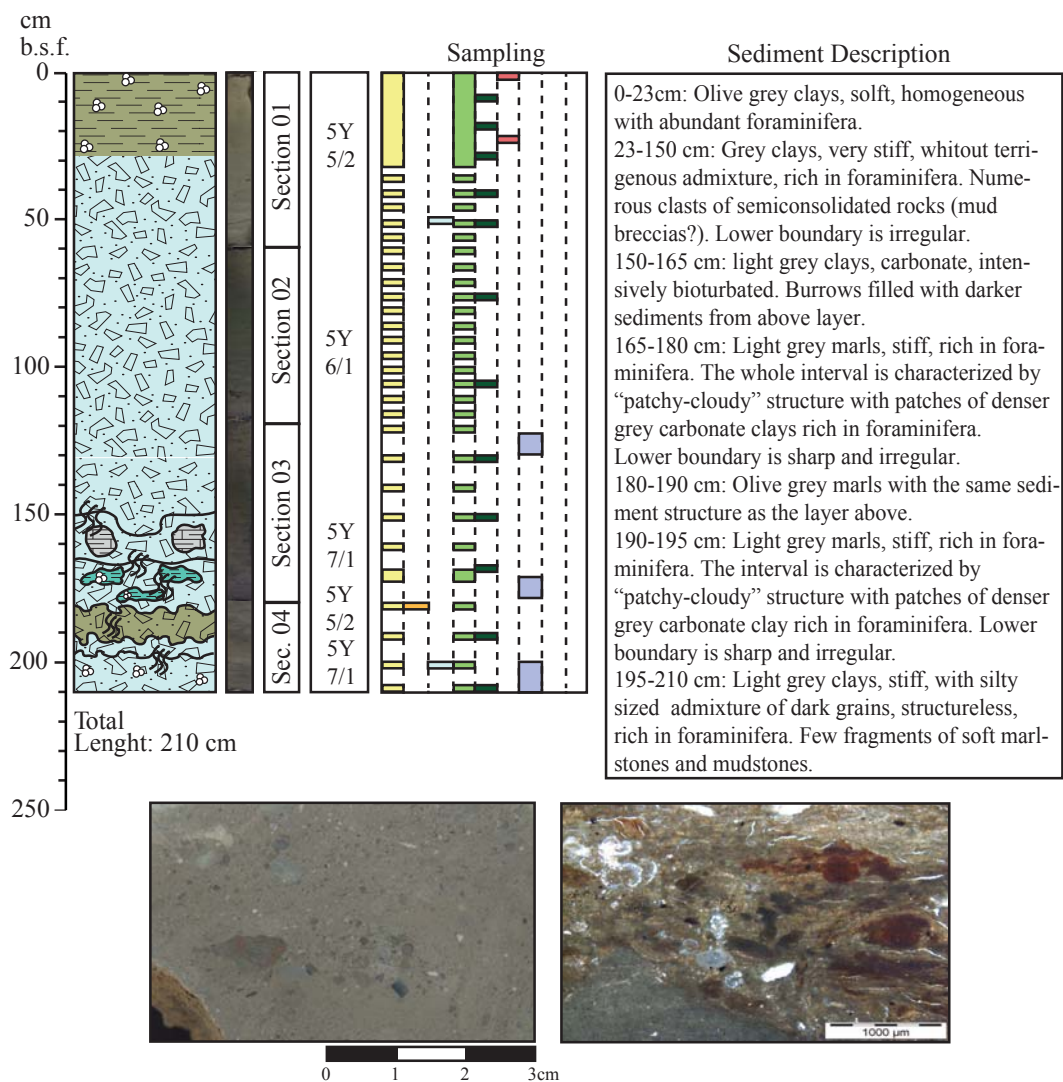


-  Sediment Analysis (X-ray diffraction, XRD)
-  Sediment Analysis (Transmission electron microscopy, TEM)
-  Sediment Analysis (Scanning electron microscopy, SEM)
-  Sediment Analysis (X-ray fluorescence, XRF and Inductively coupled plasma mass spectrometry, ICP-MS)
-  Sediment Analysis (TC, TOC and TN)
-  Sediment Analysis (Radiocarbon dating)
-  Sediment Analysis (Polished hand-samples and thin sections)
-  Pore waters (Inductively coupled plasma mass spectrometry, ICP-MS; Inductively coupled plasma atomic emission spectrometry, ICP-OES; stable and radiogenic isotopes)
-  Lipid biomarkers (Gas chromatography, GC; Gas chromatography mass spectrometry, GC-MS and High-performance liquid chromatography, HPLC)

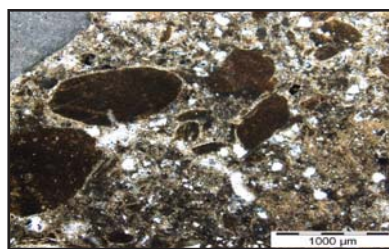
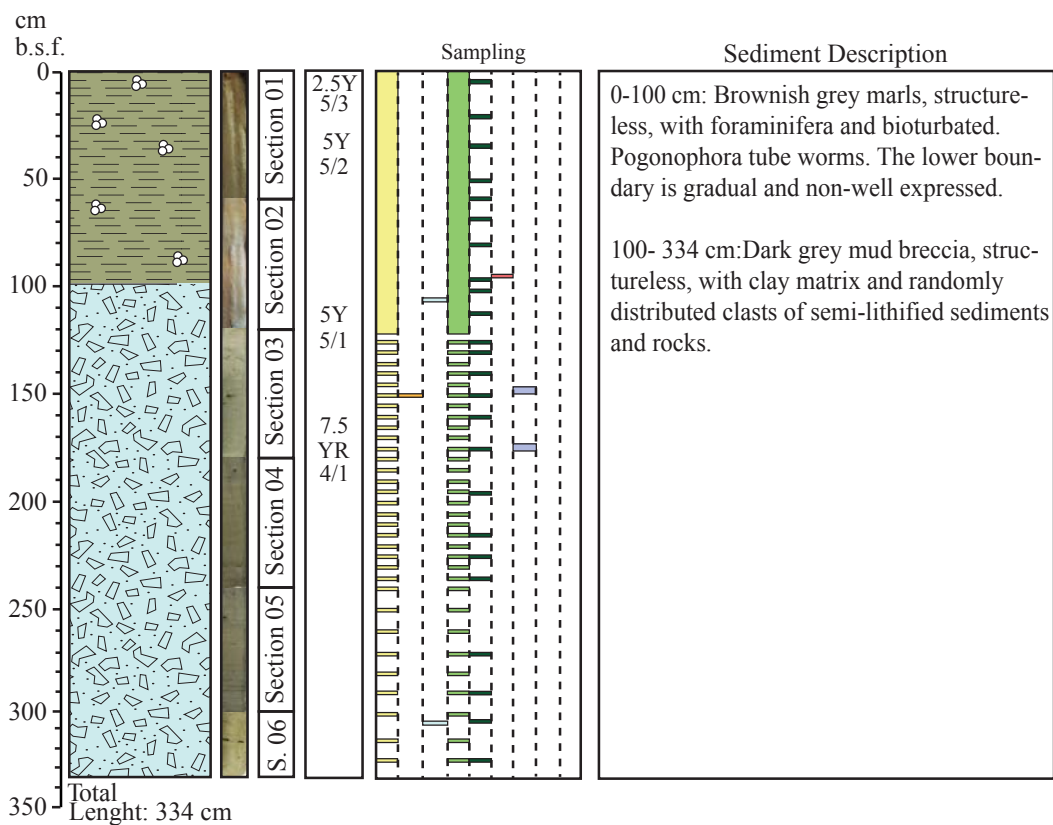
Oceanographic cruise: TTR-9 BASACALB		Core: MS258G
Location: Granada mud volcano, the Alboran Sea		Date: 19/07/99
Latitude: 35° 33.72' N	Longitude: 04° 37.40' W	
Recovery: 144 cm	Water Depth: 583 m	



Oceanographic cruise: TTR-9 BASACALB	Core: MS262G
Location: Marrakech mud volcano, the Alboran Sea	Date: 19/07/99
Latitude: 35° 37.51' N	Longitude: 04° 29.66' W
Recovery: 210 cm	Water Depth: 1086 m

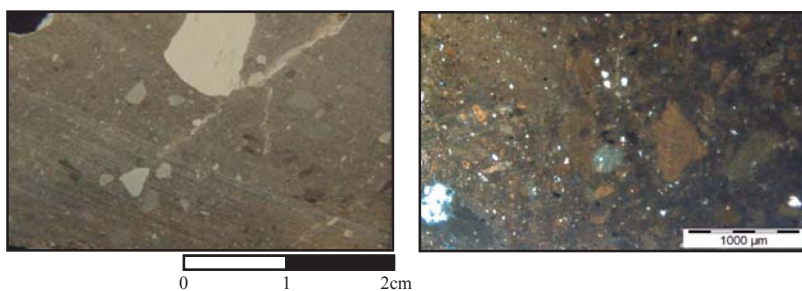
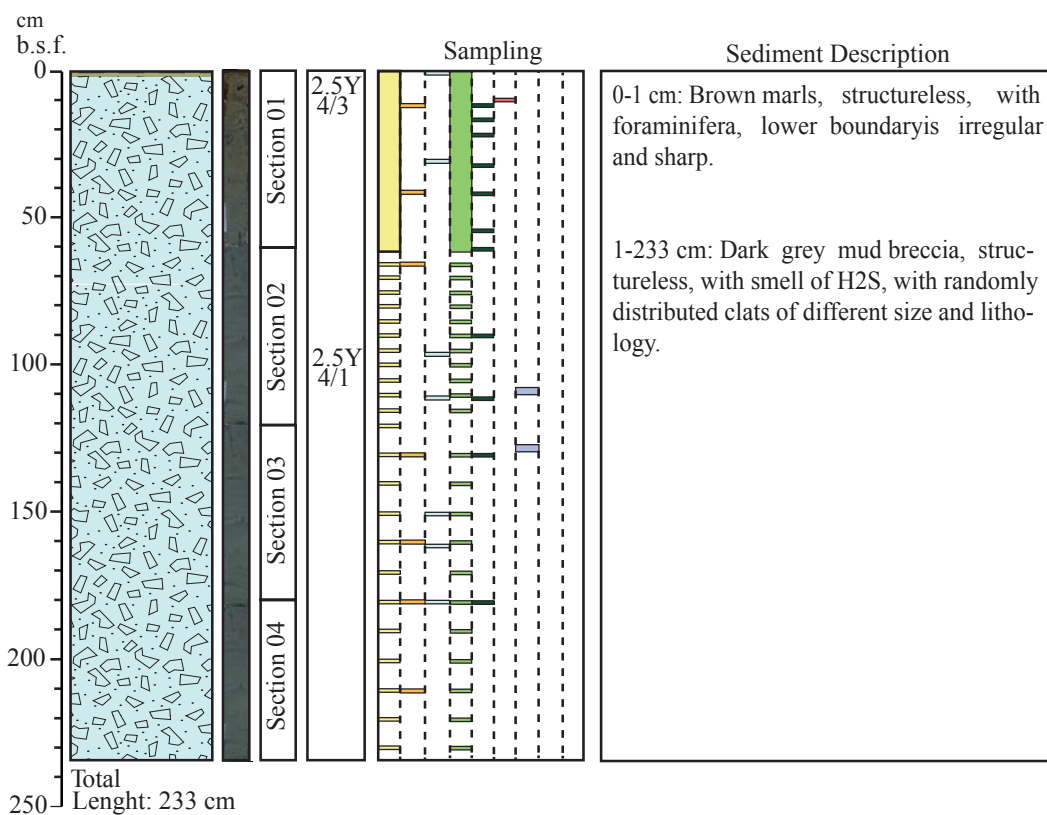


Oceanographic cruise: TTR-12 Leg 3, MARSIBAL	Core: MS280G
Location: Kalinin mud volcano, the Alboran Sea	Date: 21/07/02
Latitude: 36° 02.828' N	Longitude: 04° 55.973' W
Recovery: 334 cm	Water Depth: 908 m

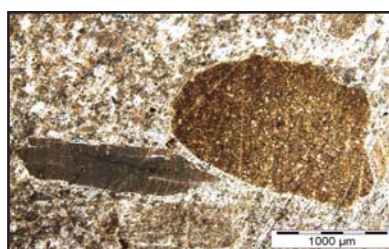
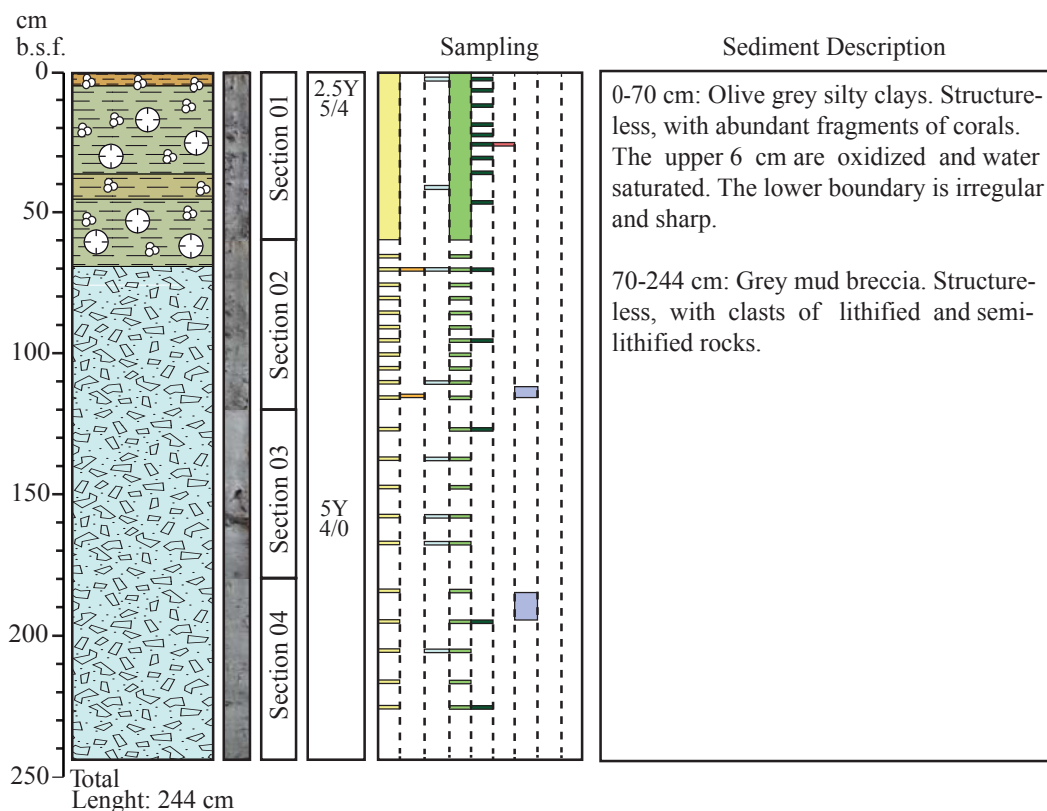


0 1 2 3cm

Oceanographic cruise: TTR-12 Leg 3, MARSIBAL	Core: MS283G
Location: Perejil mud volcano, the Alboran Sea	Date: 21/07/02
Latitude: 36° 06.018' N	Longitude: 04° 53.158' W
Recovery: 233 cm	Water Depth: 841 m

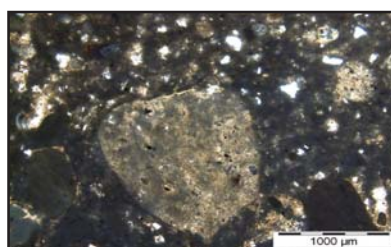
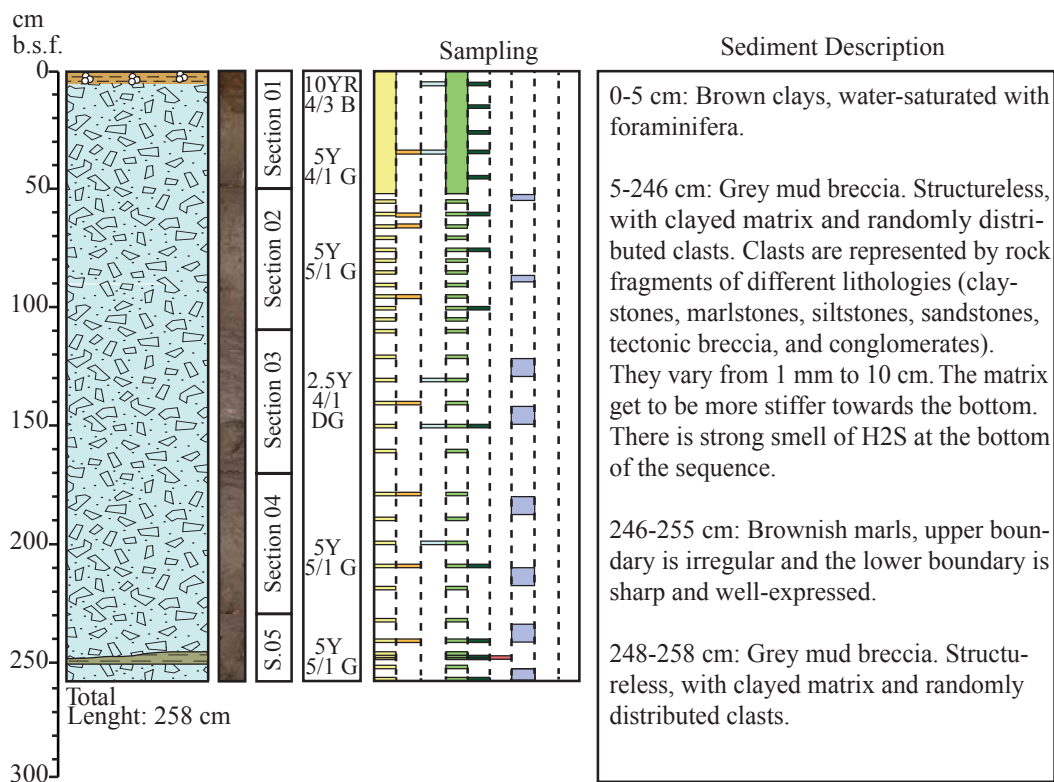


Oceanographic cruise: TTR-12 Leg 3, MARSIBAL		Core: MS285G
Location: Dhaka mud volcano, the Alboran Sea		Date: 22/07/02
Latitude: 36° 25.398`N	Longitude: 04° 31.853`W	
Recovery: 244 cm	Water Depth: 360 m	



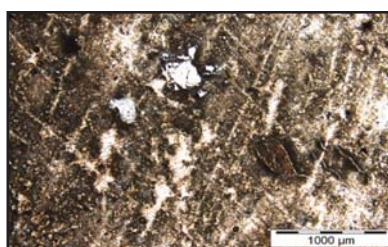
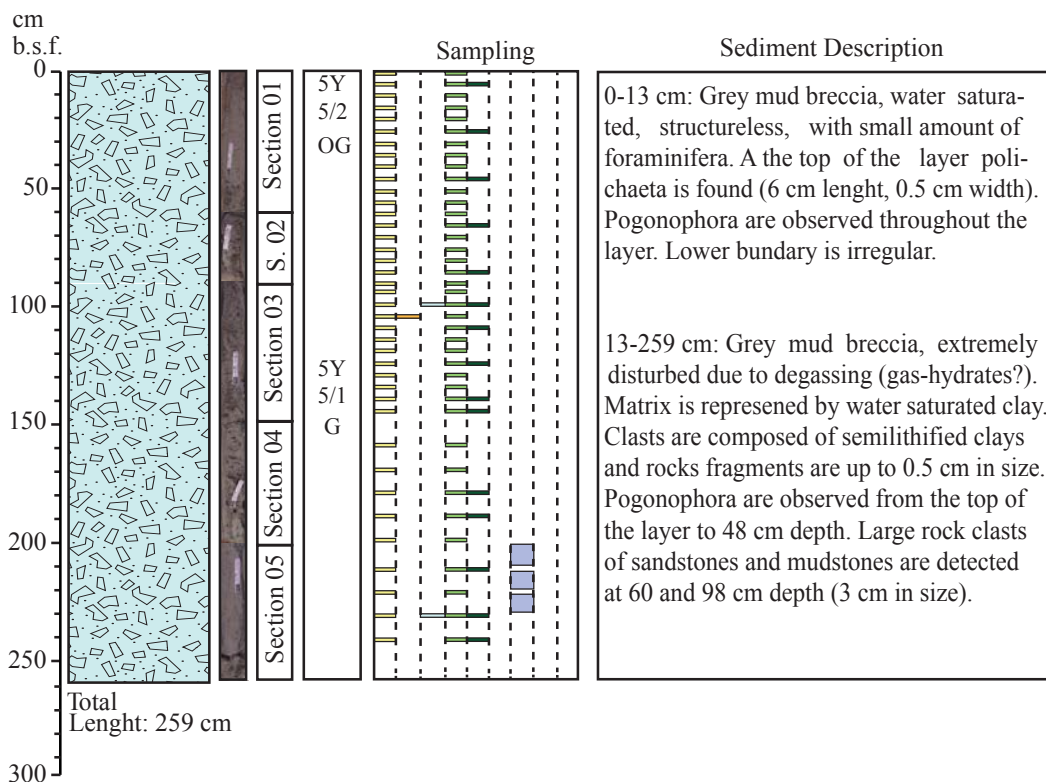
0 0.5 1cm

Oceanographic cruise: TTR-17 Leg 1, SAGAS-08		Core: MS385G
Location: Carmen mud volcano, the Alboran Sea		Date: 13/06/08
Latitude: 35° 43.306`N	Longitude: 04° 44.060`W	
Recovery: 258 cm	Water Depth: 806 m	



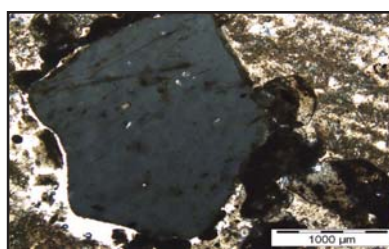
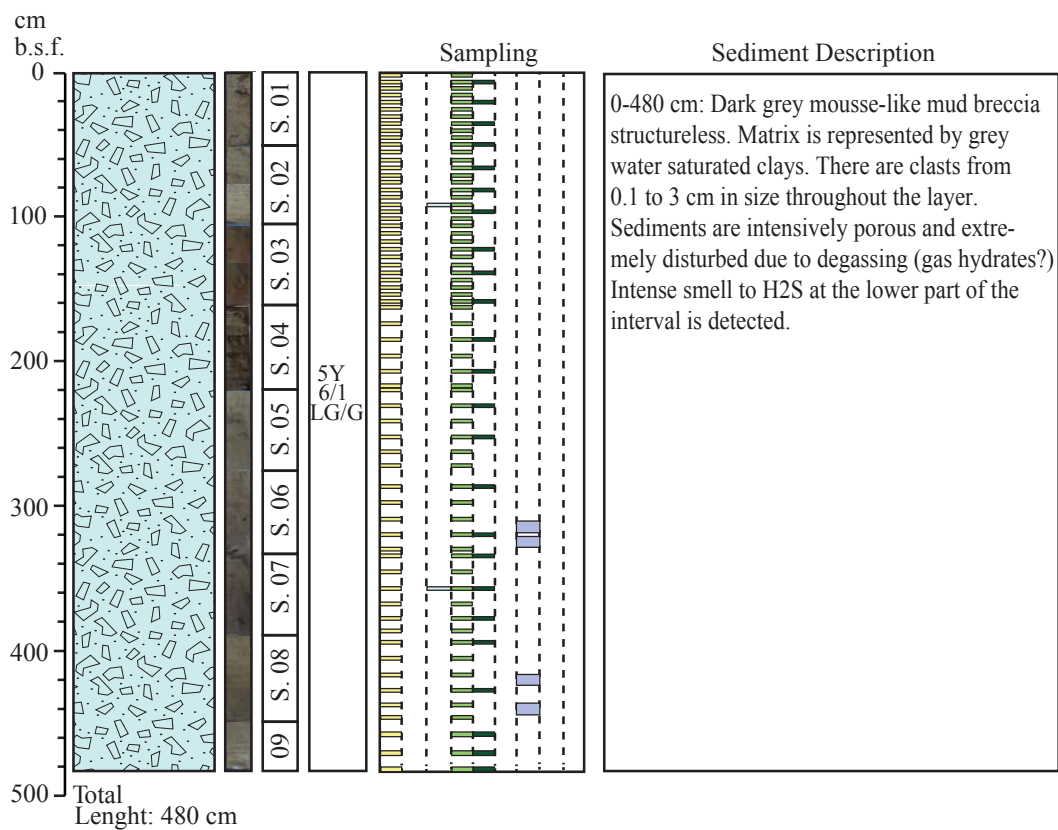
0 1 2cm

Oceanographic cruise: TTR-17 Leg 1, SAGAS-08		Core: MS386G
Location: Carmen mud volcano, the Alboran Sea		Date: 13/06/08
Latitude: 35° 43.309'N	Longitude: 04° 44.008'W	
Recovery: 259 cm	Water Depth: 809 m	



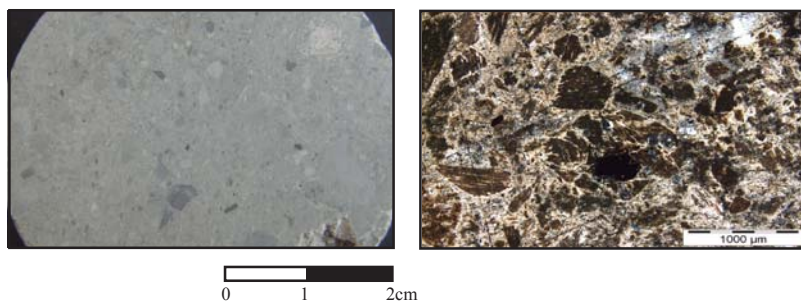
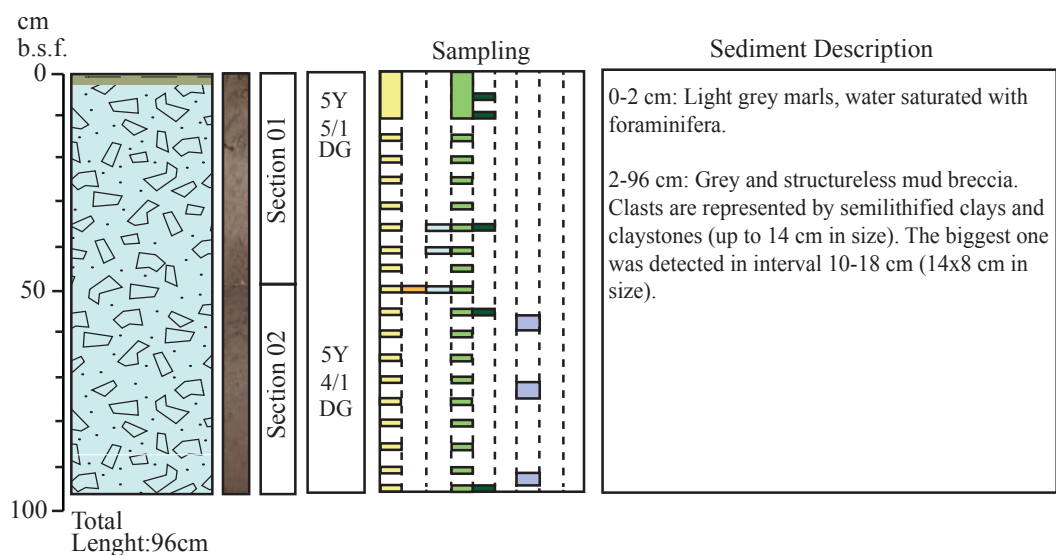
0 1 2cm

Oceanographic cruise: TTR-17 Leg 1, SAGAS-08		Core: MS390G
Location: Carmen mud volcano, the Alboran Sea		Date: 13/06/08
Latitude: 35° 43.306' N	Longitude: 04° 44.017' W	
Recovery: 480 cm	Water Depth: 806 m	

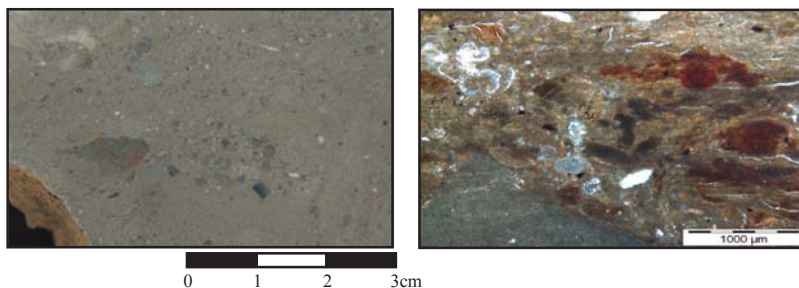
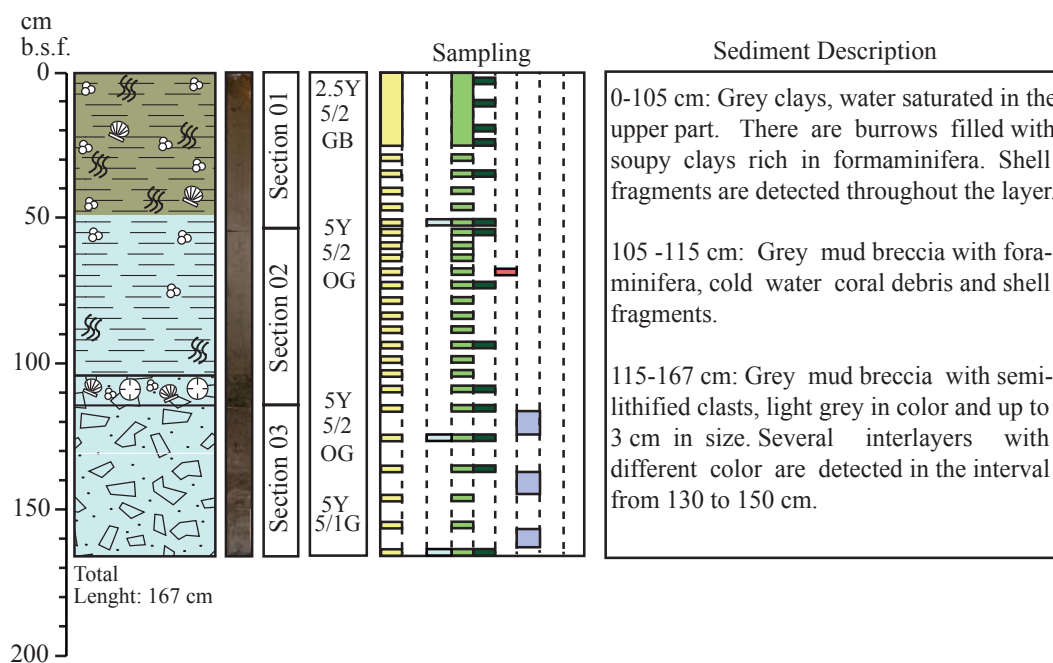


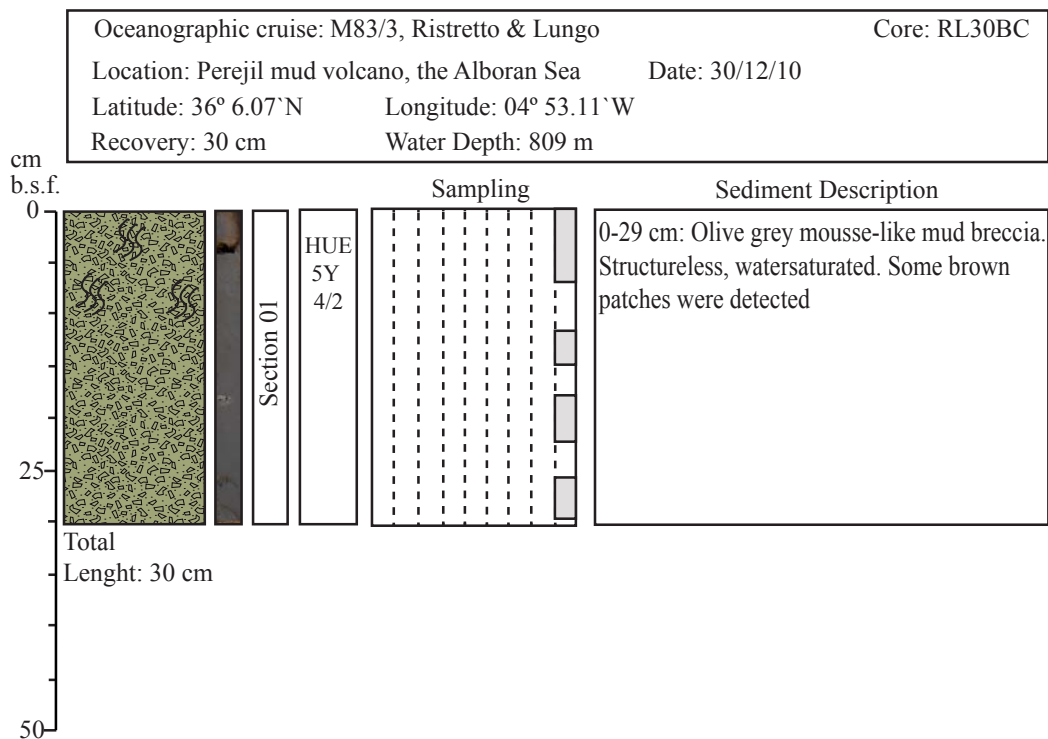
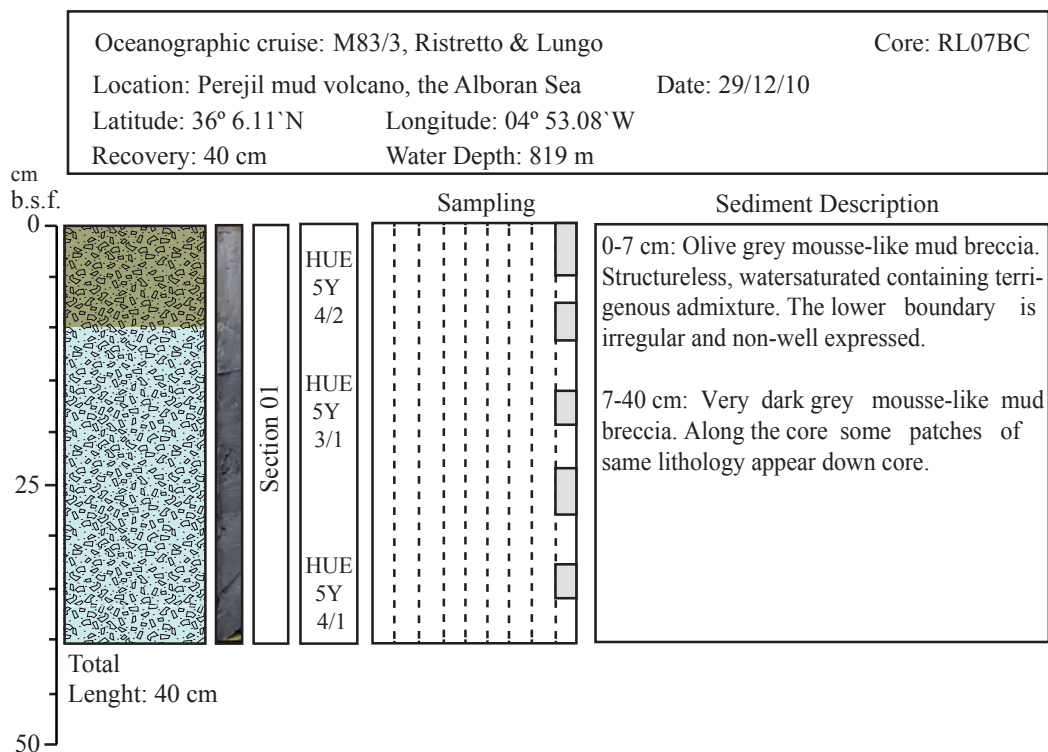
0 1 2cm

Oceanographic cruise: TTR-17 Leg 1, SAGAS-08		Core: MS414G
Location: Mulhacen mud volcano, the Alboran Sea		Date: 19/06/08
Latitude: 35° 24.426'N	Longitude: 04° 34.126'W	
Recovery: 96 cm	Water Depth: 365 m	

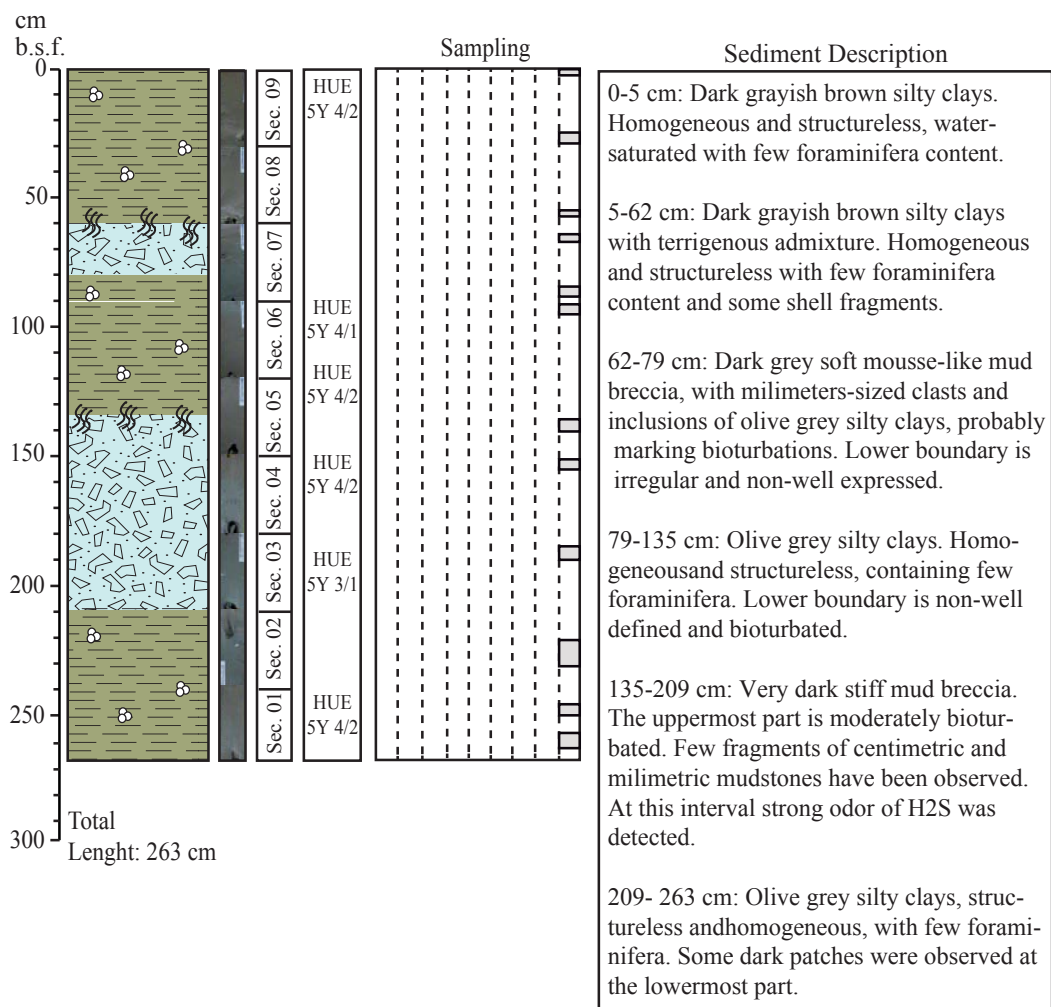


Oceanographic cruise: TTR-17 Leg 1, SAGAS-08		Core: MS419G
Location: Maya mud volcano, the Alboran Sea		Date: 20/06/08
Latitude: 35° 27.114' N	Longitude: 04° 37.138' W	
Recovery: 167 cm	Water Depth: 410 m	

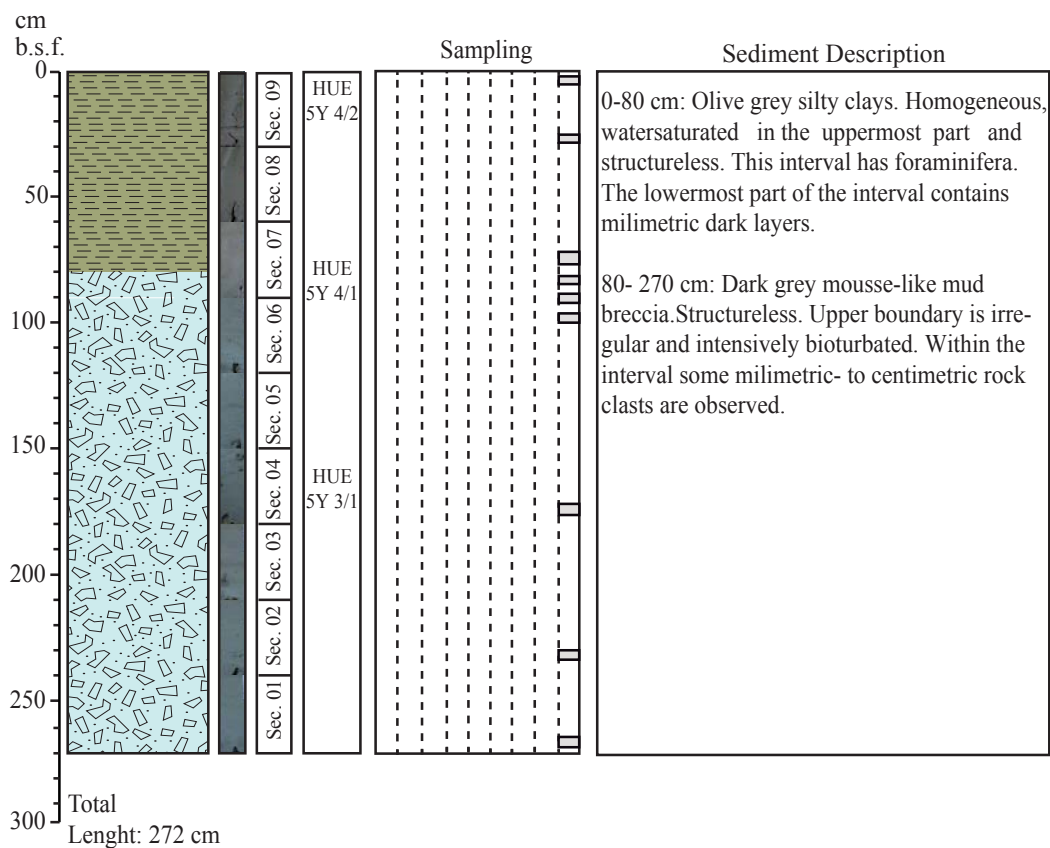




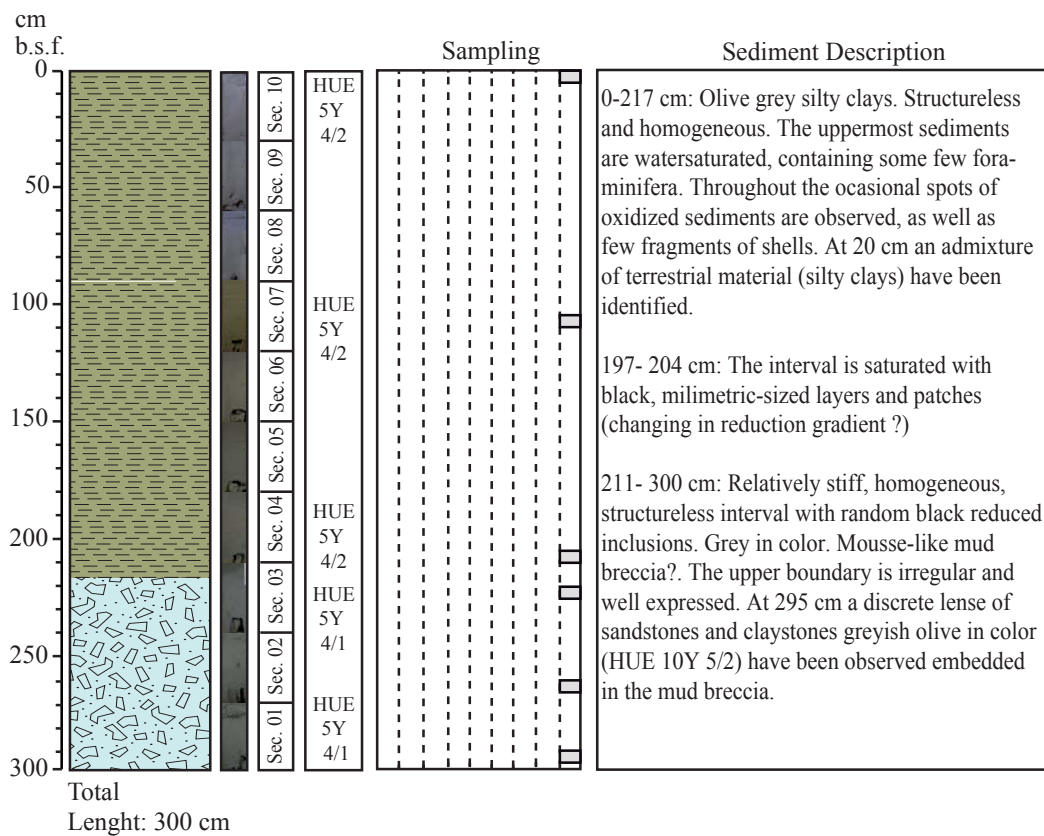
Oceanographic cruise: M83/3, Ristretto & Lungo	Core: RL08GC
Location: Perejil mud volcano, the Alboran Sea	Date: 29/12/10
Latitude: 36° 6.11' N	Longitude: 04° 53.08' W
Recovery: 263 cm	Water Depth: 822 m



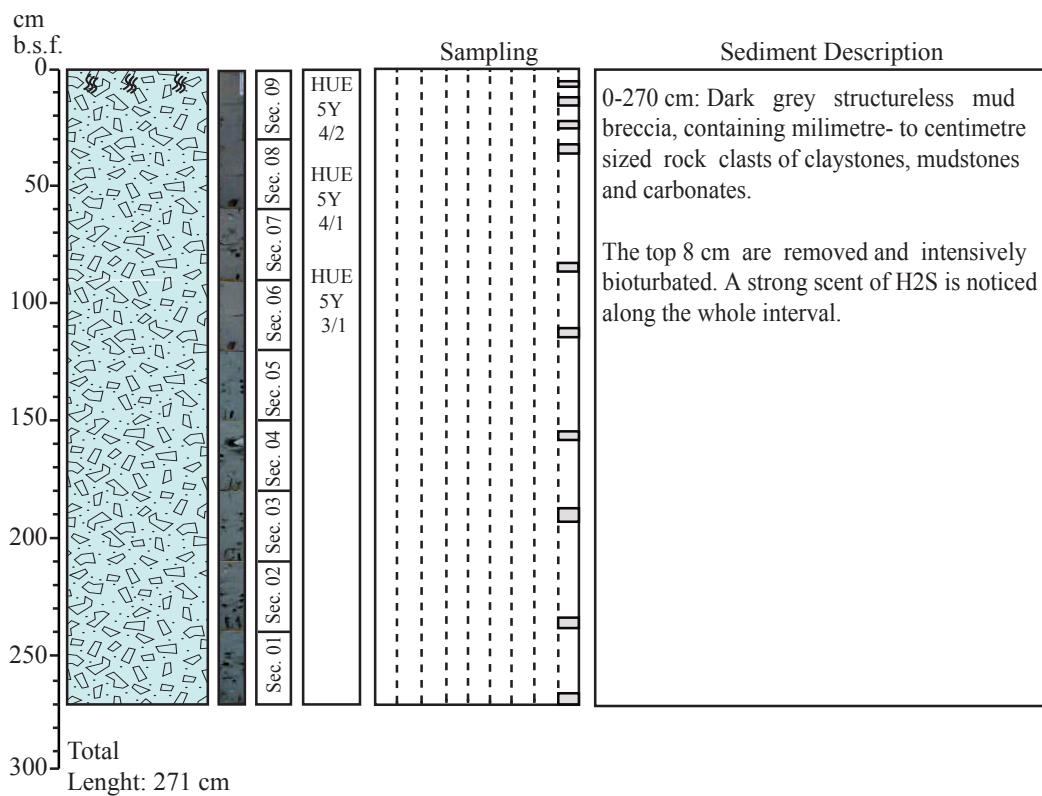
Oceanographic cruise: M83/3, Ristretto & Lungo	Core: RL12GC
Location: Kalinin mud volcano, the Alboran Sea	Date: 29/12/10
Latitude: 36° 3.00' N	Longitude: 04° 55.90' W
Recovery: 280 cm	Water Depth: 873 m



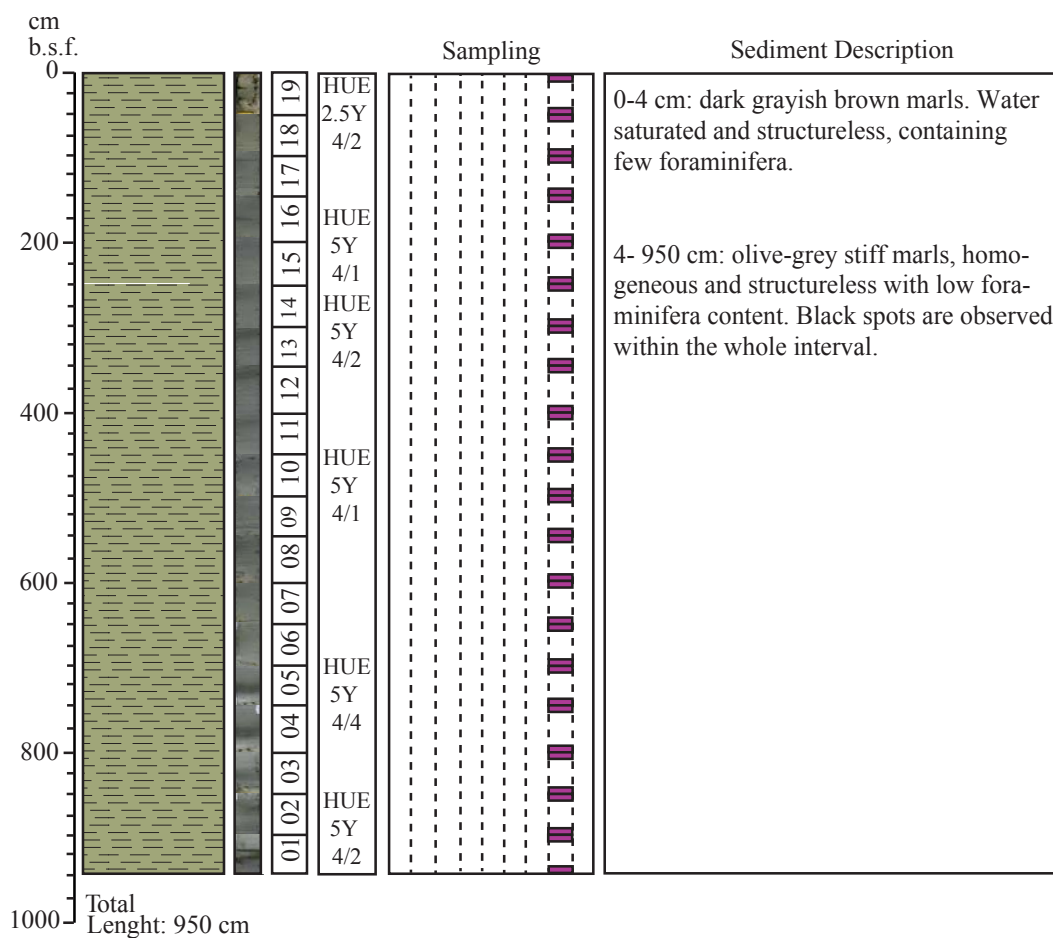
Oceanographic cruise: M83/3, Ristretto & Lungo	Core: RL25GC
Location: Schneider's Heart mud volcano, the Alboran Sea	Date: 30/12/10
Latitude: 36° 0.28' N	Longitude: 04° 57.57' W
Recovery: 310 cm	Water Depth: 924 m



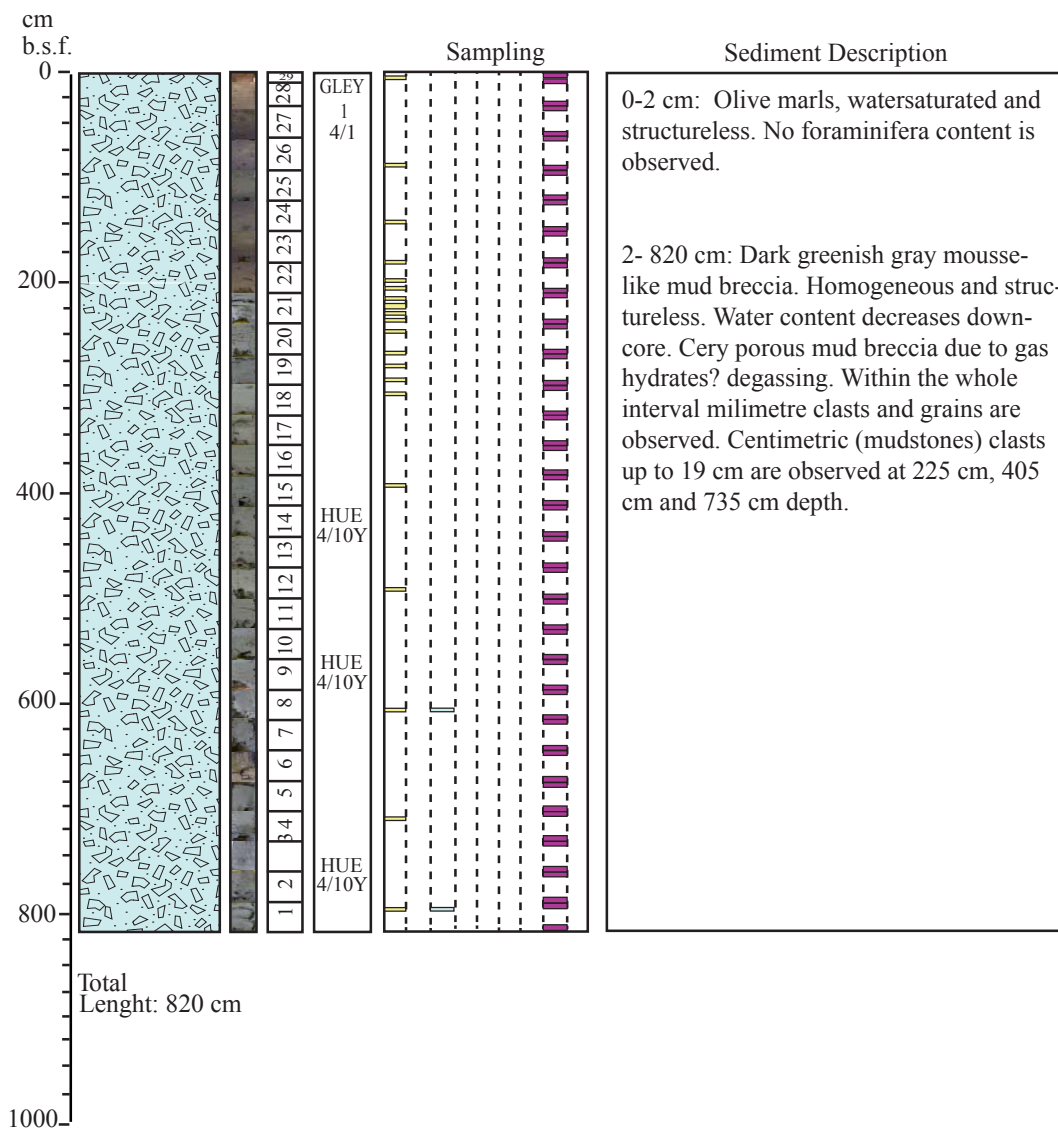
Oceanographic cruise: M83/3, Ristretto & Lungo	Core: RL31GC
Location: Perejil mud volcano, the Alboran Sea	Date: 30/12/10
Latitude: 36° 6.07'N	Longitude: 04° 53.11'W
Recovery: 271 cm	Water Depth: 808 m

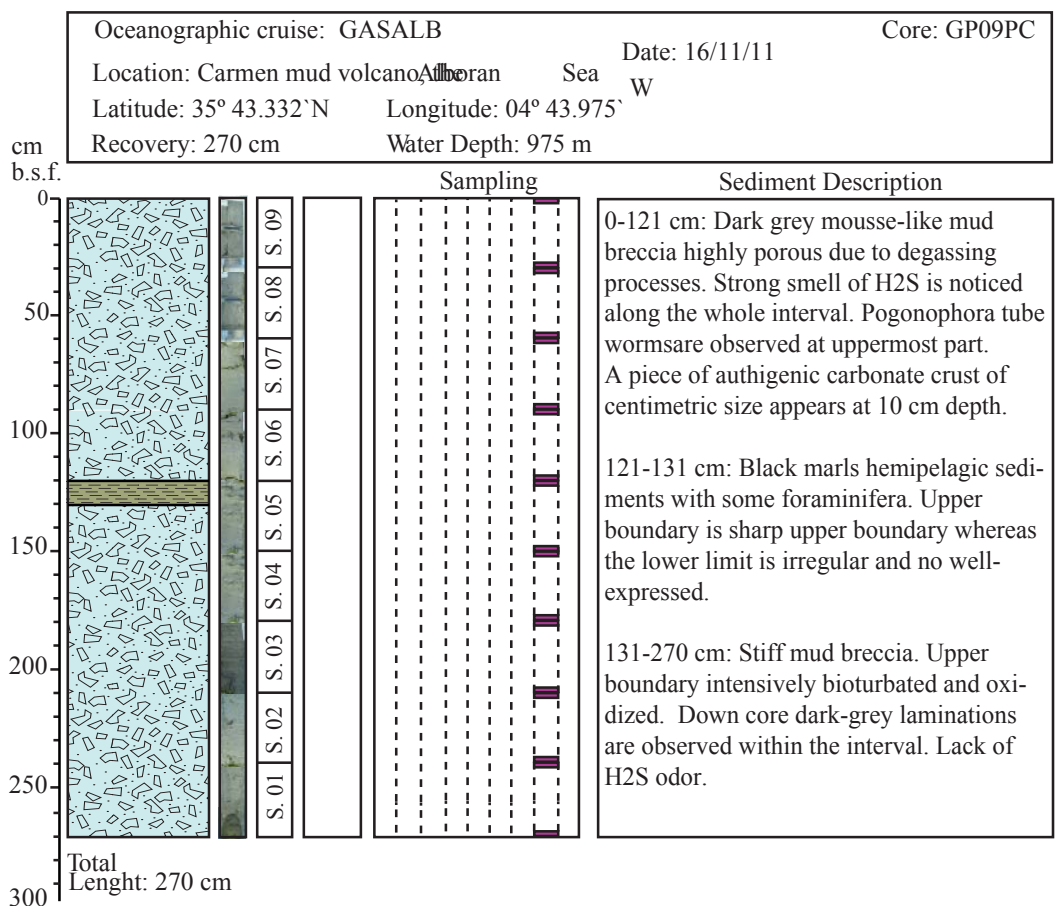
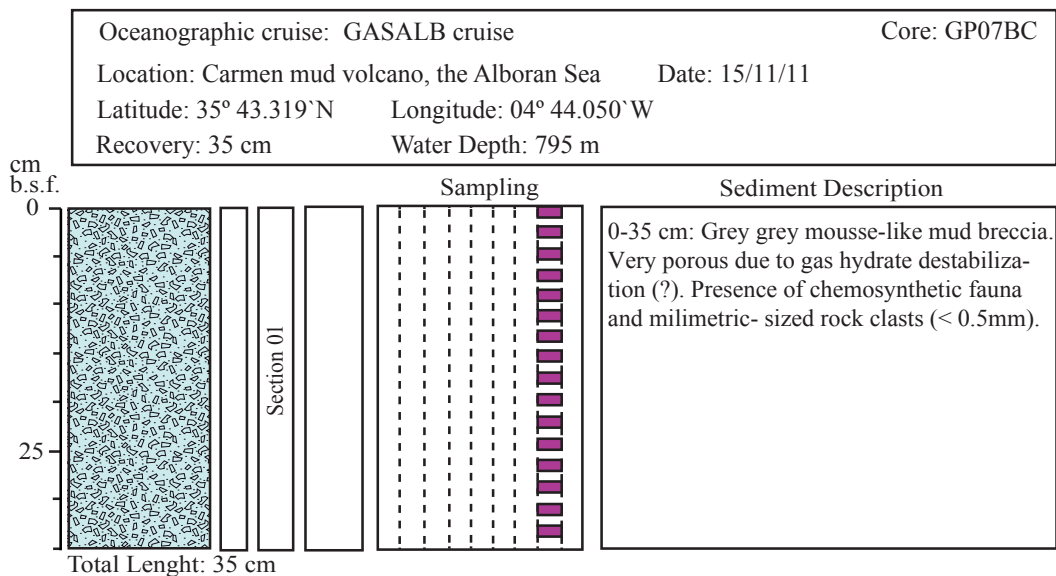


Oceanographic cruise: GASALB	Core: GP03PC
Location: Hemipelagic site, the Alboran Sea Date: 12/11/11	
Latitude: 35° 47.261' N	Longitude: 04° 32.089' W
Recovery: 950 cm	Water Depth: 1306 m



Oceanographic cruise CASALB Core: GP05PC
 Location: Carmen mud volcano, Alboran Sea Date: 14/11/11
 Latitude: 35° 43.333' N Longitude: 04° 44.046' W
 Recovery: 820 cm Water Depth: 795 m





		Structural formulae based on 11 oxygens											
Depth Sample		Tetrahedral cations		Octahedral cations					Interlayer cations				
b.s.f.		Si	Al (VI)	Al (IV)	Mg	Fe	Ti	Σ oct. cat.	K	Na	Ca	Mg	Σ Int. cat.
<i>MS283G Perejil Mud Volcano</i>													
7cm	1	3.52	0.48	1.53	0.33	0.24	0.00	2.11	0.24	0.02	0.21	0.00	0.47
	2	3.62	0.38	1.43	0.29	0.38	0.00	2.10	0.15	0.02	0.10	0.04	0.32
	3	3.84	0.16	1.37	0.41	0.36	0.00	2.13	0.10	0.00	0.07	0.00	0.17
	4	3.67	0.33	1.48	0.40	0.19	0.00	2.07	0.34	0.02	0.14	0.00	0.49
	5	3.49	0.51	1.66	0.20	0.21	0.00	2.07	0.24	0.03	0.07	0.06	0.41
	6	3.55	0.45	1.66	0.10	0.28	0.00	2.03	0.14	0.02	0.00	0.14	0.29
41cm	1	3.71	0.29	1.44	0.19	0.43	0.00	2.06	0.19	0.02	0.00	0.03	0.24
	2	3.86	0.14	1.43	0.34	0.29	0.00	2.06	0.08	0.02	0.17	0.00	0.27
	3	3.32	0.68	1.45	0.34	0.33	0.00	2.11	0.10	0.02	0.24	0.15	0.51
	4	3.52	0.48	1.25	0.36	0.51	0.00	2.12	0.21	0.02	0.12	0.06	0.40
	5	3.86	0.14	1.58	0.24	0.19	0.00	2.01	0.09	0.00	0.26	0.00	0.34
68cm	1	3.40	0.60	1.55	0.19	0.33	0.00	2.06	0.16	0.03	0.16	0.11	0.45
	2	3.88	0.12	1.52	0.29	0.22	0.00	2.04	0.20	0.01	0.08	0.00	0.29
	3	3.37	0.63	1.38	0.25	0.40	0.00	2.03	0.65	0.02	0.09	0.00	0.76
	4	3.63	0.37	1.25	0.43	0.42	0.00	2.09	0.21	0.02	0.28	0.00	0.50
	5	3.72	0.28	1.48	0.26	0.31	0.00	2.05	0.21	0.02	0.16	0.00	0.38
	6	3.60	0.40	1.51	0.29	0.30	0.00	2.10	0.12	0.02	0.21	0.02	0.37
131cm	1	3.67	0.33	1.29	0.40	0.43	0.00	2.12	0.29	0.03	0.00	0.00	0.33
	2	3.55	0.45	1.30	0.37	0.39	0.00	2.06	0.27	0.19	0.00	0.00	0.46
	3	3.65	0.35	1.42	0.28	0.39	0.00	2.09	0.19	0.05	0.00	0.03	0.27
	4	3.71	0.29	1.33	0.31	0.46	0.00	2.10	0.17	0.05	0.00	0.00	0.23
	5	3.35	0.65	1.76	0.02	0.22	0.00	2.01	0.10	0.07	0.00	0.21	0.38
	6	3.60	0.40	1.42	0.32	0.36	0.00	2.11	0.28	0.05	0.00	0.01	0.34
161cm	1	3.46	0.54	1.44	0.35	0.33	0.00	2.12	0.43	0.03	0.00	0.02	0.49
	2	3.65	0.35	1.47	0.28	0.34	0.00	2.09	0.17	0.03	0.00	0.05	0.26
	3	3.56	0.44	1.62	0.09	0.33	0.00	2.03	0.10	0.02	0.00	0.15	0.27
	4	3.64	0.36	1.42	0.30	0.28	0.07	1.99	0.17	0.02	0.21	0.00	0.40
	5	3.62	0.38	1.61	0.23	0.24	0.00	2.07	0.31	0.03	0.00	0.00	0.35
	6	3.60	0.40	1.58	0.27	0.24	0.00	2.09	0.28	0.03	0.00	0.03	0.34
181cm	1	3.62	0.38	1.33	0.38	0.28	0.00	1.99	0.21	0.12	0.33	0.00	0.66
	2	3.57	0.43	1.52	0.25	0.31	0.00	2.08	0.12	0.02	0.21	0.03	0.38
	3	3.42	0.58	1.77	0.07	0.19	0.00	2.02	0.12	0.02	0.14	0.14	0.42
	4	3.70	0.30	1.48	0.26	0.31	0.00	2.05	0.22	0.05	0.09	0.00	0.36
	5	3.60	0.40	1.23	0.54	0.39	0.00	2.17	0.19	0.03	0.17	0.00	0.40
	6	3.53	0.47	1.65	0.20	0.22	0.00	2.07	0.16	0.03	0.15	0.05	0.39
211cm	1	3.44	0.56	1.32	0.29	0.49	0.00	2.10	0.24	0.03	0.10	0.07	0.45
	2	3.62	0.38	1.46	0.26	0.33	0.00	2.05	0.29	0.02	0.16	0.00	0.47
	3	3.40	0.60	1.53	0.29	0.28	0.00	2.10	0.25	0.02	0.23	0.04	0.54
	4	3.53	0.47	1.27	0.34	0.50	0.00	2.11	0.28	0.02	0.10	0.03	0.43
	5	3.54	0.46	1.42	0.31	0.38	0.00	2.10	0.23	0.00	0.19	0.02	0.44
	6	3.52	0.48	1.27	0.41	0.45	0.00	2.12	0.30	0.02	0.17	0.00	0.49

Structural formulae based on 11 oxygens

Depth Sample	Tetrahedral cations		Octahedral cations					Interlayer cations					
	b.s.f.	Si	Al (VI)	Al (IV)	Mg	Fe	Ti	$\Sigma_{\text{oct. cat.}}$	K	Na	Ca	Mg	$\Sigma_{\text{Int. cat.}}$
MS285G Dhaka Mud Volcano													
3cm	1	3.23	0.77	1.91	0.00	0.17	0.00	2.08	0.22	0.02	0.00	0.14	0.38
	2	3.12	0.88	1.63	0.29	0.14	0.00	2.06	0.61	0.07	0.25	0.00	0.93
	3	3.34	0.66	1.80	0.04	0.17	0.00	2.01	0.28	0.03	0.00	0.15	0.47
	4	3.22	0.78	1.50	0.15	0.41	0.00	2.05	0.33	0.14	0.00	0.08	0.56
	5	3.53	0.47	1.39	0.21	0.47	0.00	2.07	0.27	0.02	0.00	0.08	0.37
	6	3.54	0.46	1.82	0.08	0.12	0.00	2.03	0.14	0.03	0.00	0.12	0.30
	7	3.65	0.35	1.91	0.04	0.07	0.00	2.01	0.09	0.03	0.00	0.10	0.22
41cm	1	3.43	0.57	1.40	0.35	0.32	0.00	2.08	0.39	0.04	0.23	0.00	0.66
	2	3.26	0.74	1.43	0.32	0.35	0.00	2.10	0.44	0.07	0.16	0.00	0.67
	3	3.42	0.58	1.60	0.26	0.21	0.00	2.07	0.44	0.04	0.12	0.00	0.60
	4	3.57	0.43	1.55	0.18	0.33	0.00	2.06	0.14	0.03	0.00	0.11	0.28
	5	3.64	0.36	1.30	0.41	0.42	0.00	2.13	0.27	0.05	0.00	0.00	0.33
67cm	1	3.52	0.48	1.40	0.36	0.31	0.00	2.08	0.16	0.23	0.00	0.00	0.38
	2	3.41	0.59	1.50	0.33	0.28	0.00	2.11	0.19	0.10	0.16	0.02	0.47
	3	3.53	0.47	1.33	0.37	0.42	0.00	2.11	0.32	0.05	0.09	0.00	0.46
	4	3.47	0.53	1.34	0.35	0.43	0.00	2.12	0.39	0.05	0.00	0.02	0.46
	5	3.34	0.66	1.41	0.32	0.38	0.00	2.11	0.23	0.05	0.00	0.16	0.45
	6	3.28	0.72	1.53	0.32	0.26	0.00	2.11	0.42	0.05	0.12	0.03	0.63
	7	3.31	0.69	1.68	0.22	0.17	0.00	2.07	0.45	0.00	0.07	0.09	0.60
112cm	1	3.42	0.58	1.54	0.27	0.28	0.00	2.09	0.39	0.07	0.00	0.03	0.49
	2	3.42	0.58	1.44	0.32	0.35	0.00	2.11	0.36	0.02	0.03	0.08	0.49
	3	3.52	0.48	1.58	0.23	0.26	0.00	2.08	0.34	0.00	0.09	0.02	0.45
	4	3.59	0.41	1.40	0.32	0.36	0.00	2.08	0.34	0.02	0.10	0.00	0.46
	5	3.56	0.44	1.45	0.33	0.29	0.00	2.08	0.23	0.02	0.28	0.00	0.52
	6	3.56	0.44	1.51	0.32	0.26	0.00	2.08	0.26	0.02	0.22	0.00	0.50
138cm	1	3.90	0.10	1.51	0.19	0.28	0.00	1.97	0.22	0.05	0.03	0.00	0.31
	2	3.59	0.41	1.53	0.33	0.21	0.00	2.07	0.29	0.05	0.14	0.00	0.48
	3	3.67	0.33	1.49	0.28	0.27	0.00	2.04	0.28	0.02	0.17	0.00	0.47
	4	3.25	0.75	1.67	0.03	0.31	0.00	2.01	0.19	0.05	0.00	0.23	0.47
	5	3.31	0.69	1.91	0.00	0.17	0.00	2.08	0.09	0.05	0.00	0.14	0.27
	6	3.58	0.42	1.48	0.35	0.28	0.00	2.12	0.26	0.03	0.00	0.04	0.34
168cm	1	3.54	0.46	1.48	0.42	0.24	0.00	2.14	0.25	0.00	0.19	0.01	0.45
	2	3.34	0.66	1.36	0.30	0.44	0.00	2.10	0.22	0.00	0.10	0.17	0.49
	3	3.59	0.41	1.55	0.34	0.19	0.00	2.08	0.26	0.04	0.18	0.00	0.47
	4	3.50	0.50	1.41	0.28	0.40	0.00	2.09	0.10	0.00	0.12	0.14	0.36
	5	3.50	0.50	1.44	0.20	0.43	0.00	2.07	0.10	0.02	0.00	0.18	0.30
	6	3.57	0.43	1.56	0.30	0.24	0.00	2.10	0.20	0.03	0.03	0.06	0.33
204cm	1	3.70	0.30	1.62	0.16	0.28	0.00	2.05	0.08	0.02	0.03	0.07	0.21
	2	3.53	0.47	1.61	0.27	0.21	0.00	2.09	0.24	0.02	0.17	0.01	0.44
	3	3.20	0.80	1.34	0.14	0.57	0.00	2.05	0.19	0.00	0.14	0.24	0.57
	4	3.52	0.48	1.49	0.30	0.24	0.00	2.03	0.25	0.12	0.19	0.00	0.56
	5	3.56	0.44	1.58	0.26	0.24	0.00	2.09	0.21	0.03	0.00	0.08	0.32

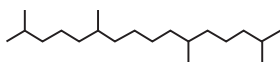
Structural formulae based on 11 oxygens

Depth Sample	Tetrahedral cations		Octahedral cations					Interlayer cations					
	b.s.f.	Si	Al (VI)	Al (IV)	Mg	Fe	Ti	Σoct. cat.	K	Na	Ca	Mg	ΣInt. cat.
MS385G Carmen Mud Volcano													
35 cm	1	3.63	0.37	1.70	0.23	0.10	0.00	2.03	0.35	0.00	0.16	0.00	0.51
	2	3.98	0.02	1.33	0.36	0.23	0.00	1.92	0.27	0.10	0.15	0.00	0.51
	3	3.90	0.10	1.43	0.26	0.23	0.00	1.93	0.25	0.10	0.13	0.00	0.48
	4	3.97	0.03	1.33	0.23	0.26	0.00	1.81	0.21	0.24	0.12	0.00	0.57
	5	3.98	0.02	1.53	0.28	0.21	0.00	2.02	0.11	0.02	0.10	0.00	0.22
	6	3.80	0.20	1.52	0.30	0.17	0.00	1.99	0.32	0.02	0.17	0.00	0.51
60 cm	1	3.99	0.01	1.42	0.26	0.23	0.00	1.90	0.23	0.05	0.23	0.00	0.50
	2	4.10	-0.10	1.41	0.31	0.22	0.00	1.95	0.21	0.00	0.16	0.00	0.36
	3	3.98	0.02	1.46	0.24	0.19	0.00	1.89	0.38	0.02	0.17	0.00	0.57
	4	4.03	-0.03	1.44	0.29	0.21	0.00	1.94	0.19	0.02	0.21	0.00	0.41
	5	4.00	0.00	1.63	0.19	0.16	0.00	1.97	0.09	0.02	0.16	0.00	0.26
	6	3.91	0.09	1.51	0.26	0.19	0.00	1.97	0.28	0.02	0.14	0.00	0.43
65 cm	1	3.71	0.29	1.57	0.31	0.23	0.00	2.10	0.24	0.00	0.00	0.02	0.26
	2	4.03	-0.03	1.37	0.42	0.21	0.00	1.99	0.19	0.02	0.19	0.00	0.40
	3	3.31	0.69	1.69	0.10	0.24	0.00	2.03	0.17	0.03	0.16	0.15	0.51
	4	3.42	0.58	1.48	0.28	0.28	0.00	2.04	0.26	0.10	0.26	0.00	0.63
	5	3.63	0.37	1.43	0.42	0.26	0.00	2.11	0.30	0.02	0.12	0.00	0.44
	6	3.52	0.48	1.42	0.37	0.26	0.00	2.06	0.37	0.05	0.21	0.00	0.63
95 cm	1	3.76	0.24	1.51	0.36	0.19	0.00	2.05	0.15	0.02	0.24	0.00	0.41
	2	3.78	0.22	1.49	0.36	0.22	0.00	2.06	0.20	0.02	0.15	0.00	0.36
	3	3.89	0.11	1.27	0.35	0.28	0.00	1.90	0.17	0.17	0.23	0.00	0.58
	4	3.86	0.14	1.21	0.57	0.33	0.00	2.11	0.20	0.02	0.15	0.00	0.36
	5	3.86	0.14	1.69	0.14	0.08	0.00	1.92	0.31	0.00	0.23	0.00	0.53
	6	3.96	0.04	1.44	0.31	0.21	0.00	1.97	0.26	0.02	0.16	0.00	0.44
140 cm	1	3.52	0.48	1.45	0.36	0.30	0.00	2.11	0.32	0.02	0.16	0.00	0.50
	2	3.52	0.48	1.50	0.33	0.28	0.00	2.11	0.17	0.02	0.19	0.04	0.42
	3	3.71	0.29	1.44	0.31	0.28	0.00	2.03	0.35	0.02	0.12	0.00	0.49
	4	3.56	0.44	1.59	0.30	0.21	0.00	2.10	0.21	0.05	0.14	0.00	0.40
	5	3.19	0.81	1.47	0.26	0.35	0.00	2.09	0.16	0.04	0.14	0.22	0.56
	6	3.28	0.72	1.19	0.38	0.56	0.00	2.13	0.28	0.00	0.21	0.12	0.61
178 cm	1	3.51	0.49	1.37	0.27	0.45	0.00	2.09	0.09	0.00	0.00	0.20	0.29
	2	3.83	0.17	1.67	0.20	0.17	0.00	2.04	0.14	0.05	0.00	0.00	0.19
	3	3.67	0.33	1.70	0.20	0.17	0.00	2.07	0.08	0.07	0.00	0.06	0.21
	4	3.71	0.29	1.66	0.21	0.20	0.00	2.07	0.09	0.07	0.00	0.03	0.19
	5	3.75	0.25	1.49	0.26	0.27	0.00	2.02	0.21	0.12	0.00	0.00	0.33
	6	3.98	0.02	1.46	0.21	0.31	0.00	1.97	0.22	0.05	0.00	0.00	0.27
	7	3.46	0.54	1.60	0.21	0.27	0.00	2.07	0.17	0.08	0.00	0.10	0.35
208 cm	1	3.73	0.27	1.47	0.33	0.31	0.00	2.11	0.19	0.03	0.00	0.00	0.23
	2	3.46	0.54	1.21	0.30	0.59	0.00	2.10	0.14	0.05	0.00	0.15	0.34
	3	3.77	0.23	1.52	0.31	0.26	0.00	2.09	0.17	0.05	0.00	0.00	0.22
	4	3.68	0.32	1.47	0.36	0.29	0.00	2.12	0.16	0.07	0.00	0.01	0.24
	5	3.59	0.41	1.68	0.20	0.19	0.00	2.07	0.19	0.02	0.00	0.09	0.30
	6	3.77	0.23	1.39	0.45	0.31	0.00	2.15	0.17	0.03	0.00	0.00	0.21
	7	3.88	0.12	1.67	0.20	0.20	0.00	2.07	0.07	0.02	0.00	0.01	0.09
	8	3.79	0.21	1.53	0.33	0.24	0.00	2.09	0.16	0.05	0.00	0.00	0.21
240 cm	1	3.50	0.50	1.14	0.46	0.55	0.00	2.15	0.43	0.03	0.00	0.00	0.46
	2	3.06	0.94	1.04	0.25	0.80	0.00	2.08	0.21	0.05	0.00	0.31	0.57
	3	3.66	0.34	1.61	0.33	0.17	0.00	2.11	0.22	0.03	0.00	0.03	0.28
	4	3.70	0.30	1.36	0.49	0.27	0.00	2.13	0.33	0.03	0.00	0.00	0.37
	5	3.52	0.48	1.62	0.18	0.26	0.00	2.06	0.26	0.03	0.00	0.08	0.37
	6	3.53	0.47	1.51	0.26	0.31	0.00	2.09	0.37	0.03	0.00	0.02	0.42
	7	3.70	0.30	1.25	0.45	0.43	0.00	2.13	0.29	0.03	0.00	0.00	0.33

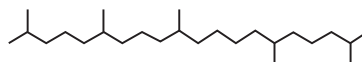
Depth Sample	Structural formulae based on 11 oxygens												
	Tetrahedral cations		Octahedral cations					Interlayer cations					
b.s.f.	Si	Al (VI)	Al (IV)	Mg	Fe	Ti	Σ Oct. cat.	K	Na	Ca	Mg	Σ Int. cat.	
MS262G Marrakech Mud Volcano													
175 cm	1	3.70	0.30	1.43	0.42	0.26	0.00	2.11	0.26	0.02	0.10	0.00	0.38
	2	3.51	0.49	1.22	0.47	0.42	0.04	2.11	0.29	0.05	0.09	0.00	0.43
	3	3.75	0.25	1.45	0.34	0.24	0.00	2.04	0.29	0.02	0.16	0.00	0.46
	5	3.59	0.41	1.45	0.20	0.40	0.02	2.04	0.26	0.02	0.03	0.04	0.36
	6	3.65	0.35	1.45	0.33	0.29	0.00	2.08	0.24	0.05	0.10	0.00	0.40
	7	3.45	0.55	1.52	0.26	0.31	0.00	2.09	0.20	0.03	0.19	0.04	0.47
	MS414G Mulhacen Mud Volcano												
56 cm	1	3.47	0.53	1.67	0.16	0.16	0.04	1.98	0.32	0.05	0.18	0.00	0.55
	2	-	-	-	-	-	-	-	-	-	-	-	-
	3	3.75	0.25	1.57	0.26	0.21	0.02	2.03	0.24	0.05	0.00	0.00	0.29
	4	3.54	0.46	1.50	0.13	0.30	0.02	1.94	0.54	0.02	0.14	0.00	0.70
	5	3.52	0.48	1.45	0.28	0.31	0.03	2.05	0.31	0.03	0.09	0.01	0.44
	6	3.58	0.42	1.13	0.40	0.45	0.02	1.99	0.68	0.05	0.00	0.00	0.74
	7	3.63	0.37	1.40	0.23	0.41	0.00	2.03	0.30	0.00	0.20	0.00	0.50
MS386G Carmen Mud Volcano													
104 cm	1	3.69	0.31	1.50	0.28	0.30	0.00	2.08	0.18	0.00	0.17	0.00	0.36
	2	3.68	0.32	1.37	0.29	0.42	0.00	2.08	0.20	0.02	0.12	0.00	0.34
	3	3.48	0.52	1.29	0.30	0.51	0.00	2.10	0.42	0.02	0.05	0.00	0.50
	4	3.46	0.54	1.43	0.24	0.39	0.02	2.06	0.29	0.04	0.12	0.03	0.47
	5	3.17	0.83	0.97	0.28	0.84	0.00	2.09	0.26	0.04	0.00	0.25	0.54
	6	3.67	0.33	1.23	0.24	0.59	0.00	2.06	0.36	0.02	0.00	0.00	0.38
	7	3.60	0.40	1.35	0.33	0.37	0.02	2.05	0.28	0.04	0.16	0.00	0.48
MS280G Kalinin Mud Volcano													
150 cm	1	3.46	0.54	1.34	0.31	0.45	0.00	2.10	0.08	0.10	0.19	0.02	0.41
	2	3.40	0.60	1.27	0.30	0.52	0.00	2.09	0.30	0.07	0.19	0.00	0.56
	3	3.52	0.48	1.38	0.27	0.32	0.00	1.97	0.54	0.05	0.18	0.00	0.78
	4	3.56	0.44	1.33	0.41	0.38	0.00	2.11	0.41	0.05	0.00	0.00	0.46
	5	3.43	0.57	1.65	0.14	0.26	0.00	2.05	0.24	0.03	0.00	0.13	0.40
	7	3.51	0.49	1.58	0.17	0.31	0.00	2.06	0.22	0.05	0.00	0.08	0.35
	8	3.57	0.43	1.03	0.16	0.86	0.00	2.05	0.23	0.09	0.00	0.02	0.33
	9	3.48	0.52	1.34	0.16	0.56	0.00	2.05	0.22	0.03	0.10	0.06	0.42
	MS258G Granada Mud Volcano												
65cm	1	3.28	0.72	1.30	0.25	0.53	0.00	2.08	0.37	0.05	0.12	0.06	0.60
	2	3.41	0.59	1.69	0.15	0.18	0.00	2.02	0.50	0.07	0.05	0.00	0.62
	3	3.33	0.67	1.76	0.04	0.21	0.00	2.01	0.18	0.05	0.11	0.14	0.48
	4	3.62	0.38	1.37	0.35	0.35	0.00	2.07	0.23	0.05	0.18	0.00	0.46
	5	3.69	0.31	1.42	0.27	0.35	0.00	2.03	0.24	0.05	0.14	0.00	0.43
	6	3.78	0.22	1.63	0.14	0.25	0.00	2.02	0.21	0.05	0.00	0.00	0.26
	8	3.56	0.44	1.58	0.19	0.30	0.00	2.06	0.25	0.03	0.12	0.00	0.41
	9	3.49	0.51	1.30	0.27	0.17	0.25	1.74	0.39	0.03	0.12	0.00	0.54
	10	3.58	0.42	1.50	0.15	0.37	0.00	2.03	0.34	0.00	0.16	0.00	0.50

Irregular Isoprenoids

Crocetane (I)

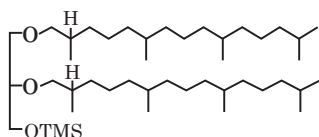


PMI (II)

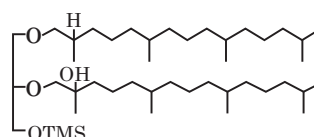


Isoprenoidal Dialkyl Glycerol Diethers

Archaeol (III)

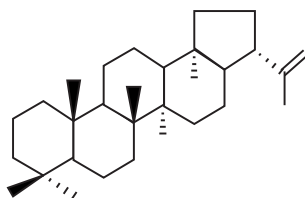


Hydroxyarchaeol (IV)

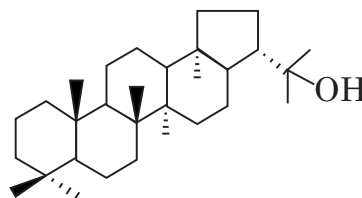


Cyclic Triterpanes

Diploptene (V)

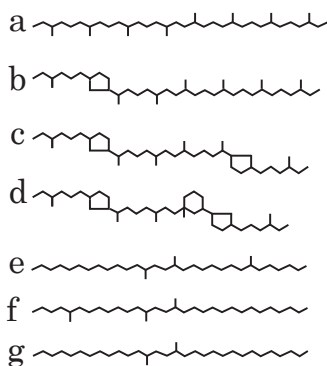
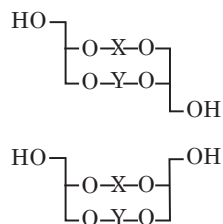


Diplopterol (VI)



Glycerol Dialkyl Glycerol Tetraethers

Basic Structure



No	X	Y
VII	a	a
VIII	a	b
IX	b	b
X	b	c
XI (+XI') Crenarchaeol (+ regioisomer)	c	d
XII	e	f
XIII	g	f
XIV	g	g

please
Clean me
☹️

Aknowledgments
Agradecimientos

Acknowledgements

We tend to think that every story and every activity has an end goal, and what really matters is achieving that ultimate goal. Until recently this is the way I saw it, but one day I suddenly realized that the most important thing is how you move along and the people and stories you encounter on your travels. From them we learn, their advice and their support allow us to progress; with them we share laughter and tears.

Many people have been present during the development of this PhD and I would like to dedicate a few words of gratitude to them.

Firstly, I would like to thank my PhD supervisors Menchu Comas and Paqui Martinez-Ruiz for entrusting me the study of the Alboran mud volcanoes. Your encouragement, affection and tireless supervision over these years are very dearly appreciated.

I would also like to express my most sincere gratitude to Professor Gert J. de Lange, my supervisor during stays at Utrecht University, who I personally think of another director of this Thesis (or at least of a substantial part of it). Gert, thanks (danke je wel) for your endless scientific motivation at delicate times when I felt unable to go on. Not only are you considered a scientific father, but also a true second father, so generously hosting me in your home and your family, which I also like to think of as mine.

I wish to express further gratitude to numerous researchers who have welcomed me during various short stays abroad: Luis Pinheiro and Vitor Magalhães for welcoming me and treating me so kindly during my stay at the University of Aveiro (Portugal); Christian Hensen, who generously and quickly welcomed me at the Helmholtz Centre for Ocean Research Kiel-GEOMAR (Kiel, Germany); and Alina Stadnitskaia, for inviting me to be part of the Department of Biogeosciences (BGC) at the Royal Netherlands Institute for Sea Research NIOZ-(Texel, Netherlands). I learned tremendously from Alina and all her instructions, and her extraordinary supervision during my short stay at NIOZ and onboard the METEOR squeezed the most productive part out of me, initiating me in biomarker research.

I would like to express my sincere thankfulness to Professor Jaap S. Sinninghe Damsté for harboring me in the BGC-Department at NIOZ and showing continuous kindness and availability.

My thanks as well the external reviewers Vitor Magalhães and Crisogono Vasconcelos, who so kindly accepted the revision and validity of this PhD. My thanks to all the members of the Thesis committee: Fernando Nieto, Conchilla Jiménez de Cisneros Vencelá, Jose Manuel Castro, Belén Rubio and Michael Böttcher, for their comments and advice. I also appreciate the careful review of my written English by Jean Louise Sanders.

Regarding the scientific paper that constitutes Chapter 6, I would like to thank all the co-authors, as well as editor Dr. Silvio Pantoja, Dr. Jincal Tuo and the anonymous reviewer for suggestions that greatly improved the quality of this publication.

I would like to extend my gratitude to all those researchers who, at some point, provided council on scientific issues; Steffan Schouten and Ellen Hopmans for their help and kindness in biomarker-

related issues; Luis Pinheiro and Maria do Rosario Azevedo for their availability and scientific advice on geochemistry; Fernando Nieto for generously offering me the facilities of the Mineralogy and Petrology Department of the University of Granada and providing advice about mineralogical issues; and Michael Böttcher for such helpful collaboration in the study of pore waters and fluids. As well I would like to extend my gratitude to the Marine Geoscience group of the University of Vigo (Belén Rubio, Daniel Rey, Federico Vilas and Isabel Rodriguez-Germade) for their collaboration and support during treatment and measurements of mud volcano samples in ITRAX-Core Scanner.

Thank you also: captains, crew, scientific and technical staff behind the oceanographic cruises: BA-SACALB; MARSIBAL-1; SAGAS-08; Ristretto & Lungo and GASALB. To all hardworking participants involved in these cruises, thank you for your effort and dedication during sampling and data recording.

My thanks to all the technical staff who helped me to process the samples and perform various analyses, at the Instituto Andaluz de Ciencias de la Tierra: Elisa Cabrera, Diana, Juan Santamarina, Miguel Martin, Carmen Niembro, Elvira Martin, Leticia. Technical staff of the Centro de Servicios Técnicos de Granada: Olga, Maria del Mar, Shell, Juande, Alicia, Bendi. All technicians who helped me during the different short stays abroad: Sara Ribeiro, Arnold van Dijk, Tom Zalm, Michiel Kienhuis, Anhelique Mets, Georges Ossebaar, Sharyn Ossebaar, Karel Bakker, Yvo Witte, Marcel Bakker, Leon Wuis, Lorendz Boom, Ruud Groenewegen, and Dirk Jan Visser.

I would also like to express special thanks to my teachers Federico Olóriz and Agustin Martin Algarra, who transmitted their love and passion for geology and the earth sciences to me. Aside from great researchers, they are great human beings.

Thank you to my scientific family of friends at the IACT (Rita, Claudia, Luis, Mari, Eli, Amel), my older siblings (David, Francis, Vanessa, Alpi) and all my colleagues, both at the Faculty of Sciences (Noel, Rute, Pili, Javier) and at the IACT (Ari, Enric, Marga, Nicole, Claudio, Meri, Laura, Lozano), for so much support and encouragement over the years. In particular, I would like to thank Nieves Torres and Marta Rodrigo-Gámiz for their very close friendship, unconditional support and love. With you two I have laughed until I cried, and you gave me comfort at some of the hardest times. I carry you in my heart as more than friends and almost sisters.

Thanks to a wide variety of wonderful people I met on different stays and oceanographic cruises: Isabel Rodriguez-Germade, Elena Piñero, Loubna, Conny Lenz, Ruud Groenewegen, Marie-Louise Godeau, Elena Grimoldi, Kiara Tessarolo, Claudia Cassalino, Agostino Rizzi, Claudio Stalder, Helge Niemann, Valentina Darakchieva, Monika Vladimirova, Marlene, Rick Hennekam, Denitsa Apostolova, Laura Villanueva, Yvonne, Elisabeth Svensson, Darci Rush, Nicole Bale, Sabine Lengger, Claudia Zell, Jonh Cluderay, Alejandra Morera, Itzel Ruvalcaba, Mathilde Hagens, Fatima SuluGambari, Alwina Hoving, Matthias Egger, Nikki; Jiawang, Tom Jilbert... and many others who offered me their friendship and assistance.

I would like to express my gratitude to friends from the HADES Cruise (RV Sarmiento de Gamboa) for crucial affection and encouragement in the final stretch. Especially to Hector Perea, Laura Becerril and Jaume Llopart for fun shared and lots of useful advice. Those moments gave me the courage needed to face this final hurdle. You are great.

Despite having so little time for other true friends during these years with the Thesis, I would like to dedicate due acknowledgement and affection to them now, just as they have always conveyed the affection and support that allowed me to continue: Eva Maestre, Alejandro Mochón, Jorge Martín, Ana Sánchez, Mari Luz López, David Fernández, Angie, Alberto... and many others!. Special thanks to Julia Ordoñez, who has always shown me an amount of love and admiration I do not deserve. "Cubs" Claudia and David are dearly appreciated for their innocence and affection, as it their father, my good friend Jose Antonio Martínez (Gato), who was not supposed to go so soon and who unfortunately could not witness the end of thesis.

Finally, I want to thank my family, especially my parents and siblings, who joined me on this adventure. Thanks for always believing in me, understanding that science is my passion, and so often letting me know that you are proud of me. I hope someday to give back all that you have done for me and recover the time I had to sacrifice being away from you. Coco and Luna, you have been so patient! Your jumps, kisses of joy and energy every time I came home were the key to keeping cheerful all these years.

And of course thanks to David, who more than anyone has experienced the daily life of this thesis. Thank you for your unconditional support and good cheer at all times. Thanks for refloating me when I was in danger of sinking, for taking care of me and sharing your love at all times.

Agradecimientos

Siempre pensamos que toda historia, todo objetivo tiene un final y que lo realmente importante es alcanzar la meta. Hasta hace poco esto es lo que pensaba, hasta que de repente me dí cuenta de que lo más importante es el camino que recorres, el rumbo de esa historia y de las personas que has ido encontrado en ella. De ellas se aprende, de sus consejos, de sus ánimos, con ellas compartes risas y también llantos.

Son muchas las personas que han formado parte y que han estado presentes durante el desarrollo de esta Tesis Doctoral y me gustaría dedicarles unas palabras de agradecimiento.

En primer lugar me gustaría agradecer a mis directoras de Tesis, Menchu Comas y Paqui Martínez-Ruiz por animarme y darme la oportunidad de realizar este trabajo. Os agradezco enormemente haberme confiado el estudio de los volcanes de Alborán, la incansable supervisión durante estos años de doctorado y todo el cariño que, cada una a vuestra manera, siempre me habéis mostrado. También me gustaría expresar mi más sincera gratitud al Profesor Gert J. de Lange, quien ha sido mi supervisor durante mis estancias en la Universidad de Utrecht y al que considero un supervisor más de esta Tesis Doctoral (o al menos de una parte importante de ella). Gracias Gert por tu incansable motivación científica, por los ánimos que siempre has dado cuando me sentí incapaz de continuar y por tu mediación en los momentos más delicados de esta Tesis. No solo te considero un padre científico, sino también un verdadero segundo padre, siendo generoso acogiéndome en tu hogar y a toda tu familia, a la que también considero un poquito propia.

También me gustaría agradecer a los diferentes investigadores que me han acogido durante las distintas estancias en el extranjero. A Vitor Magãlhaes y Luis Pinheiro por acogerme y tratarme tan cariñosamente durante mi estancia en la Universidad de Aveiro (Aveiro, Portugal), a Christian Hensen quien tan generosa y rápidamente me acogió en el Helmholtz Centre for Ocean Research Kiel- GEOMAR (Kiel, Alemania), y finalmente a Alina Stadnitskaia por invitarme a formar parte del Departamento de Biogeociencias (BGC) en el Royal Netherlands Institute for Sea Research-NIOZ (Texel, Países Bajos). En particular quisiera agradecer a Alina por todas sus instrucciones de las que he aprendido enormemente. Por su supervisión durante mi estancia en NIOZ y durante la campaña oceanográfica a bordo del METEOR, por sacar mi parte más productiva e iniciarme en el mundo de los biomarcadores.

Quiero expresar mi más sincera gratitud al Professor Jaap S. Sinninghe Damsté, por recibirme y hacerme participe del BGC-department en NIOZ, así como por su amabilidad y disponibilidad continua. A los expertos revisores Vitor Magãlhaes y Crisogono Vasconcelos que tan amablemente se han encargado de revisar y reconocer la validez de esta Tesis Doctoral. A los miembros del tribunal de esta Tesis; Fernando Nieto, Conchilla Jiménez de Cisneros Vencelá, José Manuel Castro, Belén Rubio y Michael Böttcher, por sus comentarios y consejos. Así como a la revisora de inglés Jean Louis Sanders por revisar tan cuidadosa y detalladamente este manuscrito.

En relación a la publicación científica que constituye el Capítulo 6, me gustaría agradecer a todos los co-autores, así como al editor Dr. Silvio Pantoja, Dr. Jincal Tuo así como al revisor anónimo por todas las sugerencias que han aportado. Sin duda han contribuido enormemente a mejorar la calidad de dicha publicación.

Me gustaría extender mi gratitud a todos aquellos investigadores que en algún momento me han asesorado en cuestiones científicas; a los profesores Steffan Schouten y Ellen Hopmans por su ayuda y amabilidad en cuestiones relacionadas con biomarcadores; a Luis Pinheiro y María do Rosario Azevedo por su disponibilidad y asesoramiento científico en cuestiones geoquímicas; a Fernando Nieto por ofrecerme generosamente el uso de equipos del Departamento de Mineralogía y Petrología de la Universidad de Granada, por su disponibilidad y asesoramiento en cuestiones mineralógicas; Al profesor Michael Böttcher por su ayuda y colaboración en el estudio de fluidos intersticiales, así como al grupo de Geociencias Marinas de la Universidad de Vigo (Belén Rubio, Daniel Rey, Federico Vilas, Isabel Rodríguez-Germade) por su colaboración y asesoramiento durante el tratamiento y medidas de muestras en ITRAX- Core Scanner.

A los capitanes, tripulación, personal técnico y científico que han colaborado en las campañas oceanográficas BASACALB; MARSIBAL-1; SAGAS-08; Ristretto & Lungo y GASALB. A todos los participantes, gracias por vuestro esfuerzo y trabajo tanto en la toma de muestras como en su registro.

A todo el personal técnico que me han ayudado a procesar las muestras y realizar las distintas analíticas, del Instituto Andaluz de Ciencias de la Tierra: Elisa Cabrera, Manuel Carmona, Alejandro-Juan Santamarina, Miguel Martín, Carmen Niembro, Elvira Martín, Leticia, Diana, Bárbara y todo el personal de administración que siempre me trataron con tanta amabilidad y cariño. Al personal del Centro de Servicios Técnicos de Granada: Olga, María del Mar, Concha, Juande, Alicia, Bendi. A todos los técnicos que me ayudaron en las distintas estancias: Sara Ribeiro, Arnold van Dijk, Tom Zalm, Michiel Kienhuis, Anhelique Mets, Jort Ossebaar, Sharyn Ossebaar, Karel Bakker, Yvo Witte, Marcel Bakker, Leon Wuis, Lorendz Boom; Ruud Groenewegen, Jan Dirk de Visser.

A mis profesores Federico Oloriz y Agustín Martín Algarra, que me contagiaron el amor y pasión por la geología y las ciencias de la tierra, a los que no solo tengo como ejemplo por ser grandes investigadores, sino también por ser grandísimas personas.

A mis hermanos científicos y amigos del IACT (Rita, Claudia, Luis, Mari, Eli, Amel), a mis hermanos mayores (David, Francis, Vanessa, Alpi) y a todos mis compañeros, tanto de la Facultad de Ciencias (Noel, Rute, Pili, Javier) y del IACT (Ari, Enric, Marga, Nicole, Claudio, Meri, Laura), por todo el apoyo y los ánimos que siempre me han dado. Y en especial a Nieves y Marta, que tanto me han comprendido, y que tanto cariño me ha regalado estos años. Con vosotras he reído hasta llorar, he encontrado el consuelo en algunos de los momentos más duros y por eso os llevo en el corazón. Habéis sido las mejores amigas y casi como mis hermanas.

Gracias a todas las personas que pude conocer en las distintas estancias y campañas oceanográficas: Isabel Rodríguez-Germade, Elena Piñero, Giordana Gennari Loubna, Conny Lenz, Ruud Groenewegen, Marie-Louise Godeau, Elena Grimoldi, Kiara Tessarolo, Claudia Cassalino, Agostino Rizzi, Clau-

dio Stalder, Helge Niemann, Valentina Darakchieva, Monika Vladimirova, Marlene, Rick Hennekam, Denitsa Apostolova, Laura Villanueva, Yvonne, Elisabeth Svensson, Darci Rush, Nicole Bale, Sabine Lengger, Claudia Zell, Jonh Cluderay, Alejandra Morera, Itzel Ruvalcaba, Mathilde Hagens, Fatima Sulu-Gambari, Alwina Hoving, Matthias Egger, Nikki; Jiawang, Tom Jilbert y tantos otros que me regalaron su amistad o en algún momento me ayudaron enormemente y me dieron su cariño.

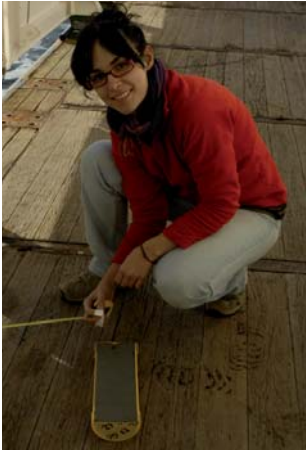
Sin duda a mis amigos de la campaña HADES (BO Sarmiento de Gamboa) también les quiero agradecer todo el cariño y los ánimos que me han regalado en la recta final. En especial a Héctor Perea, Laura Becerril y Jaume Llopart, por todos los momentos divertidos y las risas que hemos compartido, y por todos vuestros consejos. Esos momentos me han dado la vida y me han llenado de fuerza y coraje necesarios para afrontar esta recta final. Sois geniales y os llevo como hermanos también.

Me gustaría también agradecer a todos los amigos que, a pesar de haberles dedicado muy poco tiempo durante esta Tesis, siempre me han mostrado su cariño y me han transmitido toda la fuerza para continuar: Eva Maestre, Alejandro Mochón, Jorge Martín, Ana Sánchez, Mari Luz López, David Fernández. En especial a Julia Ordoñez que siempre me ha demostrado su cariño y una admiración que no merezco. A los cachorros Claudia y David por su inocencia y cariño y a su padre, mi amigo José Antonio Martínez (Gato) a quien que no le tocaba irse aún y que desgraciadamente no pudo ver esta Tesis finalizada.

Finalmente quiero agradecer a toda mi familia, en especial a mis padres y hermanos por toda su comprensión y acompañarme en esta aventura. Gracias por creer siempre en mi, entender que la ciencia es mi pasión y hacerme saber siempre que estáis orgullosos de mi. Espero poder devolveros algún día todo lo que habéis hecho por mí y recuperar todo el tiempo que he tenido que sacrificar y estar lejos de vosotros. Mis Coco y Luna, ¡vosotros sí que habéis tenido paciencia! vuestros saltos, chupeteos de alegría y energía cada vez que he llegado a casa han sido un factor fundamental para mantenerme alegre todos estos años.

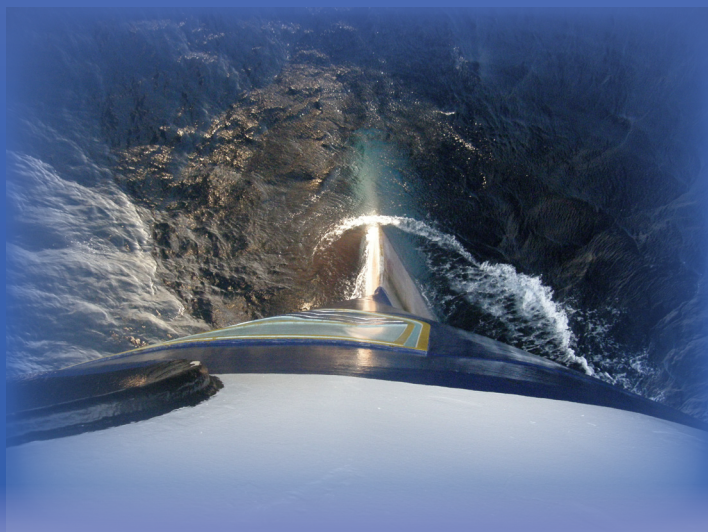
Y por supuesto a David, quien mejor que nadie ha vivido el día a día de esta Tesis. Gracias por darme tu apoyo incondicional y animarme en todo momento. Gracias por volver a ponerme a flote cuando pensaba que no podría ser capaz de llegar al final, por cuidarme y darme tu cariño en todo momento.

Curriculum Vitae



Carmina López-Rodríguez was born on the 28th of February, 1983 in Antequera, Málaga (Spain). There, Carmina graduated from secondary school at the “Colegio Maria Inmaculada” in 2000. Subsequently, she started studying “Geology” at University of Granada. In 2007 she started her master in “Geology” at the same institution. In 2008 she got a Fellowship from the Program “JAE-Predoc” (The Spanish National Research Council –CSIC) for master studies at University of Granada and for Ph.D. at the Andalusian Earth Science Institute (IACT, CSIC-UGR), in Granada, Spain. During her master she studied materials and sediments from mud volcanoes from the western Mediterranean (Alboran Sea), under supervision of Francisca Martínez-Ruiz and Menchu Comas Minondo (The Spanish National Research Council –CSIC & University of Granada - UGR). In 2009 she obtained her master degree. At

the same time she started her Ph.D also under supervision of Francisca Martínez-Ruiz and Menchu Comas Minondo at same institution (IACT, CSIC-UGR). During her Ph.D she worked sixteen months at international research centers abroad: Aveiro University, (Portugal); 2009); IFM-GEOMAR, (Germany); BGC-Department the Royal Netherland Institute for Sea Research (NIOZ) (The Netherlands); Utrecht University, (The Netherlands), doing complementary work which resulted in this thesis.



UGR

Universidad
de Granada



CSIC
CONSEJO SUPERIOR DE INVESTIGACIONES CIENTÍFICAS



PhD Program
in Earth Sciences



IACT
INSTITUTO ANDALUZ DE CIENCIAS DE LA TIERRA

cei·mar
campus de excelencia internacional del mar

